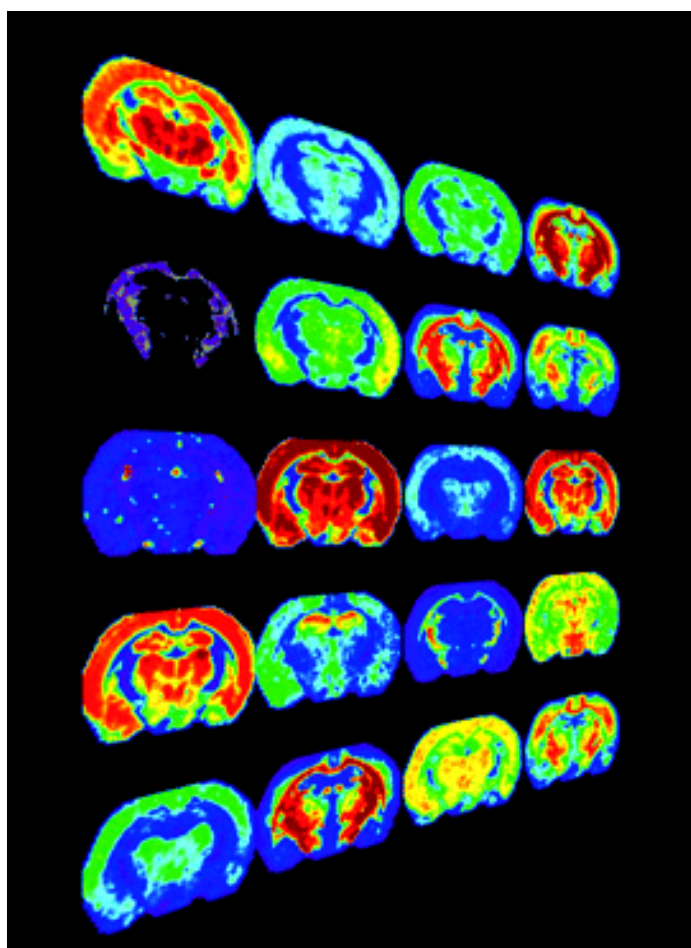UNIVERSITÀ DELLA CALABRIA

Dipartimento di CHIMICA

MASS SPECTROMETRIC METHODOLOGIES

AND

LIFE SCIENCE

PhD candidate Domenico Taverna

Academic Year 2009/2010

PhD Dissertation

Methodologies for the development of molecules of pharmacological interest

XXIII cycle (CHIM/06)

MASS SPECTROMETRIC METHODOLOGIES AND LIFE SCIENCE

Submitted in partial fulfilment of the requirements for

the degree of Doctor of Philosophy, Department of Chemistry,

University of Calabria,

Italy

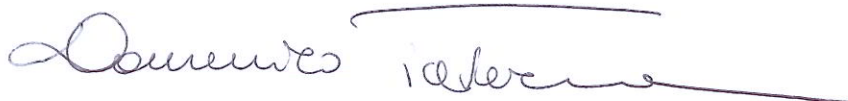| Supervisors	PhD Coordinator
Prof. Giovanni Sindona	Prof. Bartolo Gabriele
Dr. Leonardo Di Donna	

Candidate

Domenico Taverna

Academic Year 2009/2010

Declaration

I, the undersigned, certify that this thesis submitted for the degree of PhD in chemistry is the result of my own research, except where otherwise acknowledged, and that this thesis (or any part of the same) has not been submitted for a higher degree to any other university or institution.

Domenico Taverna   November, 23rd 2010

To my parents,
my brother
and who believed in me
since the beginning of this adventure into the science.

Acknowledgments

I would like to say thanks to my mentor at Università della Calabria, Prof Giovanni Sindona, and to my mentor at Vanderbilt University, Prof Richard M Caprioli, for giving me the opportunity to study my thesis in their mass spectrometry labs and for giving me the best advices ever about science. Their expert knowledge has been a great support for my work. I was always pushed to move up my limit to reach many goals in my investigations. Further, I would like to thank both my professors because they gave me the opportunity to had not only an important experience in science but also an important experience in life.

I would like also to say thanks to my PhD supervisor, Dr Leonardo Di Donna, that followed step by step even if I was so far from the lab, when I was in US. This thank is extended to Dr Fabio Mazzotti, that spent a lot of time with me in the lab working on the instruments and to Prof Giuseppina De Luca for her experience in NMR analysis and data interpretation.

Another thank is for my collaborator at Vandy's Plastic Surgery Department, Dr Lillian B Nanney and her collaborators, Alonda C Pollins and Nancy L Cardwell, for the constant support in the human skin project. I really appreciate your collaboration.

I would like to say thanks to my first "compagno di venture" in mass spectrometry, Dr Raffaele Salerno, aka Zio Raf, that really introduced me to this life science and followed me through all my thesis work.

My thanks will be never enough for all my friends and colleagues in Sindona team as well as in Caprioli team, that joined with me nights and days in the last three years.

I wanna say thanks to the Department of Chemistry family, basically all the administrative staff that supported me and all the others for orders, trips, and much more.

I wish to express my most sincere acknowledge to my PhD Coordinator, Prof Bartolo Gabriele, for his special support during all the PhD program.

How I can forget the hours spent with Mr Vanni and Mr Franco Santoro (aka Zio Franco) to try to figure out what was going on in the lab instruments.

And, Barbara, Paolo, Attilio, my "Olivicultura friends", Anna and Donatella, Antonio, Monica, Caterina, Paolo P, Hicham, Mohammed, Ashif, Will, Rita, Jeff, Junhai, Joy, Kerry, Hans, Erik, Kathleen, Whitney, Veronica, Maureen, Kristina, Noemi, Karinna, Roberto, Andrei, Peggi, Eduardo, Gwendoline, Erin, Jamie, Lisa, Mich, Patricia, Rey, and all my "family" in Nashville.

Contents

Section 1 – Food as a Source of Pharmacological Interest Compounds

Contents

Section 2 – Imaging Mass Spectrometry Applications on Human Skin Ulcers

Contents

Contents

List of Terms and Abbreviations

2D DIGE	2 dimensional difference gel electrophoresis
APCI	atmosperic pressure chemical ionization
API	atmosperic pressure ionization
AUC	area under curve
CE	capillary electrophoresis
CE	collision energy
CHCA	α-cyano-4-hydroxycinnamic acid
CID	collision-induced dissociation
CRM	charge residue model
DAD	diode array detector
DAG	diacyl glycerol
DAN	1,5-diaminonaphtalene
DE	delayed extraction
DHA	2,5-dihydroxyacetophenone
DHB	2,5-dihydroxybenzoic acid
DT	drift time
ESI	electrospray ionization
FAB	fast atom bombardment
FFPE	formalin fixed paraffin embedded
FT-ICR	fourier trasform ion cyclotron resonance
FWHM	full width half maximum
GC	gas chromatography
H&E	hematoxylin and eosin
HN-APCI	heated nebulizer atmosperic pressure chemical ionization
HPLC	high performance liquid chromatography
HR	high resolution
IC	half maximal inhibitory concentration
iCAT	isotope coded affinity tag
IDM	ion-desorption model
IHC	immunohystochemistry
IM-MS	ion mobility mass spectrometry
IMS	imaging mass spectrometry
IR	infrared
iTRAQ	isobaric tag for relative quantitation
k	capacity factor
LC	liquid chromatography
LDI	laser desorption ionization
m/q, m/z	mass to charge *ratio*
MALDI	matrix assisted laser desorption
MRM	multi reaction monitoring
MS	mass spectrometry
MS/MS	tandem mass spectrometry

MudPIT	multidimesional protein identification technology
MW	molecular weight
NMR	nuclear magnetic resonance
NPUAP	national pressure ulcer advisory panel
NS	nozzle skimmer
PC	principal components
PCA	principac component analysis
pI	isoelectric point
PSD	post source decay
PTMs	post traslatonal modifications
QIT	quadupole ion trap
Q-TOF	quadrupole time of flight
RF	radio frequency
ROC	receiver oprating characteristic curve
RP	reversed phase
RP	resolving power
RT	retention time
RTOF	reflectron TOF
SA	sinapinic acid, 3,5-dimethoxy-4-hydroxycinnamic acid
SAM	significance analysis of microarrays
SAX	strong anion exchange column
SCX	strong cation exchange column
SIM	selected ion monitoring
SIMS	secondary ion mass spectrometry
SPE	solid phase extraction
TFA	trifluoroacetic acid
THAP	2',4',6'-trihydroxyacetophenone
THF	tetrahydrofuran
TOF	time of flight
UV	ultraviolet

T his thesis work was focused on two different fields of research in order to develop methodologies for mass spectrometry investigative approaches. In the last decade, the increased interest of the scientific community for the food chemistry, especially in the South of Italy, pushed me to further investigate food and similar. Recent development in methods and instrumentations in mass spectrometry make it possible; in particular, the isolation and characterization of unknown molecules from very complex matrices can be carried out using a mass spectrometry based approach. The first part of the three year PhD was spent on food chemistry; basically, two foods, a fruit and an herbaceous plant, were used as source of compounds of suspected pharmacological interest. Thus, a mass spectrometry based approach was used to observe, separate and then collect semi-purified fractions of molecular weight specific species that were then structurally elucidated. A member of the Citrus fruit family as well as a member of Alliacee family were used as object of this thesis work also to complete the study of the citrus flavonoidic composition started several years ago in Sindona lab. The pummelo, aka Citrus Grandis, was prepared for the extraction of phenolic compounds and chromatography separation of low molecular species (below 1 KDa). The chromatography was used not only to separate different known molecular species but also to collected semi-purified fractions of unknown m/z ions by semi-preparative mode. An high resolution measurement is needed to obtain important information about the molecular formula as well as the number of double bonds present in the structure of the unknown compound of interest. The same high resolution measurement was carried out also for tandem mass spectrometry experiments, in order to fragment the unknown ions and study the obtained fragmentation patterns and assign the different part of the molecules. Many other experiments (either hydrolysis reaction and NMR analysis) were needed to validate the MS/MS spectra interpretations. According to the proved biological and pharmacological activities of such compounds (flavonoids), the characterization of new compounds extracted from food gives new clues to reach a complete and comprehensive characterization of the food molecular composition. The second part of this PhD was spent at the Mass Spectrometry Research Center in Vanderbilt University in order to develop methodologies for on tissue analysis by an emerging mass spectrometry field, Imaging Mass Spectrometry. Object of this study was the human skin: basically, human skin fresh frozen biopsies were used to investigate the proteome of a disease not completely understood, called pressure ulcer at stage IV. For this study, two main experimental approaches were used. One, termed *profiling*, involves analysis of discrete areas of the tissue sections to enable comparisons between distinct areas on tissue sections, such as normal healthy area versus a diseased area, or between two different specimens. Thus, the profiled spectra can be submitted to computational analysis and can be used to evaluate differences between two specimens. The second approach, termed *imaging*, is an high-resolution analysis of a tissue section that allows to analyze the entire tissue section from an ordered array of laser ablated spots in which spectra are acquired from those spots at intervals that define the image resolution. Imaging software generates two-dimensional ion-maps, by plotting the intensity of signals obtained as a function of *xy* coordinates. This procedure allows for rapid assessment of molecules localization and the visualization of the molecular differences between and among samples. This technology was applied to the study of human skin pressure ulcers, optimizing three different methods for proteins (mass range 2-20 kDa), in situ tryptic digested peptides (mass range 500-2000 Da) and lipids

(300-1400 Da). To further validate the preliminary findings, many statistical analysis (Significance Analysis of Microarrays, Principal Component Analysis, Receiver Operating Curves) were carried out. Data from the wound area as well as from the adjacent normal dermis/epidermis highlighted also the presence of two sub-regions within the wound bed. The IMS ion density maps for specific molecular species displayed a specific distribution and localization within two wound areas: one, the upper, most stagnant wound are bed apparently very compromised with on top a crust (death skin) and another one, the lower more mature, apparently still instance skin or on the road of healing. Mass spectrometry was used to identify the molecular features observed e recorded in the mass spectra and other techniques, such as immunohistochemistry, were used to confirm the MS/MS spactra interpretation and database search.

The present thesis work was divided in two sections: the first section regards the food chemistry part of the PhD as well as the second section was instead focused on the IMS study of the human skin ulcers. Each section was further divided in three chapters (1-Introduction on the object of the study, MS fundamentals and technologies used; 2-Results and Discussion; 3-Material and Methods).

Section 1

Chapter 1

Food as a Source of Pharmacological Interest Compounds

An Introduction

Food as a Source of Pharmacological Interest Compounds: Structural Characterization of New Flavonoids from Fruits and Plants.

It's widely known that fruits, vegetables, in general foods, can be considered as a natural source of molecules and compounds of pharmacological interest. It is also known that there are a bunch of inflammatory based processes in the human body and most of them, at date, are not yet fully understood. Fruits, vegetables, in general food, are a good source of several classes of compounds, many times interesting in terms of biological/pharmacological activity or as important component of some healthy diet. Most of the time, working on fruits and vegetables, the main problem for the identification and characterization of a compound of pharmacological interest is the isolation of lower abundant compounds due to the extreme complexity of the matrix; for instance, a fruit as pummelo (one of the object of this thesis work), also called Citrus Grandis from citrus family, is full of different classes of molecules. In particular, it is considered as a rich source of phenolic compounds.[1] All his parts, peel's albedo and flavedo, juice and also leaves are full of molecules. There are several ways to process a fruit and to try to isolate a compound of interest: in this thesis work a mass spectrometry based approach has been used, preceded by one of the classic separation technique: liquid chromatography. Following the last applications in food chemistry for structural characterization of compounds from fruits, three new, unknown glycosilated flavonoidic compounds were characterized using high resolution and tandem mass spectrometry. Other four previously uncharacterized molecules, again flavonoids, were instead structural elucidated in another vegetable matrix called allium porrum, from aliacee family.

MS Applications on Food

Mass spectrometry (MS), at date, is an analytical technique suitable in several fields of research; MS can be considered as a tool for the biological sciences to reach target that other technologies are not able to reach. According to sensitive mass analyzers capable of appropriate resolution and mass range, MS/chromatography combinations, tandem mass spectrometry and new ionization methods, MS is now an indispensable tool in the fields of proteomics, lipidomics and metabolomics; on the basis of the detection, identification, quantification, and structural characterization of peptides, lipids, and metabolites derived from biological sources. In addition to these small-molecule applications, intact biomolecules such as proteins and protein complexes (enzyme-substrate, protein-protein, and protein- DNA)[2, 3] are increasingly falling within the scope of MS, which is providing information such as molecular weight, stoichiometry, and binding affinity. All of these developments seem likely to be accelerated by the advent of ambient MS techniques[4], which allow compounds ranging from biopolymers to small drugs to endogenous biochemicals to be analyzed in unprepared samples, very rapidly and with high specificity. Further, mass spectrometry has become an important analytical tool in biology also because offers high-throughput, sensitive and specific analysis for many applications in microbiology, including clinical diagnostics and environmental research.[5]

Most of the recent applications in the food world to investigate their composition, their productive processes, for food quality and safety and to figure out their roles in diet and human health, are mass spectrometry-based. Some MS-based techniques are involved in the analysis of compounds of food concern as for instance the MALDI (matrix assisted laser desorption ionization) and ESI (electrospray ionization) sources to the analysis of proteins, peptides, lipids, phenolic compounds, etc.[6] In the last few years the role of mass spectrometry and related techniques is increasingly built up as an enabling tool in food analysis for elucidation of new compounds and also for quality control. Improvements in instrumentation, advances in on-line separation techniques and in data processing have contributed to determine a great expansion in the role of MS also in food-related analysis.[6] Liquid chromatography-mass spectrometry (LC-MS) coupling has led to the development of new interfaces, extending the possibilities and automation of various procedures even more.[7, 8] Undoubtedly, significant advances in ionization techniques having a broad range of applicability and high sensitivity for the analysis of high-polar and high-molecular mass compounds of food concern have been the key of this development in the last years. The impact of ionization technique such as electrospray (ESI) and matrix-assisted laser desorption ionization (MALDI)[9] on quadrupole, magnetic sector or time-of-flight (TOF) instruments, or coupled with instruments with tandem MS (MS-MS) capabilities has been fundamental also for food applications. Among atmospheric pressure ionization (API)-based interfacing systems are ESI, that is liquid-based interface, and heated nebulizer-atmospheric pressure chemical ionization (HN-APCI), often coupled with LC systems.[8] ESI and APCI well complement one another as regards to polarity and molecular mass of analytes and of chromatographic conditions. Although use of APCI is not yet as widespread as ESI, the number of reported applications of APCI-MS is rapidly increasing. Separation techniques such as gas chromatography (GC), liquid chromatography (HPLC) and capillary electrophoresis (CE) have become analytical techniques with many applications in study of substances of food concern, ranging from naturally occurring compounds to xenobiotics. Analysis of complex food extracts requires highly selective analytical techniques to characterize and determine targeted compounds and to characterize unknown compounds. The coupling of chromatographic techniques and MS has overcome the main analytical problem, which is scarce information about identity given by the detectors usually associated with GC and HPLC. High analytical power of GC-MS and on-line LC-MS have been convincingly proved. As for GC-MS, principles, instrumentation and analytical strategies using these techniques have been extensively discussed recently.[10] Liquid chromatography coupled to MS-MS offers a powerful tool also in food chemistry due to its selectivity, which enables the use of fast chromatography with low separation efficiency. However, in the analysis of real samples the existence of coeluting undetected components can lead to scarcely accurate method as a consequence of problems with the MS response, due to ion suppression and other effects. Thus the need for an efficient sample purification and chromatographic separation should not be undervalued. MS-MS can be accomplished using triple-quadrupole systems, which realize a tandem in-space instrument, or by performing in-source collision-induced dissociation (CID); furthermore, using ion trap (IT) instruments or LIFT cell instruments.[11, 12]

Natural Substances in Food

Mass spectrometry is considered to be a significant aid in natural substances characterization. In particular, rapid and sensitive characterization of polypeptides and proteins combined with sequence-related information can be directly obtained from MS-MS experiments of proteins. But also characterization of lipids, carbohydrates, vitamins, phenolic compounds, drugs and much more. In particular, mass spectrometry is suitable to characterize polypheolic compounds in foods; latter, play an important role as natural potent antioxidants exhibiting various physiological and biological activities, such as anti-inflammatory, anti-allergic and anti-carcinogenic activities, in the human metabolism. Owing to recognized beneficial properties toward human health, identification of antioxidant, phenolic compounds and their degradation products has been regarded as an important target successfully reached by using HPLC-MS[13-19, 20-22, 23-31] and MALDI -TOF-MS.[32-34] In fact, since polyphenolic compounds are usually found as complex mixture in plants, the composition of which changes according to the plant examined, hyphenated techniques are needed. Among these, LC-MS with different ionization modes represents a rapid and reliable technique to analyze these involatile substances. In some cases the coupled technique can afford a full on-line structural analysis involving no time-consuming isolation process. Innovative results have been demonstrated for accurate mass determination of phenolics and related compounds using MALDI-TOF-MS. The increasing interest in the characterization of phenolic compounds in food products, studied in the first part of this thesis, has created new demands for the development of rapid, sensitive, and specific analytical methodologies for the identification and quantification of this class of chemical compounds in fresh and processed foods. As described in recent overview papers[13, 14], over the past few years, various liquid chromatographic methods with UV-Vis absorption or DAD-UV, fluorescence and more recently with MS detection have been developed for the analysis of these naturally occurring antioxidant, anti-inflammatory compounds in foods. The authors evidence that using traditional approaches based on HPLC-DAD, UV spectra of phenolic compounds are often very similar and the possibility of unambiguous identification does not exist. With the introduction of bench-top instrumentation, mass spectrometry coupled to HPLC has evolved into a routine technique that enables collection of significant data on the structures of these compounds that show similar UV-Vis spectra.[15] Phenolic compounds in some vegetables matrices such as olive have been characterized by reversed-phase liquid chromatography using ESI-MS detection.[16, 17] Extracts from several olive fruit samples were examined by LC–MS using ESI in the positive and negative ion modes to generate total ion current (TIC) chromatograms.[16] With the aim to analyze phenolic compounds in olive fruit, the same authors performed semi-preparative HPLC analyses to isolate the analytes of interest into distinct fractions and then the selected fractions were analyzed by LC–ESI-MS in both negative and positive ion modes.[17] Although positive and negative analysis were complementary, the latter showed better sensitivity and selectivity for the acidic and phenolic compounds. Recently, the composition of simple phenolic compounds in fruits has been evaluated by RP-HPLC analysis and the identity of phenolic compounds was confirmed by LC–MS equipped an ESI ionization source.[18] HPLC coupled with ESI-MS was investigated as a reliable method for analyzing wine polymeric tannins.[19] The apparatus coupled to the chromatographic system was a simple quadrupole mass spectrometer with a mass range of 2400 mass

units. It was observed that the response of polyphenols (except for anthocyanins) was better in negative ion mode than in positive ion mode. Further, signal intensity decreased as the polymerization degree increased. Various series of ion peaks containing a variable number of trihydroxylated units were detected as monocharged ions [M–H]⁻ from dimers to pentamers. The largest mass detected in the analyzed wine fraction corresponded to the mass of heptamers, which were found as doubly charged ions. Both APCI and ESI interfacing systems have been explored for coupling with HPLC for determination of low-molecular-mass phenols and flavan-3-ols in wine.[35] Two different RPLC separation methods were optimized using APCI and ESI as the ion sources either in positive or negative ion mode. Data reported in this paper showed that ESI coupled with HPLC provided to be the method of choice for the analysis of low-molecular-mass phenols under negative ion mode, whereas flavan-3-ol compounds were well detected under both positive and negative ion modes. HPLC–tandem mass spectrometry has been successfully applied to the quantitation of prenylflavonoids in hops and beer.[22] After HPLC separation under reversed-phase conditions, prenylflavonoids were detected by APCI in positive ion mode. Quantitative MS–MS data were obtained by multiple-reaction monitoring using a triple–quadrupole mass spectrometer equipped with an APCI source. Attention was paid to accuracy and precision of the method, which were evaluated on spiked samples. Besides phenolic compounds such as phenolic acids and aldehydes, include flavonoids. This class of poly coumaphenols have been found to be an important part of the human diet and have become an intense focus of research interest because of their perceived health beneficial effects (ref sindona bergamotto). Sindona et al have characterized 3-hydroxymethilglutaryl flavonid glycosides in bergamot fruit.[36] Furthermore, anthocyanidins are an important class of flavonoid compounds which are widely distributed in nature. Considerable effort was put in polyphenol analysis by the group of Sporns.[32-34] The applicability of MALDI-MS for both qualitative and quantitative analysis of anthocyanins was first demonstrated in wine and fruit juice samples.[32] Anthocyanins under acidic conditions were predominantly in the aromatic oxonium ion form and easily ionized in MALDI-TOF-MS to form molecular cations [M] in the positive ion mode. Following similar analytical procedures, a MALDI-TOF-MS method was applied to identify flavonol glycosides in yellow onion and green tea.[34] Recently, the interest in these phenolic compounds has increased significantly due to their potential health benefits as antioxidants and anti-inflammatory agents.[37, 38] That's why the first part of this work was focused to the characterization of unknown flavonoids, according to their potential beneficial effect on human health. The application of LC–MS with an ESI interface has been evaluated for the analysis of flavanones, flavones and flavonols.[27] Following these studies, a method for extraction, separation and collection of unknown ions have been developed in this thesis and some di-glycosilated flavanols have been structurally elucidated using high resolution tandem mass spectrometry and ¹H-NMR to determine the position of the glycosidic part of the molecules.

Phenolic Compounds of Pharmacological Interest: Flavonoids.

Flavonoids are phenolic substances isolated from a wide range of vascular plants, with over 8000 individual compounds known. Structurally they are a polyphenols subclass which are widely distributed in

the plant kingdom, and characterized by two or more aromatics rings, each bearing at least one aromatic hydroxyl and connected with a heterocyclic pyran.[39] They act in plants as antioxidants, antimicrobials, photoreceptors, visual attractors, feeding repellants, and for light screening. Many studies have suggested that flavonoids exhibit biological activities, including antiallergenic, antiviral, anti-inflammatory, and vasodilating actions.[40-42] However, most interest has been devoted to the antioxidant activity of flavonoids, which is due to their ability to reduce free radical formation and to scavenge free radicals and to the anti-inflammatory activity, which is due to their polyphenolic structure that renders them quite sensitive to oxidative enzymes.[43] Flavonoids are formed in plants from the aromatic amino acids phenylalanine and tyrosine, and malonate.[44] The basic flavonoid structure is the flavan nucleus, which consists of 15 carbon atoms arranged in three rings (C_6-C_3-C_6), which are labeled A, B, and C (Figure 1).
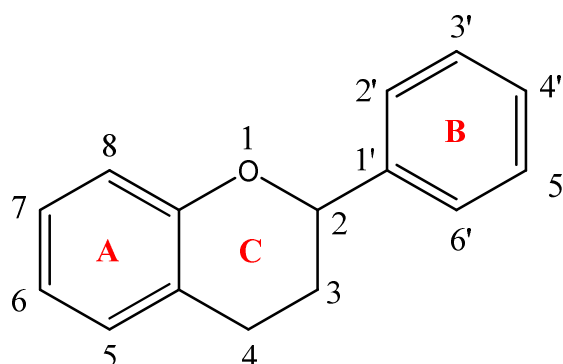
Figure 1: *basic flavonoid structure, a flavan nucleus, which consists of 15 carbon atoms arranged in 3 rings labeled A, B and C.*

The various classes of flavonoids differ in the level of oxidation and pattern of substitution of the C ring, while individual compounds within a class differ in the pattern of substitution of the A and B rings. Among the many classes of flavonoids, those of particular interest are flavones, flavanones, isoflavones, flavonols, flavanonols, flavan-3-ols, and anthocyanidins. Other flavonoid classes include biflavones, chalcones, aurones, and coumarins. Hydrolyzable tannins, proanthocyanidins (flavan-3-ol oligomers), caffeates, and lignans are all plant phenols, and they are usually classified separately. Flavonoids generally occur in plants as glycosylated derivatives, and they contribute to the brilliant shades of blue, scarlet, and orange, in leaves, flowers, and fruits.[45] Apart from various vegetables and fruits, flavonoids are found in seeds, nuts, grains, spices, and different medicinal plants as well in beverages, such as wine (particularly red wine), tea, and (at lower levels) beer.[46] More specifically, the flavones apigenin and luteolin are common in cereal grains and aromatic herbs (parsley, rosemary, thyme), while their hydrogenated analogues hesperetin and naringin are almost exclusively present in citrus fruits.[47] The flavonols quercetin and kaempferol are predominant in vegetables and fruits, where they are found mainly in the skin, with the exception of onions. Isoflavones are found most often in legumes, including soybeans, black beans, green beans, and chick peas. Alfalfa and clover sprouts and sunflower seeds also contain isoflavones.[48] The

flavan-3-ols (+)-catechin, (-)-epicatechin, (-)-epigallocatechin, and their gallate esters are widely distributed in plants, although they are very rich in tea leaves. Flavan oligomers (proanthocyanidins) are present in apples, grapes, berries, persimmon, black currant, and sorghum and barley grains.[49] Anthocyanidins and their glycosides (anthocyanins) are natural pigments and are abundant in berries and red grape.[50] Flavonoids play different roles in the ecology of plants. Due to their attractive colors, flavones, flavonols, and anthocyanidins may act as visual signals for pollinating insects. Because of their astringency, catechins and other flavanols can represent a defense system against insects harmful to the plant.[51] Flavonoids act as catalysts in the light phase of photosynthesis and/or as regulators of iron channels involved in phosphorylation.[52] They can also function as stress protectants in plant cells by scavenging ROS produced by the photosynthetic electron transport system.[53] Furthermore, because of their favorable UV-absorbing properties, flavonoids protect plants from UV radiation of sun and scavenge UV-generated ROS.[54] Apart from their physiological roles in the plants, flavonoids are important components in the human diet, although they are generally considered as non-nutrients. Indeed, the level of intake of flavonoids from diet is considerably high as compared to those of vitamin C (70 mg/day), vitamin E (7-10 mg/day), and carotenoids (β- carotene, 2-3 mg/day).[55] Flavonoid intake can range between 50 and 800 mg/day, depending on the consumption of vegetables and fruit, and of specific beverages, such as red wine, tea, and unfiltered beer.[56] In particular, red wine and tea contain high levels (approximately 200 mg per glass of red wine or cup of tea) of total phenols. Thus, variations in consumption of these beverages are mainly responsible for the overall flavonoid intake in different national diets. Another significant source of flavonoids are different medicinal plants and related phytomedicines.[57] Several epidemiological studies provide support for a protective effect of the consumption of fresh fruits and vegetables against cancer[58, 59], heart disease[60-62], and stroke.[63, 64] Normally, high consumers of fruits and vegetables have a healthy lifestyle, which may be an important factor for their resistance against chronic diseases. All in all, fruits and vegetables do play a preventive role, which is due to a variety of constituents, including vitamins, minerals, fiber, and numerous phytochemicals, including flavonoids. Thus, it is possible that also flavonoids contribute to the protective effect of fruits and vegetables. This possibility has been evidenced by several in vitro, ex vivo, and animal studies.[65] Unfortunately, the evidence in humans is still limited and somewhat controversial.[66] According to some epidemiological studies, there is no evidence that flavonoid intake is protective against some types of cancer.[67] Only one study has shown that the consumption of flavonoids is inversely correlated with lung cancer.[68] In contrast, a possible protective role against coronary heart disease of flavonoid intake (either from fruits and vegetables or red wine and tea) has been reported in four out of six epidemiological studies.[69] The dietary sources of flavonoids were fruits, vegetables, red wine, and tea, and they were found to be inversely correlated with the risk of coronary heart disease and stroke. Accordingly, the present epidemiological data (although far from conclusive) evidence a possible protective role of dietary flavonoids, thus making desirable a regular consumption of foods and beverages rich in flavonoids.

Citrus Fruits as well as Aliacee Plants as Source of Phytochemical Substances

Food, in general, is full of nutrients with some beneficial effects on human health, if the dietary intake is regulated. The possible beneficial effects of foods are due to micronutrients (for example vitamins and minerals) and to functional food ingredients and antioxidant nutraceuticals, ''phytochemical substances''.[1] Phytochemicals can be defined as substances found in edible fruits and vegetables that, daily ingested, may exhibit a potential for modulating human metabolism in a manner favourable for the prevention of chronic and degenerative diseases. Nowadays, many studies are carried out on the thousands of phytochemicals that may have important physiological effects. An increased consumption of fruit and vegetables, typical Mediterranean diet foods, may protect against degenerative pathologies, such as cancer and atherosclerosis.[70, 71] Epidemiological studies have shown an inverse relationship between dietary flavonoid intake and cardiovascular diseases.[72] Among the phytochemicals, flavonoids are widely contained in Citrus fruits.[73] Citrus fruits are the principal source of such important nutrients. They contain vitamin C, folate, dietary fibre and other bioactive components, such as carotenoids and flavonoids, which are suggested to be responsible for the prevention of cancer and degenerative diseases.[74]

As described, according to their molecular structures flavonoids are divided into six classes: flavones, flavanones, flavonols, isoflavones, anthocyanidins and flavanols (or catechins) (Figure 2).[75] Flavonoids identified in Citrus fruits cover over 60 types, according to the five classes mentioned[76]: flavones, flavanones, flavonols, flavans and anthocyanins (the last only in blood oranges). Table 1 shows the main chemical structures of some flavonoids isolated from Citrus fruits, their structures (flavanone, flavone, or flavonol) and their chemical groups. Citrus flavanones are present in the glycoside or aglycone forms. Among the aglycone forms, naringenin and hesperetin are the most important flavanones (Table 1). Among the glycoside forms, two types are classified: neohesperidosides and rutinosides.[77, 78] Neohesperidosides, flavanones, naringin, neohesperidin and neoeriocitrin consist of a flavanone with neohesperidose (rhamnosyl-a-1,2 glucose) and they have a bitter taste (Table 1), while rutinosides (flavanones, hesperidin, narirutin and didymin) have a flavanone and a disaccharide residue e.g. rutinose (ramnosyl-a-1,6 glucose) and they are without taste (Table 1). Flavanones are usually present in diglycoside form, conferring the typical taste to Citrus fruits.[78] Phenolic compounds and flavonoid profiles are detected by HPLC-MS. These compounds can be divided into two groups according to the lag-times: the first eluted are flavanone glycosides while the second group are polymethoxylated flavones (subsequently eluted they are less polar).[79] Among flavonoids, the anthocyanins are structurally derived from pyran or flavan and, in particular, oxygen attributes a basic property to this molecule. They can be present as aglycones (anthocyanidins metabolites of flavones) (Figure 2). Catechins, leucoanthocyanin and proanthocyanins are in the flavan group, as also are tannins. They can be found in monomer, dimer and polymer forms, respectively monoflavans, biflavans or triflavans.[80]
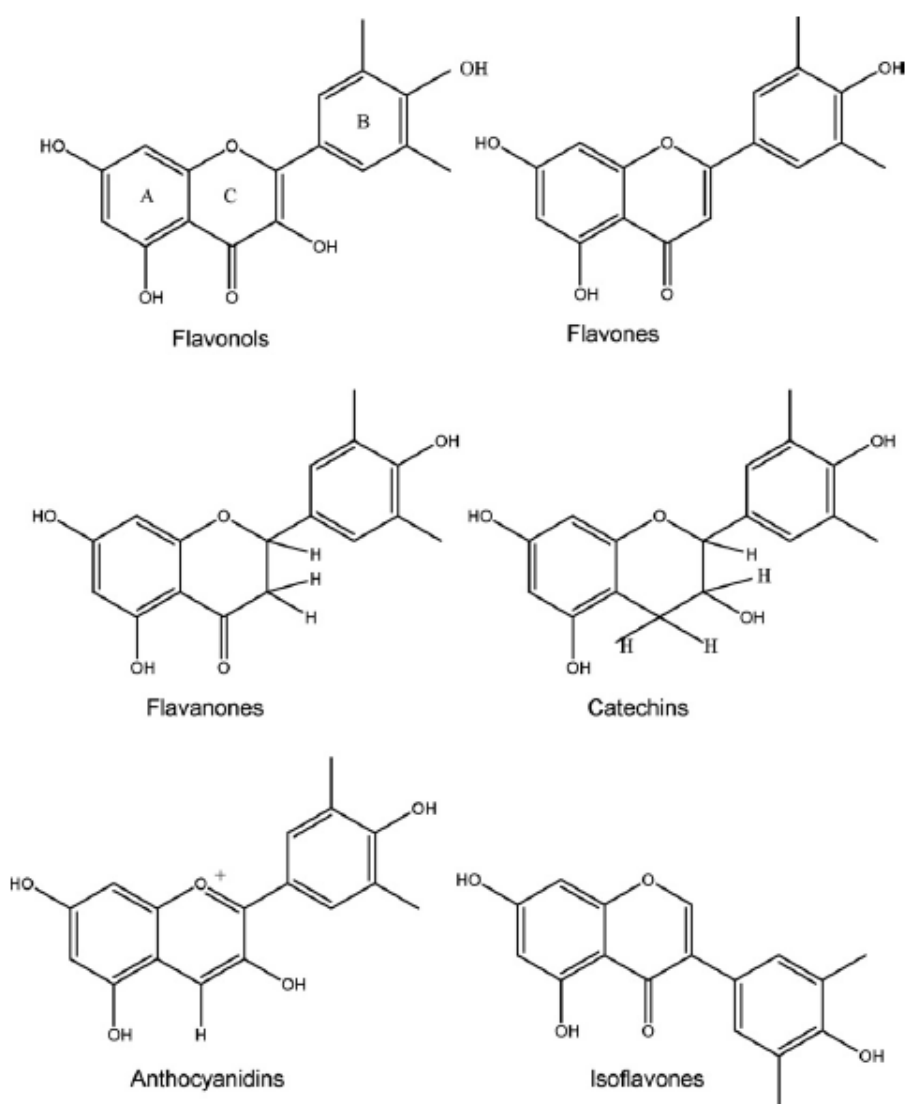
Figure 2: *molecular structures of flavonoide. The basic structure consists of the fused A and C ring, with the phenyl ring B attached to through its 1' position to the 2-position of the C ring (numbered from the pyran oxygen).*

Flavonoids are a group of pigments contained in plants and they are responsible for flower and fruit coloration. Flavonoids are present in dietary fruits and vegetables.[78] The Citrus peel and seeds are very rich in phenolic compounds, such as phenolic acids and flavonoids. The peels are richer in flavonoids than are the seeds.[81] Since a Citrus fruit is peeled, peel and seeds are not used. It is necessary to estimate these by-products as natural antioxidants in foods.[82] The 7-O-glycosylflavanones are the most abundant flavonoids in all Citrus fruits[83, 84]; for example, lemon peel is rich in glycosidic flavonoids.[85]

Compounds	Structural formula	Molecular weight	Molecular formula
Flavanone aglycone forms			
Naringenin	$R_1 = OH$; $R_2 = OH$; $R_3 = H$; $R_4 = OH$	271 Da	$C_{15}O_5H_{11}$
Hesperetin	$R_1 = OH$; $R_2 = OH$; $R_3 = OH$; $R_4 = OCH3$	288 Da	$C_{15}O_6H_{13}$
Isosakuranetin	$R_1 = OH$; $R_2 = OH$; $R_3 = H$; $R_4 = OCH3$	285 Da	$C_{16}O_5H_{13}$
Heridictyol	$R_1 = OH$; $R_2 = OH$; $R_3 = OH$; $R_4 = OH$	287 Da	$C_{15}O_6H_{11}$
Flavone and flavonol aglycone forms			
Apigenin	$R_1 = OH$; $R_2 = OH$; $R_3 = H$; $R_4 = OH$; $R_5 = H$	270 Da	$C_{15}O_5H_{10}$
Luteolin	$R_1 = OH$; $R_2 = OH$; $R_3 = OH$; $R_4 = OH$; $R_5 = H$	286 Da	$C_{15}O_6H_{10}$
Diosmetin	$R_1 = OH$; $R_2 = OH$; $R_3 = OH$; $R_4 = OCH3$; $R_5 = H$	288 Da	$C_{15}O_6H_{12}$
Quercetin	$R_1 = OH$; $R_2 = OH$; $R_3 = OH$; $R_4 = OH$; $R_5 = OH$	302 Da	$C_{15}O_7H_{10}$
Kämpferol	$R_1 = OH$; $R_2 = OH$; $R_3 = H$; $R_4 = OH$; $R_5 = OH$	286 Da	$C_{15}O_6H_{10}$
Flavanone neohesperidoside forms			
Naringin	$R_2 = OH$; $R_3 = H$; $R_4 = OH$	604 Da	$C_{29}O_{14}H_{32}$
Neohesperidin	$R_2 = OH$; $R_3 = OH$; $R_4 = OCH3$	634 Da	$C_{30}O_{15}H_{34}$
Poncirin	$R_2 = OH$; $R_3 = H$; $R_4 = OCH3$	588 Da	$C_{29}O_{13}H_{32}$
Neoeriocitrin	$R_2 = OH$; $R_3 = OH$; $R_4 = OH$	620 Da	$C_{29}O_{15}H_{32}$
Flavanone rutinside forms			
Narirutin	$R_3 = H$; $R_4 = OH$	551 Da	$C_{29}O_{11}H_{27}$
Hesperidin	$R_3 = OH$; $R_4 = OCH_3$	583 Da	$C_{30}O_{12}H_{31}$
Didymin	$R_3 = H$; $R_4 = OCH_3$	567 Da	$C_{30}O_{11}H_{31}$
Eriocitrin	$R_3 = OH$; $R_4 = OH$	571 Da	$C_{29}O_{12}H_{31}$
Diosmin	$R_3 = OH$; $R_4 = OCH_3$	583 Da	$C_{30}O_{12}H_{31}$

Table 1: *structural characteristics and molecular weights of Citrus flavonoide in the aglycone and glycoside forms.*

Among the neohesperidoside flavanones, naringin, neohesperidin and neoeriocitrin, are mainly present in bergamot, grapefruit and bitter orange juices. Among rutinoside flavanones, hesperidin, narirutin and didymin, are present in bergamot, orange, mandarin and lemon juices.[86] Flavanone chemical structures are specific for every species, which renders them markers of adulteration in commercial juices.[87-89] The

seed and peel compositions are not always the same in Citrus fruits. For example, the lemon seed mainly contains eriocitrin and hesperidin, while the peel is rich in neoeriocitrin, naringin and neohesperidin. Moreover, the glycosylated flavanone concentrations are different; neoeriocitrin and naringin have similar concentrations in peel while, in seed, eriocitrin is 40 times more abundant than is naringin.[90] Neohesperidin, naringin and neoeriocitrin are extracted from peel in great amounts. Bitter orange is a very interesting neohesperidin and naringin source; these compounds can be useful for the production of sweeteners. The seeds of bergamot are the most important source of the glycosylated flavanones, naringin and neohesperidin; lemon is rich in eriocitrin and hesperidin. All the other Citrus fruits have small amounts of glycosylated naringin.[91] Flavanone glycosyl compositions of peels and seeds are quite unlike those of juices. Naringin has been found in lemon peel and seed and in mandarin seed, but it is not present in the juices of these fruits.[92] This glycosylated flavanone is never present in sweet orange juice, and its presence is used to detect adulteration.[88] Although flavones and flavonols have been found in low concentrations in Citrus tissues, these compounds are studied to evaluate their antioxidant ability.[93] Miyake et al. isolated two C-glucosylflavones from the peel of lemon fruit (Citrus Limon BURM. f.). They identified 6,8-di-C-b-glycosyldiosmin and 6-C-b-glycosyldiosmin by UV, IR, FABMS, ^{1}H NMR, and ^{13}C NMR analyses. In lemon juice extracted from several cultivars, there is little difference in the glycosylated flavonoids amounts. Eriocitrin, 6,8-di-C-b-glycosyldiosmin and 6-C-b-glycosyldiosmin are particularly abundant in lemon and lime, while they are almost absent in other Citrus fruits.[94] Anthocyanins constitute the colouring compounds of flowers and fruits, but sometimes also of leaves, buds and roots. They are in the epicarp, but they also colour the mesocarp of oranges. The anthocyanin content is strongly dependent on the level of maturation. Catechins, leucoanthocyanin and proanthocyanins are not Citrus fruit specific compounds because they are also found in other vegetables.

Also plants of the genus Allium have been recognized as rich sources of secondary metabolites endowed with interesting biological activities.[95] As a part of a systematic phytochemical study on Mediterranean Allium species, Fattorusso et al. have recently obtained a number of new kaempferol glycosides from the wild garlic, A. ursinum L.[96], and from the ornamental garlic, A. neapolitanum Cyr [97], this latter plant also contained some quercetin and isorhamnetin glycosides. They investigated also the flavonoid glycosides of leek, A. porrum L. (Alliaceae). Although this plant is widely distributed and commonly used as a food, no systematic evaluation of its flavonoid composition has been reported yet. The isolation from bulbs of leek of five flavonol glycosides, two of which, based on a kaempferol aglycone and acylated with a 3-methoxy-4-hydroxycinnamoyl moiety, were proposed. All the isolated compounds were evaluated for their inhibitory activity on human platelet aggregation, an action already evidenced for kaempferol. In particular, kaempferol was reported to inhibit markedly (IC50 20 mM) platelet aggregation and ATP release of platelets induced by arachidonic acid or collagen. In addition, kaempferol also acts as a thromboxane receptor antagonist, and it has been claimed as an active agent in the prevention of atherosclerosis and acute platelet thrombus formation. In this thesis work Allium porrum was investigated to furher characterize new unknown flavonoids.

Distribution of Flavonoids in Citrus Fruits and Tissues

The detailed flavonoid composition in fruit tissues of the Citrus species was analyzed by Nogata et al. in 2006; this study provide data that would enable more effective utilization of flavonoids constituents and to examine the agreement of their flavonoids composition with Tanaka's classification system. The latter was made in 1969 and can be considered as a morphological classification of the Citrus genus divided into 2 subgenera, 8 sections and 16 subsections, involving 149 species.[98] Swingle, an advocator of another system, classified Citrus into 2 subgenera and 16 species including 8 varieties in 1948.[99] The major difference between these two systems is in how mandarins were treated: Swingle placed all mandarins except C. tachibana and C. indica in C. reticulata, whereas Tanaka separated mandarins into 36 species. Nogata et al. evaluated flavonoids concentration in each tissue of citrus fruits on a fresh weight basis. The composition data for each fruit were calculated from all the different parts of the fruit: from those of the flavedo, albedo, segment epidermis, and juice vesicle tissues, and that for the peel tissue was from those of the flavedo and albedo tissue. Albach and Redman have shown that Citrus species could be differentiated on the basis of their content of neohesperidosides or rutinosides.[100] Basically, all neoesperidosyl flavanones present in citrus fruits and also some neohesperidosyl flavones were found as principal components in the segment epidermis; on the other hand, the rutinosyl flavonoids (with some exceptions) had opposite score in the same fruit tissues. The presence and the relative concentration of all the flavonoids species in Citrus fruits was found different. Although some study have suggested that the sugar type largely contribute to the principal components, the flavonoid glycosides generally decreased with decreasing polarity of the fruit.[101] Therefore, the polarity of the flavonoids constituents is suggested to contribute in the second principal components of the fruit. In respect of the principal component of the segment epidermis, the flavonoid glycosides had inverse values to those of the fruit and the contribution of polymethoxylated flavonoids was smaller than that of the fruit. Further, values for the flavonoids in the juice vesicle had different patterns from those in the other parts of fruits, and no clear trend apparent. According to several study it's clear that the composition data are influenced by the flavonoid localization, pulp content, and water content. And also the flavanone glycoside composition of some Citrus juice was demonstrated as differentiated by Mouly et al.. Provided that the number of citrus biotypes is limited, the flavonoid composition should enable their differentiation. In conclusion, the flavonoid composition in the tissues of more than 45 Citrus species may differ with the recognition of morphological differences due also to the geographic area. Although, most of the flavonoids present in the citrus fruits as principal or secondary components are already structurally elucidated and is known their action, physiological and pharmacological, many compounds are still unknown, especially the minor components. The first part of this PhD was focused to discover, isolate and characterize unknown flavonoids in Citrus fruit as Pummelo. The pummelo (*Citrus maxima* or *Citrus grandis*) is a citrus fruit native to South East Asia. It is usually pale green to yellow when ripe, with sweet white (or, more rarely, pink or red) flesh and very thick pudgy rind. It is the largest citrus fruit, 15–25 cm in diameter, and usually weighing 1–2 kg. Other spellings for pomelo include pummelo, and pommelo, and other names include Chinese grapefruit, jabong, lusho fruit, grapefruit (aka pomplemous), papanas, and shaddock. The pomelo tastes like a sweet, mild grapefruit, though the typical pomelo is much larger in size than the grapefruit. It has very little, or none, of the

common grapefruit's bitterness, but the enveloping membranous material around the segments is bitter, considered inedible, and thus usually discarded.

Mass Spectrometry Fundamentals

Ion Sources

The function of an ion source is to convert sample molecules or atoms into gas-phase ionic species. Several different types of ion-source designs are in use, some operating at very low pressures and some at atmospheric pressure, and not all are alike in construction. Some common elements of these sources are (1) a source block, (2) a source of energy (e.g., an electron, particle, or ion beam), (3) a source heater, (4) a short ion-extraction region that accelerates the ions to a specified fixed kinetic energy, and (5) an exit slit assembly. The accelerating potential is set to several kilovolts in magnetic-sector and time-of-flight (TOF) instruments, but to only a few volts in quadrupole-based mass spectrometers. The ion source should have the following desirable characteristics: (1) high ionization efficiency (a requirement for high detection sensitivity), (2) a stable ion beam, (3) a low-energy spread in the secondary-ion beam, (4) minimum background ion current, and (5) minimum cross-contamination between successive samples.

Electrospray

Electrospray ionization (ESI) is also an API technique that is applicable to a wide range of liquid-phase samples. In particular, it has made an enormous impact in the characterization of large biomolecules. It has also become the most successful interface for LC/MS and CE/MS applications.[102, 103] Although the concept of electrospray was put forward by Malcom Dole in 1968[104], the development of ESI–MS is credited to John Fenn[105, 106], who was awarded the 2002 Nobel Prize in Chemistry for that contribution. As the name implies, electrospray ionization is a process that produces a fine spray of highly charged droplets under the influence of an intense electric field. Evaporation of the solvent converts those charged droplets into gas-phase ions. A simplistic view of the ESI process is depicted schematically in Figure 3.
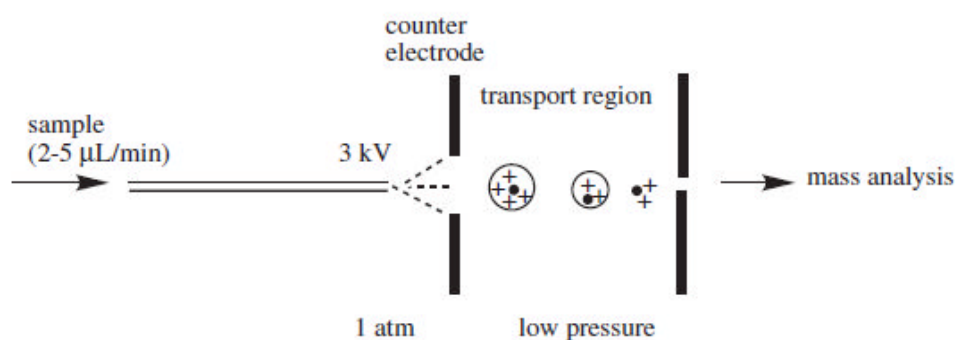
Figure 3: *basic components of electrospray.*

The sample solution in a suitable solvent mixture flows continuously through a stainless steel capillary tube whose tip is held at a high potential (3 to 4 kV) with respect to the walls of the surrounding atmospheric-pressure region, called a *counter-electrode*. The solvent consists of a 1 : 1 (v : v) mixture of water and acetonitrile and typically contains <1% acetic acid, formic acid, or trifluoroacetic acid. The potential difference between the tip of the capillary and the counterelectrode produces an electrostatic field that is sufficiently strong to disperse the emerging solution into a fine mist of charged droplets. Evaporation of the charged droplets is assisted by a flow of hot nitrogen. During the process of droplet evaporation, some of the dissolved ions are released into the atmosphere. The resulting ions are transported from the atmospheric-pressure region to the high vacuum of the mass analyzer via a series of pressure-reduction stages. Two designs of the transport region are commonplace in the commercial version of the ESI source; one consists of a heated metal or glass capillary several centimeters long (shown in Figure 4) and the other of small-orifice skimmer lenses (Figure 5) similar to those outfitted in an APCI source. To improve the iontransmission efficiency, radio-frequency rf) multipoles (quadrupoles, hexapoles, or octopoles) or "ion funnels" are placed between the ESI source and the mass analyzer. Optimum operation of a normal ESI source is achieved at flow rates of 2 to 10 μL/min. For stable operation at higher flow rates (0.2 to 1.0 mL/min^{-1}; e.g., effluents from narrow- and wide-bore analytical HPLC columns), some form of an additional source of energy, such as heat or a high velocity annular flow of gas, is supplemented to disperse the liquid into fine droplets. Electrospray analysis can be performed in positive and negative ionization modes. The polarity of the ions to be analyzed is selected by the capillary voltage bias. A novel feature of the ESI mass spectrum is the formation of intact molecular ions of the analyte. Fragmentation, if desired, can be induced in the ion transport region of the ESI source by increasing the sampling cone voltage. This process is known as *in source collision-induced dissociation* (CID) or *nozzle–skimmer* (NS) *dissociation*.
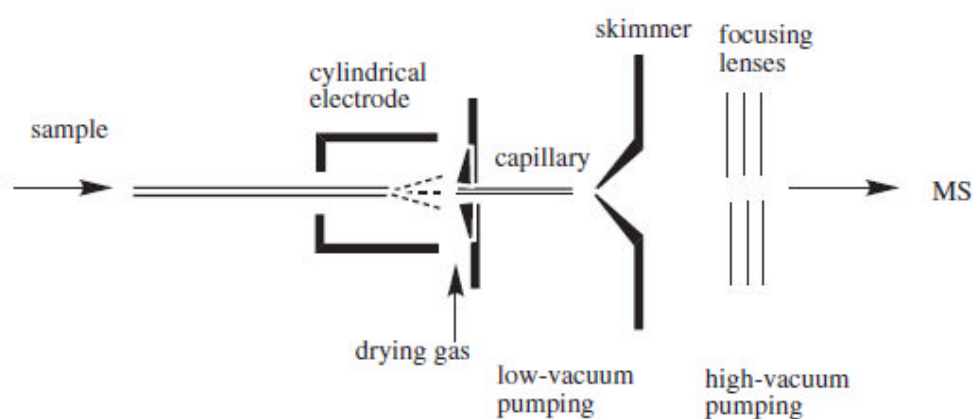
Figure 4: *heated capillary design of electrospray ionization source.*
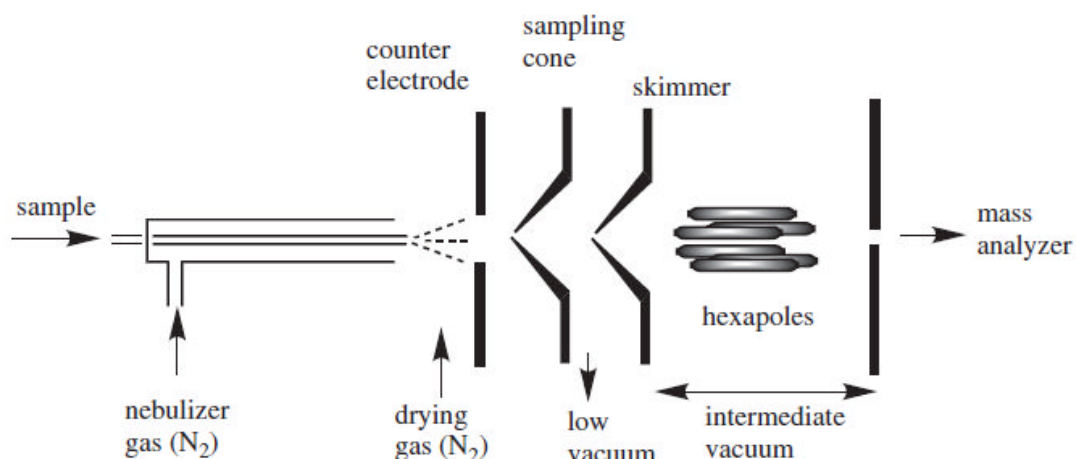
Figure 5: *block diagram of an electrospray ionization source that uses skimmer lenses.*

The mechanism of ESI is a highly debated topic.[106-112] It is generally believed that ionization in electrospray involves three different processes: droplet formation, droplet shrinkage, and desorption of gaseous ions. At the onset of the electrospray process, the electrostatic force on the liquid leads to a partial separation of charges. In the positive-ion mode, cations concentrate at the tip of the metal capillary and tend to migrate toward the counter-electrode, whereas anions migrate inside the capillary away from the tip (Figure 6a). The migration of the accumulated positive ions toward the counter-electrode is counterbalanced by the surface tension of the liquid, giving rise to a Taylor cone at the tip of the capillary (Figure 6b). If the applied electric force is large enough, a thin cylinder of the liquid extends from this cone and breaks into a mist of fine droplets. The continuous production of charged species is assisted by electrochemical redox processes. In the positive-ion mode, electrochemical oxidation occurs in solution at the metal contact of the sprayed solution and reduction at the counter-electrode. In the negative-ion mode, the migration of anions and direction of electrochemical processes are reversed. A number of factors, such as applied potential, flow rate of the solvent, capillary diameter, and solvent characteristics influence the size of the droplets formed initially. Evaporation of the solvent from these droplets leads to droplet shrinkage. A cascade of droplet-fission processes follows. As the droplets shrink in size, the charge density on their surface increases until it reaches the Rayleigh instability limit. At this point, the repulsive coulombic forces exceed the droplet surface tension, causing fission of the droplets into smaller and highly charged offspring droplets. Further evaporation of the solvent results in Coulomb fission of the offspring droplets into second-generation droplets. Two mechanisms have been proposed to explain ion desorption from the droplets: the charge-residue model (CRM) and the ion-desorption model (IDM).[108] According to the CRM proposal (see Figure 7a), the sequence of solvent evaporation and droplet fission is repeated several times, until the drop size becomes so small that it contains only one solute molecule. As the last of the solvent is evaporated, that molecule is dispersed into the ambient gas, retaining the charge of the droplets. As shown in Figure 7b, the IDM proposal also relies on the sequence of solvent evaporation and droplet fission.
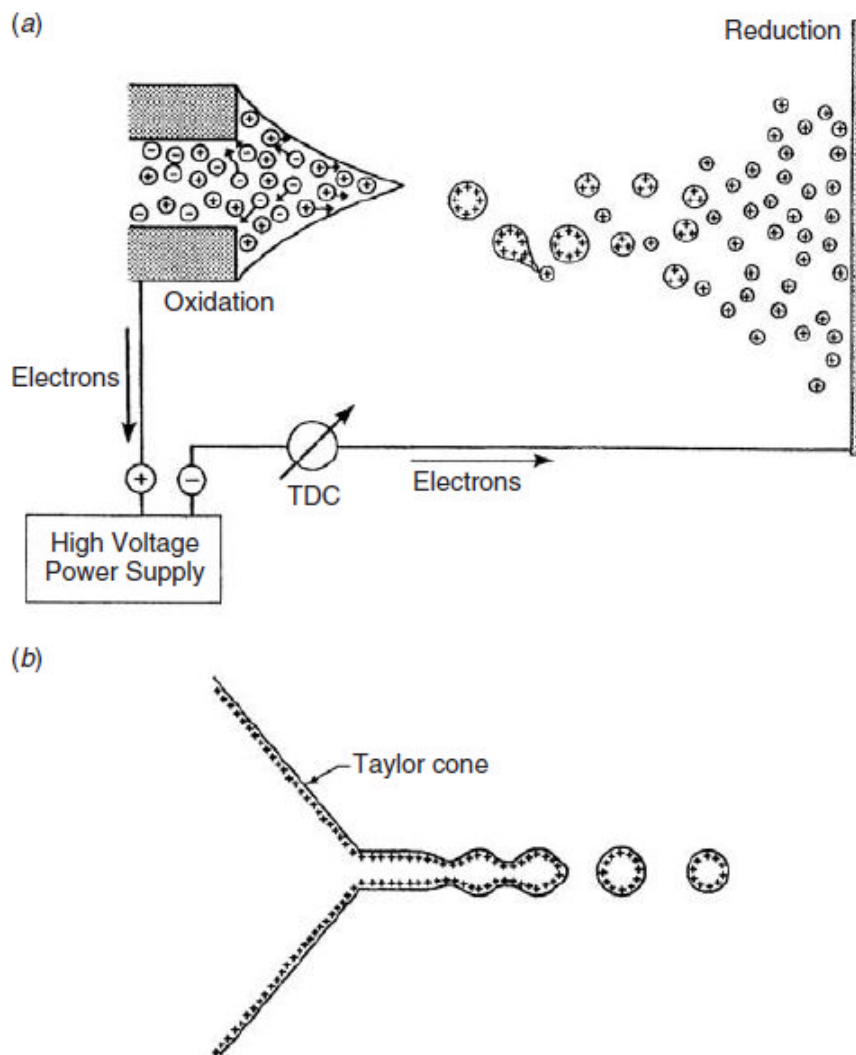
Figure 6: *depiction of electrochemical processes and Taylor cone formation in the ESI.*
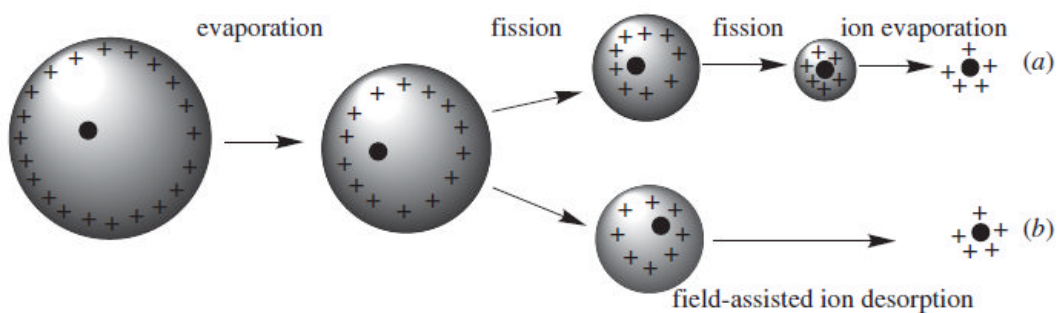
Figure 7: *desorption of ions from charged droplets into the gas phase: (a) Charge residue model; (b) ion-desorption model (From ref. 81.).*

Expulsion of the solvated ions into the gas phase, however, takes place at some intermediate droplet size (10 to 20 nm in radius) when the electric field due to the surface charge density is sufficiently high but less than the Rayleigh instability limit. Currently, it is generally believed that the IDM model applies to ions with significant surface activity (i.e., hydrophobic molecules) and the CRM model applies largely to hydrophilic species. Thus, proteins and metal cations may follow CRM, whereas peptide and fatty acids follow IDM. As a consequence, the ESI response depends on the nature of the analyte. Enke has put forward an equilibrium partitioning model to explain differences in ESI response.[113] This model predicts that surface-active analytes compete favorably with excess droplet surface charge and thus exhibit a higher ESI response. Because of this relationship between the nonpolar character of the analytes and their ESI response[114], a correlation exists between ESI response and the HPLC retention time.[115]

Mass Analyzers and Mass Resolving Power

High resolution is a desirable figure of merit of a mass spectrometer because it helps to (1) perform accurate mass measurements, (2) resolve isotopically labeled species when the percent incorporation of the label is to be determined, (3) resolve an isotopic cluster when the charge state of high-mass compounds is to be determined, (4) enhance the accuracy of quantification, and (5) unambiguously mass-select precursor ions in MS/MS experiments. By definition, the *mass resolution* of a mass spectrometer is its ability to distinguish between two neighboring ions that differ only slightly in their mass (Δm). Mathematically, it is the inverse of resolving power (RP), given as

$$\text{RP} = \frac{m}{\Delta m} \qquad\qquad \textbf{Eq. 1}$$

where *m* is the average of, and Δm is the difference in, the accurate masses of two neighboring ions. A larger RP means that a smaller mass differences can be resolved. According to the 10% valley definition (depicted in Figure 8), the two equal-height peaks are considered resolved when the valley between the two ions is 10% of the height of either one (i.e., each contributes 5% to the valley). The value of RP can also be expressed in terms of the width of a single symmetrical well-resolved peak. Here *m* is the *m/q* value at the apex of the peak and Δm is the width of the peak at a specified height. The peak-width definition is depicted pictorially on the right-hand side of Figure 8. Use of the 10% valley definition is a common practice with magnetic-sector and quadrupole instruments. In TOF, QIT, and FT-ICR mass analyzers, the peaks separated by 50% valley are considered as resolved. In such cases, resolution is reported in terms of full width at half maximum (FWHM; see Figure 8). The RP value in FWMM definition is larger by a factor of 2 than the 10% valley definition.
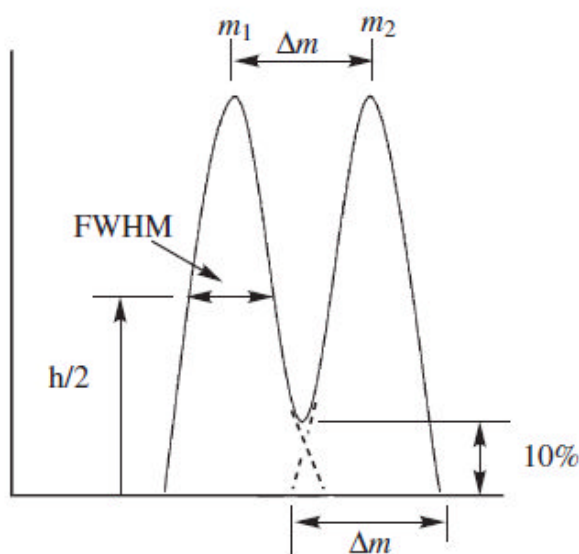
Figure 8: *resolving power: 10% valley definition (depicted by separation of two ions of mass m_1 and m_2) and FWHM definition (h/2 is half the height of the peak).*

The Quadrupole

Quadrupole instruments are probably the most widely used type of mass spectrometer. A *quadrupole* consists of four precisely matched parallel metal rods (Figure 9). The mass separation is accomplished by the stable vibratory motion of ions in a high-frequency oscillating electric field that is created by applying direct-current (dc) and radio-frequency (rf) potentials to these electrodes.[116-118] Under a set of defined dc and rf potentials, ions of a specific *m/q* value pass through the geometry of quadrupole rods. A mass spectrum is obtained by changing both the dc and rf potentials while keeping their ratio constant. Four metallic rods (electrodes) are arranged symmetrically in a square array (Figure 9).
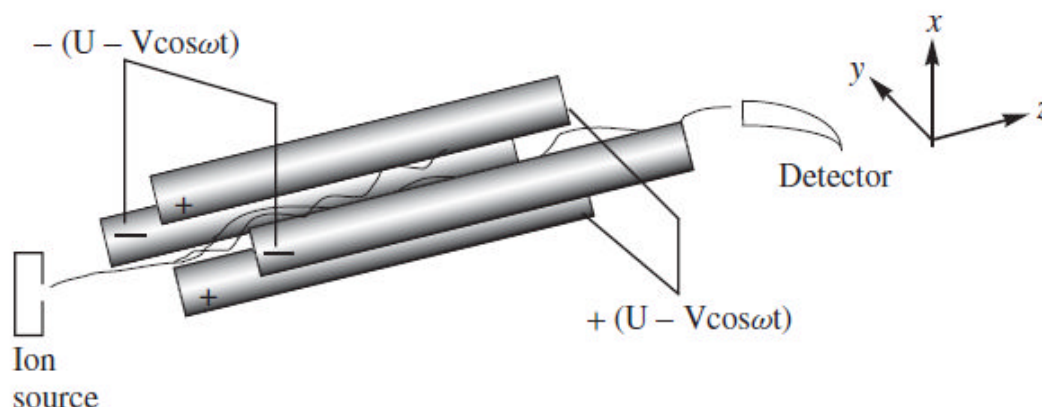
Figure 9: *quadrupole mass analyzer. At a certain values of dc potential U and rf potential V , ions of a specific range of m/q value have stable trajectories in the x- and y-directions and travel in the z-direction*

within the quadrupole field to reach the detector; all other ions are lost because they follow unstable trajectories.

Ideally, the rods should be of hyperbolic geometry, but for convenience, precisely machined circular rods are acceptable. The field within the square array is created by connecting opposite pairs of electrodes electrically. One pair receives a superimposed positive dc potential U and a time-dependent rf potential V cos ωt, where ω is the angular frequency (in rad s^{-1}) of the applied rf voltage, V its amplitude, and t the time. The angular frequency is related to the radio-frequency f (in hertz) by $\omega = 2\pi f$. The other adjacent pair of rods receives a dc potential $-U$ and an rf potential of the same magnitude, V cos ωt, but out of phase by 180° [i.e., $-(U - V \cos\omega t)$]. Application of these voltages creates an oscillating field within the rods that is given by

$$\Phi_{(x,y)} = \Phi_0 \frac{x^2 - y^2}{r_0^2} = (U - V \cos \omega t)\frac{x^2 - y^2}{r_0^2} \qquad \textbf{Eq. 2}$$

where Φ_0 is the applied potential (i.e., $U - V \cos \omega t$), r_0 the inscribed radius (i.e., one-half the distance between the opposite electrodes), and x and y the distances from the center of the field. Ions are injected at one end of the quadrupole structure in the direction of the quadrupole rods (the z-direction). Separation of ions of different m/q value is accomplished through the criterion of path stability within the quadrupole field. At a given set of operating parameters, ions of a narrow but adjustable m/q range have stable trajectories (i.e., their motion is confined within the field-defining electrodes), whereas the remainder of the ions will have unstable trajectories (i.e., the amplitude of their motion exceeds the boundaries of the electrodes). Thus, the mass separation action of a quadrupole is similar to that of a narrow bandpass filter rather than a conventional mass spectrometer (i.e., ions of a narrow mass window can survive within the quadrupole geometry). To obtain a mass spectrum, the quadrupole field is varied to force other mass window ions to sweep through the quadrupole. The mass-filtering action of a quadrupole can be explained as follows[118]: consider first the action of a positive pair of electrodes (i.e., those acting in the xz-plane). As shown in Figure 10a, the positive dc potential applied to these rods will accelerate positive ions toward the central axis (point a). The simultaneous action of the rapidly changing rf potential during its negative half-cycle will accelerate these ions toward the rods (point b); the low-m/q ions will be accelerated to the highest velocities on each half cycle and will ultimately be eliminated from the field-defining space. In contrast, the higher-m/q ions will respond sluggishly to this rf potential and will remain confined within the boundaries of the rods. Thus, a positive pair of rods acts as a high-pass filter for positive ions. Now consider the action of the negative pair of electrodes the ($y - z$-plane). Because of the continuous action of the negative dc potential, all positive ions will be attracted toward the rods (point a in Figure 10b).
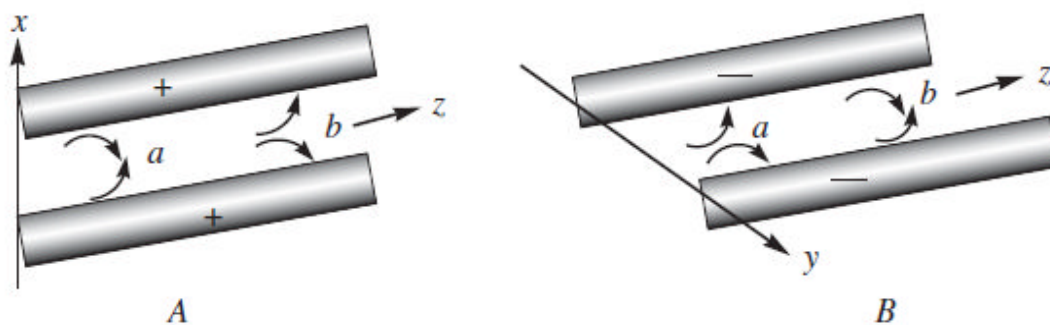
Figure 10: operation *of a quadrupole in (A) the xz-plane and (B) the yz-plane. In the xz-plane, the positive rods act as a high-pass filter for positive ions. The ions converge toward the z-axis (at point a) due to the action of the positive dc potential and are defocused due to the action of the negative half-cycle of the rf potential. Similar actions make the negative pair of rods low-pass filter in the yz-plane.*

During the short period of the positive half-cycle of the rf potential, only the motion of lower-m/q ions will be reversed toward the center of the rods (point *b*). Because of their inertia, the higher-m/q ions will be lost to the rapidly changing positive rf potential. Thus, the negative pair of electrodes acts as a low-pass filter. The combination of these actions creates a stability window for ions of a narrow m/q range to travel through the rods (in the *z*-direction)

The Time-of-Flight

A *time-of-flight* (TOF) *mass spectrometer*, one of the simplest mass-analyzing devices, is currently in high demand. In combination with matrix-assisted laser desorption/ionization (MALDI), it has emerged as a mainstream technique for the analysis of biomolecules. The basic principle of ion separation by TOF mass spectrometry was conceptualized by Stephens in 1946.[119] This mass analyzer consists of a long (ca. 100 cm in length) field-free flight tube in which ions are separated on the basis of their velocity differences. A short pulse of ions of defined kinetic energy is dispersed in time when it travels a long flight tube (of length L). The velocities, v, of ions are an inverse function of the square root of their (m/q or m/z) values:

$$v = \sqrt{\frac{2qV}{m}} \qquad\qquad \textbf{Eq. 3}$$

Therefore, the lower-m/q ions travel faster and reach the detector earlier than the higher m/q ions. Thus, a short pulse of ions is dispersed into packets of isomass ions (Figure 11).
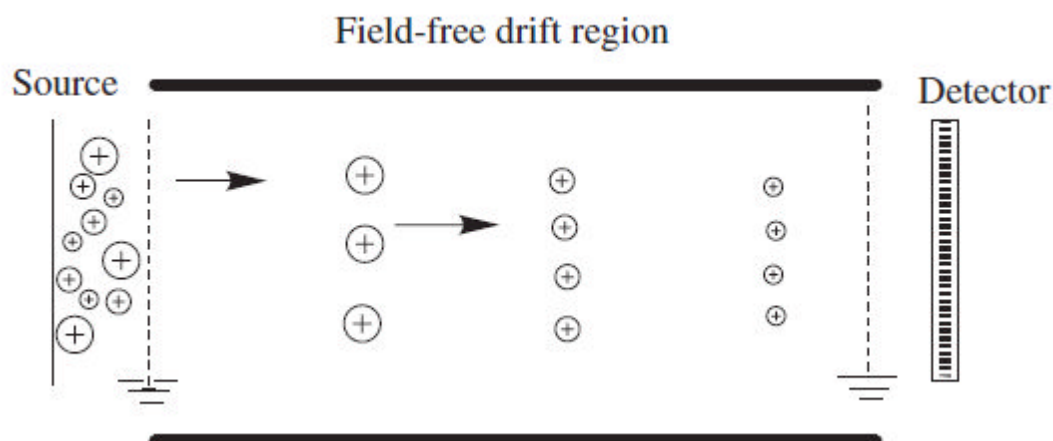
Figure 11: *principle of mass separation by a time-of-flight mass analyzer. Ions are separated on the basis of their m/q; high m/q ions (big circles) travel slower than the lower m/q ions (smaller circles).*

The time of arrival of an ion is given by

$$t = \frac{L}{v} = L\sqrt{\frac{m}{2qV}} \qquad \textbf{Eq. 4}$$

The measured arrival times of all ions provides a time spectrum that is converted into a mass spectrum by calibrating the instrument. A generally accepted calibration equation is

$$\frac{m}{q} = at^2 + b \qquad \textbf{Eq. 5}$$

which is valid with currently popular delayed-extraction TOF. In these instruments, the linear relation between m/q and t^2 no longer exists. In this equation, a is the constant of proportionality between the arrival time of an ion and its m/q, and b is a time offset that arises from the difference in time between the ion extraction and the data acquisition start pulse. These constants are determined with two different ions of known m/q values.

Because a defined start–stop signal is required for the measurement of time, an essential prerequisite in the TOF operation is that all ions enter the flight tube at exactly the same time. This arrangement would also avoid any artifact left behind from the previous ionization event. For this reason, TOF instruments are optimally combined with pulsed-mode ion sources such as 252Cf plasma desorption or MALDI. Alternatively, pulsing the accelerating potential can provide a pulsed ion beam from continuous ion beam sources (e.g., electron ionization, and electrospray ionization). In the past, conventional TOF–MS, popularly known as *linear TOF–MS*, found limited application owing primarily to its poor resolution

(<500) and incompatibility with continuous-beam ion sources. The limitation of poor resolution has been circumvented to some extent by the current developments described next. In TOF–MS, mass resolution is related to the temporal width of the isomass ions packet when that packet arrives at the detector (i.e., $R = t/\Delta t$). In the ion source, ions are accelerated out of the source region with inherent dispersion in time (instant of ion formation), space (location of ion at the time of acceleration), and velocity (owing to differences in the initial kinetic energy of ions). These are the three primary factors that limit the resolution in a TOF instrument.[120-122] The initial kinetic energy (KE) of ions (i.e., KE before acceleration) is given by KE = 1/2 mv_0^2, where v_0 is the initial velocity, which will be in a random direction; after acceleration, KE = qV + 1/2 mv_0^2. The temporal dispersion creates uncertainty in the ions' arrival time at the detector. The contribution of this factor can be minimized by the use of a very short ionization pulse and/or a fast-rise ion-extraction pulse, and also by increasing the flight path. Multiturn and multipass research TOF mass spectrometers are available to increase the ion flight path without increasing the size of the instrument significantly.[123, 124] The spatial distribution gives rise to differences in kinetic energies and source exit times of ions after their acceleration. Consider two same-mass ions formed at different locations in the ion source. Because the ion formed to the left of the central axis is subjected to a higher potential, it will be accelerated to a higher velocity than the ion formed to the right of the central line, but it will exit the source later. Convergence of spatially dispersed ions is achieved at the *space focus plane*, where the faster later ions catch up with the slower earlier ones. The spatial distribution of MALDI-formed ions is inherently low because the plane of ion formation is well defined. The initial kinetic energy spread 1/2 mv_0^2 is the dominating factor that restricts resolution in TOF instruments. The spatial distribution and initial kinetic-energy spread of ions are minimized by incorporating delayed-extraction and reflectron devices. With gas-phase ionization techniques, the initial kinetic energy variations in both magnitude and direction gives rise to a resolution factor called the *turnaround time*, the extra time that an ion traveling initially away from the exit slit must take to exit the ion source. Because this ion must reverse its direction before it begins its journey toward the detector, it lags behind other ions of identical initial velocity that were moving toward the exit slit. Longer flight tubes and longer flight times can reduce the effect of the turnaround time. The difference in the arrival times of ions that differ in mass by 1 u (say, 2000 and 2001 u) is very short (in nanosections). Therefore, the mass resolution of TOF instruments is also limited by the time-resolving power of the ion detection system. *Delayed extraction* (DE), the principle of which was first enumerated by Wiley and McLaren in 1956 in the form of *time-lag focusing*[125], is one way to improve the resolution of linear TOF mass spectrometers.[126-128] This procedure uses a dual-stage ion-extraction optics with two distinct extraction and acceleration regions (Figure 12). During the ionization pulse, no potential is applied to the extraction region. Therefore, ions drift in this region in a field-free environment with their initial velocities $v0$. After a short delay of a few hundred nanoseconds, the acceleration potential is applied to extract the ions from the source. During this delay period, the slow-moving ions lag behind the fast-moving ions.
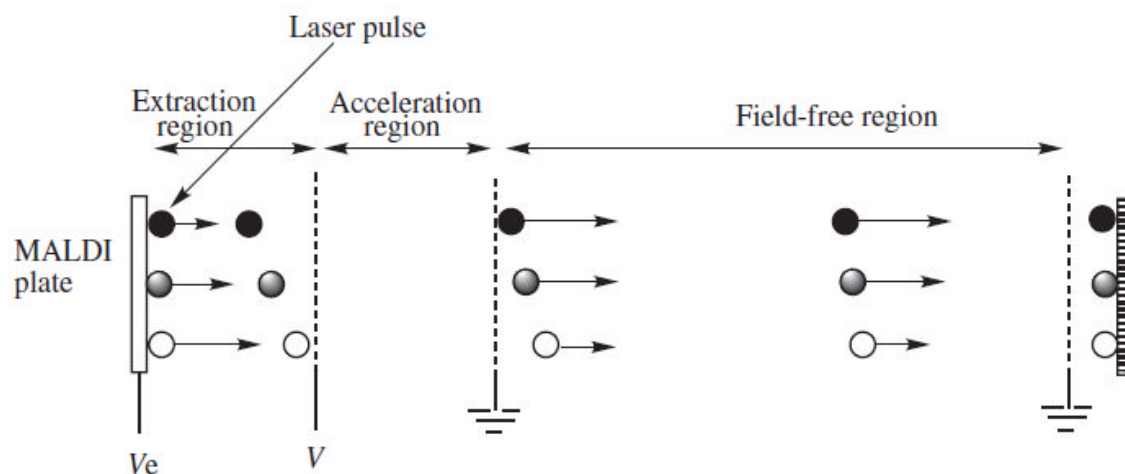
Figure 12: *principle of time-lag focusing. Ions with initial velocity dispersion drift to a different extent in the field-free environment of the extraction region; the slower-moving ions lag behind the faster-moving ions. After a short delay, when an acceleration pulse is applied, the slower ions are subjected to a higher field than the faster ions and thus are accelerated to a higher velocity than the faster ions. In the FFR region, all isomass ions will get closer to each other, and ultimately will arrive at the detector simultaneously.*

As mentioned above, ions near the repeller electrode (i.e., farther from the extraction grid) will be subjected to a greater electrical potential than will ions closer to the extraction grid. Because of this difference in the accelerating field, the ions that were lagged behind are accelerated to a higher velocity. With a proper setting of the delay time and amplitude of the extraction pulse, all ions of a particular mass but of different initial kinetic energy can be made to reach the detector at the same time. A DE device has also been useful to gain knowledge of the structure-specific fragment ions.[128, 129] That information is missing in a conventional linear TOF mass spectrum because the molecular ions are usually promptly extracted from the ion source before they have a chance to fragment. During the delayed-extraction period, the energetic ions are given the opportunity to fragment and subsequently are mass-analyzed.

The Reflectron TOF

A *reflectron* is an energy-correcting device that can minimize the effects of initial spatial and energy spreads.[130] This electrostatic mirror consists of grids and a series of ring electrodes, each with a progressively increasing repelling potential (Figure 13). The mirror is placed at the end of the flight tube [i.e., the first field-free region (FFR) of length $L1$] and works on the principle that after entering this device, ions are slowed down by the repelling electric field until they come to rest; subsequently, their direction of motion is reversed, and they are reaccelerated into a second FFR of length $L2$.
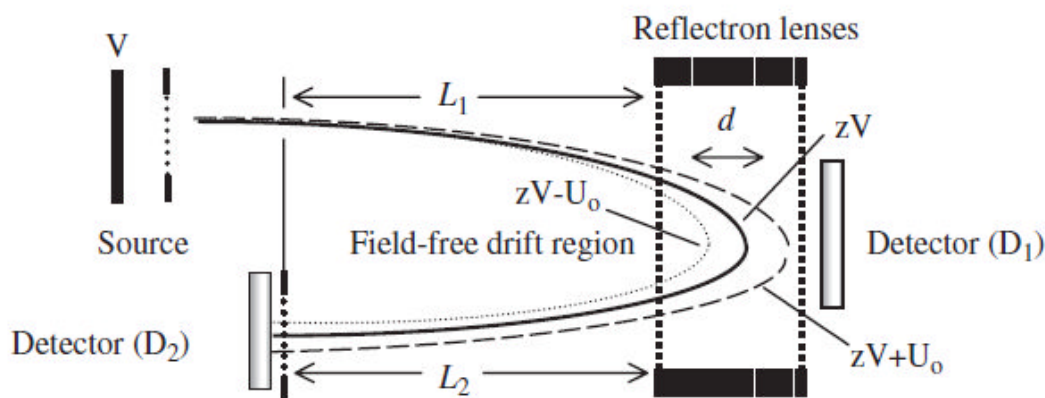
Figure 13: *reflectron time-of-flight mass analyzer. All ions of the same mass, but that differ in kinetic energy, are made to arrive at the same time at a detector (D_2) that is located at the end of the second field-free region (L_2).*

In principle, an ion with excess energy $qV + U_0$ (where $U_0 = 1/2 \ (mv_0^2)$ will arrive earlier at the reflectron but will spend more time in the reflecting field as it penetrates to a greater depth (*d*) than does an ion with average energy qV. Thus, with a proper setting of ring voltages, the shorter flight time of the faster ion in the drift regions is compensated by this extra time in the mirror. As a consequence, all ions of the same m/q value arrive simultaneously at the detector placed at the end of the second FFR; the result is an improvement in mass resolution. The additional flight path due to the second FFR also contributes to improved resolution. The mirror also recreates the space focus plane at a useful distance from the source. It allows use of a high extraction field, which reduces the turn around time. Linear-field reflectrons with a single or dual stage and nonlinear-field reflectrons have been described in the literature.[130-132] A single-stage reflectron consists of an entrance grid electrode and a series of ring electrodes and uses a single retarding or reflecting field to provide first-order correction of the kineticenergy distribution. The dual-stage device contains two linear retarding-voltage regions that are separated by an additional grid. The *orthogonal acceleration* (oa) feature of a TOF mass analyzer enables it to be used with continuous-beam ion sources.[133-136] The ion beam from the external source enters an ion acceleration region from a direction perpendicular to the main axis of the TOF instrument (see Figure 14). A short pulse of an orthogonal accelerating field is applied to eject the ions efficiently in a section of the beam out of the ion-sampling region. This approach provides high efficiency (a high duty cycle) to gate ions from an external source. It also reduces the spatial and energy spreads of source-formed ions because of minimization of the turnaround effect.[137] Coupling an external continuous-beam ion source with the ion-sampling region of an oa–TOF mass spectrometer is achieved via tube lenses, rf-only multipoles, a QIT, or a linear ion trap. In each case, the intent is to minimize an ion beam's divergence and to increase ion-transport efficiency.
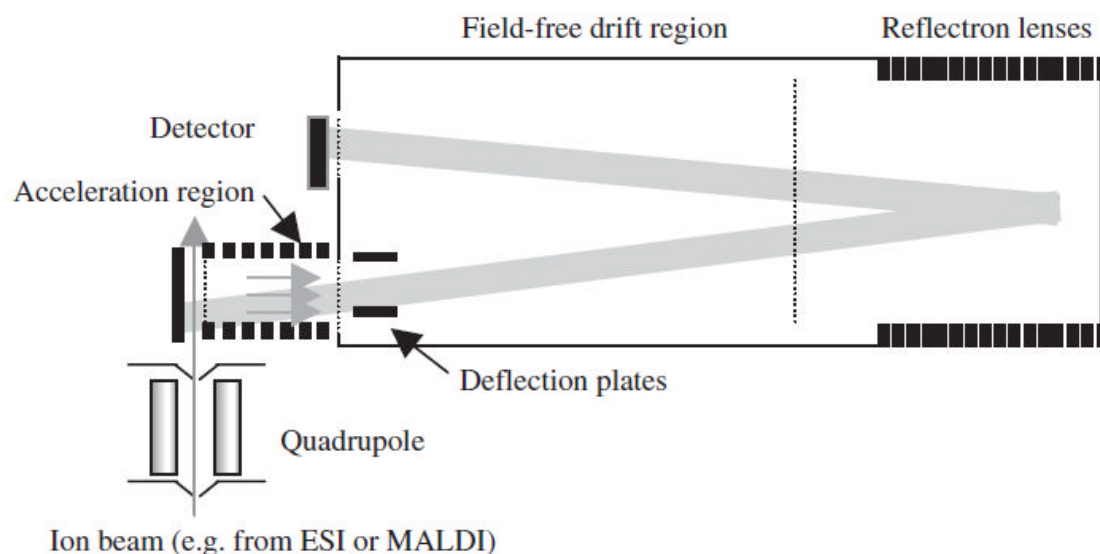
Figure 14: *principle of an orthogonal time-of-flight mass analyzer. A beam of ions from a continuous ionization source, such as ESI, are transmitted between the orthogonal ion extraction plate and grid. A segment of the beam is then pushed into the field-free region by a pulse in the orthogonal direction.*

Ion Mobility Mass Spectrometer

Ion mobility (IM) *mass spectrometers* are hybrid instruments that combine an IM separation system with conventional MS systems. An *ion mobility spectrometer* (IMS) can also serve as a stand-alone ion detection system.[138] An IMS uses gas-phase mobility rather than the m/q ratio as a criterion to separate ions.[139-140] The mobility of ions is measured under the influence of an electrical field gradient and cross flow of a buffer gas, and depends on ion's collision cross section and net charge. A typical IMS is shown in Figure 15. It consists of a reaction region and a much longer drift region; both regions contain a series of uniformly spaced electrodes that are connected via a series of high resistors to provide a uniform electric field strength. The two regions are separated by an electrical shutter. Buffer gas is also circulated in the drift tube. The ions are generated in the reaction chamber and are allowed to enter the drift region by opening the electrical shutter for a brief period. Under the influence of an electrical field, ions drift into the drift tube, where they are separated according to their size-to-charge ratio. The mobility of ions is a combined effect of ion acceleration by the electric field and retardation by collisions with the buffer gas.

At the end of the drift region is placed an ion detector (e.g., a Faraday cup) for the detection of the separated ions. This type of instrument has been highly successful for national security in the detection of explosives in commercial aviation, mass transportation, and urban centers.[138] For more accurate mass analysis, an IMS is coupled to a quadrupole or TOF mass analyzer.[141-145]
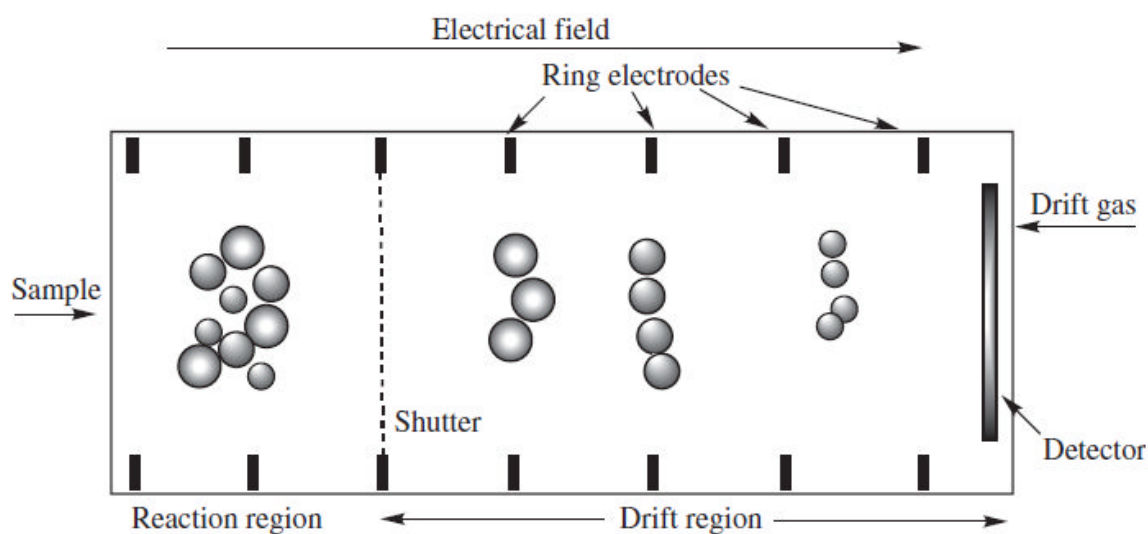
Figure 15: *depiction of the principle of ion mobility spectrometry.*

Similar to LC–MS systems, the IMS serves as a separation device and the quadrupole or TOF mass analyzer as a detection device, but has the added advantage that separation times are in milliseconds. ESI and MALDI ion sources have both been coupled to IM–MS instruments.[141-144] Such systems can be employed for the analysis of mixtures of proteins and tryptic peptides.[141-143] An instrument that depicts the coupling of IM with TOF mass spectrometry is shown in Figure 16. It consists of a MALDI source, an ion mobility cell, a CID cell, and an oa–TOF mass analyzer. Ions exit the drift tube when the axial field strength of the ion mobility cell is ramped up, and enter the source region of an oa–TOF instrument, where the ions are detected intact in the usual manner. Alternatively, ions can be fragmented in the CID prior to their detection by the TOF–MS. The resolution of an IMS, usually very low (10 to 12) can be increased to 200 to 400 by increasing the pressure of the buffer gas, connecting the ion source directly with the drift tube, increasing the length of the drift tube, and increasing the electric field gradient of the drift tube. Unlike LC/MS separation, an ion chromatogram can be obtained within 1 s. Other applications of IM–MS include the detection of drugs, chemical warfare agents, and environmental pollutants; size distribution of aerosol particles; structure information of gas-phase clusters; and conformational studies of proteins and oligonucleotides.[145] A variation of IMS is field-ion spectrometry (FIS), which functions as an ion filter to allow one type of ion to be transmitted continuously.[146] In FIS the electric field is applied as a high-frequency asymmetric waveform rather than as a dc voltage. Ions travel in the axial direction of the drift tube in a flowing stream of a buffer gas, and the electric field is applied perpendicular to the direction of the gas flow.
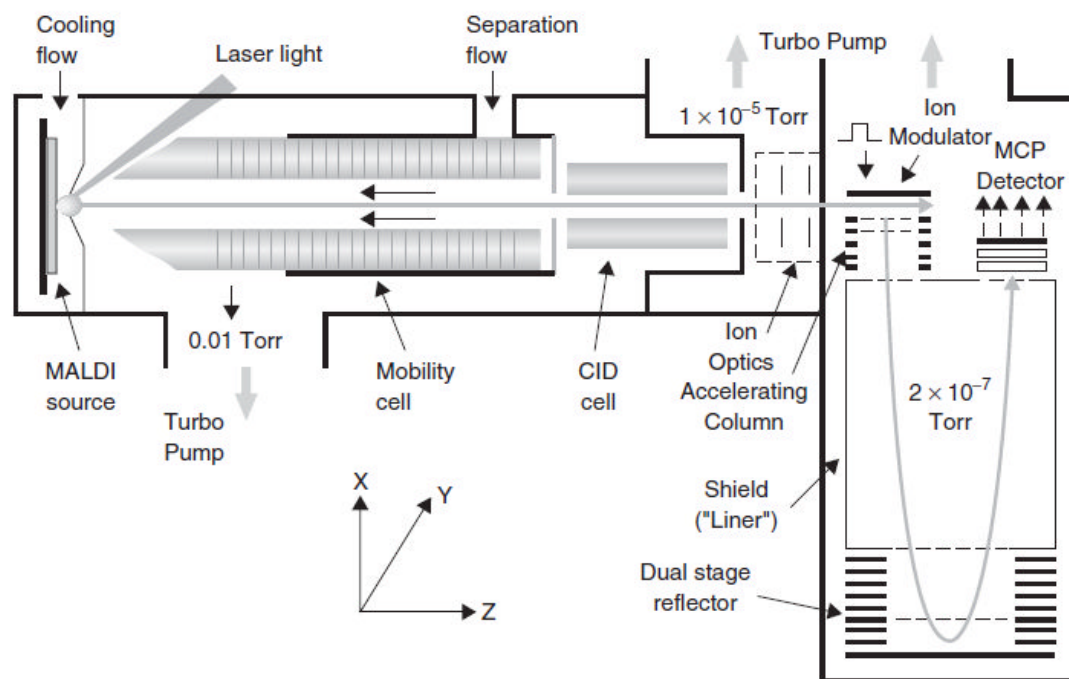
Figure 16: *schematic of the ion mobility/oa–TOF instrument.*

Tandem Mass Spectrometry

The concept of *in-space tandem mass spectrometry* is illustrated in Figure 17. It involves two mass spectrometry systems; the first system (MS-1) performs the mass selection of a desired target ion from a stream of ions produced in the ion source. This mass-selected ion undergoes either unimolecular fragmentation (equation 6) or a chemical reaction in the intermediate region.
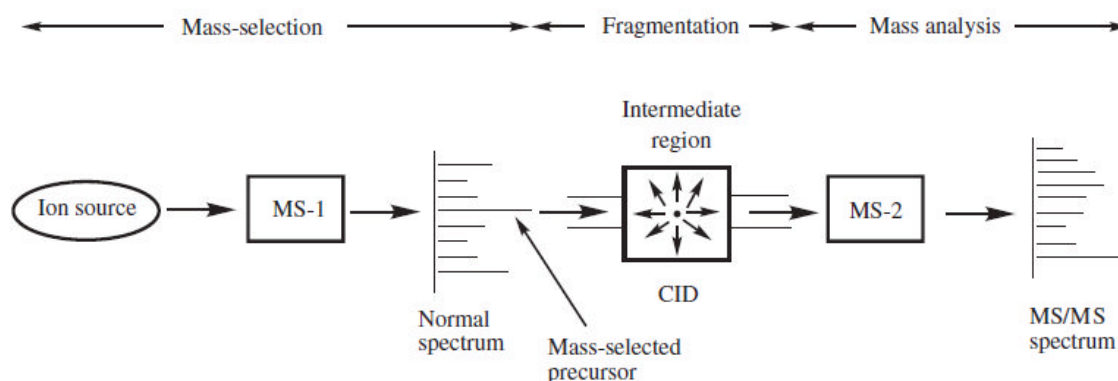
Figure 17: *basic principle of tandem mass spectrometry.*

The second MS system (MS-2) performs the mass analysis of the product ions that are formed in the intermediate step.

$$m_p{}^+ \longrightarrow m_1{}^+ + m_n'$$
$$\longrightarrow m_2{}^+ + m_n''$$
$$\longrightarrow m_3{}^+ + m_n'''$$

Eq. 6
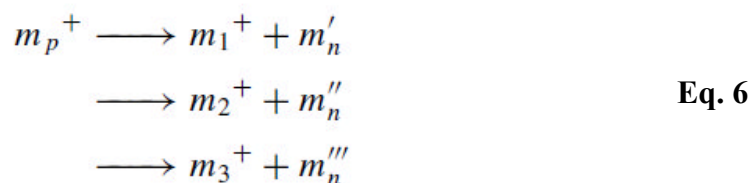
The MS/MS operation can be likened to the sorting of cards in a playing card deck. First, cards can be sorted according to their rank (e.g., aces from rest of the cards). After all four aces have been sorted, it is important to know their identity: that is, the suit. The MS-1 operation is similar to the sorting of cards according to their rank (e.g., aces here), whereas the MS-2 function is identification of the suit of each ace. The operation of tandem MS is also similar to the function of the gas chromatography (GC)-MS system. The first stage of MS/MS separates a mixture of ions into individual components as GC resolves a mixture of compounds, and the second stage acts as an identification system for the mass-resolved ions. By convention, the mass-selected ion is called the *precursor ion* ($m_p{}^+$) and its fragments are called *product ions* (e.g., $m_1{}^+, m_2{}^+, m_3{}^+$, etc. in Equation 6). The *mn* species in Equation 6 are neutral losses. Because of the incontrovertible link between the precursor ion and all of its product ions, the molecular specificity of MS/MS approaches unambiguity. This unique attribute of tandem mass spectrometry is a highly useful feature that plays a role in the unequivocal identification of a target compound in real-world samples. Tandem mass spectrometry is not restricted to two stages of mass analysis (i.e., MS/MS or MS^2); it is also possible to perform *multistage MS* (i.e., higherorder MS) experiments, abbreviated as MS^n. These experiments can determine the genealogical relation between a precursor and its ionic products. For example, MS^3 indicates three stages of tandem mass spectrometry, which involves mass selection of one of the products, say either $m_1{}^+, m_2{}^+$, or $m_3{}^+$, formed from the precursor $m_p{}^+$ of the first-stage MS (Equation 6), and determination of the second-generation products of that mass-selected ion. Multistage MS experiments are performed mostly with ion-trapping instruments. A maximum of 12 MS/MS experiments has been envisioned with a quadrupole ion trap. Beam-type instruments can also be used for MS^n experiments but require as many discrete mass analyzers as there are number of stages in the experiment, making it difficult to perform more than four stages of MS/MS experiments. As an example, a three-sector magnetic field instrument can perform up to MS^3 experiments. Practical applications of tandem mass spectrometry require data to be acquired in the following four scan modes. A pictorial representation of these scans and their symbolism is given in Figure 18.
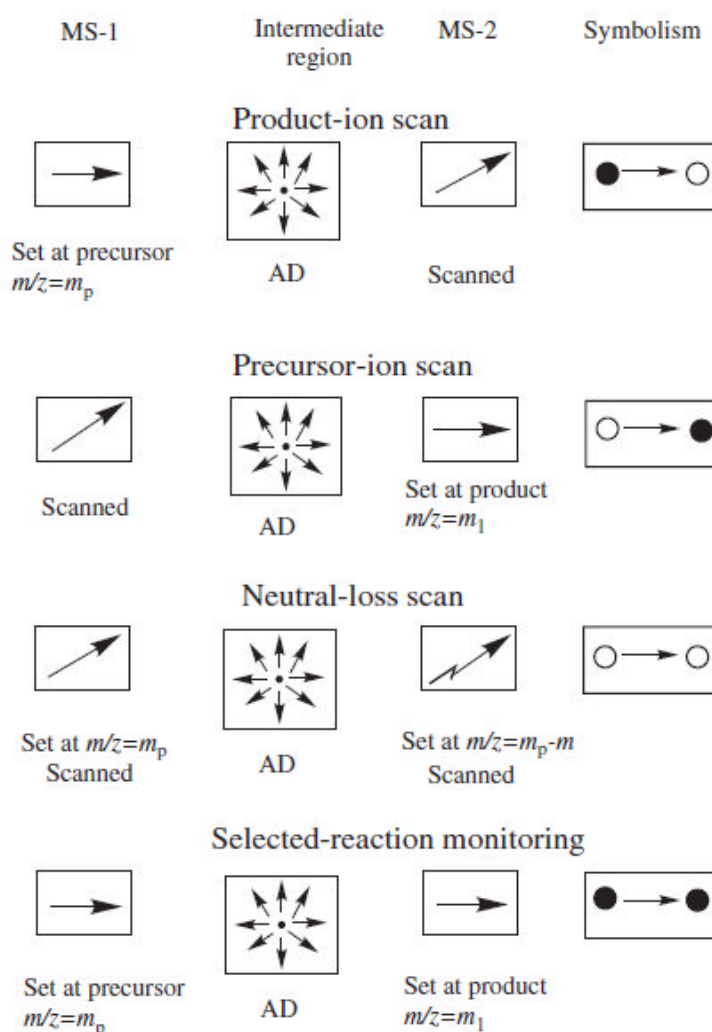
Figure 18: *pictorial representation of four scan modes of tandem mass spectrometry. AD refers to ion activation and dissociation, and the filled and open circles stand for fixed and scanning mass analyzers, respectively.*

The *product-ion scan* (the old, now-unaccepted term, still used by some, is *daughter-ion scan*) is the most common mode of MS/MS operation. That spectrum is useful in the structure elucidation of a specified analyte. Information obtained in this scan is similar to that derived from a normal mass spectrum, except that the spectrum contains only those product ions that are formed exclusively from a mass-selected precursor ion. To acquire this spectrum, the first mass analyzer is set to transmit only the precursor ion chosen, and the second mass spectrometer is scanned over a required *m/z* range. Another popular MS/MS scan is the *precursor-ion scan* (the past, now-unaccepted term is *parent-ion scan*). It provides a spectrum of all precursor ions that might fragment to a common, diagnostic product ion. The spectrum is obtained by adjusting the second mass spectrometer to transmit a chosen product ion (e.g., *m*1) and scanning the first mass analyzer over a certain *m/z* range to transmit only those precursor ions that fragment to yield the chosen product ion. This scan is useful for the identification of a closely related class of compounds in a

mixture. A typical example is the detection of phosphopeptides from biological samples. A major product of fragmentation of phosphopeptides is the PO− 3 ion at *m/z* 79. The precursor-ion scan of this *m/z* value will detect the presence of phosphopeptides selectively in a mixture of peptides from biological samples (see Figure 19).
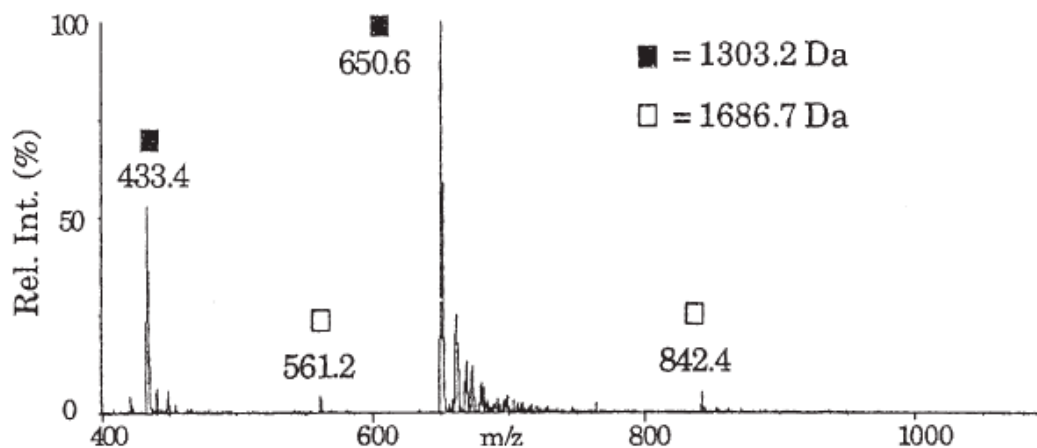
Figure 19: *precursor-ion scan of m/z 79 for selective detection of phosphopeptides. Two tyrosine phosphorylated peptides (1303.2 and 1686.7 Da) are detected in an LC fraction.*

In a *constant-neutral-loss scan*, all precursors that undergo the loss of a specified common neutral are monitored. To obtain this information, both mass analyzers are scanned simultaneously, but with a mass offset that correlates with the mass of the specified neutral. Similar to the precursorion scan, this technique is also useful in the selective identification of closely related class of compounds in a mixture. For example, the loss of 44 Da is a common reaction of carboxylic acids. Through the constantneutral loss scan, the identity of all carboxylic acids present in a complex mixture can be revealed. Similarly, by monitoring the 98-Da neutral loss, the presence of phosphopeptides can be detected in a complex mixture.[147] The fourth scan, *selected-reaction monitoring* (SRM), is useful in quantitative measurements of analytes present in complex mixtures. Conceptually, this scan mode is similar to the product-ionscan. However, instead of scanning the second mass spectrometer in abroad mass range, the two mass analyzers are adjusted to monitor one or more chosen precursor–product pairs of the analyte. This operation is identical to the selected-ion monitoring mode (SIM) of data acquisition. Monitoring more than one reaction is termed *multiple-reaction monitoring* (MRM). All four scan modes can be implemented with magnetic sector- and quadrupole-based true or hybrid tandem instruments. Time-of-flight (TOF) and tandem-in time devices are also suitable for product scan experiments, but they are unable to perform the other three scans.

Tandem Mass Spectrometry with TOF Instruments

Post-source Decay

One of the attempts in this direction is the development of a technique known as *post source decay* (PSD).[148] A substantial portion of ion source–formed ions undergoes metastable dissociation in the flight tube FFR. Normally, these fragments escape detection in a linear TOF mass analyzer because the charged fragment and the corresponding neutral formed in a metastable decay both retain the velocity of their precursor and thus arrive at the detector along with their precursor. The kinetic energy of the product ions, however, is reduced in proportion to the change in their mass. The energy-resolving characteristic of a reflectron TOF (RTOF) instrument has the ability to distinguish ions on the basis of differences in their kinetic energy. Thus, a reflectron can serve as a tandem MS to detect the flight tube fragmentation reactions. To enhance the FFR metastable fragmentation of MALDI-produced ions, a PSD spectrum is usually acquired using "hot" MALDI matrices, such as α-cyano- 4-hydroxycinnamic acid. Figure 20 shows a conceptual diagram of the PSD method.
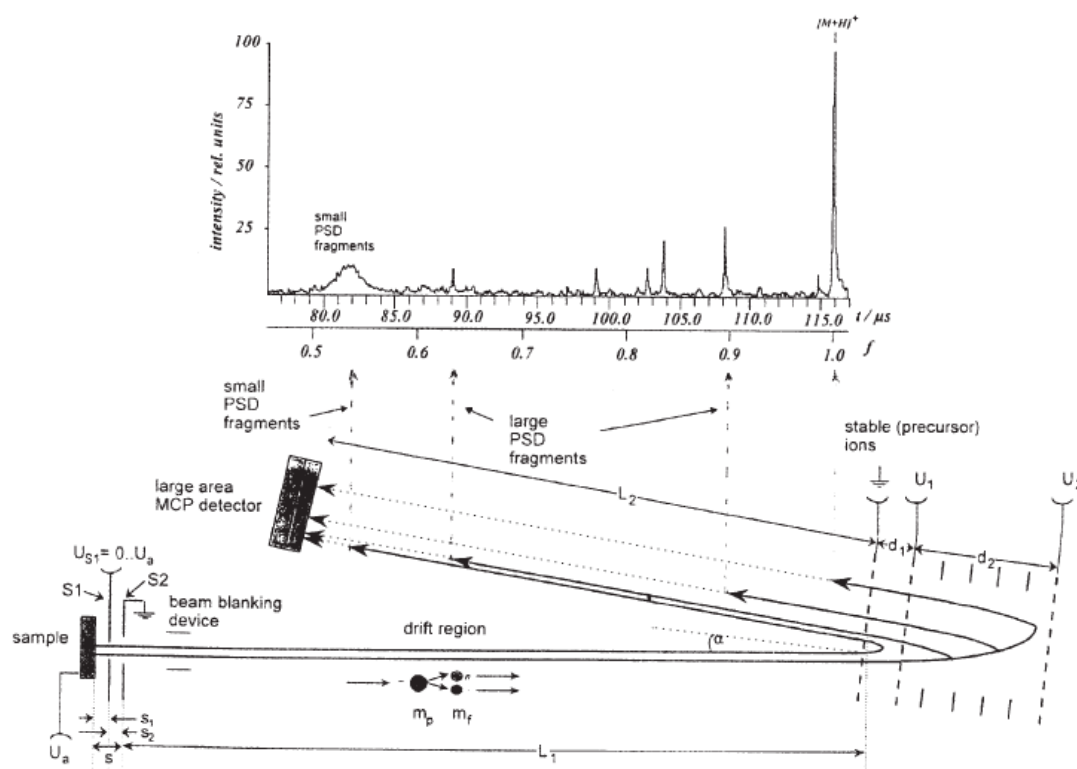
Figure 20: *post-source decay measurements with a reflectron TOF mass spectrometer.*

A fast computer controlled ion gating provides mass selection of the precursor ion. The ion gate is a timed-deflection device that remains active all the time except for a very brief period to allow passage of ions of chosen *m/z* value. Scanning of the spectrum is initiated when the neutral products strike the detector placed behind the reflectron. The charged products of the metastable decay of the precursor ion

are mass-resolved by the reflectron and are detected by a detector located at the end of the second drift region. Because the energy range of PSD products far exceeds the bandwidth of a common reflectron, at a specific reflectron voltage setting (potentials U_1 and U_2 in Figure 20), only a small segment of the product-ion spectrum can be brought to focus at the detector. A complete spectrum, however, can be obtained by piecing together several segments, each acquired by stepping up the reflectron voltage. The quality of the mass spectral data is modest: first, because the mass resolution of the ion gate–selection is poor (ca. 40 to 70 at FWHM), and second, because not all fragmentation channels are accessible, owing to the inherent inefficiency of the metastable fragmentation process. Bleeding air or a collision gas into the flight tube might enhance the fragment ion yield. Two alternative approaches have been suggested as a possible solution to the mismatch between the wide energy range of the product ions and the reflectron bandwidth. First, a wideband reflectron can be employed to acquire a complete mass spectrum with a single set of reflectron potentials. A curved-field reflectron, which has a wide energy-acceptance window, can be employed for this purpose.[149-151] Second, the precursor ions are slowed down to lower kinetic energies by using a lower accelerating potential. An alternative approach to slow precursor ions is to decelerate them to acceptable energies prior to dissociation and to reaccelerate all ions for the mass analysis before their entry into the reflectron.[152] The latter approach is useful specifically for CID-formed products.

Tandem TOF Instruments

A significant step to overcome limitations of the PSD approach is to combine two discrete TOF mass analyzers into a true tandem instrument.[151-153] An ion activation–fragmentation region is added between the two analyzers. All permutations of TOF and RTOF combinations have been tested (e.g., TOF/TOF, TOF/RTOF, and RTOF/RTOF). Primarily, it consists of three sections: a linear TOF for the MS-1 (TOF1) function, a collision region that serves as an ion source for the MS-2 section, and a reflectron that acts as an MS-2. The precursor ions are generated in the TOF1 and focused in the center of a timed-ion selector (TIS) device by setting the appropriate delay between the ion-extraction pulse and the laser-triggering event. The TIS is a double-sided deflection gate, the first gate of which acts as a high-pass filter, and the second gate, as a low-pass filter. With a proper setting of voltages at predetermined times, the double-sided gate prevents all m/z values that are lower and higher than the precursor ion m/z to enter the collision cell. The gate-selected ions are decelerated to 1- to 2-keV energies prior to their entry into the collision cell. After the CID event, ions exit the collision cell and travel through a short FFR region at reduced velocities before they are reaccelerated into the TOF2 region, where the mass dispersion and energy focusing of product ions are achieved. With this arrangement, it is feasible to obtain a complete MS/MS spectrum with a single extraction pulse. This commercial design has recently been modified to incorporate a curved field reflectron as a TOF2. With this modification, there is no need to decelerate the ions prior to CID and to reaccelerate the CID products because the curved field reflectron can accept broad-energy-range ions. As a consequence, CID can be performed at the full 20-keV collision energy to increase the extent of fragmentation. Another tandem TOF/TOF design uses a LIFT cell for post-acceleration to higher energy.[154] This instrument also consists of a linear TOF as an MS-1 and a gridless space-angle reflectron

as an MS-2. In addition, it contains a TIS for gated-ion selection, a LIFT cell to raise the potential energy, a post-lift metastable-suppression device to remove unfragmented precursors. A collision cell is also added between the first ion source and the TIS gate to acquire a true CID spectrum. Raising the potential with a lift device allows the mass analysis of fragment ions in a single spectrum.

Coupling Separation Devices – Hyphenated Separation Techniques

The role of GC, HPLC, and CE in high-resolution separation of complex mixtures is unquestionable. Similarly, mass spectrometry has attained an indisputable position in analytical chemistry as a highly structure-specific technique that can provide structural identity of a wide range of compounds. Chromatography and mass spectrometry both, however, have their limitations in stand-alone operation. First, the separation power of any chromatography system is finite. It will be nearly impossible to achieve complete separation of all components of a complex mixture. Second, identification of a compound in chromatography is less than reliable because of marginal information content. The basis of identification of the target analyte in chromatography is comparison of its retention time with that of a reference material. Therefore, the common separation techniques of GC, LC, and CE cannot provide unequivocal identity of the analyte when used with conventional detection systems. Uncertainty may arise because another component of the mixture may elute at the desired retention time. A compound-specific detector is thus an essential adjunct to characterize unambiguously the components that elute from any separation system. In this respect, mass spectrometry offers the unique advantages of high molecular specificity, detection sensitivity, and dynamic range. Only mass spectrometry has the ability to provide confirmatory evidence of an analyte because of its ability to distinguish closely related compounds on the basis of the molecular mass and structure-specific fragment ion information. The confidence in identification of a target compound, however, diminishes when it is present in a mixture. Because of the universal nature of mass spectrometry detection, the data obtained might also contain signal due to other components of the mixture. The coupling of a separation device with mass spectrometry thus benefits mutually. The result is a powerful two-dimensional analysis approach, where the high-resolution separation and the highly sensitive and structure-specific detection are both realized simultaneously. Following are some of the benefits that accrue when a separation technique and mass spectrometry are coupled.

- The capabilities of the techniques are enhanced synergistically. As a consequence, both instruments may be operated at subpar performance levels without compromising the data outcome.
- The high selectivity of mass spectrometry detection allows one to identify coeluting components.
- The certainty of identification is enhanced further because, in addition to the structure-specific mass spectral data, the chromatographic retention time is also known.
- Multicomponent samples can be analyzed directly without prior laborious off-line separation steps, resulting in a minimal sample loss and saving of time.

- The sensitivity of analysis is improved because the sample enters the mass spectrometer in the form of a narrow focused band.

- Less sample is required than the amount required for off-line analysis by the two techniques separately.

- Because of the removal of interferences, the quality of mass spectral data is improved and any mutual signal suppression is minimized.

- The confidence in quantitative analysis is increased because mass spectrometry permits the use of a stable isotope analog of the analyte as an internal standard.

Chromatography Fundamentals

The primary function of chromatography is separation of a mixture of compounds into individual components. It is a dynamic separation system that is composed of two media, a stationary phase and a mobile phase. The stationary phase in most applications is a liquid supported on the surface of an inert solid support and is usually packed in a column. The mobile phase can be a gas, a liquid, or a supercritical fluid. Its purpose is to transport the sample through the column, a process known as *elution*. The components in a separation mixture distribute between these two phases to a different extent. A component that interacts strongly with the stationary phase moves slowly, and as a result it is separated from the fast-moving components, which have less affinity for the stationary phase. The emerging components are detected by a detector placed at the end of the column. A chromatographic peak should be narrow and Gaussian in nature. In practice, the peaks are often broad and non-Gaussian; the more time the solute spends in a column, the broader the peak. The performance of a chromatographic system is described in terms of a number of parameters, including capacity factor, selectivity factor, plate height, plate number, and resolution. The *capacity factor*, k', describes the migration rate of the solutes, and is defined as the ratio of the time a solute spends in the stationary phase versus the time it spends in the mobile phase. In practice, it can be measured from a given chromatogram (Figure 21) using the relation

$$k' = \frac{t_r - t_m}{t_m} \qquad \textbf{Eq. 7}$$

where t_r is the retention time of the solute and t_m is the dead time, the time taken by an unretained component to elute from the column. Ideal separation is obtained when k' lies between 1 and 5. The *selectivity factor*, α, defines the extent of separation between two components A and B, and is given by the ratio of their capacity factors
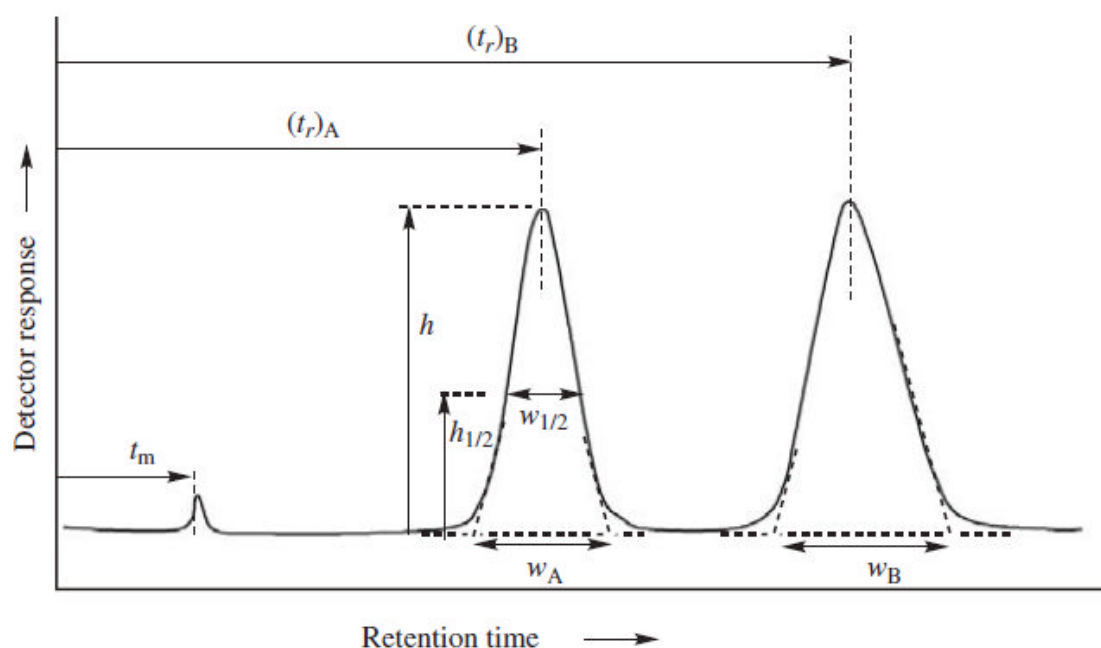
Figure 21: *typical chromatogram of a two-component (A and B) sample. The first little peak is of an unretained component.*

. Experimentally, it is determined by Eq. (8), where B refers to a late-eluting component (i.e., $t_B > t_A$ and $\alpha > 1$):

$$\alpha = \frac{k'_B}{k'_A} = \frac{(t_r)_B - t_m}{(t_r)_A - t_m}$$

Eq. 8

The quantitative measures of column efficiency are the plate height and plate number. *The plate height, H, is defined as the length of column that participates in one mass transfer equilibrium between the stationary phase and the mobile phase. The plate number, N, is the measure of the total number of plates in a column.* The two terms are related to each other through the column length, L, by the expression $N = L/H$. The value of N can be measured from the chromatogram using the equation

$$N = 16 \left(\frac{t_r}{w} \right)^2 = 5.54 \left(\frac{t_r}{w_{1/2}} \right)^2$$

Eq. 9

where w is the peak width at the base and $w_{1/2}$ at half-peak height (see Figure 21). The separation of two components A and B is expressed in terms of the resolution, R, given by

$$R = \frac{2[(t_r)_B - (t_r)_A]}{w_A + w_B}$$

$$R = \frac{\sqrt{N}}{4} \frac{\alpha - 1}{\alpha} \frac{k'_B}{1 + k'_B}$$

Eq. 10

Careful scrutiny of these two equations reveals that separation of the two target components can be optimized by manipulation of the k', α, and N terms. The first two terms are known as *thermodynamic effects*, and the third term is associated with kinetic features of the column. The k' term is optimized by increasing the temperature of the column (as in GC) and by changing the mobile-phase composition (as in LC). The options available to optimize α are a change in the mobile-phase composition, column temperature, and stationary-phase composition. N can be improved by increasing the length of the column and reducing H, which is accomplished by changing the mobile-phase flow rate and reducing the size of the solid support, the thickness of the liquid stationary phase, the viscosity of the mobile-phase solvent, the temperature of the column, and the diameter of the column. The use of capillary columns and columns packed with small particles is a common practice in GC/MS and LC/MS applications.

Coupled LC/MS

The coupling of LC with mass spectrometry is not as straightforward as a similar combination of GC with MS. There are several fundamental differences in the operating environment of HPLC and mass spectrometry. The first mismatch is the solvent flow rate. The separation in conventional wide-bore analytical columns is accomplished at liquid flow rates of 0.5 to 1.5 mL/min. Unlike GC/MS, this liquid produces a gas flow too large for safe operation of the mass spectrometry vacuum system (10^{-5} to 10^{-8} torr). For example, 1.0 mL of water will produce about $1.0 \times 10^5 \, \text{m}^3$ of gas load when introduced in a mass spectrometer at 10^{-5} torr pressure. Liquid flow rates below 10 μL/min can be accepted safely by a mass spectrometry system. Another problem is the incompatibility of common HPLC solvents and nonvolatile additives with mass spectrometry operation. The third problem in the early years of LC/MS efforts was unavailability of ionization methods that could be used for thermally labile and nonvolatile compounds. Over the years, a suite of different LC/MS interfaces has emerged; as of today, some of them are of historical importance only and are discussed here only for pedagogic interest. Advances in the liquid introduction devices have been reviewed.[155-159] With the development of an atmospheric-pressure ionization (API) source, coupling of LC with MS has become a routine matter. The ESI format of API is the most appropriate interface for the LC/MS combination because (1) of its potential for the analysis of a variety of nonvolatile and thermally labile molecules of low to very high molecular mass at unprecedented low detection sensitivity, (2) ionization occurs at atmospheric pressure, (3) of its compatibility with RP–LC solvents, and (4) a range of solvent flow can be accepted. As a consequence, the LC/ESI–MS combination has gained prominence in several areas of research, such as to sequence proteins; to identify

mixtures of compounds, tryptic maps, and post-translational modifications in proteins; to elucidate structure of metabolic products; to analyze drugs, pesticides, and toxins; and to screen combinatorial libraries. The development of LC/ESI–MS has also greatly advanced the science of quantification. Several reviews of LC/ESI–MS technology have appeared in the literature.[160-163] The composition and flow rate of the solvent are two variables that are paramount for optimum operation of the ESI system. The flow rate determines the size as well as the size distribution of the droplets formed during ESI. A conventional ESI source operates at a flow rate of 1 to10 μL/min. At higher flow rates, the spray is not stable because of the formation of larger droplets, which lead to electrical breakdown. Similarly, a fluid with high surface tension, such as pure water, is difficult to electrospray, but many polar solvents commonly used in RP–HPLC (e.g., methanol, ethanol, isopropanol, and acetonitrile) are suitable for the electrospray operation. Nonpolar solvents are difficult to disperse; therefore, normal-phase HPLC is not easy to implement with the ESI process unless a polar solvent is admixed with the nonpolar mobile phase. HPLC is performed with various size columns that range from 0.1 to 4.6 mm in i.d. The optimum mobile-phase flow rate is lower when the size of the column is reduced. For example, a decrease in the column i.d. from 4.6 mm to 320 μm reduces the solvent flow rate from 1 mL/min to 4.9 $\mu Lmin^{-1}$. The sensitivity, efficiency, sample-loading capacity, and sample size are the other important criteria in the selection of a specific-size column. Smaller-diameter columns provide increased efficiency of separation. Although the injection volume and loading capacity of capillary columns are much lower than they are for wide-bore columns, the former offers much higher sample peak concentration at the detector, to provide greater detection sensitivity. As an example, the sensitivity of microbore columns is greater than that of wide-bore columns by a factor of 100. A fourfold increase in sensitivity can be realized when the column diameter is reduced by one-half. Small columns also have the advantage of less solvent consumption and waste disposal. To accommodate a wide range of HPLC flow rates and columns, several designs of the ESI interface have emerged. With a proper ESI interface and flow splitting, a column of any dimension can be combined with mass spectrometry. The duty cycle of most mass analyzers is long compared to the chromatography peak width. This mismatch might pose a problem in obtaining representative data with capillary LC systems. The high scan speed of a TOF mass spectrometer is a highly attractive feature for an LC/MS combination. Also, a TOF instrument has multiplex detection capability. However, the coupling of TOF–MS with LC is not straightforward because of the pulse nature of the TOF operation. Nevertheless, some success has been achieved to couple LC with ESI and MALDI modes of ionization. The most common approach to couple ESI with TOF–MS makes use of the orthogonal ion-extraction concept, in which ESI-produced ions are stored between each duty cycle and are pushed into the flight tube by a high-voltage pulse.

References

1. Tripoli E, La Guardia M, Giammanco S, Di Majo D, Giammanco M, *Food Chemistry*, **2007**, *104*, 466.

2. Ganem B, Li Y, Henion JD, *J. Am. Chem. Soc.*, **1991**, *113* (20), 7818.

3. Bonk T, Humeny A, *The Neuroscientist*, **2001**, *7*, 1, 6.

4. Cooks RG, Ouyang Z, Takats Z, Wiseman JM, *Science*, **2006**, *311*, 5767, 1566.

5. Chace DH, *Clinical Chemistry*, **2003**, *49*, 1227.

6. Careri M, Bianchi F, Corradini C, *Journal of Chromatography A*, **2002**, *970*, 3.

7. Cole RB (Ed.), Electrospray Ionization Mass Spectrometry-Fundamentals, Instrumentation and Applicatios, Wiley, New York, 1997.

8. Niessen WMA, in: Niessen WMA (Ed.), Liquid Chromatography-Mass Spectrometry, 2nd edition, Chromatographic Science Series, Vol. 79, Marcel Dekker, New York, 1999.

9. Karas M, Hillenkamp, *Anal. Chem.*, **1988**, *60*, 2299.

10. Niessen WMA (Ed.), Principles and Instrumentation of Gas Chromatography-Mass Spectrometry, Current Practice of Gas Chromatography-Mass Spectrometry, Chromatographic Science Series, Vol. 86, Marcel Dekker, New York, 2001.

11. Johnson JV, Yost RA, *Anal. Chem.*, **1990**, *62*, 2162.

12. Groseclose MR, Andersson M, Hardesty WM, Caprioli RM, *J. Mass Spectrom.*, **2007**, *42*, 254.

13. Da Costa CT, Horton D, Margolis SA, *J. Chromatogr. A*, **2000**, *881*, 403.

14. Merken HM, Beecher GR, *J. Agric. Food Chem.*, **2000**, *48*, 577.

15. He XG, *J. Chromatogr. A*, **2000**, *880*, 203.

16. Ryan D, Robards K, Lavee S, *J. Chromatogr. A*, **1999**, *832*, 87.

17. Ryan D, Robards K, Prenzler P, Jardine D, Herlt T, Antolovich J, *J. Chromatography A*, **1999**, *855*, 529.

18. Lesage-Meessen L, Navarro D, Maunier S, Sigoillot JC, Lorquin J, Delattre M, Simon JL, Asther M, Labat M, *Food Chem.*, **2001**, *75*, 501.

19. Fulcrand H, Remy S, Souquet JM, Cheynier V, Moutounet M, *J. Agric. Food Chem.*, **1999**, *47*, 1023.

20. Cappiello A, Famiglini G, Mangani F, Careri M, Lombardi P, Mucchino C, *J. Chromatogr. A*, **1999**, *855*, 515.

21. Cappiello A, Bruner F, *Anal. Chem.*, **1993**, *65*, 1281.

22. Stevens JF, Taylor AW, Deinzer ML, *J. Chromatogr. A*, **1999**, *832*, 97.

23. Chandra A, Rana J, Li Y, *J. Agric. Food Chem.*, **2001**, *49*, 3515.

24. Dugo P, Mondello L, Errante G, Zappia G, Dugo G, *J. Agric. Food Chem.*, **2001**, *49*, 3987.

25. Wybraniec S, Platzner I, Geresh S, Gottlieb HE, Haimberg M, Mogilnitzki M, Mizrahi Y, *Phytochemistry*, **2001**, *58*, 1209.

26. Pazmino-Duran EA, Giusti MM, Wrolstad RE, Gloria MBA, *Food Chem.*, **2001**, *75*, 211.

27. Careri M, Elviri L, Mangia A, *Rapid Commun. Mass Spectrom.*, **1999**, *13*, 2399.

28. Fabre N, Rustan I, De Hoffmann E, Quetin-Leclercq J, *J. Am. Soc. Mass Spectrom.*, **2001**, *12*, 707.

29. Baptista JAB, Da P. Tavares JF, CArvalho RCB, *Food Res. Int.*, **2001**, *34*, 345.

30. Dominguez C, Guillen DA, Barroso CG, *J. Chromatogr. A*, **2001**, *918*, 303.

31. Wang Y, Catana F, Yang Y, Roderick R, Van Breemen RB, *J. Agric. Food Chem.*, **2002**, *50*, 431.

32. Wang J, Sporns P, *J. Agric. Food Chem.*, **1999**, *47*, 2009.

33. Wang J, Sporns P, *J. Agric. Food Chem.*, **2000**, *48*, 5887.

34. Wang J, Sporns P, *J. Agric. Food Chem.*, **2000**, *48*, 1657.

35. Perez-Magarino S, Revilla I, Gonzalez-SanJose ML, Beltram S, *J. Chromatography A*, **1999**, *847*, 75.

36. Di Donna L, De Luca G, Mazzotti F, Napoli A, Salerno R, Taverna D, Sindona G, *J. Nat. Prod.*, **2009**, *72* (7), 1352.

37. Martinez-Florez S, Gonzalez-Gallego J, Culebras JM, Tunon MJ, *Nutr. Hosp.*, **2002**, *17*, 6, 271.

38. Gonzalez-Gallego J, Garcia-Mediavilla MV, Sanchez-Campos S, Tunon MJ, *Bri. J. of Nutr.*, **2010**, *104*, S15.

39. Garcia-Lafuente A, Guillamon E, Villares A, Rostagno MA, Martinez JA, *Inflamm. Res.*, **2009**, *58*, 537.

40. Kaul TN, Middleton E, Ogra PL, *J. of Med. Virology*, **1985**, *15*, 1, 71.

41. Cushnie TPT, Lamb AJ, *Int. J. of Antimicrobial Agents*, **2005**, *26*, 343.

42. Nishida S, Satoh H, *Clin. Chim. ACTA*, **2004***, 339*, 129.

43. Pietta PG, *J. Nat. Prod.*, **2000**, *63*, 1035.

44. Harborne, J. B. In *Plant Flavonoids in Biology and Medicine*; Cody, V., Middleton, E., Harborne, J. B., Eds.; Alan R. Liss: New York, **1986**; pp 15-24.

45. Brouillard R, Cheminat A, *Prog. Clin. Biol. Res*. **1988**, *280*, 93.

46. Kuhnau J, *World Rev. Nutr. Diet*. **1976**, *24*, 117.

47. Pietta PG, Mauri PL, Simonetti P, Testolin GF, J. *Anal. Chem*. **1995**, *352*, 788.

48. Herrman KJ, *Food Technol*. **1976**, *11*, 433.

49. Franke A, Custer LJ, Cerna CM, Narala KK, *J. Agric. Food Chem*. **1994**, *42*, 1905.

50. Haslam E, *Plant Polyphenols*; Cambridge University Press: Cambridge, U.K., **1989**.

51. Mazza G, Miniati E, *Anthocyanins in Fruits, Vegetables and Grains*; CRC Press: Boca Raton, FL, **1993**.

52. Pietta PG, Simonetti P In *Antioxidant Food Supplements in Human Health*; Packer L, Hiramatsu M, Yoshikawa T, Eds.; Academic Press: San Diego, **1999**; pp 283.

53. Harborne, JB In *Flavonoids: Advances in Research Since 1986*; Harborne, JB, Ed.; Chapman and Hall: London, **1994**; pp 589.

54. Shirley BW, *Trends Plant Sci*. **1996**, *31*, 377.

55. Yamasaki H, Sakihama Y, Ikehara N, *Plant Physiol*. **1997**, *115*, 1405.

56. Larson RA, *Phytochemistry* **1988**, *27*, 969.

57. Pietta PG In *Flavonoids in Health and Disease*; Rice-Evans CA, Packer L, Eds.; Marcel Dekker: New York, **1998**; pp 61-110.

58. Ingram D, Sanders K, Kolybaba M, Lopez M, *Lancet* **1997**, *983*, 990.

59. Block G, Patterson B, Subar A, *Nutr. Cancer* **1992**, *17*, 1.

60. Frei BC, *Crit. Rev. Food Sci.* **1995**, *35*, 83.

61. Gei KF, *J. Nutr. Biochem.* **1995**, *6*, 206.

62. Gillman MW, Cupples LA, Gagnon D, Posner BM, Ellison C, Castelli WP, Wolf P, *J. Am. Med. Assoc.* **1995**, *273*, 1113.

63. Ness AR, Powles JW, *Int. J. Epidemiol.* **1997**, *6*, 1.

64. Peterson J, Dwyer J, *Nutr. Res.* **1998**, *12*, 1995.

65. Gorinstein S, Barnitkowska E, Kulasek G, Zemser M, Trachtenberg S, *J. Nutr.* **1998**, *128*, 2023.

66. Wang W, Goodman MT, *Nutr. Res.* **1999**, *19*, 191.

67. Hertog MG, L. *Proc. Nutr. Soc.* **1996**, *55*, 385.

68. Knekt P, Jarvinen R, Seppanen R, Heliovaara M, Teppo L, Pukkala, Aromaa A, *Am. J. Epidemiol.* **1997**, *146*, 223.

69. Hertog MGL, Katan MB In *Flavonoids in Health and Disease*; Rice-Evans CA, Packer L, Eds.; Marcel Dekker: New York, 1998; pp 447-467.

70. Hertog MGL, Hollman PCH, Katan MB, *Journal of Agricultural and Food Chemistry*, **1992**, *40*, 2379.

71. Keys A, *American Journal of Clinical Nutrition*, **1995**, *61*, 1321.

72. Hertog MG, Hollman PCH, Katan MB, Kromhout D, *Lancet*, **1993**, *342*, 1007.

73. Yao LH, Jiang YM, Shi J, Tomas-Barberan FA, Datta N, Singanusong R, et al., *Plant Foods for Human Nutrition*, **2004**, *59*, 113.

74. Ejaz S, Ejaz A, Matsuda K, Chae WL , *Journal of the Science of Food and Agriculture*, **2006**, *86*, 339.

75. Peterson JMS, Dwyer J, Dsc RD, *Nutrition Research*, **1998**, *18*, 1995.

76. Horowitz R, Gentili B (1977). *Flavonoids constituents of citrus*. In Nagy S, Shaw PE, Vedhuis MK (Eds.), Citrus science and technology (pp. 397–426). Westport, CT: AVI Publishing.

77. Gionfriddo F, Postorino E, Bovalo F, *Essenze-Derivati agrumari*, **1996**, *66*, 404.

78. Macheix JJ, Fleuriet A, Billot J (1990). *The main phenolics of fruits*. In Fruit phenolics (pp. 1–103). Boca Raton, FL: CRC Press.

79. Mouly P, Gaydou EM, Auffray A, *Journal of Chromatography A*, **1998**, *800,* 171.

80. Cook NC, Samman S, *Nutritional Biochemistry*, **1996**, *7*, 66.

81. Yusof S, Mohd Ghazali H, Swee King G, *Food Chemistry*, **1990**, *37*, 113.

82. Pratt DE, Hudson BJF (1990). *Natural antioxidants not exploited commercially*. In BJF (Ed.), Food Antioxidants Hudson (pp. 171–192). New York: Elsevier.

83. Benavente-Garcıa O, Castillo J, Sabater F, Del Rio JA, *Plant Physiology and Biochemistry*, **1995**, *33*, 227.

84. Lewinsohn E, Berman E, Mazur Y, Gressel J, *Plant Science*, **1989**, *61*, 23.

85. Park GL, Avery SM, Byers JL, Nelson DB, *Food Technology*,**1983**, *37*, 98.

86. Horowitz RM, *Progress in Clinical and Biological Research*, **1986**, *213*, 163.

87. Marini D, Balestrieri F, *Italian Journal of Food Science*, **1995**, *3*, 255.

88. Mouly P, Arzouyan CR, Gaydou EM, Estienne JM, *Journal of Agricultural and Food Chemistry*, **1994**, *42*, 70.

89. Ooghe WC, Detavernier CM, *Journal of Agricultural and Food Chemistry*, **1997**, *45*, 1633.

90. Bocco A, Cuvelier ME, Richard H, Berset C, *Journal of Agricultural and Food Chemistry*, **1998**, *46*, 2123.

91. Bocco A, Cuvelier ME, Richard H, Berset C, *Sciences des Aliments*, **1997**, *18*, 13.

92. Mouly P, Arzouyan CR, Gaydou EM, Estienne JM, *Analusis*, **1995**, *23*, 336.

93. Benavente-Garcıa O, Castillo J, Marin FR, Ortuno A, Del Rıo JA, *Journal of Agricultural and Food Chemistry*, **1997**, *45*, 4505.

94. Miyake Y, Yamamoto K, Morimitsu Y, Osawa T, *Food Science and Technology International*, **1998**, *4*, 48.

95. Augusti KT, 1990. *Therapeutic and medicinal values of onions and garlic*. In: Brewster JL, Rabinowitch HD (Eds.), Onions and Allied Crops, Vol. 3. CRC Press, Boca Raton, pp. 93–104.

96. Carotenuto A, De Feo V, Fattorusso E, Lanzotti V, Magno S, Cicala C, *Phytochemistry*, **1996**, *41*, 531.

97. Carotenuto A, Fattorusso E, Lanzotti V, Magno S, De Feo V, Cicala C, *Phytochemistry*, **1997**, *44*, 949.

98. Tanaka T, *Bull. Univ. Osaka Pref. Ser. B*, **1969**, *21*, 139.

99. Swingle, WT, *The botany of Citrus and its wild relatives of the orange subfamily*. In The Citrus Industry Vol. I: History, Botany, and Breeding, eds. Webber, HJ and Batchelor LD, University of California Press, Berkeley, pp. 129-474 (1943).

100. Albach, RF, *Redman GH, Phytochemistry*, **1969**, *8*, 127.

101. Kawai S, Tomono Y, Katase E, Ogawa K, Yano M, *J. Agric. Food Chem.*, **1999**, *47*, 3565.

102. Smith RD, Loo JA, Ogorzalek Loo RR, Busman M, and Udseth HR, *Mass Spectrom. Rev.*, **1991**, *10*, 359.

103. Dass C, *Curr. Org. Chem.*, **1999**, *3*, 193.

104. Dole M, Mack LL, Hines RL, Mobley RC, Ferguson LD, and Alice MB, *J. Chem. Phys.*, **1968**, *49*, 2240.

105. Fenn JB, Mann M, Meng CK, Wong SF, and Whitehouse CM, *Science*, **1989**, *246*, 64.

106. Fenn JB, Mann M, Meng CK, Wong SF, and. Whitehouse CM, *Mass Spectrom. Rev.,* **1990**, *9*, 37.

107. Wilm MS and Mann M, *Int. J. Mass Spectrom. Ion Proc.*, **1994**, *136*, 167.

108. Fenn JB, Rosell J, Nohmi T, Shen S, and Banks FJ, Jr., Electrospray ion formation: desorption versus desertation, in A. P. Snyder, ed., *Biochemical and Biotechnological Applications of Electrospray Ionization Mass Spectrometry*, American Chemical Society, Washington, DC, 1995, pp. 60–80.

109. Amad MH, Cech NB, Jackson GS, and Enke CG, *J. Mass Spectrom.*, **2000**, *35*, 784.

110. Gamero-Castano M and de la Mora JF, *J. Mass Spectrom.*, **2000**, *35*, 790.

111. Kebarle P, *J. Mass Spectrom.*, **2000**, *35*, 804.

112. De la Mora JF, Van Berkel GJ, Enke CG, Martinez-Sanchez M, and Fenn JB, *J. Mass Spectrom.*, **2000**, *35*, 939.

113. Enke CG, *Anal. Chem.*, **1997**, *69*, 4885.

114. Cech NB and Enke CG, *Anal. Chem.*, **2000**, *72*, 2717.

115. Cech NB, Krone JR, and Enke CG, *Anal. Chem.*, **2001**, *73*, 208.

116. Dawson PH, *Mass Spectrom. Rev.*, **1986**, *5*, 1.

117. Campana JE, *Int. J. Mass Spectrom. Ion Proc.*, **1980**, *33*, 101.

118. Miller PE and Bonner Denton M, *J. Chem. Educ.*, **1986**, *63*, 617.

119. Stephens WE, *Phys. Rev.*, **1946**, *69*, 691.

120. Cotter RJ, *Anal. Chem.*, **1992**, *64*, 1027A.

121. Guilhaus M, *J. Mass Spectrom.*, **1995**, *30*, 1519.

122. Cotter RJ, *Anal. Chem.*, **1999**, *71*, 445A.

123. Toyoda M, Ishihara M, Yamaguchi S, Ito H, Matsuo T, Roll R, and Rosenbauer H, *J. Mass Spectrom.*, **2000**, *35*, 163.

124. Piyadasa CK, Hakansson P, and Ariyarathe TR, *Rapid Commun. Mass Spectrom.*, **1999**, *13*, 620.

125. Wiley WC and McLaren IH, *Rev. Sci. Instrum.*, **1955**, *26*, 1150.

126. Brown RS and Lenon JJ, *Anal. Chem.*, **1995**, *67*, 1998.

127. Whittal RM, Russon LM, Weinberger SR, and Li L, *Anal. Chem.*, **1997**, *69*, 2147.

128. Vestal ML, Juhasz P, and Martin SA, *Rapid Commun. Mass Spectrom.*, **1995**, *9*, 1044.

129. Brown RS and Lenon JJ, *Anal. Chem.*, **1995**, *67*, 3990.

130. Mamyrin BA, *Int. J. Mass Spectrom. Ion Proc.*, **1994**, *131*, 1.

131. Cornish TJ and Cotter RJ, *Anal. Chem.*, **1997**, *69*, 4615.

132. Zhang J and Enke CG, *J . Am. Soc. Mass Spectrom.*, **2000**, *11*, 759.

133. Dawson JHJ and Guilhaus M, *Rapid Commun. Mass Spectrom.*, **1989**, *3*, 155.

134. Verentchikov AN, Ens W, and Standing KG, *Anal. Chem.*, **1994**, *66*, 126.

135. Chernushevich IV, Ens W, and Standing KG, *Anal. Chem.*, **1999**, *71*, 452A.

136. Guilhaus M, Selby D, and Mlynski V, *Mass Spectrom. Rev.*, **2000**, *19*, 65.

137. Krutchinsky AN, Chernushevich IV, Spicer VL, Ens W, and Standing KG, *J . Am. Soc. Mass Spectrom.*, **1998**, *9*, 569.

138. Eiceman GA and Stone JA, *Anal. Chem.*, **2004**, *76***,** 391A.

139. Wu C, Siems WF, Asbury GR, and Hill HH, Jr., *Anal. Chem.*, **1998**, *70***,** 4929.

140. Clemmer DE and Jarrold MF, *J . Mass Spectrom.*, **1997**, *32*, 577.

141. Laboda A, *J . Am. Soc. Mass Spectrom.*, **2006**, *17*, 691.

142. Hoaglund-Hyzer CS and Clemmer DE, *Anal. Chem.*, **2001**, *73***,** 177.

143. Ruotolo BT, Gillig KJ, Stone EG, Russell DH, Fuhrer K, Gonin M, and Schultz JA, *Int. J. Mass Spectrom.*, **2002**, *219*, 253.

144. Ruotolo BT, McLean JA, Gillig KJ, Stone EG, and Russell DH, *J . Am. Soc. Mass Spectrom.*, **2005**, *16*, 158.

145. Srebalus Barnes CA and Clemmer DE, *Anal. Chem.*, **2001**, *73*, 424.

146. Guevremont R and Purves RV, *J . Am. Soc. Mass Spectrom.*, **1999**, *10*, 492.

147. Schlosser A, Ripkorn R, Bossemeyer D, and Lehmann WD, *Anal. Chem.*, **2001**, *73*, 170.

148. Spengler B, *J. Mass Spectrom.*, **1997**, *32*, 1019.

149. Cornish TJ and Cotter RJ, *Anal. Chem.*, **1997**, *69*, 4615.

150. Cornish TJ and Cotter RJ, *Rapid Commun. Mass Spectrom.*, **1994**, *8*, 781.

151. Cotter RJ, Gardner BD, Ilchenko S, and English RD, *Anal. Chem.*, **2004**, *76*, 1976.

152. Beussman DJ, Vlasak PR, McLane RD, Seeterlin MA, and Enke CG, *Anal. Chem.*, **1995**, *67*, 3952.

153. Yergey AL, Coorssen JR, Backlund PS, Blank PS, Humphrey GA, Zimmerberg J, Campbell JM, and Vestal ML, *J. Am. Soc. Mass Spectrom.*, **2002**, *13*, 784.

154. Suckau D, Rosemann A, Schuerenberg M, Hufnegel P, Franzen J, and Holle A, *Anal. Bioanal. Chem.*, **2003**, *376*, 952.

155. Abian J, *J. Mass Spectrom.*, **1999**, *34*, 157.

156. Arendale RF, Severson RF, and Chortyk OT, *Anal. Chem.*, **1984**, *56*, 1533.

157. Ryhage R, *Anal. Chem.*, **1964**, *36*, 759.

158. Watson JT and Biemann K, *Anal. Chem.*, **1965**, *37*, 844.

159. Black DR, Flath RA, and Teranishi R, *J. Chromatogr. Sci.*, **1969**, *7*, 284.

160. Tomer KB, Moseley MA, Deterding LJ, and Parker CE, *Mass Spectrom. Rev.*, **1996**, *13*, 431.

161. Abian J, Osterkamp AJ, and Gelpi E, *J. Mass Spectrom.*, **1999**, *34*, 244.

162. Dass C, High-performance liquid chromatography–electrospray ionization mass spectrometry, in F. Settle, ed., *Handbook of Instrumental Techniques for Analytical Chemistry*, Prentice Hall, Upper Saddle River, NJ, 1998, pp. 647–664.

163. Dass C, *Curr. Org. Chem.*, **1999**, *3*, 193.

Section 1

Chapter 2

Food as a Source of Pharmacological Interest Compounds

Results and Discussion

Structural Characterization of Phenolic Compounds in Allium Porrum by High Resolution Tandem Mass Spectrometry.

Vegetables kingdom is full of plants rich of phenolic compounds. Usually, the synthesis of compounds involved in a bunch of human metabolic process as secondary metabolites take place in some of these plants.[1, 2] *Allium porrum*, object of this study, is an herbaceous plant rich source of phenolic compounds. Basically, allium porrum origins from the Mediterranean region; it is an important outdoor vegetable in West Europe, where it is cultivated on about 30,000 ha.[3] Together with *onion* and *garlic*, *Allium porrum* belonging to *Alliacee*'s family. The genus Allium comprises around 750 species according to Hirschegger et al.[4] The subgenus Allium, including around 280 species, is the largest; 114 of these species are made of its largest section, called allium. This section includes economically important species, such as garlic (A. sativum L.) and leek (A. ampeloprasum L.), as well as other minor crops of local importance, such as great headed garlic (GHG), and kurrat.[5-7] This study was focused on Mediterranean allium species, in particular to discover and characterize unknown phenolic compounds by mass spectrometry. Some of these phenolic compound are flavonoids; they are considered as important factors of the overall antioxidant activity of dietary plants.[8] Generally, plant polyphenols, a large group of natural antioxidants ubiquitous in a diet rich in vegetables and fruits, have protective effects, independent of those of known nutrients and micronutrients. A large variety of plant (poly)phenols exist, including cinnamic acids, benzoic acids, flavonoids including proanthocyanidins, stilbenes, coumarins, lignans, and lignins as important polyphenols involved in various disease.[9] In addition to their antioxidant properties, polyphenols show several interesting effects in animal models and in vitro systems; they trap and scavenge free radicals, regulate nitric oxide, decrease leukocyte immobilization, induce apoptosis, inhibit cell proliferation and angiogenesis, and exhibit phytoestrogenic activity.[10,11] These effects may contribute to their potentially protective role in cancer and cardiovascular diseases.[12, 13] Furthermore, vegetables as leek and also onion and garlic are used as food in Mediterranean diet.[14] Actually, according to many literature works, the presence of flavonoids in *leek* is already known; we investigated this vegetable focusing on *kaempferol* glycosides (Figure 1).[15]
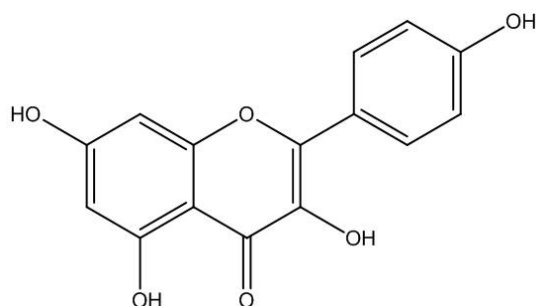
Figure 1: *kaempferol structure, aglycone of the four unknown structure characterized in this study.*

Plants belong to *Allium* genus are rich of these secondary metabolites with important biological activities and utilized for prevention of many disease including cancer, obesity, hypertension, hypercholesterolemia.[15] Herein we describe the isolation from leek leaves of unknown flavonol glycosides, based on a kaempferol aglycone and acylated with a ferulic moiety by means of LC/MS and high resolution ESI-MS and MS/MS methods, through the use of appropriate standards isolated from other plants such as *Coarse Fresee* (*Endive*).[16, 17]

Results

The first part of this study concerned of chromatography separation.[18] *Allium porrum* leaves methanolic extract, properly prepared and solubilized as described in the extraction procedure (see *Materials and Methods*), was injected in the LC/MS instrument, operating in positive ionization mode. Such technique, called *hiphenate*, can be considered as a meeting point between chromatographic separation and the use of mass spectrometry as an investigative tool.[19-21] The full chromatogram as well as the UV chromatogram of the methanolic *leek* leaves extract showed a peak corresponded to the ion at m/z 873 [M+H]$^+$ at 65.04 min (Figure 2 & 3); in the same analysis ions at m/z 843, m/z 697 and m/z 535, respectively at RT 64.43 min, 54.20 min and 55.01 min, were also detected. So four previously uncharacterized flavonoidic structures were elucidated (Figure 4).
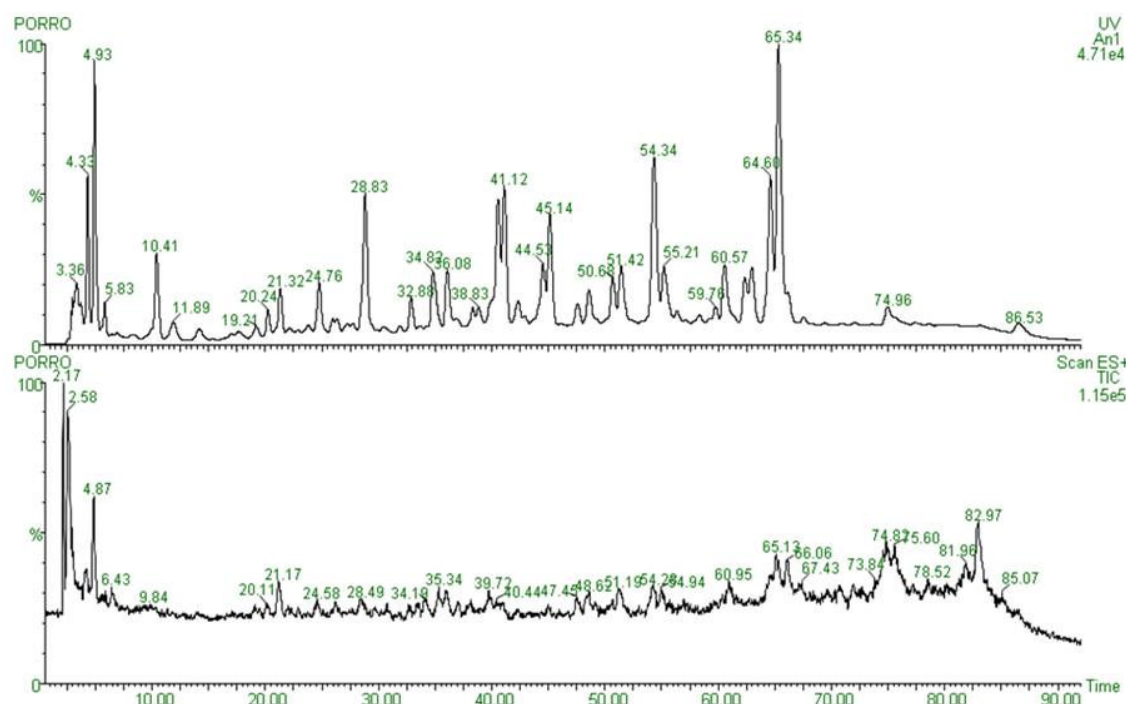
Figure 2: *LC/UV/MS positive ion mode chromatogram of a leek leaves extract. Run time 90 min. UV absorbance λ 280.*
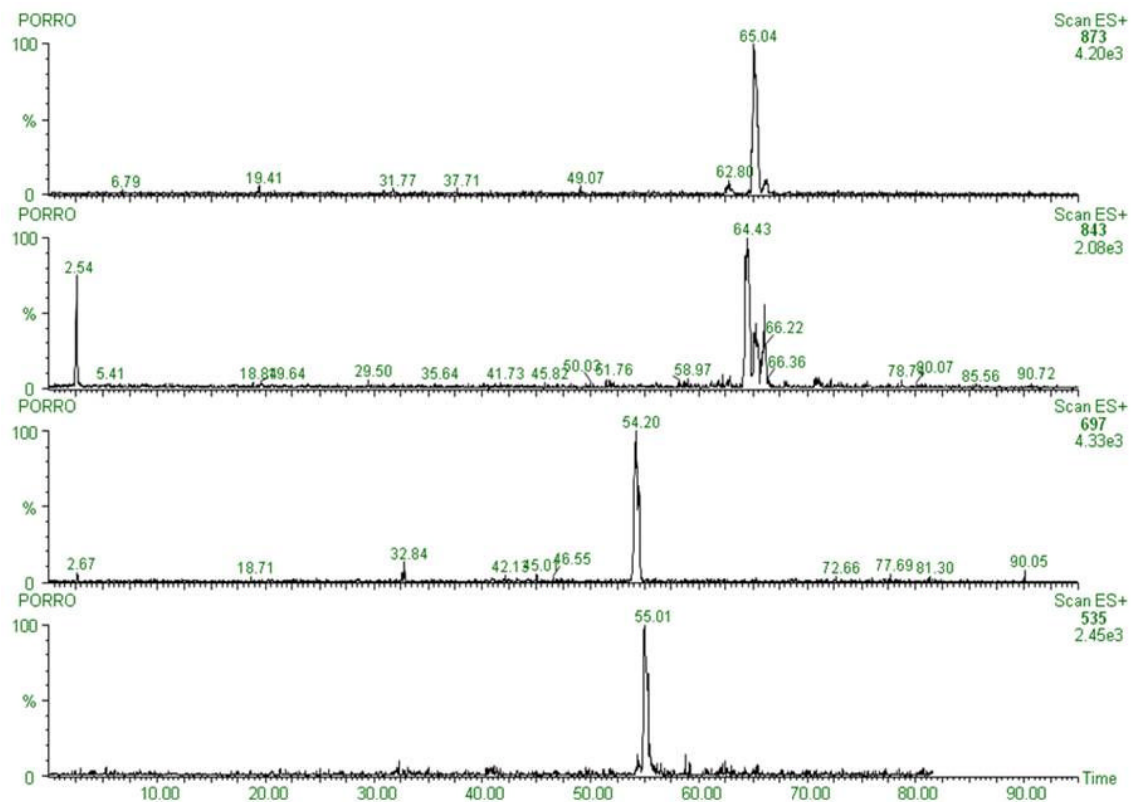
Figure 3: *UV chromatograms of the four unknown ions object of this study.*
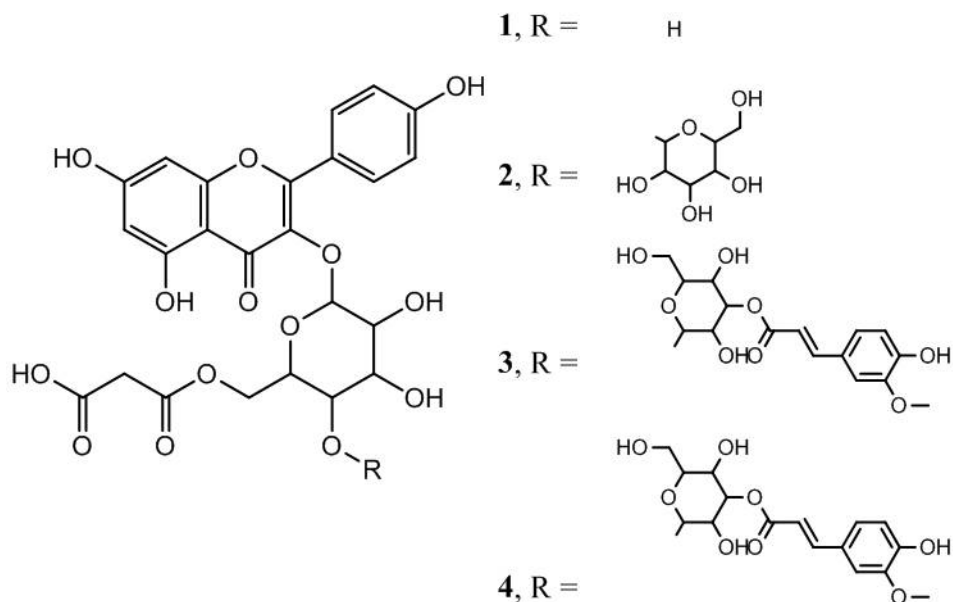
Figure 4: *structures of the four kaempferol glycosides characterized in this study.*

The semi-purified fractions of the unknown compounds from the methanol extract were properly stored at -20°C until MS analysis the same day. The first mass spectrometry measurement was performed by an high resolution Q-TOF instrument in order to obtain information about the elemental composition of the ions as well as the number of double bonds present in the structures.

The first compound isolated by semi-preparative HPLC and than collected was the ion at m/z 535 (9.4 mg from 8.8 gr of porrum leaves extract – 400 gr of leaves), a kaempferol glycoside already known in literature as a kaempferol glycoside molecule in another vegetable.[16]   The MS/MS fragmentation of the latter was used as validation of our findings. The leek ion at m/z 535 was eluted at RT 55.01 min and displayed an UV peak with an absorbance (λ) at 280, the typical absorbance of phenolic compounds such as flavonoids (Figure 3). Once the elemental composition $C_{24}H_{23}O_{14}$ with 2.3029 ppm error and 5 ppm tolerance was highlighted Table 1, tandem mass spectrometry experiments were performed. The fragmentation pattern obtained working in positive ionization mode displayed two main indicative fragments: the base peak, the ion at m/z 287 (Y_0), corresponding to the aglycone moiety of the molecule and the ion at m/z 231 (B_1) corresponding to the glycosilated part of the structure (Figure 5).

Measured mass	Calculated mass	Error (ppm)	Tolerance (ppm)	Formula	DBE
535.1070	535.1082	2.3029	5	$C_{24}H_{23}O_{14}$	13.5
697.1576	697.161	4.9571	5	$C_{30}H_{33}O_{19}$	14.5
843.1963	843.1978	1.8209	5	$C_{39}H_{39}O_{21}$	20.5
873.2080	873.2084	0.4582	5	$C_{40}H_{41}O_{22}$	20.5

Table 1: *high resolution MS measurements of four unknown masses detected in the leek extract.*

We suggest the fragment B_1 origins from the loss of the aglycone and the loss of a molecule of water. Moreover, these are the more common fragmentations occurring in the spectra of glycoconjugates and glycosides, involving cleavage of the glycosidic bond with retention of the glycosidic oxygen atom by the species formed from the reducing end. According to the typical cleavage of the glycosidic bond for this kind of molecules in positive ion mode[22], some fragments result from the protonation of the glycosidic bond, which subsequently broken to yield the B_1 and a smaller glycoconjugate. In the structure we suggest in this study, the conjugate corresponds to a malonil moiety, a malonic acid esterified on the glycosidic part of the molecule, in our case an hexose. The presence of an hexose moiety as glycosidic part of the molecule was suggested by Fattorusso et al. Another fragment ($X_0^{0,2}$) was assigned according to the typical sugar ring fragmentation observed by Domon and Costello in 1988: since several fragmentations involving the cleavage of carbon-carbon bond are possible, we suggest the break of the sugar ring at the

position 0,2. Further, the ion at m/z 145 (just labeled F) was observed in the MS/MS spectrum; we suggest a rearrangement for the sugar (dehydrated) due to the loss of the aglycone and the malonyl moiety Figure 5.
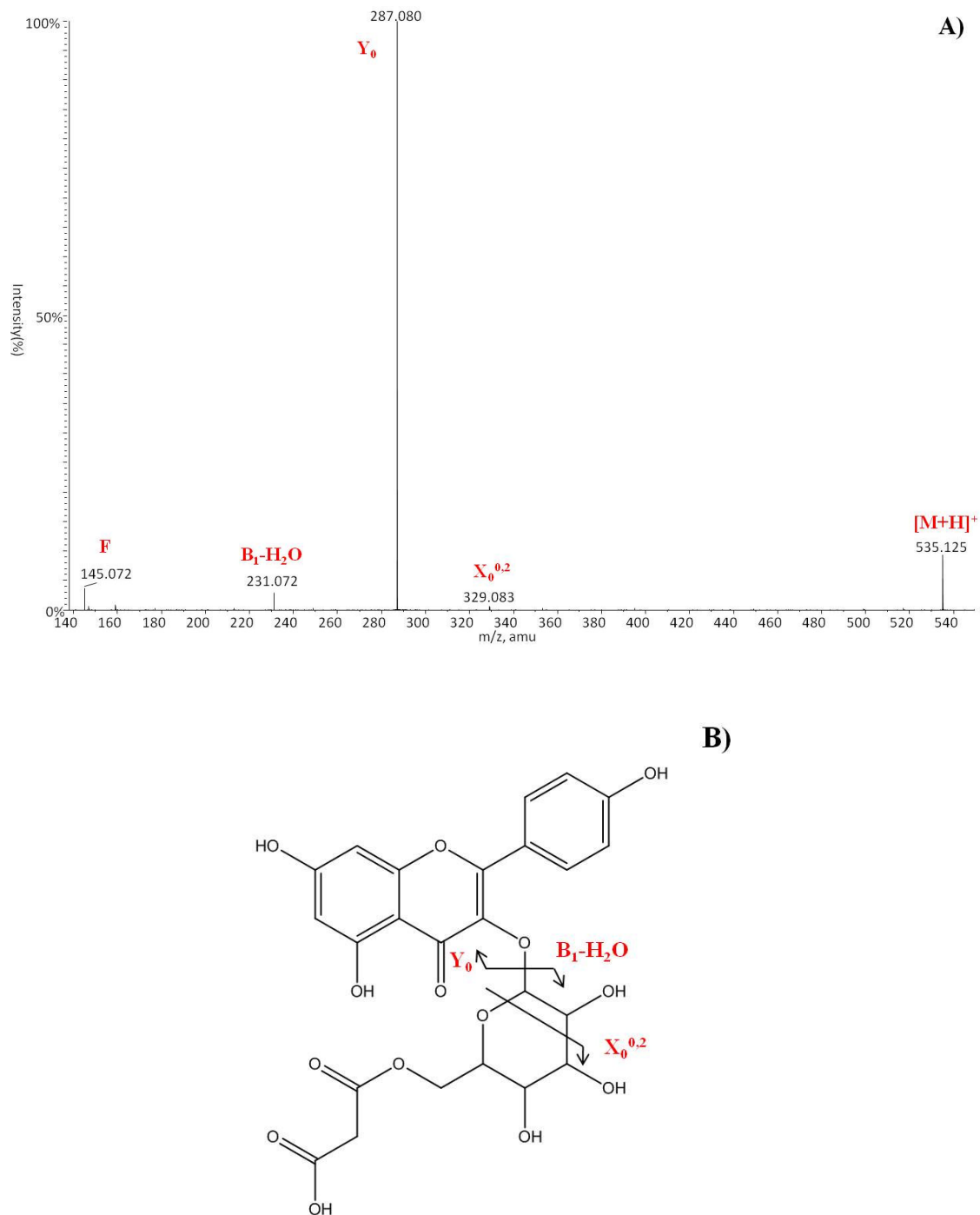
Figure 5: *a) MS/MS spectrum in positive ion mode of the species at m/z 535 and b)the suggested fragmentation.*

Finally, this leek unknown structure (the ion at m/z 535) was confirmed extracting and fragmenting the same ion already known in another vegetable, endive.[16]
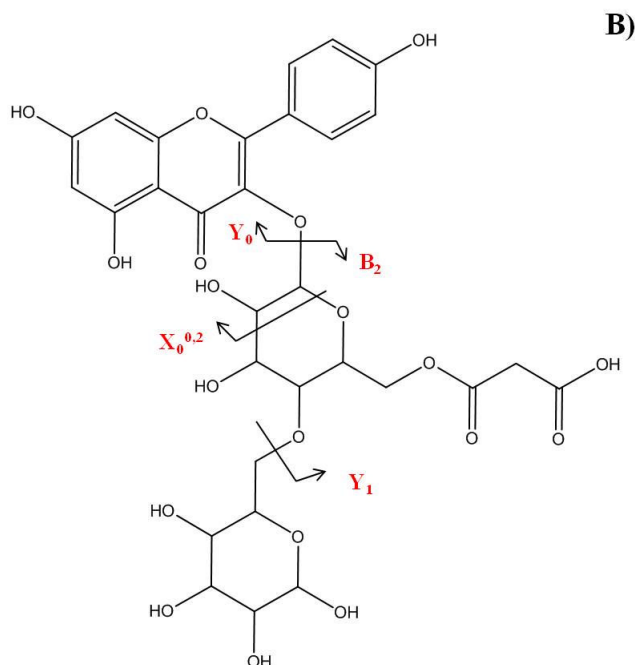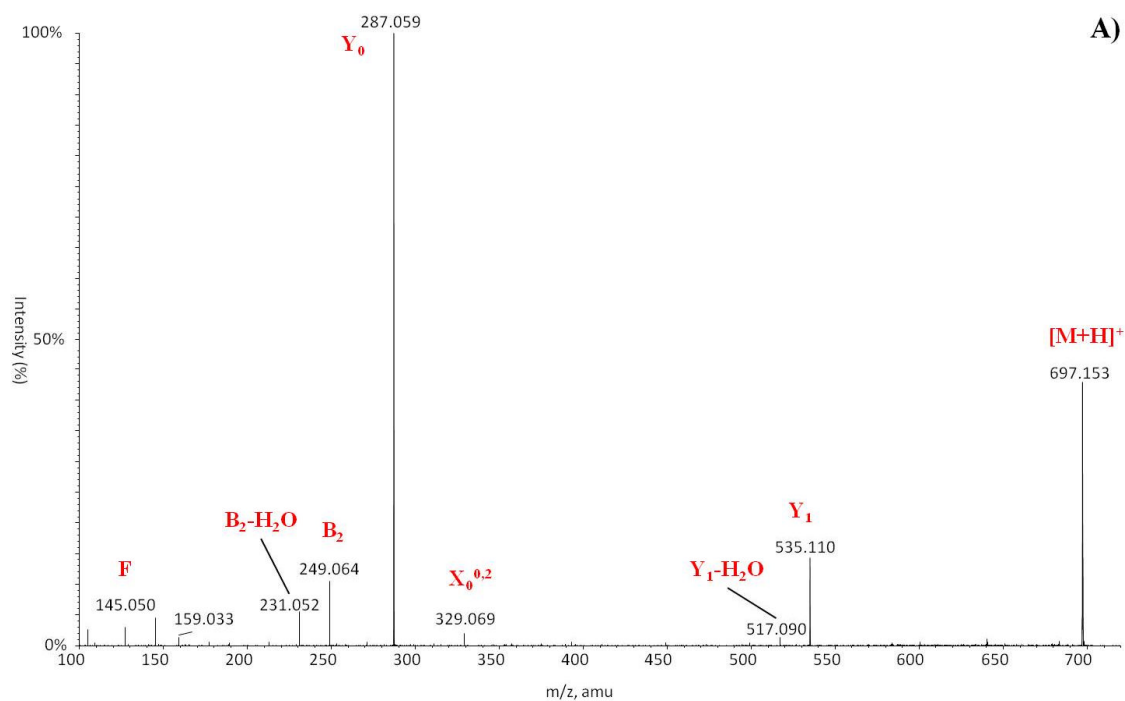
Figure 6: *a) MS/MS spectrum in positive ion mode of the species at m/z 697 and b)the suggested fragmentation.*

The comparison between the RT and UV peaks performed in the same experimental conditions allowed to highlight the presence of a glucose moiety in the structure. The presence of this hexose was confirmed also by the NMR work of Fattorusso et al. The HPLC run displayed another unknown ion at RT 54.20 min Figure 3; this ion at m/z 697 was characterized using the same experimental approach. The collected fraction generate 5.82 mg of the ion at m/z 697. The high resolution MS measurements gave us an elemental composition $C_{30}H_{33}O_{19}$ (Table 1). The MS/MS spectrum displayed the same ions of the previously molecule (m/z 287 Y_0, m/z 231 B_2-H_2O and m/z 329 $X_0^{0,2}$) and also another ion at m/z 535 assigned as Y_1 because is due to the break of a glycosidic bond and the loss of 163 amu (the external sugar) from the parent ion (m/z 697 $[M+H]^+$). Further, the ion at m/z 145 (just labeled F) was observed in the MS/MS spectrum; we suggest a rearrangement for the internal sugar (dehydrated) due to the loss of the aglycone, the external sugar and the malonyl moiety (Figure 6). To further validate this finding a basic hydrolysis reaction by $NaCO_3$ was carried out; the reaction was checked by mass spectrometry analysis until the complete formation of the final product expected after 2 hours. Thus, the loss of 87 amu in the final product, compared with the molecular ion (m/z 697), confirmed our hypothesis about the presence of a malonyl moiety linked on the glucose (Figure 7).
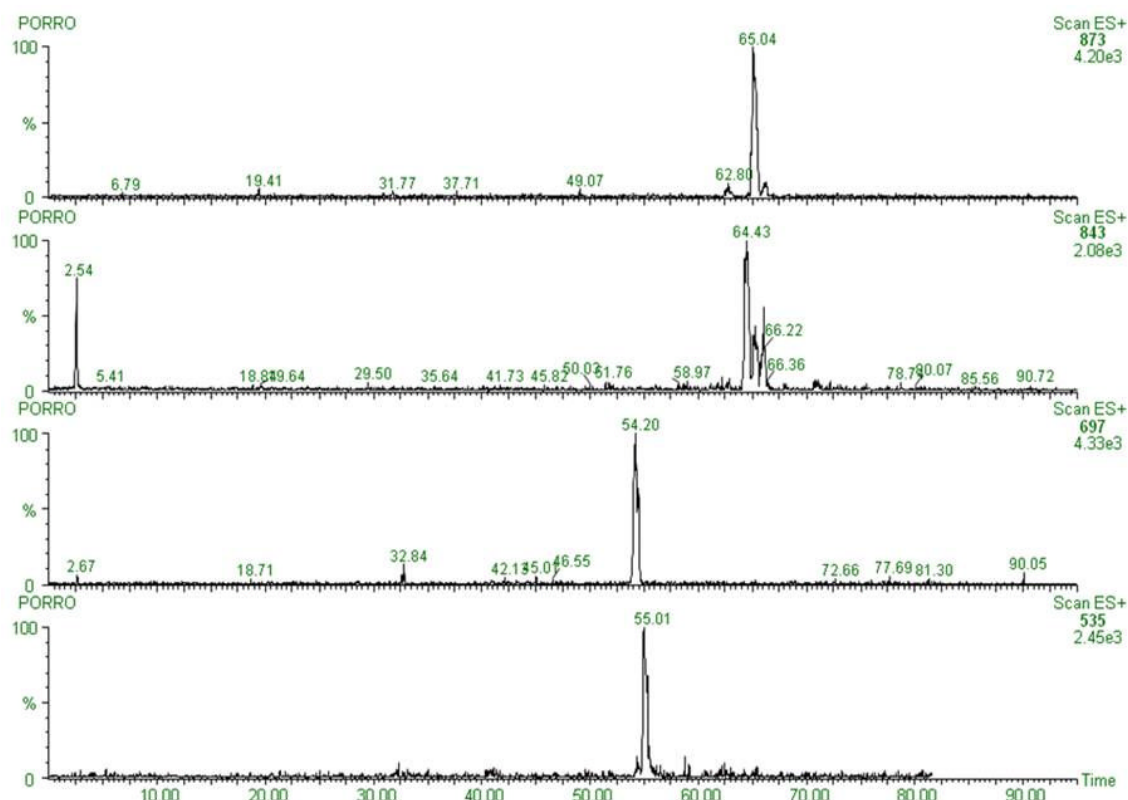
Figure 7: *UV/MS chromatograms of the basic hydrolysis reaction on the semi-purified collected fraction of the species at m/z 697 in positive ion mode. Spectra at time 0 and at complete reaction after 5 hours are displayed.*

The UV chromatogram of the leek leaves methanol extract highlighted other two unknown ions at m/z 843 and 873, eluted at RT 64.43 min and 65.04 min, respectively (Figure 3).
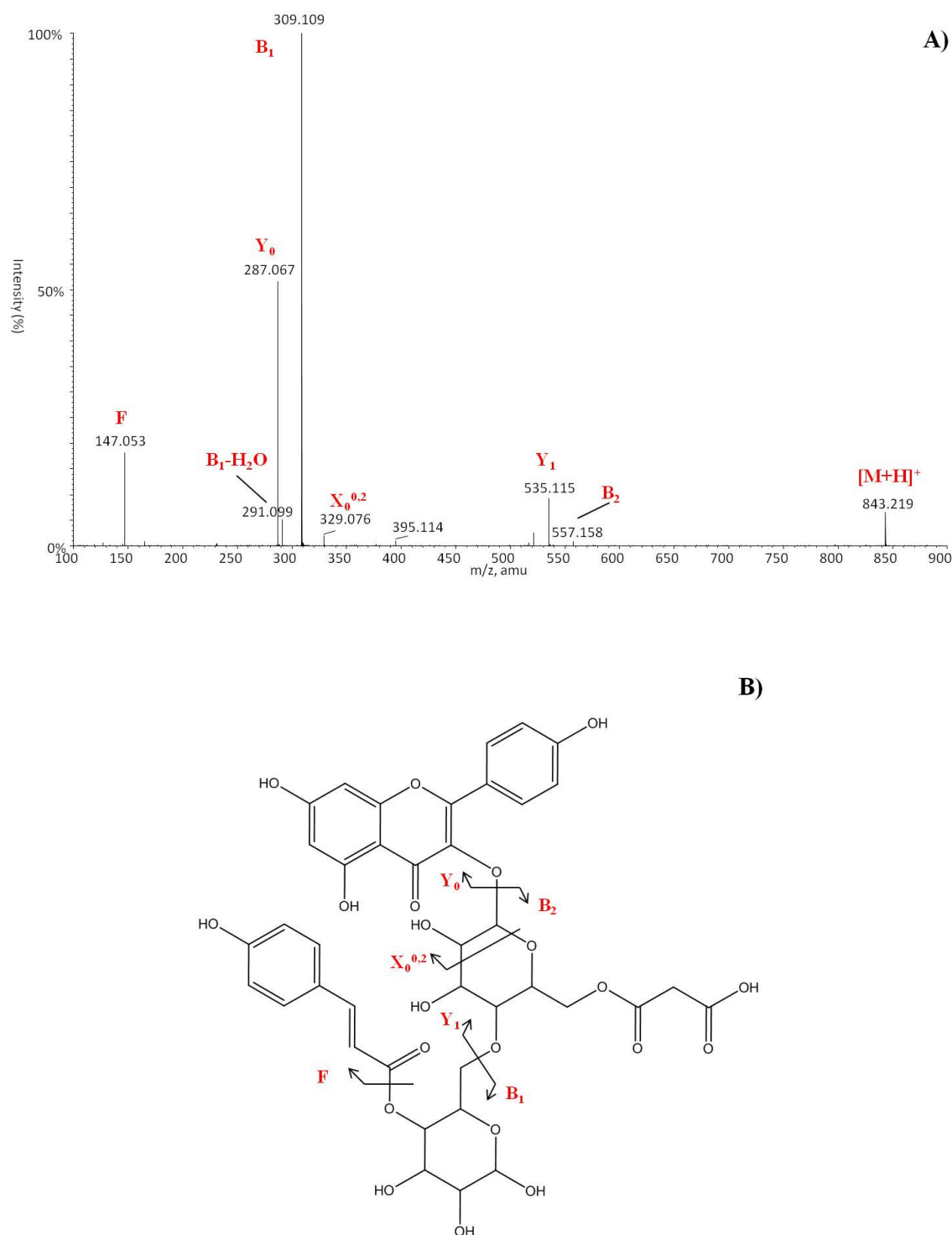
Figure 8: *a) MS/MS spectrum in positive ion mode of the species at m/z 843 and b)the suggested fragmentation.*

Lower amount of these ions were purified and collected by semi-preparative chromatography, respectively 4.6 mg for the m/z 843 and 3 mg for the m/z 873. The high resolution MS measurements suggested $C_{39}H_{39}O_{21}$ and $C_{40}H_{41}O_{22}$ respectively (Table 1).
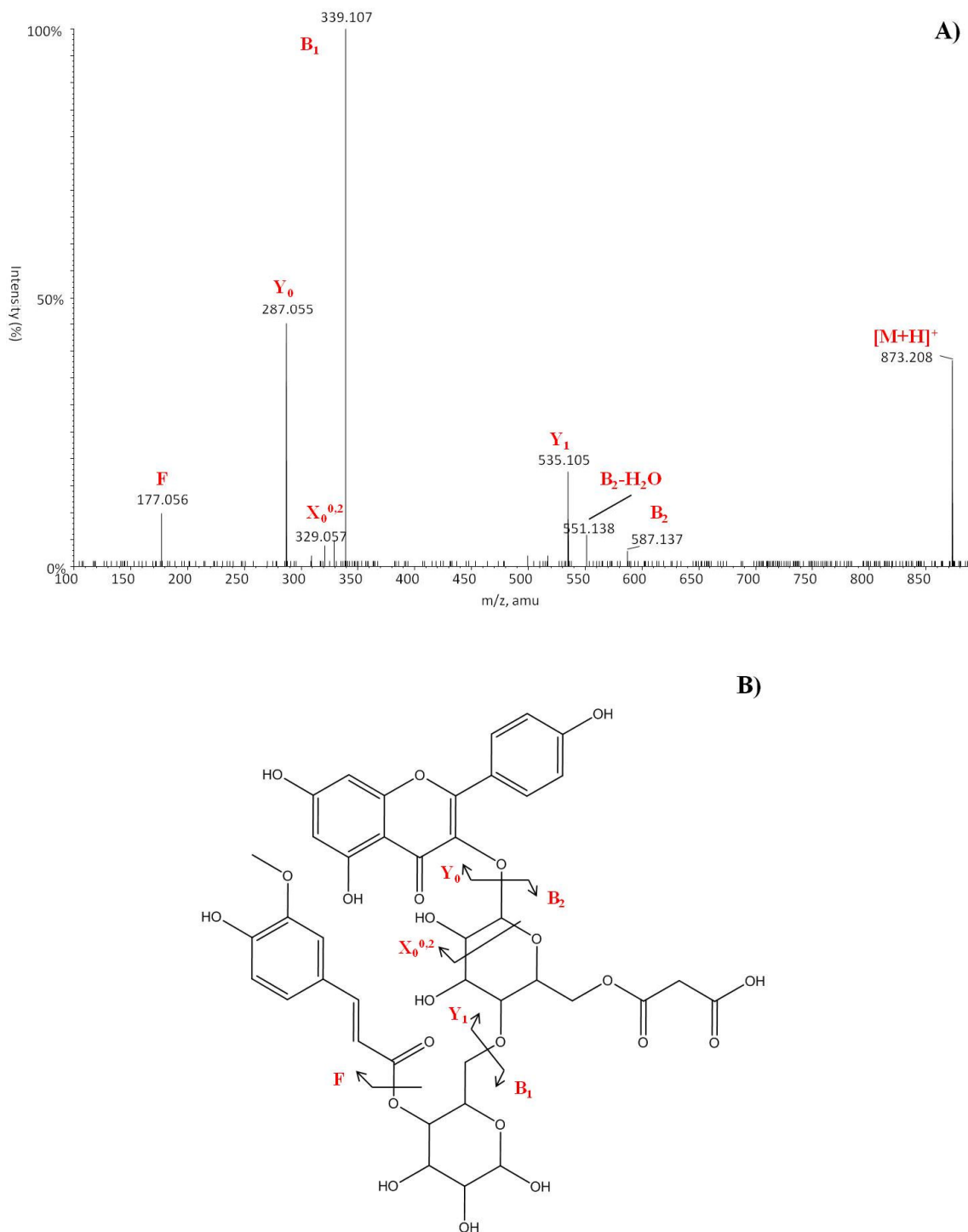
Figure 9: *a) MS/MS spectrum in positive ion mode of the species at m/z 843 and b) the suggested fragmentation.*

The tandem mass spectrometry experiments produced fragmentation patterns pretty similar for these two unknown leek species (Figure 8 & 9): in both cases the fragment Y_0 corresponds to the aglycone (m/z 287) as well as the $X_0^{0,2}$ results from the internal cleavage of a carbon-carbon bond in the sugar ring linked at the flavonol C ring. The ion at m/z 147 (just labeled F) observed in the MS/MS spectrum suggested a cumaric moiety linked on the external sugar. This suggestion was validated by the assignment of the fragment Y_1 (m/z 535) resulting from the loss of a glycoconjugate moiety (the external sugar and the cumaric moiety). In the uknown leek species at m/z 873 instead (Figure 9), this glycoconjugate fragment was observed at m/z 177; according also to the high resolution MS measurement, this finding suggested a ferulic acid esterified on the external sugar ring. Thus, the B_1 fragment were both assigned: in the case of the first species (m/z 843) the break of the glycosidic bond of the external sugar ring generated the ion at m/z 309, corresponding to the glycoconjugate made of the external hexose and the coumaric moiety.
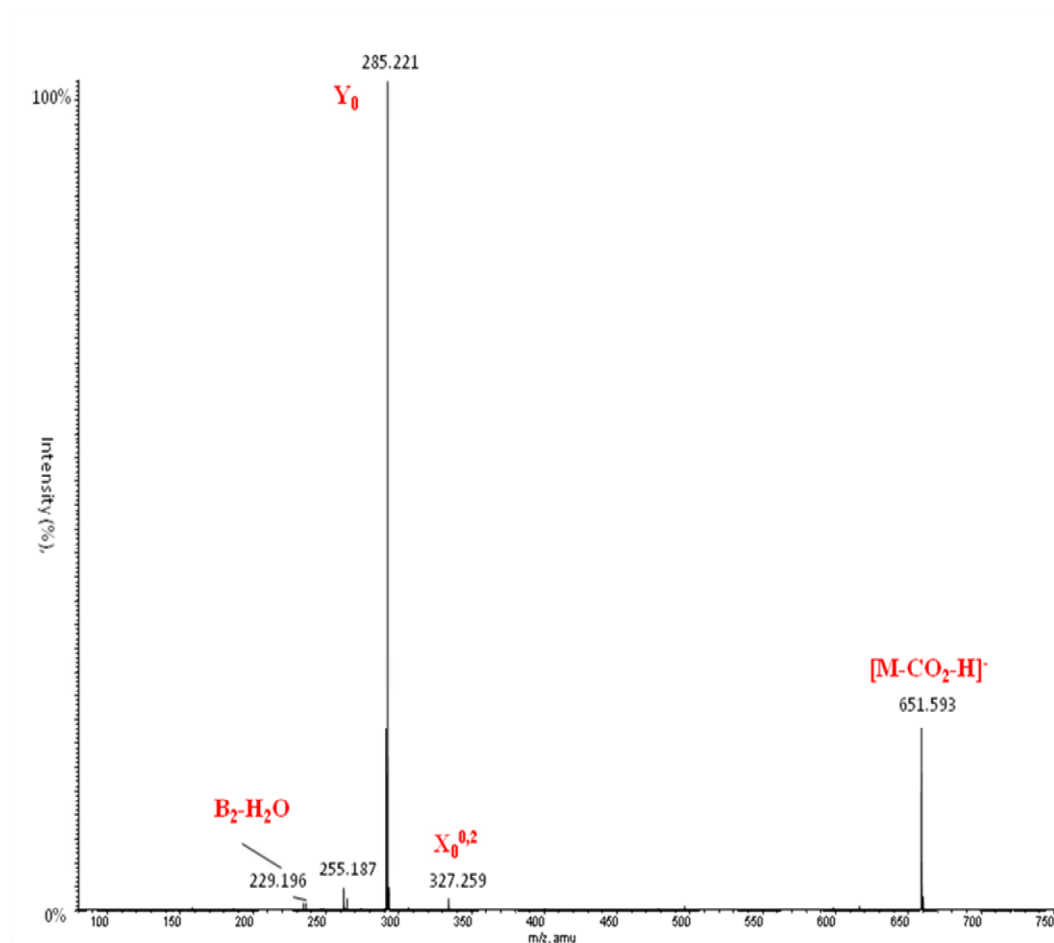
Figure 10: *MS/MS spectrum in negative ion mode of the species at m/z 695.*

The MS/MS spectrum of the last unknown leek species characterized in this study (m/z 873) displayed instead the ion at m/z 339 as B_1 fragment because of the ferulic moiety (Figure 9). Further, the species at m/z 843 highlighted the fragment at m/z 557 assigned as B_2 because corresponds to the glycoconjugate moiety due to the loss of the aglycone (m/z 287), as highlighted in Figure 8. The same fragment (B_2) was assigned in the other unknown leek species to the ion at m/z 587 (Figure 9).

Finally, the MS/MS spectrum of the ion at m/z 873 displayed also the fragments at m/z 551: we suggest this fragment result from the loss of two molecules of water from the B_2 fragment. Tandem mass spectrometry experiments were also carried out in negative ion mode in order to further study the fragmentation patterns of these previously uncharacterized molecules isolated from allium porrum. The negative MS/MS spectra did not suggest many information useful for the structural characterization. Figure 10 displays a representative example of negative fragmentation of one of these glycosilated flavonoids which shows the characteristic loss of -CO_2 from the *quasi-molecular* ion as well as the characteristic Y_0 fragment (m/z 285) related to the aglycone (the kaempferol moiety) and also the B_2-H_2O.

Discussion

Allium porrum as well as many other plants are still object of study because they are considered as a source of natural products with healthy properties otherwise unknown to the people. Many of these plants are often included in diet even if some of them are difficult to be found. Studying complex mixture as an herbaceous plan, a purification and separation technique is necessary before mass analysis. In the last decade, MS based approach was used for the structural elucidation of unknown natural compounds is hundreds of foods. This was due to two main reasons: primarily, because mass spectrometry as investigative and analytical tool appeared as the only one able to give information related to the chemical composition of a complex mixture; secondly, either the last advancements in the technology and in the instrumentation allow investigators to quickly measure with an incredible accuracy and immediately evaluate many important information such as the number of double bonds or the elemental composition of an unknown molecule. Further, the availability on line of big and daily updated database as well as the availability of known standard molecules on sale, need to be mentioned as facilities in the investigation of natural products such as food. Mass spectrometry in the food chemistry word play a key role not only in investigation of something unknown, but also in the food safety and quality control. Many pharmaceutical companies are also interested to the food chemistry world: in the last decade hundreds of new drugs were prepared using natural components extract from plant. In this business mass spectrometry as investigative tool find its perfect application and at date it is considered as the best, fastest and most accurate way for the measurements of plant metabolites as well as drugs discovery. The genus *Allium* is know in literature since the '800 and his molecular composition is still object of study. Even if new technologies and new software for data processing and data comparison make investigators life a little bit easier, the knowledge on the flavonoidic composition of many dietary plants is still in its infancy. Following the last trends in food chemistry the interest on lower abundant compounds is growing up and the methods optimized in this

thesis work for extraction, separation as well as for MS analysis can be further used for a complete elucidation of natural compounds, candidate drugs or candidate dietary members.

Citrus Grandis Glycosilated Flavonoids Structural Characterization by High Resolution Tandem Mass Spectrometry.

Plants contain several compounds that have powerful pharmacological activities. Antioxidant activity as well as anti-inflammatory activity are not only produced by the plant but is also produced by microorganisms.[23, 24]   In the last decade the attention of the scientific world was focused also on natural products such as fruits, for instance, as a source of compounds of pharmacological interest. In a study of the total antioxidant activities of 12 fruits and 5 commercial fruit juices it has been recorded that strawberry has the highest antioxidant activity followed by plum, orange, red grape, kiwi fruit, pink grapefruit, white grape, banana, apple, tomato, pear and honeydew melon.[25]   Citrus seeds possessed greater antioxidant activity than peel.[26] Genus Citrus, with several species cultivated worldwide, produces a large amount of waste materials, including flavedo, albedo, segment membrane and seed waste.[27]   It's known that high consumption of fruits and vegetables is associated with a lowered incidence of degenerative diseases, such as cancer, heart disease, inflammation, arthritis, immune system decline, brain dysfunction and cataracts.[28-30] Some activities that help to prevent some deseases depend to the presence of antioxidants, especially polyphenolic compounds, such as tannins and anthocyanins, and antioxidant vitamins, including ascorbic acid, tocopherol and b-carotene.[31-33] Citrus plants are also rich in naturally-occurring flavonoids, which are primarily found in peel. Flavonoids have a wide range of biological activities, such as cell proliferation-inhibiting, apoptosis-inducing, enzyme-inhibiting, antibacterial, and antioxidant effects.[34, 35] Statistical analysis revealed that the total phenolic contents in the pumelo juice were positively correlated to the antioxidant activity; in particular, free radical-scavenging activity is greatly influenced by the phenolic composition of the sample and the total phenolic contents could be used as an index for free radical-scavenging ability and reducing power in the butan pumelo fruit pulp juice or its fermented product.[36] According to some studies, free radical-scavenging activity depends on the structural conformation of phenolic compounds.[37, 38] Thus, free radical-scavenging activity is greatly influenced by the phenolic composition of the sample; and not only. In fact, there are specific functional group with antioxidant capacity, such as both 3-(a) and 5-(b)-hydroxyl groups; but the flavonoids antioxidant capacity is linked both to a combination of chemical and structural elements, for instance, glycoside presence or absence (glycosides or aglycones) and the presence of free hydroxyls or number and position of hydroxyls eventually esterified. However, flavonoids can exercise their antioxidant activity in several ways: antiradical activities, anti-lipoperoxidation activities, activities of methal chelation; in particular, their radical scavengin activity is attribuited to their hydrigen-donating ability.[39] The butan fruit, object of this study, called also *pummelo* (aka buntan, pampaleone, *Citrus Maxima*) belong to the

genus *Citrus* and Species *Grandis*.[40] It is thought to be one of the three species from which all citrus derive. The others species are *citron* and *mandarin*.[41] *Pummelo* is native from Southeast Asia, but it can be found also in Fiji, Tonga and Hawai. Later it has been introduced in China. There are two *Citrus Grandis* varieties: the "red" and the "white" pummelo.[42] Moreover, literature shows differences between these two varieties. The diversity could be related to the quantities of the flavonoidic compounds contained into the different parts of the fruit.[43] For instance, the flavone *naringin* is more aboundant in peel tissue on white pummelo than in juice; in the red pummelo is the opposite.[43] Following the results obtained from Mokbel et al.[27] showing that the extract of flavedo and albedo can be used as easily accessible source of natural antioxidant and as a possible food supplement or in pharmaceutical industries, the flavonoidic composition of this fruit was investigated in this thesis work and three unknown flavonoids were structurally characterized. Flavonoids properties are already known: in particular, their physiological actions and their beneficial effects on human health.[39] The best documented characteristic of flavonoids is their ability to act as antioxidants and also as antibacterial, as noted previously.[44-46] Many researchers have proved that these compounds act to protect living organism from oxidative damages and to prevent various disease, such as cancer, cardiovascular disease and diabetes.[47, 48] Citrus fruit have been recorded also as sources of pigments.[49] This indicated that citrus fruits (flavedo and albedo) contained various compounds, not only antioxidants, but also those that may have antibacterial effects.[27]

Results

The same MS based approach used for the allium porrum project was used to further investigate the molecular contents of the citrus grandis, fruit object of this study. The investigation was focused on phenolic compounds. Also in this case, the first step of the study concerned the optimization of a method for the extraction of such compounds. Thus, analytical chromatography using a RP C18 column was used to investigate the pummel extract. In particular, three unknown compounds were structurally characterized in this study (Figure 11).The optimized LC/UV ESI-MS method for the mass spectrometry analysis highlighted a series of peaks corresponding to already known molecules as well as not yet assigned masses (Figure 12): species such as rutin (m/z 579), naringin (observed as sodium adduct at m/z 603) as well as rhoifolin (m/z 595) were eluted at RT 29.75 min, 43.68 min, 49.95 min, respectively (Figure 13).[50] The presence in the pummelo extract of such molecules was confirmed by the comparison between RT of appropriate standard molecules injected in the mass spectrometer in the same setup for the chromatography. Furthermore, this run was able to resolve many other peaks: the investigation was focused on three signals, corresponding to three masses non previously characterized in this fruit. The chromatogram displayed signals related to the m/z species 667, 765 (that is the sodium adduct of the ion at m/z 743) and 829 (Figure 14). Following Sindona et al.[51-54] , the collected fractions of those compounds were submitted to a Q-TOF instrument for high resolution MS measurements (Table 2); the aim of these experiments was to obtain mass accurate information for either the elemental composition and the number of double bonds of such masses. The latter was the first step of the structural characterization.

Measured mass	Calculated mass	Error (ppm)	Tolerance (ppm)	Formula	DBE
667.1879	667.1868	1.5337	5	$C_{30}H_{35}O_{17}$	13.5
743.2391	743.2393	0.2775	5	$C_{33}H_{43}O_{19}$	12.5
829.2397	829.2397	0.0003	5	$C_{36}H_{45}O_{22}$	14.5

Table 2: *high mass accuracy measurements of three unknown pummelo species.*
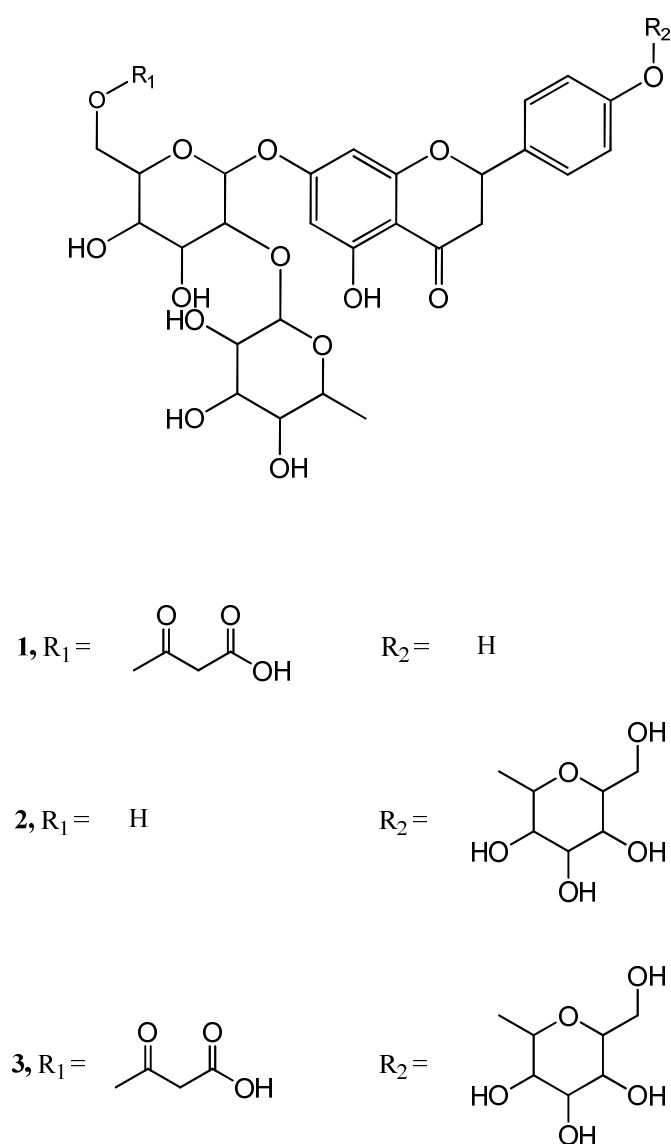
Figure 11: *scheme of pummelo unknown phenolic compounds characterized in this thesis work.*
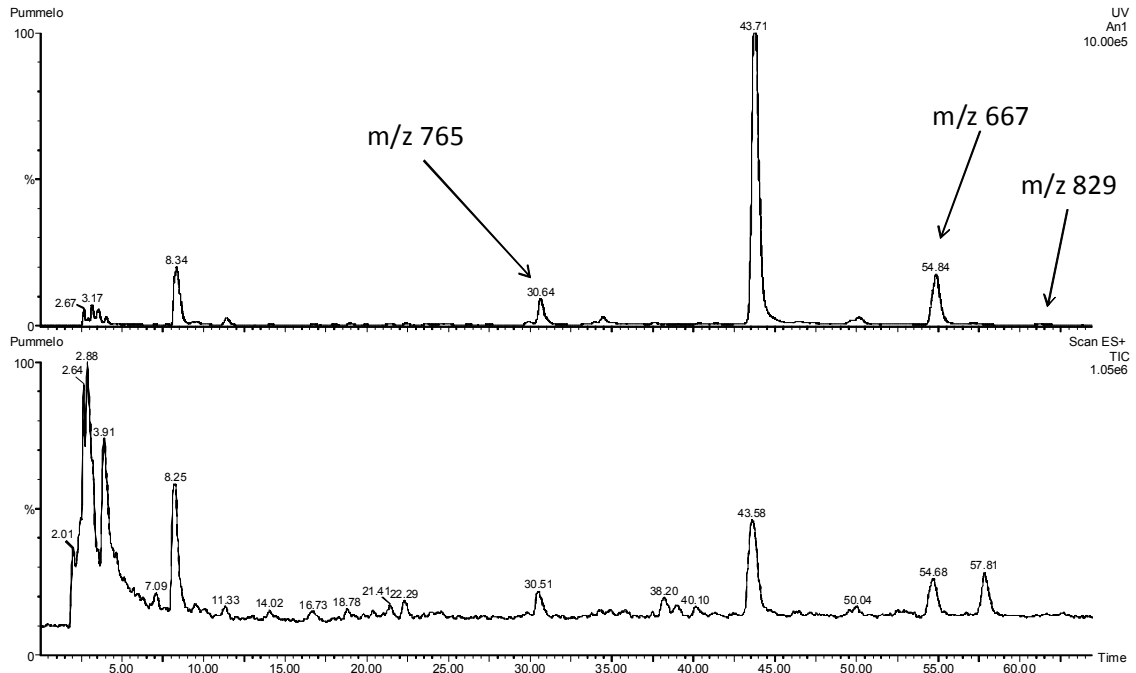
Figure 12: *LC/UV ESI-MS chromatogram of pummelo extract, at 90 min total run time through a RP C18 column.*
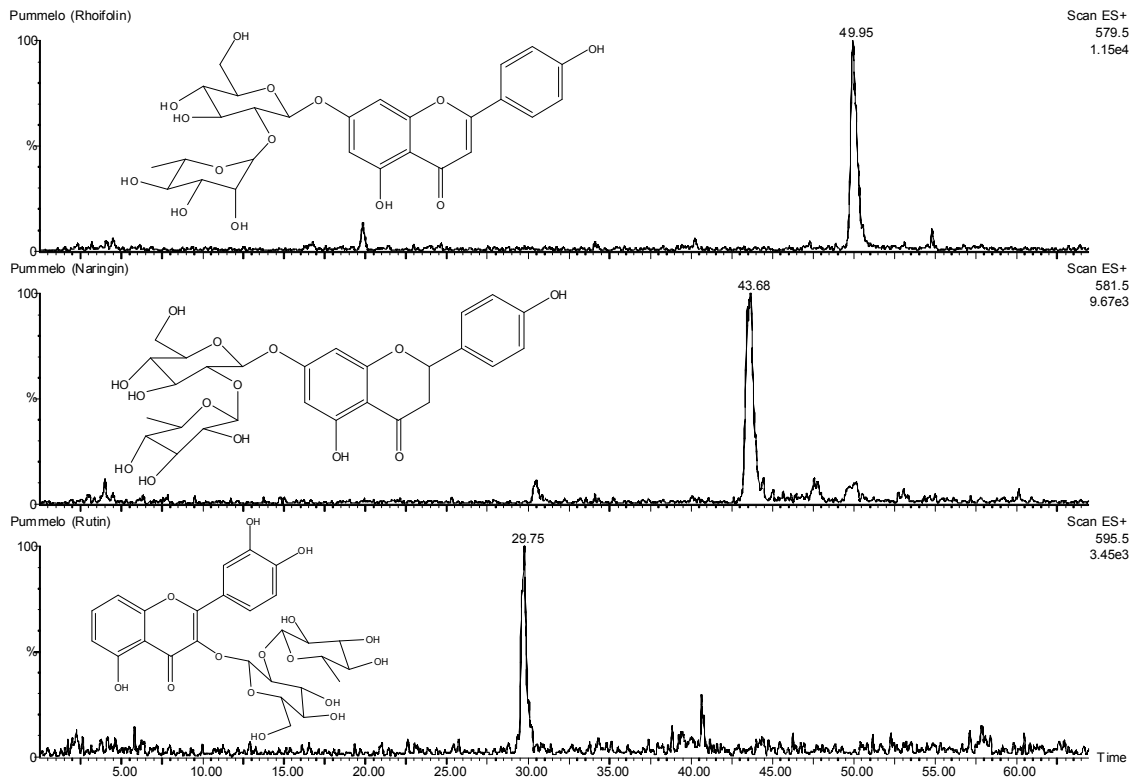
Figure 13: *LC/UV ESI-MS chromatograms of pummelo extract known flavonoids, rhoifolin (top), naringin (middle), rutin (down).*
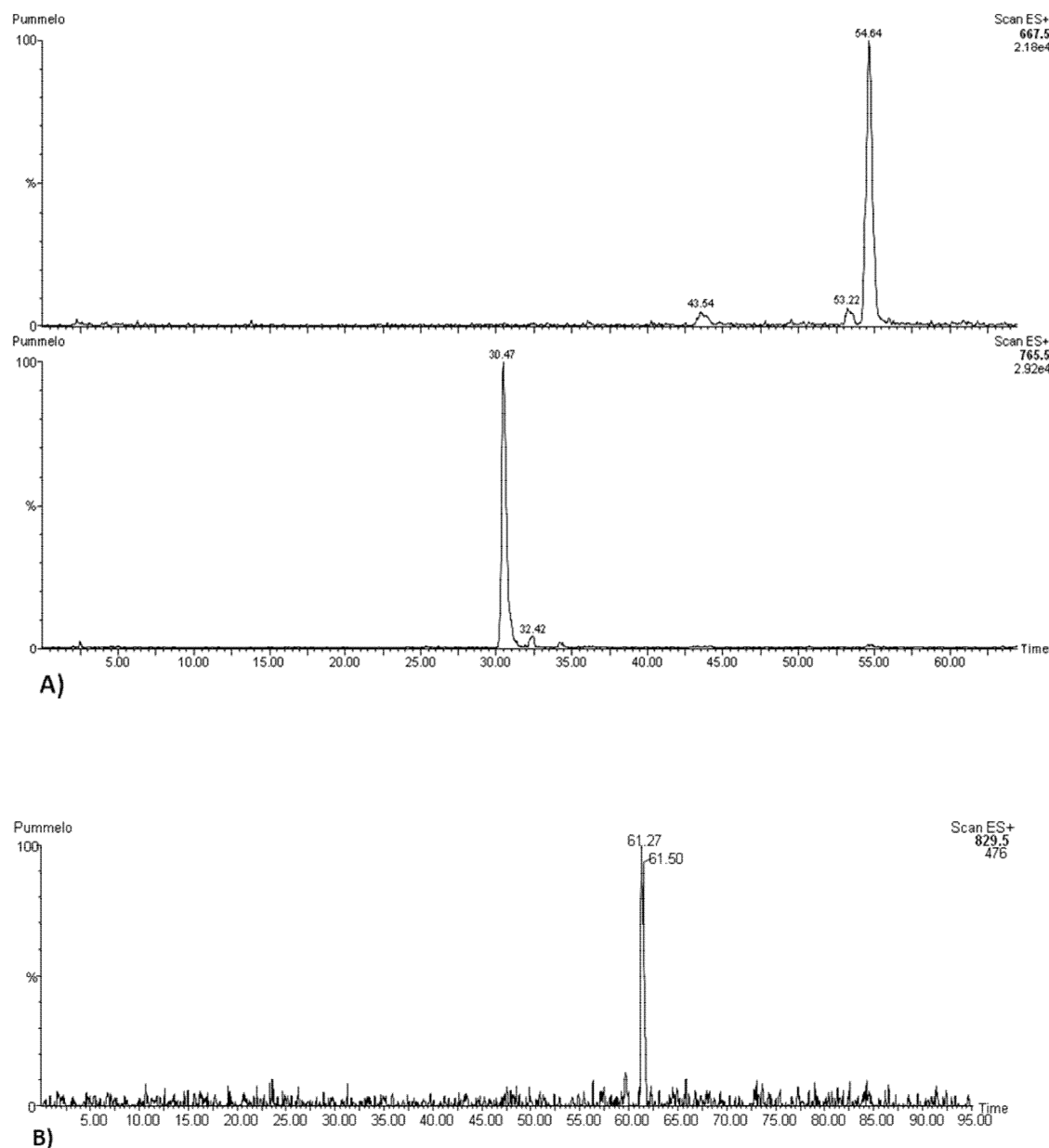
Figure 14: *LC/UV ESI-MS chromatograms of three pummelo extract unknown compounds investigated in this study. A) Ions at m/z 667, 743 (observed as m/z 765, [M+Na]$^+$) and B) 829. A) and B) were generated by two different LC-MS runs, 90 min and 95 min respectively, using the same mobile phase.*

In fact, the high mass accuracy data suggested an hypothetic structure for that mass (MW 666) pretty similar to that of the naringin. So, the semi-purified fraction of the ion at m/z 667 (35.4 mg from 670 of pummelo extract), collected by semi-preparative chromatography, was used for a basic hydrolysis reaction and the resulting final product highlighted the m/z 603, sodium adduct of a naringin (m/z 581) (Figure 15). Thus, considering all the findings, the elemental composition, the number of double bonds, the product of

the hydrolysis as well as the fragmentation pattern from the MS/MS experiment, we assigned a malonyl moiety.
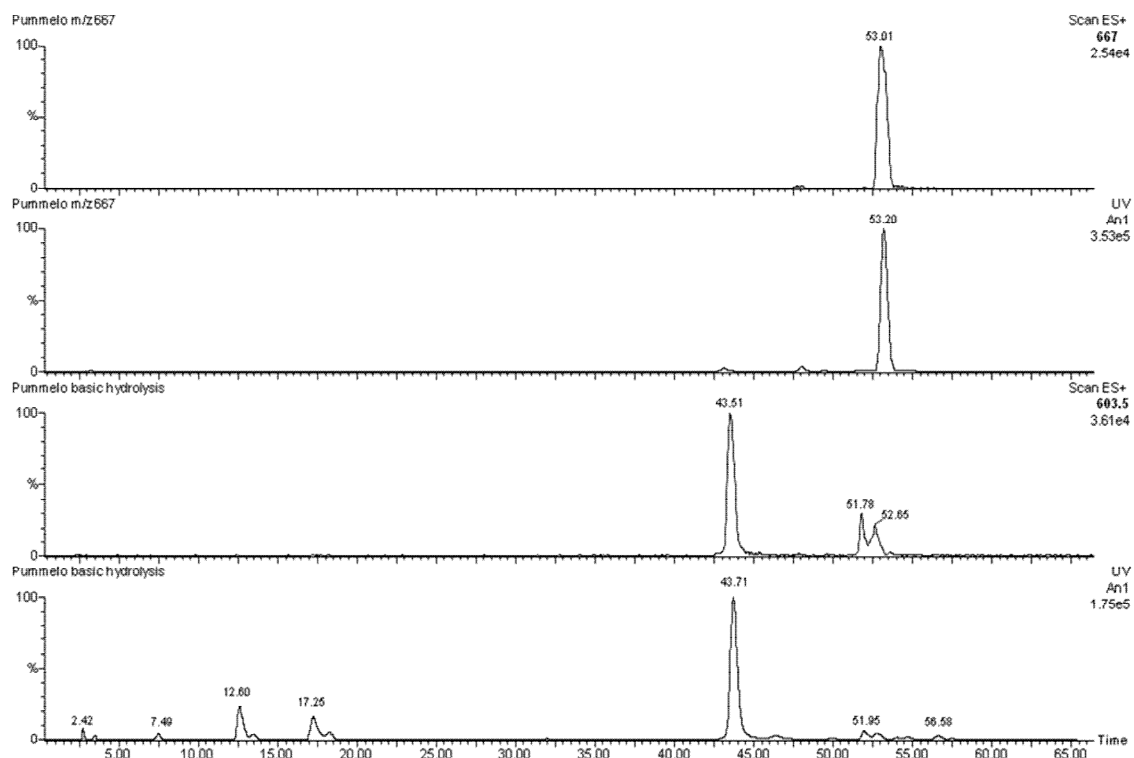
Figure 15: *LC/UV ESI-MS of the basic hydrolysis reaction performed on the semi-purified collected fraction of the uncharacterized ion at m/z 667.*

About the fragmentation pattern: the tandem MS experiment for that ion was performed in positive ion mode and many fragments were assigned according to the glycoconjugate nomenclature introduced in 1988 by Domon & Costello.[22] So, the base peak (m/z 273) was assigned as Y_0, the aglycone as well as the fragment at m/z 521 was assigned as Y_1 (Figure 16). The latter fragment results by the loss of the external hexose (a rhamnose as in the naringin structure) from the molecular ion. This is a typical cleavage at the glycosidic O-linkage with a concomitant H-rearrangement leads to the elimination of monosaccharide residue. Other fragments were found useful for the elucidation of the m/z 667 structure: for instance, the ion at m/z 503, assigned as Z_1, originated by the loss of a molecule of water from the Y_1; also the complementary monosaccharide residue was observed in the low mass range (m/z 147, B_1) as well as the fragment at m/z 395 (B_2) related to the two sugar residues and the esterified malonyl moiety, practically the molecule without the aglycone. For these reasons we suggest a structure for this ion (m/z 697) with a naringin and a malonic acid esterified on the sugar moiety, a naringin-O-malonate. Anyway, this is a typical fragmentation pathway of glycosylated flavonoids.[55] To further validate our findings about the structure suggested for the unknown pummelo species at m/z 667, 40mg of this compound were collected by multi stage semi-preparative chromatography and then submitted to ^{1}H NMR (proton nuclear magnetic

resonance) spectroscopy experiment. Once acquired, the ^{1}H NMR spectrum of the ion at m/z 667 was compared with the ^{1}H NMR spectrum of the naringin standard[56]; this comparison was necessary because the structure suggested for the pummelo unknown compound was a naringin derivate with a malonyl moiety esterified on the sugar linked on the aglycone A ring.
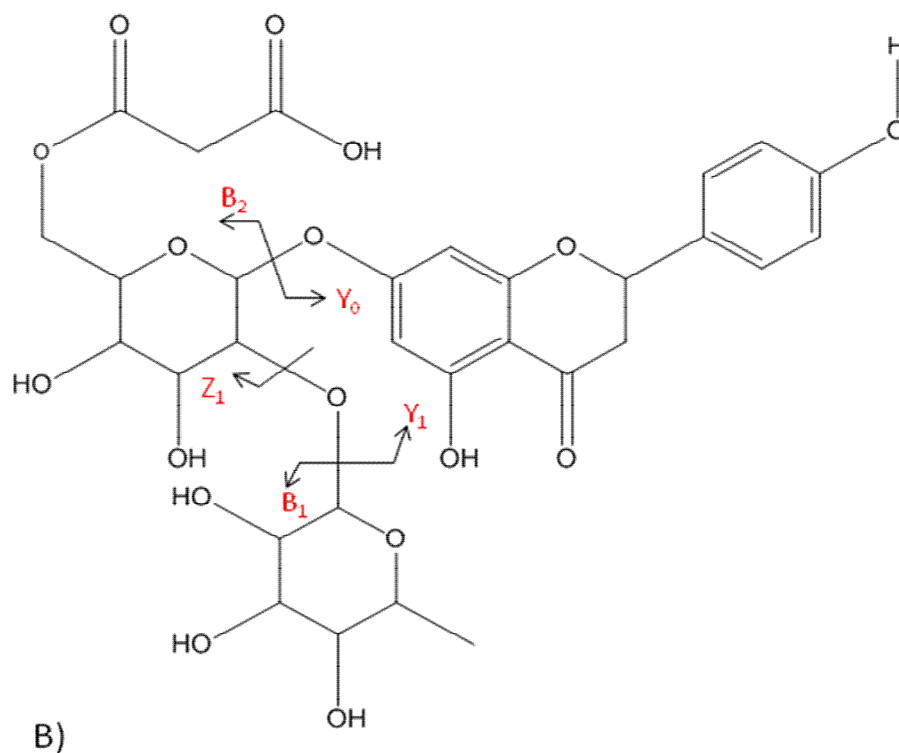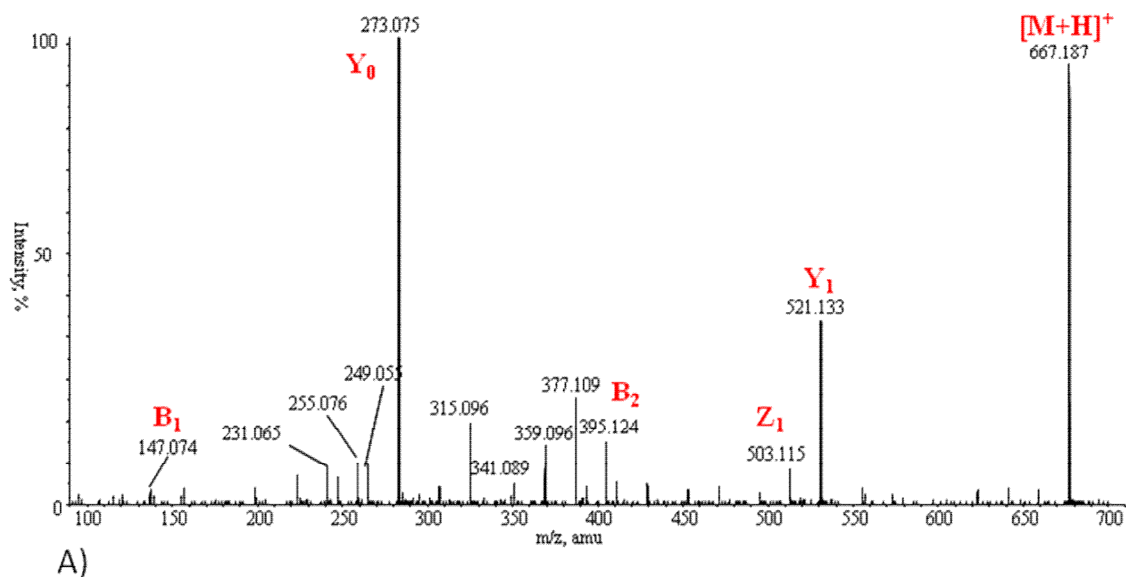
Figure 16: *A) MS/MS m/z 667 and B) the purposed structure.*

Even if either the pummelo compound and the naringin were prepared by the same protocol dissolved in methanol, the comparison between the two ^{1}H NMR spectra highlighted many differences and confirmed the structural our hypothesis (Figure 17). Thus, the pummelo compound spectrum gave glucose C-6 signal when in the naringin spectrum the same signal was shifted. This finding definitively clarified that the malonic ester suggested by the high resolution MS measurement as well as by the basic hydrolysis final product was linked on the glucose in 6-position in the case of the pummelo compound.
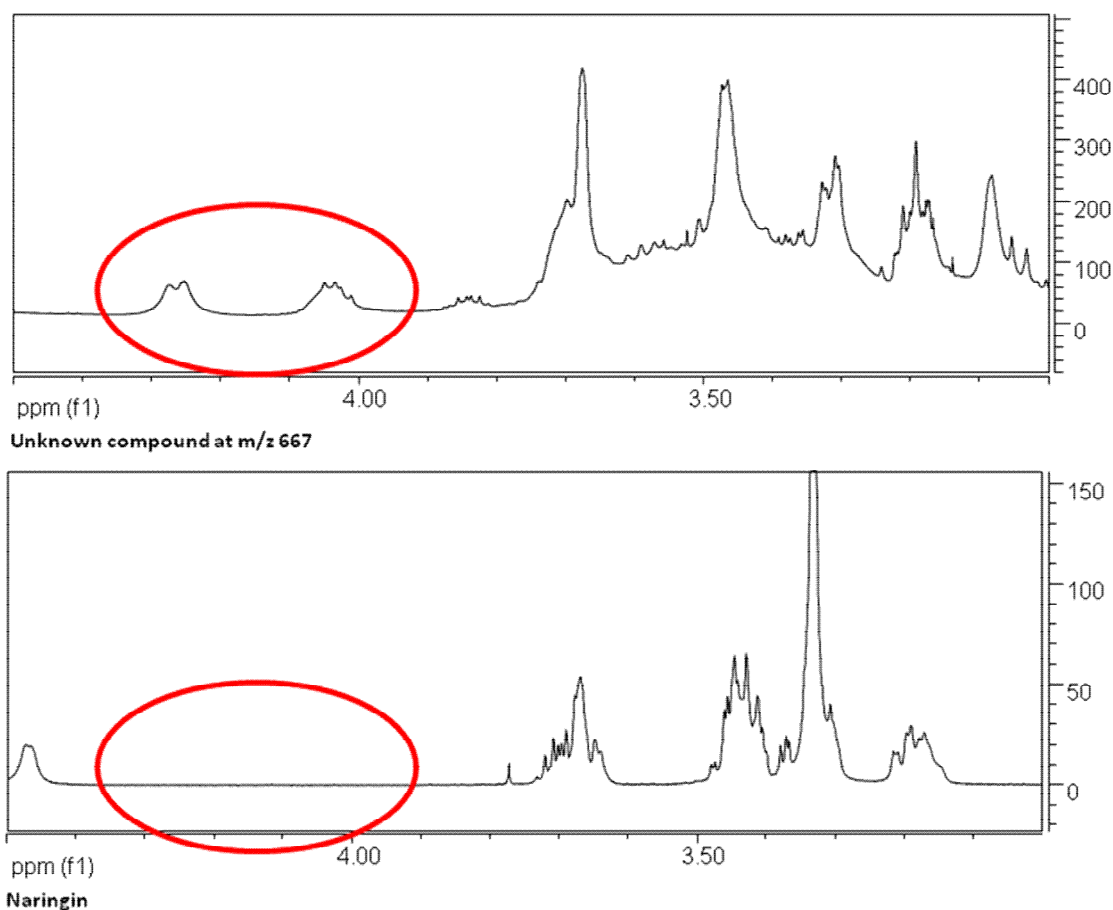
Figure 17: *NMR spectra of the m/z 667 species and the naringin standard.*

Berhow et al. characterized in 1991 a malonic ester derivate of naringin grapefruit[56] : so, grapefruit leaves extract was injected into the mass spectrometer and the resulting LC/UV ESI-MS chromatogram highlighted the same m/z 667 at the same RT in the same operating conditions (Figure 18). This strategy further validated our finding in pummelo. After the structural characterization of this first previously unknown compound extracted from the pummelo fruit, the project was focused on the isolation and purification of other two molecular species: ions at m/z 743 and 829 (from 100 mg of pummelo extract, 14,5 mg and 9,6 mg were collected, respectively). The study of the elemental composition and the number of double bonds obtained by high resolution MS measurements (Table 2) suggested two structures pretty similar to that defined for the previously ion (m/z 667). In particular, in the case of the MS/MS spectrum

65

of the ion at m/z 743 performed in positive ion mode, the fragment Y_0 was immediately assigned to the base peak, the ion at m/z 243 (the aglycone), while the fragment at m/z 581 resulting from the loss of 162 amu was assigned as Y_0^1: we suggest that this glucose is linked on the B ring of the aglycone. Moreover, the fragments Y_1 (m/z 435) and B_1 (m/z 147) were both assigned: Y_1 origins by the loss from the molecular ion of the external rhamnose corresponding to B_1. Furthermore, in literature is described a rearrangement according to the elimination of the internal sugar residue (in our case a glucose) by the break of hemiacetal acid-label bond: the resulting fragment is called Y^* and was assigned to the ion at m/z 419 (Figure 19).[57]
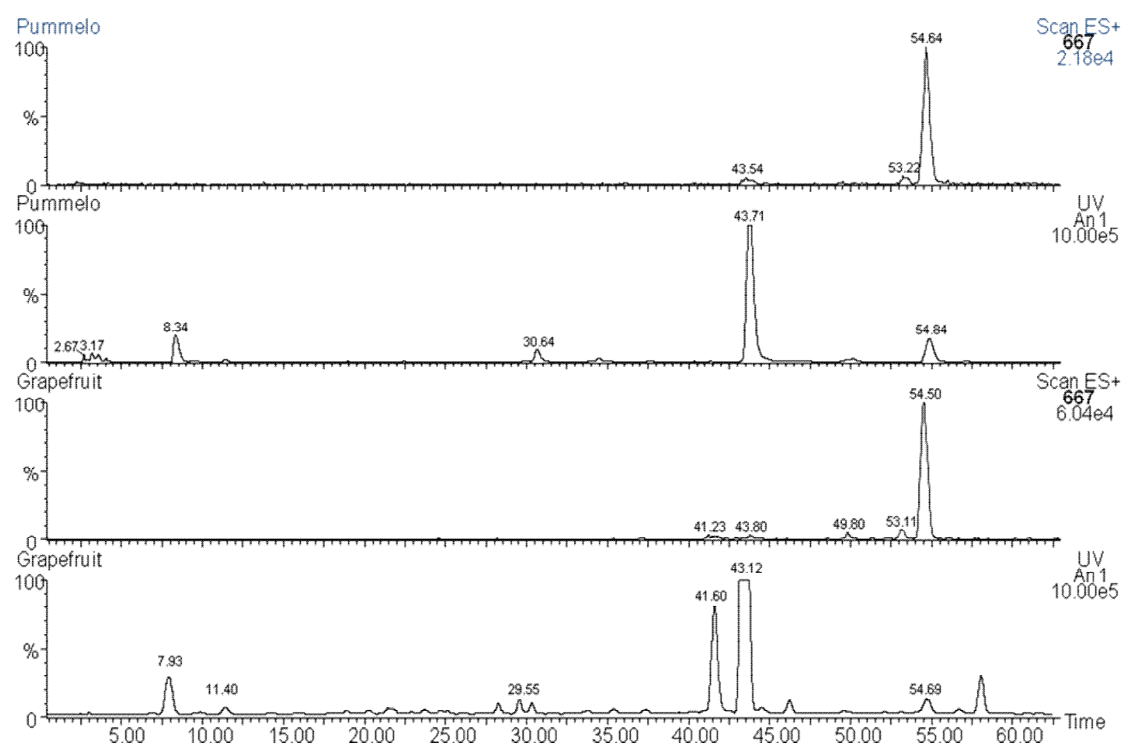
Figure 18: *grapefruit/pummelo LC/UV MS chromatograms about the m/z 667 species.*

The last one compound characterized in this study was the ion at m/z 829: the MS/MS fragmentation pathway suggested a structure pretty similar to that one characterized for the ion at m/z 667 (Figure 20). In fact, the structure we suggested for the ion at m/z 829 corresponds to the m/z 667 with one more sugar residue. Again, the aglycone fragment was immediately assigned as Y_0 as well as Z_1 and Y_1 generated by the loss of the external rhamnose. In particular, Z_1 (m/z 503) is due to a simple cleavage, but more likely a two-step process involving a loss of water from the corresponding Y ion; Y_1 (m/z 521) is due to a cleavage of the protonated glycosidic bond followed by an H-transfer. Finally, another fragment was assigned as Y_0^1: the ion at m/z 667 that origins by the loss of 162 amu, a rhamnose.

Analyzing all the acquired data, we compared also the Y_1 fragments of the ion at m/z 743 and 829: the difference in terms of mass is 86, practically the malonyl moiety. This finding further validated our suggestion about the presence of the malonic acid esterified on the one of the sugar residue, generating a glycoconjugate naringin-O-malonate.
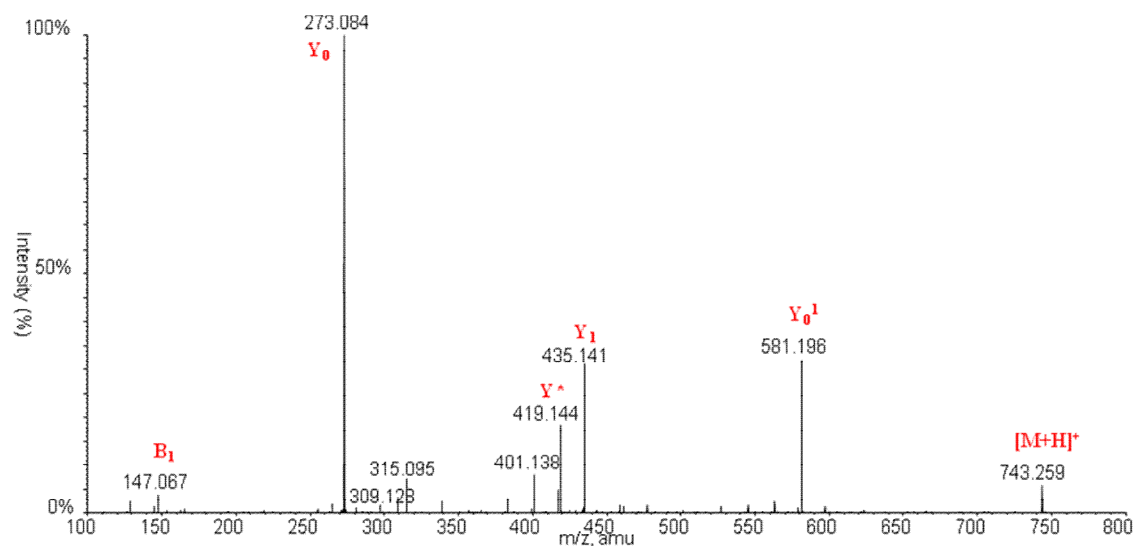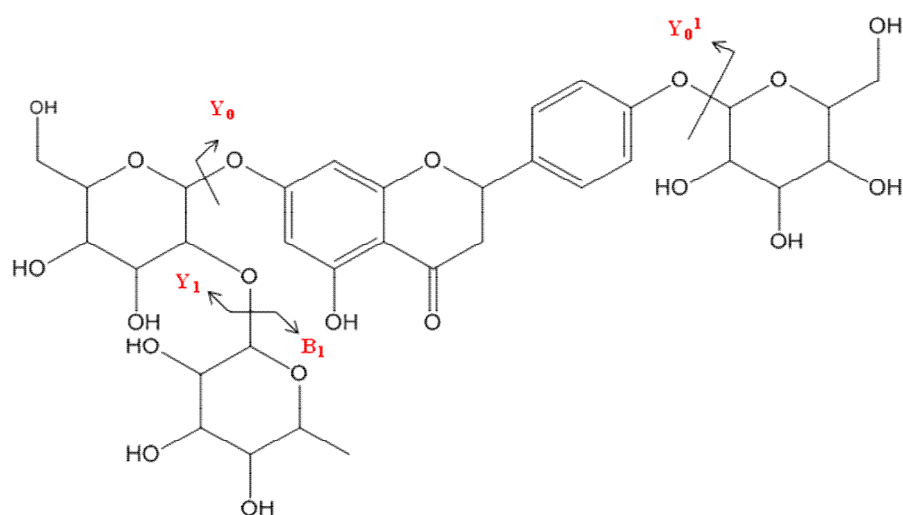
Figure 19: *A) positive ion mode MS/MS of the species at m/z 743 and B) the purposed structure.*
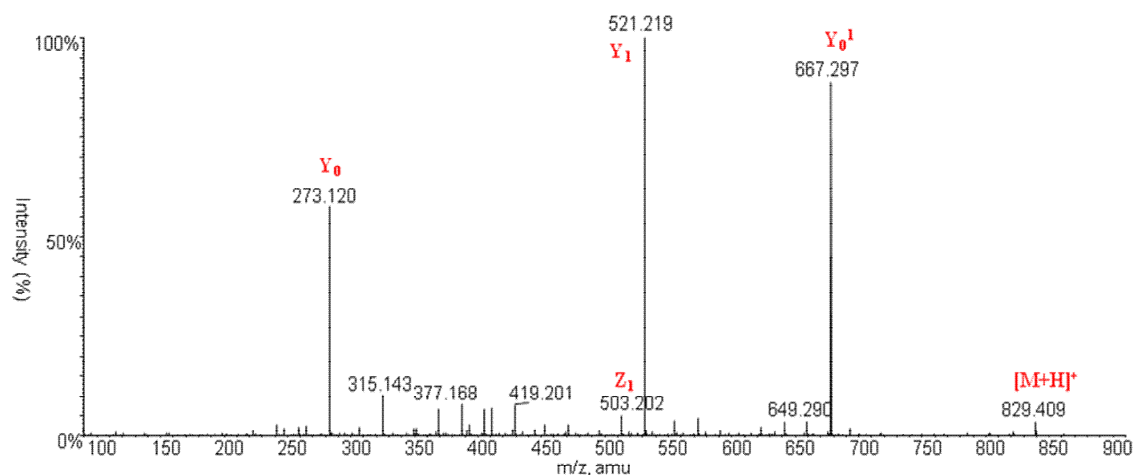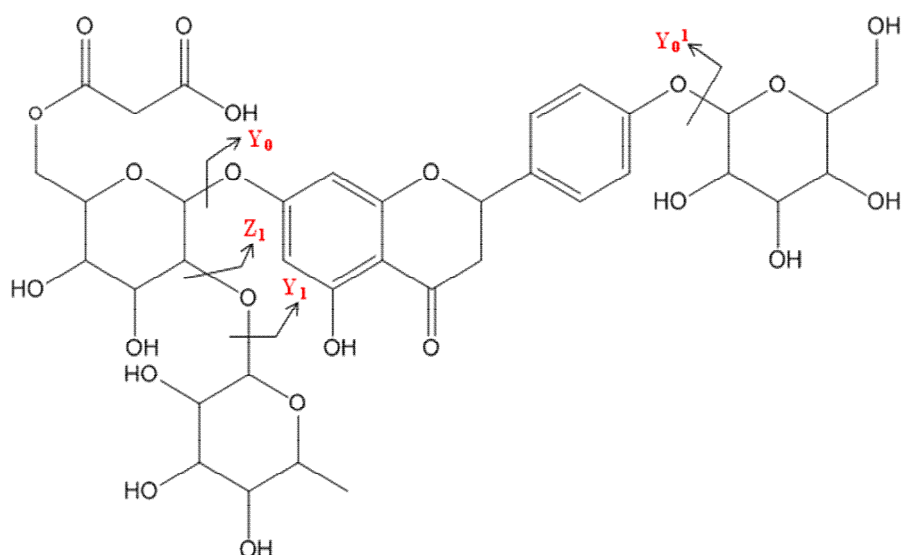
Figure 20: *A) positive ion mode MS/MS of the species at m/z 829 and B) the purposed structure.*

Tandem mass spectrometry experiments were performed also in negative ion mode (Figure 21): for instance, in the case of the species at m/z 827 (the third compound isolated in this study), the loss of $-CO_2$ from the quasi-molecolar ion [M-H]$^-$ was observed, generating the fragment at m/z 783; the loss of the one of the rhamnose (162 amu) instead origins the fragment at m/z 621 (Y_0^1) as well as the C-O bond breaking with the loss of the malonyl moiety origins the fragment at m/z 579. Further, the ion at m/z 271 was assigned as Y_0, the aglycone and the fragment at m/z 501 was assigned as Z_1. This MS/MS spectrum was acquired at low collision energy (20 ev) and when the same parent ion was fragmented using higher collision energy (up to 50 ev) only two main fragments were highlighted: the quasi-molecular ion

disappeared and the fragment generated by the CO_2 loss was the first mass detected. All the other fragments still were observed.
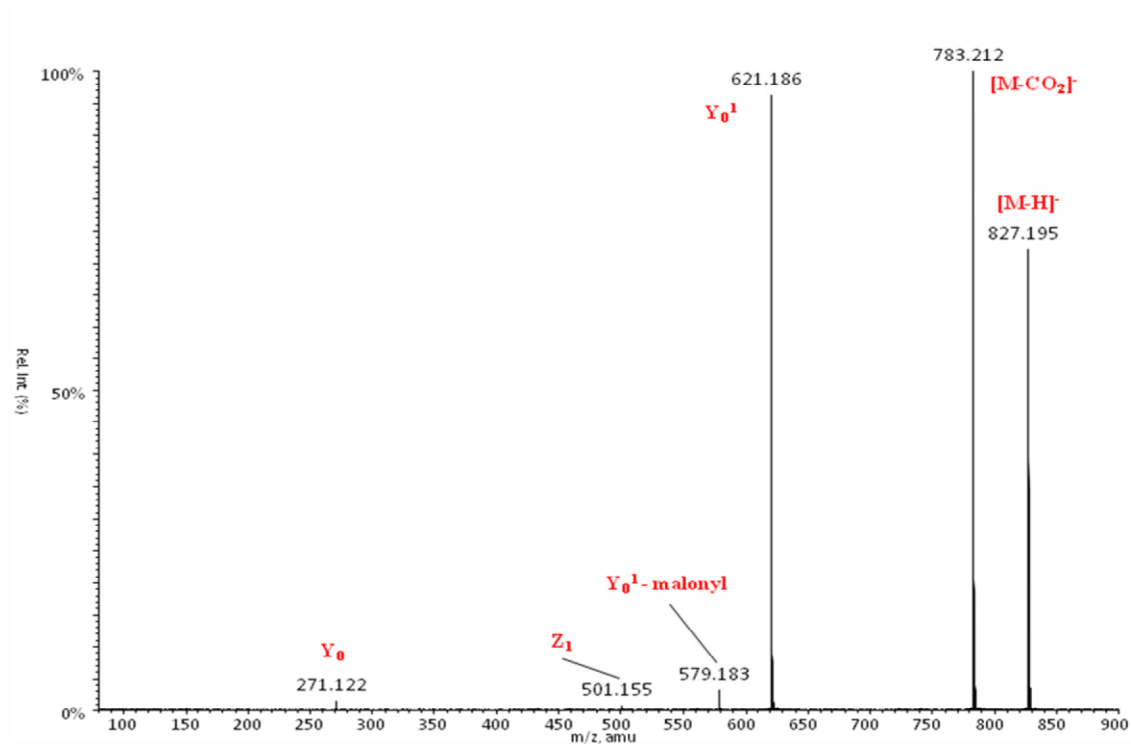
Figure 21: *A) negative ion mode MS/MS of the species at m/z 829.*

Discussion

Mass spectrometry appears as a perfect investigative tool for the elucidation and the chemical and structural characterization of natural compounds isolated from complex mixtures such as foods. In particular, the use of high resolution measurements coupled with the tandem mass spectrometry is an unchangeable approach for the study of foods composition. The investigation of *Citrus Grandis* add new clues to the challenge of citrus investigators because is one of the three citrus that generate all the others. The molecular composition of most of the citrus fruits is already known; anyway, there are still challenges especially with the lower abundant compounds. Advanced in sample processing and sample preparation for mass analysis give now the possibility to investigate also parts of the fruits that were not possible to analyze in the past. Further, the use of separation technique such as chromatography, in particular in the semi-preparative mode, allows investigators to isolate and collect semi-purified fractions of compounds (often unknown) at a specific molecular weight. These procedures coupled with spectroscopic analysis (e.g. NMR) allow for a complete and accurate characterization of molecular features. This is extremely

important for the evaluation of candidate pharmaceutical compounds from natural products, since it is proved the activity of such molecules (e.g. flavonoids).

Flavonoids health properties as well as their important role in many diets are already known. This study was focused to the optimization of chromatographic and MS methods for a faster and accurate characterization of unknown structures from complex mixtures. The use of the fast HPLC separation as well as of high mass measurements of collected fractions give the possibility to obtain many important information on the phenolic composition of different parts of the pummelo fruit. Further, the tandem mass spectrometry and the interpretation of the MS/MS spectra in either positive and negative ion modes, allowed to clarify the structures of di- and tri-glycosilated flavonols. Finally, the confirmation of the internal or external position of the glycanic part of the molecule, obtained using NMR after collection of semi-purified fraction by semi-preparative chromatography, completed and validated the identification.

Actually, three unknown compounds were completely elucidated in their structure but the optimized MS methods as well as the sample preparation and the semi-purification procedures, seems able to further investigate lower abundant compounds present in the citrus fruits. The ability of semi-preparative chromatography (coupled with a mass analyzer) to collect many milligrams of a molecular feature at a specific molecular weight give rise the availability of a semi-purified compound for further investigation. This appears as an easy, fast and cheap way to obtain a relative amount of a flavonoid to make some in vitro/in vivo tests for pharmacological property evaluation.

The use of a mass spectrometry based approach in the workflow of this thesis work open the road for the evaluation of the health properties of natural products as food for new pharmacological uses.

Detection of Isomeric Dioleyl Glycerides by Ion Mobility Mass Spectrometry. A Modern Approach to the Evaluation of Olive Oil Aging.

The isomerisation of 1,2 to 1,3 dioleyl glycerides is a marker of aging of olive oil.[58] [31]P magnetic resonance measurements allow the evaluation of the relative ratio of the two isomers as a function of time.[59] The two isomers are hardly to be distinguished by mass spectrometry and, even if suitable ionization method could be exploited, the isobaricity of the two glycerides poses problems when the analysis has to be performed on real samples. The ideal approach should consider the determination of the DAGs isomeric ratio without any chemical modification and chromatographic separation. According to the different mobility of isobaric ions, ion mobility mass spectrometry (IM-MS) allowed the separation of previously unresolvable isobaric ions in complex mixtures such as olive oil. Different Italian olive oil cultivars (carolea, cassanese, coratina) were analyzed.[60] A diacylglycerol molecule (DAG) was identified and separated by drift time.

The project was focused to the investigation of fresh pressed extra virgin olive oil from different cultivars to use diacylglycerol (DAG) isomers ratio as a parameter of the olive oil ageing. Structural isomers show

atoms and functional groups joined together in different ways. Basically, two isobaric molecules show the same molecular weight and the same molecular formula but different positions of the bond with a substituent (e.g., a carbon chain, a functional group). Most of the isobaric DAGs molecules are already known in the literature of extra virgin olive oils; anyway, this work was focused to distinguish isobaric DAGs using ion mobility separation. Extra virgin olive oil is a complex mixture which shows 1,2-1,3 isomers mixture of DAG compounds; the 1,2 isomer is not so stable and tends to isomerize in the 1,3 isomer (Figure 22).

1,2-DAG   1,3-DAG
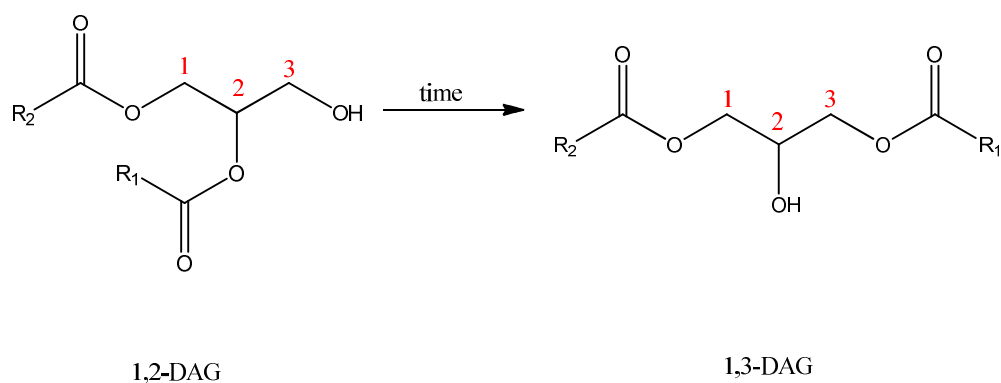
Figure 22: *scheme of DAGs 1,2/1,3 isomerization occurring during the olive oil aging.*

So, the isomers ratio changes over time and measuring that should be possible follow the ageing of the oil. Many research labs are working to measure the olive oil ageing through the 1,2-1,3 isomers ratio, using ^{31}P NMR for instance or using MS^3 experiments. The proposal of this project was to reach the same target using ion mobility mass spectrometry (IM-MS) bypassing chromatography or other separation techniques.

Results

Signals arising from analyzed samples, 1,2-1,3-dioleate mixture and extra virgin olive oils, were baseline-resolved on the basis of the ion mobility separation. The first step of the project was to optimize the MS method for the investigation of small molecules in the mass range 300-1500 Da. Further, in order to optimize the MS method for ion mobility separation of small isobaric molecules such as lipids, a mixture of diolein standard isomers was analyzed by MALDI (Figure 23). The diolein standard mixture was first analyzed by MALDI and then by ESI in positive ion mode. Results were observed using both sources, so we decide to use for the real sample the electro spray ionization because in the case of the sample preparation for MALDI analysis the sample, once spotted onto the conductive plate, needs to dry before to be submitted into the mass spectrometer. Further, we decide to use the ESI source because of the matrix clusters that are detected in the mass range of interest and can cause also ion suppression.
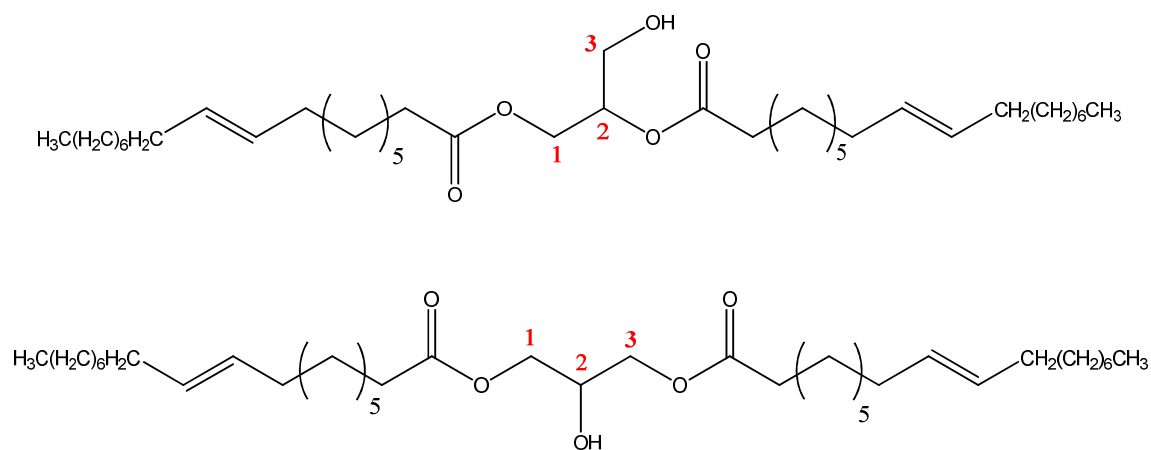
Figure 23: diolein glycerol-*1,2-1,3-dioleate standard.*

The diolein ionized using MALDI as source was observed as sodium adduct (m/z 643) (Figure 24). The IM-MS instrument was able to separate the diolein mix standard according to the different mobility in space (space related to the drift region) (Figure 25).
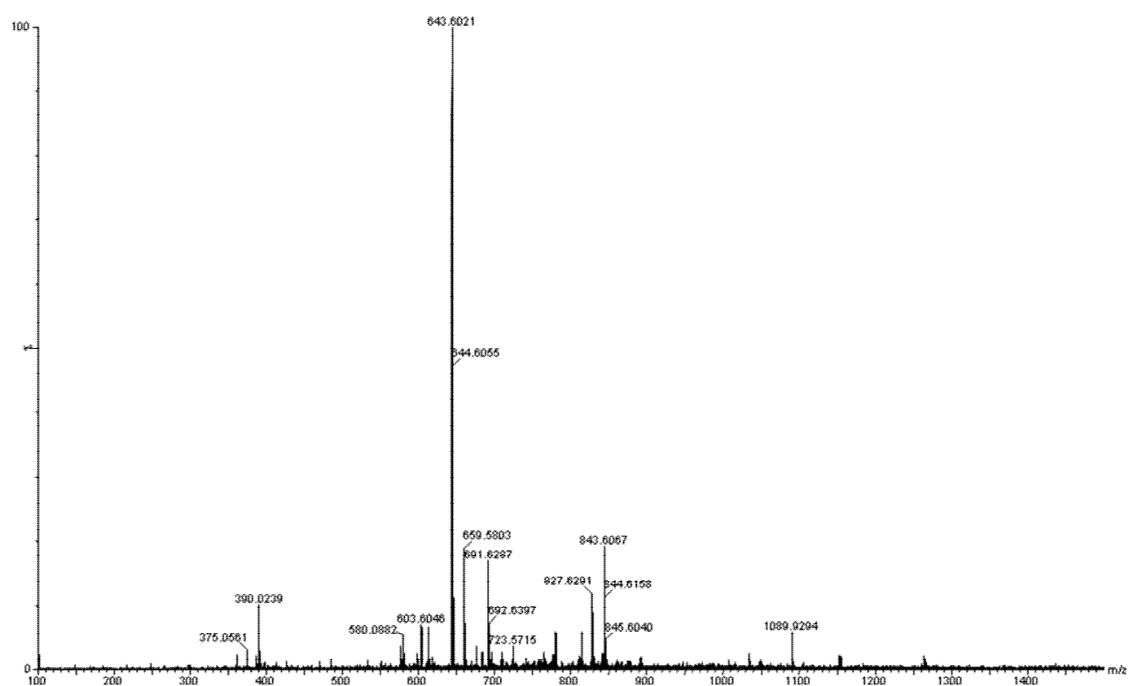
Figure 24: *diolein standard mix MS MALDI full scan. Diolein was observed as sodium adduct The standard was prepared at a concentration of 1000 ppm.*
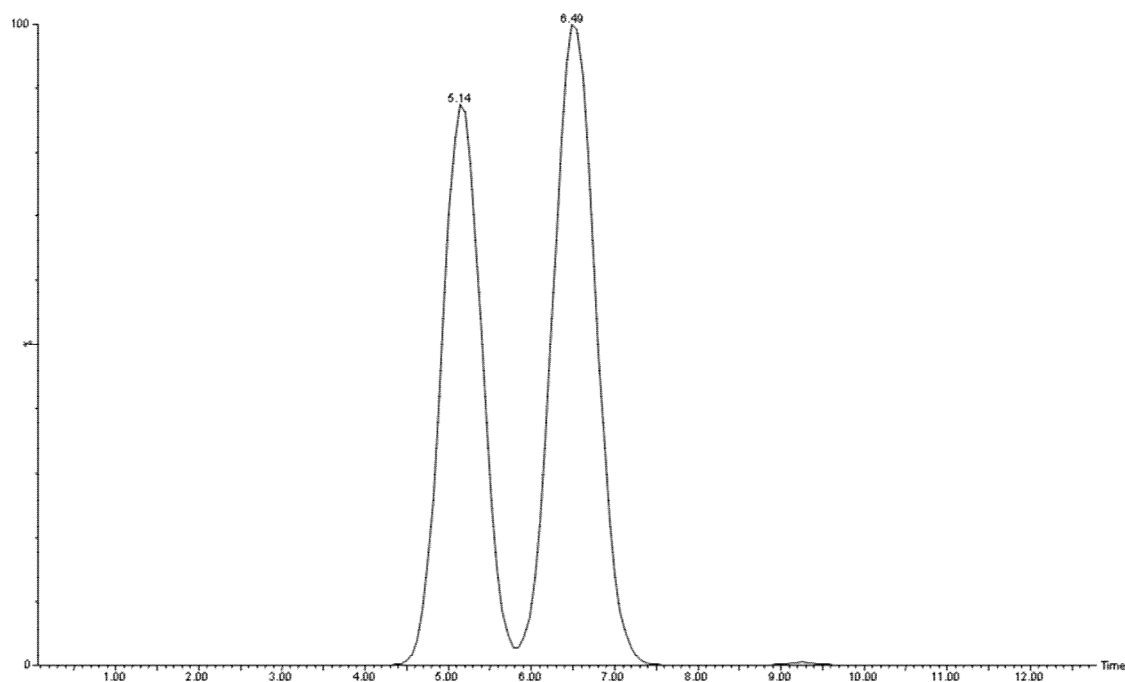
Figure 25: *diolein standard mix drift chromatogram highlighting a different mobility for the dioleins isomers. The two isobars ions.were separated in the mobility space.*
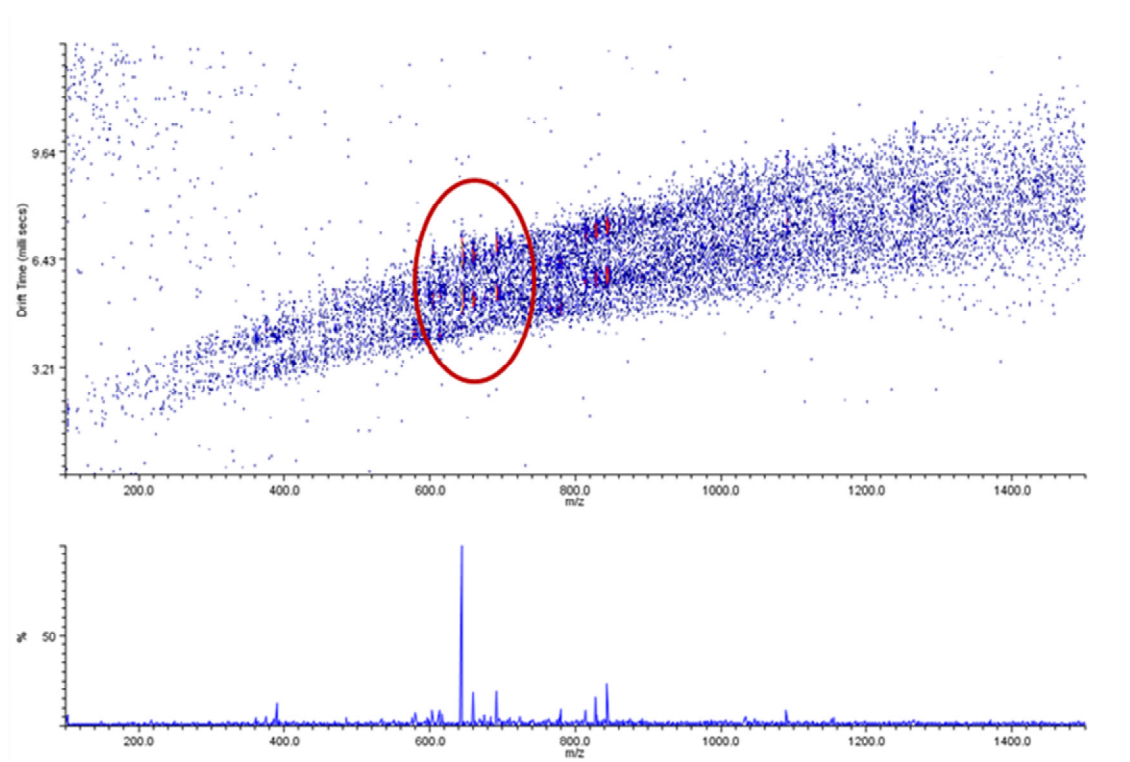
Figure 26: *two dimensional drift time chromatogram displaying the separation of the dioleiin standard isomers.*

Basically, the diolein mix highlighted a different drift time for the ion at m/z 643: flying through the drift tube this ion was separated into two signals that were detected in the drift chromatogram with two different drift times (Figure 25 & 26). Once the IM-MS method was optimized, the next step of this project was to apply this ion mobility approach on a real sample, such as a extra virgin olive oil. The sample was prepared as described in the *Materials and Methods* section bypassing chromatography and other separation techniques; so, the sample was directly injected in the mass spectrometer using the ESI as source operating in positive polarity. N=3 olive oil cultivars, carolea, cassanese and coratina, with a different age were analyzed. Thus, the presence of DAG isomers was expected. When the extra virgin olive oil was injected into the IM-MS instrument, an ion at m/z 643 was observed in the MS full scan of each cultivar; the latter ion was assigned as a DAG molecule (Figure 27) loading the high mass accuracy meauserd mass into LipidMaps web database and then validated by tandem mass spectrometry experiment. IM-MS allowed drift time separation of the DAG ion in carolea and coratina cultivars (Figure 28). Cassanese cultivar showed the ion at m/z 643 only at DT (drift time) 4.44 ms while carolea and coratina displayed the same ion separated into two peaks: the signal at DT 4.88 ms was observe in both culivars as well as other signals were detected at DT 3.66 ms (carolea) and 6.81 (coratina). So, these finding suggested that according the literature (olive oil aging connected with the DAG isomers ratio), the three analyzed samples (differentially aged) highlight a DAG molecule present in two isomers.
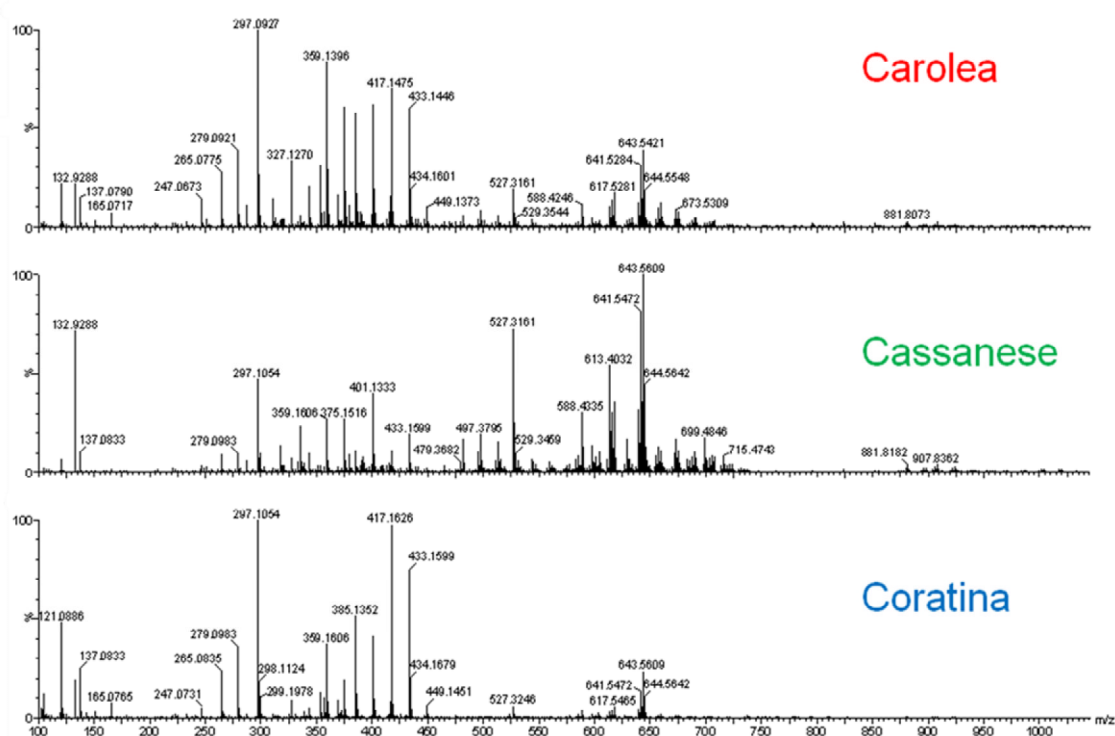
Figure 27: *ESI positive ion mode MS full scan of three olive oil cultivars. The analysis were forcute on the lipid species at m/z 643 identified as a DAG.*
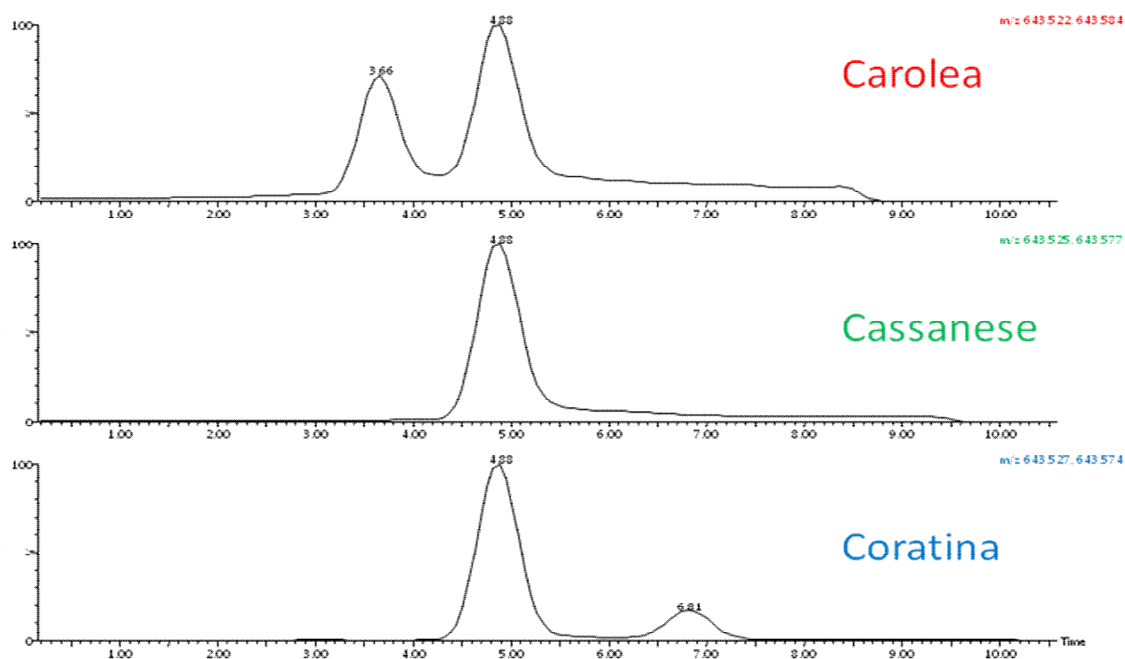
Figure 28: *DT chromatogram of the species at m/z 643, a DAG, observed in three different aged olive oil cultivars. The separation of the m/z 643 species into two peaks in coratina and carolea cultivars suggested the presence of two DAG isomers. The analyzed samples had a different age.*
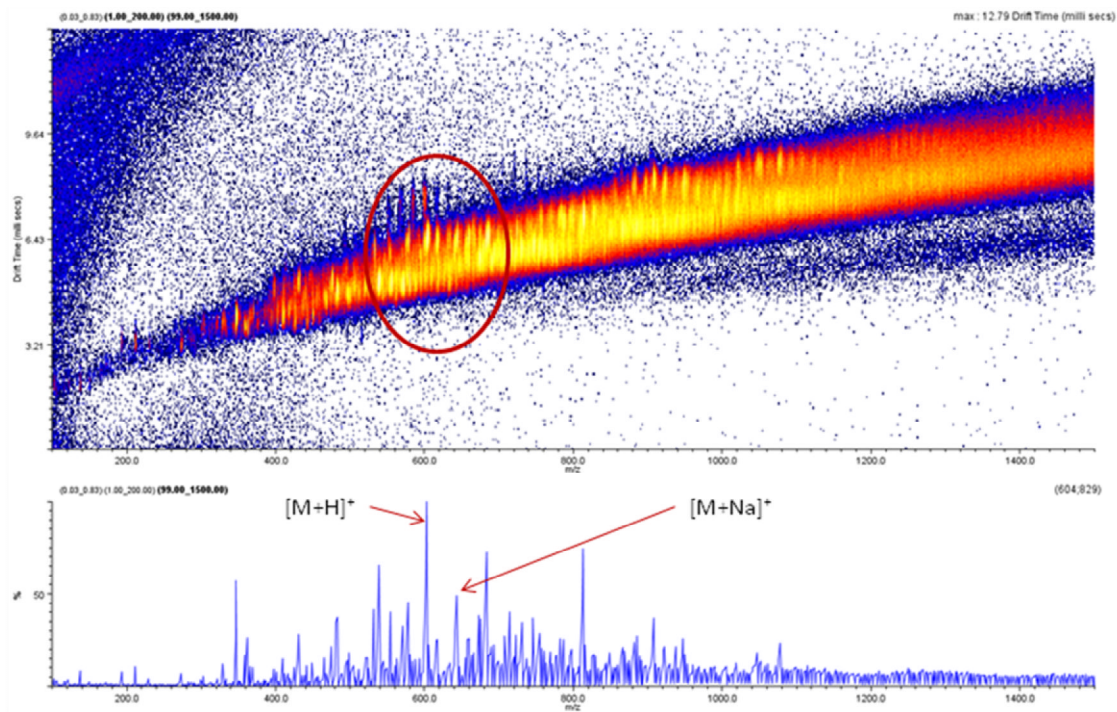
Figure 29: *two dimensional DT chromatogram displaying the separtion of the DAGs isomers (m/z 621 [M+H]$^+$ and m/z 643 [M+Na]$^+$) within the extra virgin olive oil mixture, carolea clutivar.*

Discussion

The IM-MS approach for the separation of isobaric molecules is not new; it is newer the application of this powerful technology to the complex mixture such as extra virgin olive oil. Most of the time, working on complex mixtures such as food or generally vegetables, there are many issues occurring in the sample preparation. Usually, several steps are needed for selective extraction, purification and separation of molecules of interest as well as of particular molecular classes (e.g. phenolic compounds, polar or non-polar molecules). One of the aim of this study was to try to use the real sample without any purification; that why the extra virgin olive oil was just added of an organic solvent and the centrifuged before the injection into the mass spectrometer. Furthermore, also the IM-MS method appear as faster and more accurate than other technologies such as NMR. Ion mobility separation was obtained in few minutes, once all the parameters for the drift region flight were optimized.

In conclusion, the combination of ion mobility and mass spectrometry offers a rapid method for the analysis of small molecules in which many isobars are separated in the mobility space before mass analysis. This combination brings new perspectives to the study of complex mixture. IM-MS method appears able to discern signals from isobaric ions in olive oil samples. Different aged olive oil samples were analyzed: two of them showed a DAG molecule with a different drift time. The last one showed just one isomer. Future study could consider a larger number of cultivars and a screening of the same olive oil sample every 2 weeks for instance in order to monitor the isomers ration on time.

References

1. Willibald Schliemann, Barbara Kolbe, Jurgen Schmidt, Manfred Nimtz, Victor Wray, Accumulation of apocarotenoids in mycorrhizal roots of leek (Allium porrum), *Phytochemistry*, **2008**, 69, 1680–1688.

2. A.J. Parr, G.P. Bolwell, *J. Agric. Food Chem.*, **2000**, 80, 985–1012.

3. Herve' De Clercq, Dirk Peusens, Isabel Roldan-Ruiz, Erik Van Bockstaele, Causal relationships between inbreeding, seed characteristics and plantperformance in leek (*Allium porrum* L.), *Euphytica*, **2003**, 134: 103–115.

4. Pablo Hirschegger, Jernej Jakše, Peter Trontelj, Borut Bohanec, Origins of Allium ampeloprasum horticultural groups and a molecular phylogeny of the section Allium (Allium: Alliaceae), *Molecular Phylogenetics and Evolution*, **2009**, xxx, xxx–xxx.

5. Hanelt, P., Schultze-Motel, J., Fritsch, R., Kruse, J., Maass, H., Ohle, H., Pistrick, K., **1992**, Infrageneric Grouping of Allium — The Gatersleben approach. In: Hanelt, P., Hammer, K., Knupffer, H. (Eds.), *The Genus Allium — Taxonomic Problems and Genetic Resources*, IPK, Gatersleben, Germany, 107–123.

6. Mathew, B., **1996**. A Review of Allium section Allium. Royal Botanic Gardens, Kew, Richmond, Surrey, UK. pp. 1–176.

7. Stearn, W.T., 1992. How many species of Allium are known? Kew Magazine 9, 180–182.

8. Pier-Giorgio Pietta, Flavonoids as Antioxidants, *J. Nat. Prod.*, **2000**, *63,* 1035-1042.

9. Ilja CW Arts and Peter CH Hollman, Polyphenols and disease risk in epidemiologic studies, *Am J Clin Nutr*, **2005**, 81(suppl):317S–25S.

10. Higdon JV, Frei B. Tea catechins and polyphenols: health effects, metabolism, and antioxidant functions. *Crit Rev Food Sci Nutr*, **2003**, 43: 89–143.

11. Adlercreutz H, Mazur W. Phyto-oestrogens and Western diseases. *Ann Med*, **1997**, 29:95–120.

12. World Cancer Research Fund. Vegetables and fruits. In Food, nutrition and the prevention of cancer: a global perspective. Washington, DC, *World Cancer Research Fund/American Institute for Cancer Research*, **1997**:436–46.

13. Law MR, Morris JK. By how much does fruit and vegetable consumptionreduce the risk of ischaemic heart disease?, *Eur J Clin Nutr*, **1998**; 52:549 –56.

14. G.A. Fista, J.G. Bloukas, A.S. Siomos, Effect of leek and onion on processing and quality characteristics of Greek traditional sausages, *Meat Science*, **2004**, 68, 163–172.

15. Fattorusso E., Lanzotti V., Taglialatela-Scafati O., Cicala C., The flavonoids of leek, Allium Porrum, *Phytochemistry*, **2001**, 57, 565-569.

16. DuPont, S.M.; Mondin, Z. *J. Agric. Food Chem*. **2000**, *48*, 3957.

17. Filip Cuyckens and Magda Claeys, Mass spectrometry in the structural analysis of flavonoids, *J. Mass Spectrom.* **2004**; 39: 1–15.

18. Di Donna L., Mazzotti F., Salerno R., Tagarelli A., Taverna D. and Sindona G., Characterization of new phenolic compounds from leaves of Olea europea L. by high

resolution tandem mass spectrometry, *Rapid Commun. Mass Spectrom*, **2007**, 21: 3653-3657.

19. De Nino A., Di Donna L., Mazzotti F., Muzzalupo E., Perri E. & Sindona G., Absolute method for the assay of oleuropein in olive oils by Atmospheric pressure chemical ionization tandem mass spectrometry, *Analytical Chemistry*, **2007**, 77, 18, 5961-5964.

20. Di Donna L., Mazzotti F., Napoli A., Salerno R., Sajjad A. & Sindona G., Secondary metabolism of olive secoiridoids. New microcomponents detected in drupes by electrospray ionization and high-resolution tandem mass spectrometry, *Rapid Commun. Mass Spectrom.*, **2007**, 3, 21, 273-278.

21. Di Donna L., De Nino A., Maiuolo L., Mazzotti F., Napoli A., Salerno R. & Sindona G., High-throughput mass spectrometry: the mechanism of sudan azo dye fragmentation by ESI tandem mass spectrometry and estensive deuterium labeling experiments, *J. Mass Spectrom.*, **2007**, 42, 1057-1061.

22. Domon B., Costello CE., A Systematic Nomenclature for Carbohydtrate Fragmentations in FAB-MS/MS Spectra of Glycoconjugates, *Glycoconjugates J*, **1988**, 5, 397, 409.

23. Hirota, A., Morimitsu, Y., & Hojo, H., New antioxidative indophenol reducing phenol compounds isolated from the Mortierella sp. Fungus., *Bioscience Biochemistry*, **1997**, 61, 647–650.

24. Yen, G. C., & Lee, C. A., Antioxidant activity of extracts from Molds, *Journal of Food Protection*, **1996**, 59(12), 1327–1330.

25. Wang, H., Cao, G., & Rrior, R. L., Total antioxidant capacity of fruits, *Journal of Agricultural and Food Chemistry*, **1996**, 44, 701–705.

26. Bocco, A., Cuvelier, M. E., Richard, H., & Berset, C., Antioxidant activity and phenolic compound composition of citrus peel and seed extracts, *Journal of Agricultural and Food Chemistry*, **1998**, 46, 2123–2129.

27. Mokbel M. S., Hashinaga F., Evaluation of the antioxidant activity of extracts from butan (Citrus grandis Osbeck) fruit tissue, *Food Chemistry*, **2006**, 94, 529-534.

28. Di Matteo, V., & Esposito, E., Biochemical and therapeutic effects of antioxidants in the treatment of Alzheimer's disease, Parkinson's disease, and amyotrophic lateral sclerosis, *Current Drug Targets-CNS and Neurological Disorder*, **2003**, 2, 95–107.

29. Gerber, M., Boutron-Ruault, M. C., Hercberg, S., Riboli, E., Scalbert, A., & Siess, M. H., Food and cancer: State of the art about the protective effect of fruits and vegetables, *Bulletin du Cancer*, **2002**, 89, 293–312.

30. Kris-Etherton, P. M., Hecker, K. D., Bonanome, A., Coval, S. M., Binkoski, A. E., Hilpert, K. F., et al., Bioactive compounds in foods: Their role in the prevention of cardiovascular disease and cancer, *American Journal of Medicine*, **2002**, 113(Suppl. 9B), 71S–88S.

31. Saskia, A. B. E., Van Acker, S., Van de Berg, D., Tromp, M., Griffoen, D., Van Bennekom, W., et al., Structural aspect of antioxidant activity of flavonoids, *Free Radical Biology and Medicine*, **1996**, 3, 331–342.

32. Soong, Y. Y., & Barlow, P. J, Antioxidant activity and phenolic content of selected fruit seeds, *Food Chemistry*, **2004**, 88, 411–417.

33. Wang, H., Cao, G., & Prior, R. L., Oxygen radical absorbing capacity of anthocyanins, *Journal of Agricultural and Food Chemistry*, **1997**, 45, 304–309.

34. Cao, G., Sofic, E., & Prior, R. L., Antioxidant and pro-oxidant behavior of flavonoids: Structure activity relationships, *Free Radical Biology and Medicine*, **1997**, 22, 749–760.

35. Havsteen, B. H., The biochemistry and medical significance of the flavonoids, *Pharmacology and Therapeutics*, **2002**, 96, 67–202.

36. Jang H. D., Chang K. S., Chang T. C., Hsu C. L., Antioxidant potentials of butan pumelo (Citrus Grandis Osbeck) and its ethanolic and acetified fermentation product, *Food Chemistry*, **2010**, 118, 554-558.

37. Bors W., Michel C., & Stettmaier K., Antioxidant effects of flavonoids, *Biofactors*, **1997**, 6, 399–402.

38. Larrauri, J. A., Ruperez, P., & Calixto, F. S., Antioxidant activity of wine pomace, *American Journal of Enology and Viticulture*, **1996**, 47, 369–372.

39. Elisa Tripoli, Maurizio La Guardia, Santo Giammanco, Danila Di Majo, Marco Giammanco, Citrus flavonoids: Molecular structure, biological activity and nutritional properties: A review, *Food Chemistry*, **2007***, 104, 466–479.

40. Calabrese, Francesco: Origin and history. In: Dugo, Giovanni & Di Giacomo, Angelo (eds.) (**2002**): Citrus. Taylor & Francis. ISBN 0-415-28491-0

41. Andrews, A.C. (**1961**): Acclimatization of citrus fruits in the Mediterranean region. *Agricultural History* **35**(1): 35-46.

42. A. Ortufio, D. Garcia-Puig, M. D. Fuster, M. L. Perez, F. Sabater, I. Porras, A. Garcia-Lidbn,S and J. A. Del Riot, Flavanone and Nootkatone Levels in Different Varieties of Grapefruit and Pummelo, *J. Agric. Food Chem.*, **1995,** Vol. 43, No. 1.

43. Yoichi NogT, Koji Sakamoto, et al., Flavonoid Composition of Fruit Tissues of citrus Species, *Biosci. Biotechnol. Biochem.*, **2006,** 70 (1), 178-192.

44. Zia-ur-Rehman, Citrus peel extract – A natural source of antioxidant, *Food Chemistry*, **2006**, 99, 450–454.

45. Matook Saif Mokbel á Toshihiko Suganuma, Antioxidant and antimicrobial activities of the methanol extracts from pummelo (Citrus grandis Osbeck) fruit albedo tissues, *Eur Food Res Technol*, **2006**, 224: 39–47.

46. Guddadarangavvanahally K. Jayaprakasha, Basavaraj Girennavar, Bhimanagouda S. Patil, Antioxidant capacity of pummelo and navel oranges: Extraction efficiency of solvents in sequence, **2008**, *LWT* 41, 376–384.

47. Lorenzo Camarda, Vita Di Stefano, Sergio Fatta Del Bosco, Domenico Schillaci, Antiproliferative activity of Citrus juices and HPLC evaluation of their flavonoid composition, *Fitoterapia*, **2007**, 78, 426–429.

48. Devinder Singh, Kanwaljit Chopra, The effect of naringin, a bioflavonoid on ischemia-reperfusion induced renal injury in rats, *Pharmacological Research*, **2004**, 50, 187–193.

49. Kyoung-Cheol, F., Chan-Shick, K., Nam, H. L., Sam-pin, Lee, & Doo-Khil, M., Determination of b-cryptoxanthin in peel and flesh of citrus fruits produced in Cheju Island. *Food Science and Biotechnology*, **2000**, 9(5), 288–291.

50. Gorinstain S., Huang D., et al., Determination of naringin and hesperidin in citrus fruit by high-performance liquid chromatography. The antioxidant potential of citrus fruit, *Acta Chromatographica*, **2006**, No.17, 108-...

51. Di Donna L., Mazzotti F., Salerno R., Tagarelli A., Taverna D. and Sindona G., Characterization of new phenolic compounds from leaves of Olea europea L. by high resolution tandem mass spectrometry, *Rapid Commun. Mass Spectrom*, **2007**, 21: 3653-3657.

52. Di Donna L., Mazzotti F., Napoli A., Salerno R., Sajjad A. & Sindona G., Secondary metabolism of olive secoiridoids. New microcomponents detected in drupes by electrospray ionization and high-resolution tandem mass spectrometry, *Rapid Commun. Mass Spectrom.*, **2007**, 3, 21, 273-278.

53. De Nino A., Di Donna L., Mazzotti F., Muzzalupo E., Perri E. & Sindona G., Absolute method for the assay of oleuropein in olive oils by Atmospheric pressure chemical ionization tandem mass spectrometry, *Analytical Chemistry*, **2007**, 77, 18, 5961-5964.

54. Leonardo Di Donna, Giuseppina De Luca, Fabio Mazzotti, Anna Napoli, Raffaele Salerno, Domenico Taverna, and Giovanni Sindona, Statin-like Principles of Bergamot Fruit (*Citrus bergamia*): Isolation of 3 Hydroxymethylglutaryl Flavonoid Glycosides, *J. Nat. Prod.,* **2009**, *72,* 1352–1354.

55. Peiying Shi, Qing He, Yue Song, Haibin Qu, Yiyu Cheng, Characterization and identification of isomeric flavonoid *O*-diglycosides from genus *Citrus* in negative electrospray ionization by ion trap mass spectrometry and time-of-flight mass spectrometry, *Analytica Chimica Acta*, **2007**, 598, 110–118.

56. Berhow M. A., Bennet R.D., Kanes K., Poling M. and Vandercook C.E., A malonic ester derivate of naringin grapefruit, *Phytochemistry*, **1991**, 30, 12, 4198-4200.

57. Filip Cuyckens and Magda Claeys, Mass spectrometry in the structural analysis of flavonoids, *J. Mass Spectrom.*, **2004**, 39: 1–15.

58. Perez-Camino M.C. Et al., J. Agric. Food Chem., 2001, 49, 699-704.

59. Fronimaki P et al, J. Agric. Food Chem., 2002, 50, 2207-2213.

60. Di Donna et al., Rapid Commun. Mass Spectrom., 2007, 21 (22), 3653-7.

Section 1

Chapter 3

Food as a Source of Pharmacological Interest Compounds

Materials and Methods

82

Structural Characterization of Phenolic Compounds in Allium Porrum by High Resolution Tandem Mass Spectrometry.

Chemicals

Allium porrum plants as well as endive plants were organic and purchased from a local grocery store in Cosenza (Calabria, ITALY). HPLC grade solvents were purchased from Carlo Erba (Rodano, Italy): methanol, ultra pure water, petroleum ether. Formic acid (99%) was purchased from Sigma Aldrich (Milan, ITALY). Sodium carbonate for basic hydrolysis reactions was purchased from Sigma Aldrich (Milan, ITALY). HPLC filters (0.45 µm) were instead purchased from Supelco (Sigma Aldrich, Milan, ITALY).

Sample Preparation

Plants were collected near Cosenza (Italy) in September/October 2008, then stored in -20° C freezer. Leek is made at least of two parts: the bulb and green leaves. Both parts were processed but our study was focused on the investigation of the leaves contents. The latter were cut in small parts and homogenized by vortex. Fresh leaves (500 gr) were extracted at room temperature by methanol. The resulting extract was stirred for 15 min and then place in an ultrasonic bath for 15 min at room temperature. After centrifugation and filtration into a buchner funnel, the extract was concentrated under vacuum on a rotary evaporator. The sample was washed by petroleum ether and finally dried under vacuum on a rotary evaporator. The residue was re-dissolved in 1 ml solvent (H_2O/MeOH, 1:1 v/v) to be ready for HPLC analysis . Prior to be submitted in the LC/MS instrument for chromatography separation and fraction collection, the solution was centrifuged again and then filtered by a 0.45 µm HPLC filter. The same extraction method was used to obtain the standard compound from *Coarse Fresee (Endive)*.

Separation of Microcomponents

Fractions containing each unknown compound of interest were collected using a FractionLynx semi-preparative HPLC system (Waters Corporation, Milford, MA, USA) composed of a autosampler/collector (Waters 2767 sample manager), a 600E pump working in both analytical and preparative mode, a 486 UV detector and a ZMD mass spectrometer equipped with an ESI source. The instrument was operating in positive polarity. The separation was performed using a 250 x 4.6 mm 5mm reversed-phase C18 Luna-Phenomenex column at a flow rate of 1 mL/min. The run time was 90min and the gradient was built using 0.1% HCOOH in water (solvent A) and methanol (MeOH) (solvent B) as eluting phase. The solvent run

was composed by the following steps: isocratic 80% A for 10min; linear gradient from 80% A to 74% A in 2min; linear gradient from 74% A to 31% A in 65min; isocratic 50% A for 8min; linear gradient from 31% A to 80% A in 18min; equilibration of the column for 10 min. The MS conditions were as follows: capillary voltage 3.15 kV, cone voltage 7V, extractor 2V, RF lens 0.34 V, source block and desolvation temperature 120, 250℃, respectively, ion energy 0.5V, LM resolution 14.5, HM resolution 15.0 and multiplier 650 V. The nebulizer gas was set to 650 L/h.

The semi-preparative chromatography was performed by the same equipment; a Synergy Fusion RP 80Å, 100 x 21.20 mm, 4µm column was used; the isocratic run time was performed in 15 min using a mobile phase made of 75% H_2O, HCOOH and 25% ACN.

High Resolution MS and MS/MS Experiments

The high resolution MS experiments were carried out using an hybrid Q-Star Pulsar-i (AB Sciex, Toronto, Canada) mass spectrometer, equipped with an ion spray source. Samples were introduced by direct infusion (5µL/min) of the solution coming from the HPLC separation at the optimum ion spray voltage of 4800 V. The nitrogen gas flow was set at 30 psi and the declustering and the focusing potentials were kept at 70 and 140V relative to ground, respectively. MS/MS experiments were performed in the collision cell q on the isotopically pure (^{12}C) peak of the selected precursor ions by keeping the first quadrupole analyzer at unit resolution, and scanning the time-of-flight (TOF) analyzer. The collision energy was set to between 20 and 50 eV, for each compound, while the gas pressure of the collision chamber was regulated at the instrumental parameters CAD 5, which corresponds to a pressure of the chamber of 6.86 x 10^{-3} Torr and a gas thickness of 9.55 x 10^{15} molecules/cm^2. All the acquisitions were averaged over 60 scans at a TOF resolving power of 8000. The molecular formula was evaluated by means of Analyst^{TM} QS software (AB Sciex). Tandem mass spectrometry experiments were also performed in negative ion mode using the same setup.

Hydrolysis Reactions

In order to further validate the findings from the high resolution measurements as well as from the MS/MS experiments, basic hydrolysis reactions were performed on the collected fraction of the unknown molecules of interest. The basic hydrolysis was carried out using sodium carbonate saturated solution. The sample was stored at room temperature in the dark for 48 hours. The reaction was monitored every 30 min by direct injection in the mass spectrometer until was complete.

Citruis Grandis Glycosilated Flavonoids Structural Characterization by High Resolution Tandem Mass Spectrometry.

Chemicals

HPLC grade solvents, methanol, ethanol, chloroform, were purchased from Carlo Erba (Rodano, Italy). Flavonoids standard (naringin, rhoifolin and rutin) and formic acid were purchased from Sigma-Aldrich (Milan, ITALY). C_{18} Reversed phase cartridges for SPE were purchased from Supelco (Sigma Aldrich, Milan, ITALY). Citrus Grandis fruit were purchased from a local graucery store.

Sample Preparation

Albedo tissue was removed and residuals parts were homogenized by vortex in a solution containing methanol, ethanol and chloroform (65% MeOH, 25% EtOH, 10% $CHCl_3$). The resulting extract, after centrifugation and filtration, was concentrated under vacuum on a rotary evaporator to reach a volume of 10 ml. Next step was very important to obtain a rapid purification and preconcentration of flavonoids. Solid phase extraction was used, with C_{18} reversed phase material: the sample was poured on a C_{18} cartridge, previously activated with water, and washed by water to remove sugars and then by methanol to recover flavonoids. The collected fraction was dried and used for LC/UV/MS analysis. Before to submit the resulting solution in the instrument, the sample was again centrifuged and the supernatant was injected into the mass spectrometer.

Separation of Microcomponents by HPLC/MS

The collected fractions containing each compound were obtained using a Fractionlynx semi-preparative HPLC system (Waters Corporation, Milford, MA, USA) composed of a autosampler/collector Waters 2767 sample manager, a 600E pump working in analytical mode, a 486 UV detector and a ZMD mass spectrometer equipped with an ESI source. The separation was performed using a 250 x 4.6mm 5mm reversed-phase C18 Luna-Phenomenex column at a flow rate of 1 mL/min. The run time was 115 min and the gradient was built using 0.1% HCOOH in water (solvent A) and methanol (MeOH) (solvent B) as eluting phase. The solvent run was composed by the following steps: isocratic 80% A for 10min; linear gradient from 80% A to 74% A in 2min; linear gradient from 74% A to 31% A in 65min; isocratic 50% A for 8min; linear gradient from 31% A to 80%A in 18min; equilibration of the column for 12 min. The MS conditions were as follows: Capillary voltage 3.15 kV, cone voltage 7V, extractor 2V, RF lens 0.34 V, source block and desolvation temperature 120, 250℃, respectively, ion energy 0.5V, LM resolution 14.5,

HM resolution 15.0 and multiplier 650 V. The nebulizer gas was set to 650 L/h. Concentration and collection of the single ion fractions were performed by semi-preparative column Synergy Fusion RP 80Å, 100 x 21.20 mm, 4μm, in the following operating conditions: the isocratic run time was performed in 15 min using a mobile phase made of 75% H_2O, HCOOH and 25% ACN.

High Resolution MS and MS/MS Experiments

The high-resolution ESI experiments were carried out in a hybrid Q-Star Pulsar-i (MDS Sciex Applied Biosystems, Toronto, Canada) mass spectrometer equipped with an ion spray ionization source. Samples were introduced by direct infusion (5μL/min) of the solution coming from the HPLC separation at the optimum ion spray voltage of 4800 V. The nitrogen gas flow was set at 30 psi and the declustering and the focusing potentials were kept at 70 and 140V relative to ground, respectively. MS/MS experiments were performed in the collision cell *q* on the isotopically pure (^{12}C) peak of the selected precursor ions by keeping the first quadrupole analyzer at unit resolution, and scanning the time-of-flight (TOF) analyzer. The collision energy was set between 20 and 50 eV, for each compound, while the gas pressure of the collision chamber was regulated at the instrumental parameters CAD 5, which corresponds to a pressure of the chamber of 6.86 x 10^{-3} Torr and a gas thickness of 9.55 x 10^{15} molecules/cm^2. All the acquisitions were averaged over 60 scans at a TOF resolving power of 8000. The molecular formula was evaluated by means of Analyst^{TM} QS software (MDS-Sciex).

Flavonoids Nomenclature

The nomenclature proposed by Domon and Costello for glycoconjugates was adopted to denote the product ions.[1] Ions containing the aglycone are labeled *k,lXj, Yj* and *Zj*, where *j* is the number of the interglycosidic bond broken, counted from the aglycone, and the superscripts *k* and *l* indicate the cleavages within the carbohydrate rings. The glycosidic bond linking the glycan part to the aglycone is numbered 0.

Detection of Isomeric Dioleyl Glycerides by Ion Mobility Mass Spectrometry. A Modern Approach to the Evaluation of Olive Oil Aging.

Materials and Chemicals

Diolein standard, 1,2-1,3 dioleate (dioleoyl glycerol) were purchased from Sigma Aldrich. HPLC grade solvents were purchased from Fluka. MALDI matrices tryhydroxyactophenone (THAP) and dihydroxybenzoic acid (DHB) were purchased from Across Organics. Lipid standard for intstrumental calibration were purchased from Avanti.

Sample Preparation

A solution containing a diolein, glycerol-1,2-and-1,3-dioleate, was prepared in chloroform in order to reach the concentration of 1000 ppm (stock solution) and mixed by 2,4,6-tryhydroxyacetophenone (THAP) {10 mg/ml in 50% chloroform (aq.) and 0.1% TFA } for MALDI MS analysis.
Extra virgin olive oil (300 mg) was prepared mixed by ethanol, stirred and centrifuged. The supernatant was mixed 1:1 with 2,5-dihydroxy benzoic acid (DHB) {10 mg/ml in 50% acetonitrile (aq.) and 0.1% TFA} for MALDI MS analysis and directly injected in the mass spectrometer for ESI analysis.

Ion Mobility Spectrometer

All measurements were performed using an Ion Mobility mass spectrometer (Waters, Synapt G1), with both MALDI and ESI sources in positive ion mode.
MALDI MS setup: the cooling gas was set at 4.80 ml/h; the collision energy was set at 6.0 for the trap and 4.0 for the transfer; the TOF detector was set at 1650 and the LM resolution for the resolving quadrupole at 12.0; the trap DC entrance was set at 5.0 while the bias at 22.0; the IMS DC entrance was set at 5.0 as well as the exit at 2.0; the transfer DC was set for both entrance and exit at 2.0. Th e IMS wave velocity was set at 300 m/s while the wave height at 10.0 V. The mobility trapping was set for the trap height at 10.0 V and for the extract height at 5.0 V.
ESI MS setup: the IMS wave velocity was set at 200 m/s and the wave height at 8.0 V.

References

1- Domon B and Costrello CE, *A Systematic Nomenclature for Carbohydrate Fragmentations in FAB-MS/MS Spectra of Glycoconjugates*, Glycoconjugate J, **1988**, 5, 397-409.

88

Section 2

Chapter 1

Imaging Mass Spectrometry Applications on Human Skin Ulcers

An Introduction

Skin Ulcers as Social and Economic Problem

Cutaneous ulcers currently affect 6.5 million patients in the United States.[1] The problems associated with chronic wounds are large in scope imposing physical, psychosocial and economic burdens on patients, while piling up tremendous economic cost.[2] Many issues in health care are related to these kind of wounds because they are very hard to prevent (Figure 1). By definition, chronic wounds are those that fail to progress through the expected stages of healing (hemostasis, inflammation, proliferation, remodeling) and instead enter a state of prolonged inflammation (Figure 2). In February 2007 the National Pressure Ulcer Advisory Panel (NPUAP) has redefined the definition of a pressure ulcer and the stages of pressure ulcers, including the original 4 stages and adding 2 stages on deep tissue injury and unstageable pressure ulcers.[3] This work is the culmination of over 5 years of work beginning with the identification of deep tissue injury in 2001. The staging system was defined by Shea in 1975 and provides a name to the amount of anatomical tissue loss. The original definitions were confusing to many clinicians and lead to inaccurate staging of ulcers associated or due to perineal dermatitis and those due to deep tissue injury. The proposed definitions were refined by the NPUAP with input from an on-line evaluation of their face validity, accuracy clarity, succinctness, utility, and discrimination. This process was completed online and provided input to the Panel for continued work. The proposed final definitions were reviewed by a consensus conference and their comments were used to create the final definitions.[3]

What's a Pressure Ulcer

A pressure ulcer is localized injury to the skin and/or underlying tissue usually over a bony prominence, as a result of pressure, or pressure in combination with shear and/or friction. A number of contributing or confounding factors are also associated with pressure ulcers; the significance of these factors is yet to be elucidated.

Pressure Ulcer Stages

Suspected Deep Tissue Injury

Purple or maroon localized area of discolored intact skin or blood-filled blister due to damage of underlying soft tissue from pressure and/or shear. The area may be preceded by tissue that is painful, firm, mushy, boggy, warmer or cooler as compared to adjacent tissue. Deep tissue injury may be difficult to detect in individuals with dark skin tones. Evolution may include a thin blister over a dark wound bed. The wound may further evolve and become covered by thin eschar. Evolution may be rapid exposing additional layers of tissue even with optimal treatment.

Stage I

Intact skin with non-blanchable redness of a localized area usually over a bony prominence.
Darkly pigmented skin may not have visible blanching; its color may differ from the surrounding

area. The area may be painful, firm, soft, warmer or cooler as compared to adjacent tissue. Stage I may be difficult to detect in individuals with dark skin tones. May indicate "at risk" person, a heralding sign of risk.

Stage II

Partial thickness loss of dermis presenting as a shallow open ulcer with a red pink wound bed, without slough. May also present as an intact or open/ruptured serum-filled blister. Presents as a shiny or dry shallow ulcer without slough or bruising (bruising indicates suspected deep tissue injury). This stage should not be used to describe skin tears, tape burns, perineal dermatitis, maceration or excoriation.

Stage III

Full thickness tissue loss. Subcutaneous fat may be visible but bone, tendon or muscle are not exposed. Slough may be present but does not obscure the depth of tissue loss. May include undermining and tunneling. The depth of a stage III pressure ulcer varies by anatomical location. The bridge of the nose, ear, occiput and malleolus do not have subcutaneous tissue and stage III ulcers can be shallow. In contrast, areas of significant adiposity can develop extremely deep stage III pressure ulcers. Bone/tendon is not visible or directly palpable.

Stage IV

Full thickness tissue loss with exposed bone, tendon or muscle. Slough or eschar may be present on some parts of the wound bed. Often include undermining and tunneling. The depth of a stage IV pressure ulcer varies by anatomical location. The bridge of the nose, ear, occiput and malleolus do not have subcutaneous tissue and these ulcers can be shallow. Stage IV ulcers can extend into muscle and/or supporting structures (e.g., fascia, tendon or joint capsule) making osteomyelitis possible. Exposed bone/tendon is visible or directly palpable.

Unstageable

Full thickness tissue loss in which the base of the ulcer is covered by slough (yellow, tan, gray, green or brown) and/or eschar (tan, brown or black) in the wound bed. Until enough slough and/or eschar is removed to expose the base of the wound, the true depth, and therefore stage, cannot be determined. Stable (dry, adherent, intact without erythema or fluctuance) eschar on the heels serves as "the body's natural (biological) cover" and should not be removed.[3]

Chronic wounds comprise a large catch-all category that includes major types such as venous stasis wounds, diabetic wounds, and pressure ulcers as well as other minor catagories. Among these, pressure ulcers are the least studied and understood.
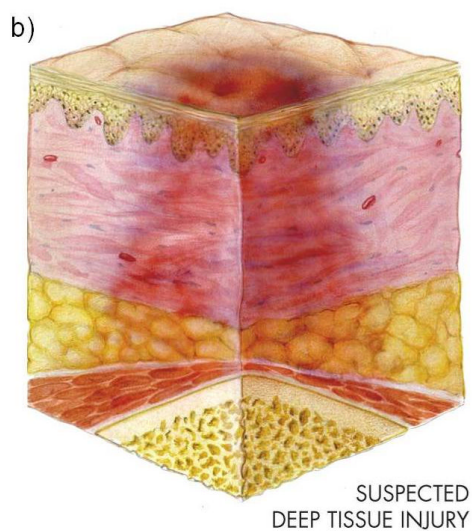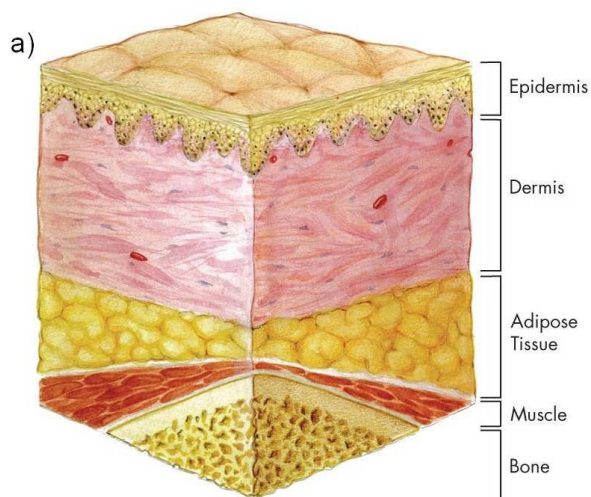
Figure 1: *representative scheme of human skin a) intact and b) suspected deep tissue injury; in particular, the latter highlights the beginning of the tissue inflammatory response due to many causative factors, e.g. co-morbidities often occurring in aged patients. Pictures from NPUAP, National Pressure Ulcer Advisory Panel.*

In the US population, a higher incidence of pressure ulcers has been reported in African-American patients as well as patients who are trapped by a low socio-economic status.[4,5] Chronic wounds rarely develop in individuals who are otherwise healthy, and chronic wound patients frequently suffer from co-morbidities such as obesity, diabetes and peripheral vascular disease.[1]
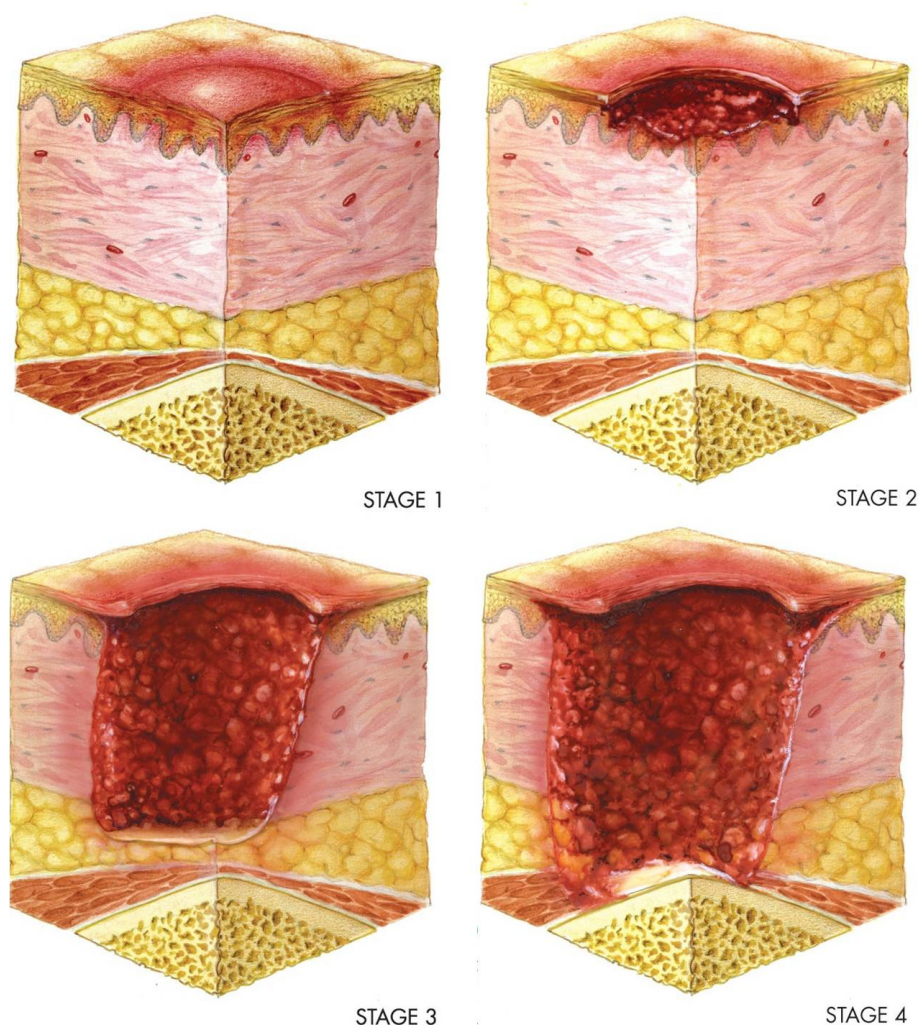
Figure 2: *skin pressure ulcers at different inflammatory stages; pictures from: NPUAP, National Pressure Ulcer Advisory Panel.*

Although Mustoe *et al*. proposed a unifying hypothesis of chronic wound pathogenesis based on four main causative factors (local tissue hypoxia, bacterial colonization, repetitive ischemia-reperfusion injury and altered stress responses in the aged patient)[6], these remain unproven hypotheses. The existing and sparse literature on chronic wounds has historically focused on single molecules or a single signaling pathway.[7-11] A recent global, proteomic analysis compared a wound fluid profile between an acute wound to a venous stasis ulcer and proposed several new biomarkers of chronic wound repair.[12] Nevertheless, the interplay between multifocal disturbances that concurrently maintain the chronic inflammatory dynamics within pressure ulcers remains unexplored. Currently wound care providers are limited by a paucity of diagnostic and prognostic indicators. Pressure ulcers are staged by crude visual impressions of wound depth. Moreover, the presence of a prominent eschar over the wound's surface often prevents any staging at all.

The determination as to whether a wound is remaining stagnant on a given therapeutic regime or is on the road to recovery is often based on longitudinal photographic measurements and guesswork. Thus lack of modern diagnostic tools and a paucity of scientific understanding of the molecular events within pressure ulcers has not produced breakthrough advancements. Meanwhile, proteomics has become a vital component for elucidating cellular processes in both health and disease in many other settings.[7,8] Advances in mass spectrometry (MS) have provided opportunities to examine molecular interactions within intact tissue while maintaining architectural features.[9] In particular, matrix assisted laser desorption/ionization (MALDI) imaging mass spectrometry (IMS) has allowed for analysis of the spatial distribution of proteins.[10] Such technology generates robust molecular-weight-specific data, requires no target-specific reagents (such as antibodies), can sample intact large proteins of 100 kDa or less, and uses simple and rapid sample preparation protocols.[11] The use of MALDI mass spectrometry makes it possible to simultaneously investigate hundreds of molecular species, especially those of higher molecular weight such as proteins, by depositing matrix on tissue sections. From a generic sample, hundreds of peptide and protein peaks are recorded in the mass spectrum produced from a single laser ablated area on the histologic specimen providing a quick and convenient tool in situations where spatial distribution is paramount.

Modern Proteomics

Understanding the complex nature of numerous interacting proteins in many diseases such as cancer is due in large part to the development of proteomics and proteomic technologies. Proteomics is the focused study of proteins, in particular their structure, function, and quantity on a global scale. The global expression of proteins within a cell determines nearly every behavior, function, and interaction within and in conjunction with other cells. In contrast to a static genome, the proteome is expressed differently from cell to cell and from time to time. In addition to this fluctuation, proteins range in size from a few kDa to several MDa and can differ by 6 orders of magnitude in concentration. A protein may further undergo any number of post-translational modifications (PTMs) or form complexes with other proteins which may dramatically alter its function. Clearly proteomics remains one of the most important and analytically challenging feats of our time.

Experimental procedures for large-scale global proteome analyses typically examine the difference in expression of hundreds of proteins between two or more biological states. The objective is to understand protein alterations resulting either directly or indirectly from a biologic process. Proteomic differences are expected to be present, for example, between benign and invasive disease, brains from Alzheimer's patients, as well as between native tissue and those exposed to pharmaceuticals or toxins. Proteins that differ between biological states can then be studied to understand the nature of a disease or the effect of a drug. In many cases, these differentially expressed proteins may become potential biomarker candidates and eventual therapeutic targets.

Proteomics is fundamentally reliant on the power of mass spectrometry (MS) for rapid and specific protein analysis. Mass spectrometry involves three basic components: ionization, mass separation, and detection. The gas-phase analyte, M, must be charged, typically via:

$$(1) \quad M + H^+ \rightarrow [M+H]^+ \text{ or } M + xH^+ \rightarrow [M+nH]^{n+}$$
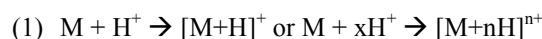
Electric and/or magnetic fields manipulate and separate ions by their mass-to-charge (*m/z*) ratio. Once separated, the ions are detected, typically by collision into an electron multiplier device. The result is a display of the measured intensity vs. the *m/z* value for all ions detected. Two ionization methods have revolutionized proteomics by allowing the direct soft ionization of large protein molecules and appropriately shared the Nobel Prize in chemistry in 2002. Electrospray ionization (ESI) and matrix-assisted laser desorption/ionization (MALDI) instruments are now the core of proteomics workflows.[13]

Current Proteomic Technologies

Large scale approaches to characterize the proteome generally fall under two categories, gel-based separation of intact proteins (pseudo top-down) and multidimensional liquid chromatography (LC) of digested proteins (bottom-up). Both of these technologies require the sample to be homogenized into a solution form, effectively removing any spatial information. Gel electrophoresis, which separates proteins by their molecular weight (MW) in 1-dimension or by their isoelectric point (pI) and MW in 2-dimensions, produces an easily visible map of the proteins in the sample. Protein "maps" are compared between biological states to find specific protein differences between groups.[14,15] Multiple samples can be labeled with fluorescent tags and analyzed simultaneously on a single gel using 2D difference in-gel electrophoresis (2D-DIGE).[16] Proteins contained in the spots are digested, extracted, and analyzed by LC-tandem MS or confirmed by immunoblotting. The clear advantage afforded is the ability to visualize a map of numerous intact proteins, and to then positively identify them. Multiplex and scaling complications keep 2D gel technology "low-throughput" and analysis of each protein spot, even when automated, can be both laborious and time consuming. In the other approach, liquid chromatography is extensively used to reduce the complexity of complex biological samples prior to MS analysis. In the "shotgun-proteomics" approach (also termed multidimensional protein identification technology MudPIT),[17] all of the extracted proteins are enzymatically digested together to form a more complex peptide mixture. The peptides are then separated in two dimensions, typically using strong cation/anion exchange (SCX/SAX) followed by reverse-phase (RP) LC. The eluent from the second separation goes directly into the mass spectrometer for peptide identification. While it may seem that initial digestion of the intact proteins further convolutes an already complex mixture, the speed at which this analysis can be done is much faster than for the 2D DIGE approach. Also, peptides are more easily separated and identified than intact proteins. This platform has been driven in large part by tremendous advances ion trap technology[18] and in the construction of genomic-based protein databases[19] and advanced algorithms to search and identify peptides and their precursor protein.[20] Comparison of biological states can be

accomplished by relative quantitation of peptides between separate analyses using spectral counting[21,22] or by direct comparison of isotopically labeled peptides, such as ICAT[23] or iTRAQ[24], from a single run. Despite the overwhelming strengths and its widespread use, bottom-up proteomics suffers from describing intact biologically active proteins, resulting in limited concrete evidence for intact protein character and function.

MALDI Imaging MS of Biological Tissues

Matrix-assisted laser desorption/ionization (MALDI) imaging mass spectrometry (IMS) of intact proteins records and combines proteomic data with location information directly from thin sections of biological samples.[25,26] The spatial integrity of the proteins within the biopsy section is maintained, allowing specific cellular regions to be analyzed. For the analysis, matrix is applied uniformly or in a discrete grid array across the tissue, Figure 3.

Figure 3. MALDI IMS process from tissue (a), coating with matrix (b), MS data acquisition at every x,y location (c), and image reconstruction from each ion (d).

*Adapted with permission from Cornett, et al. *Nature Methods* - **4**, 828 - 833 (2007)
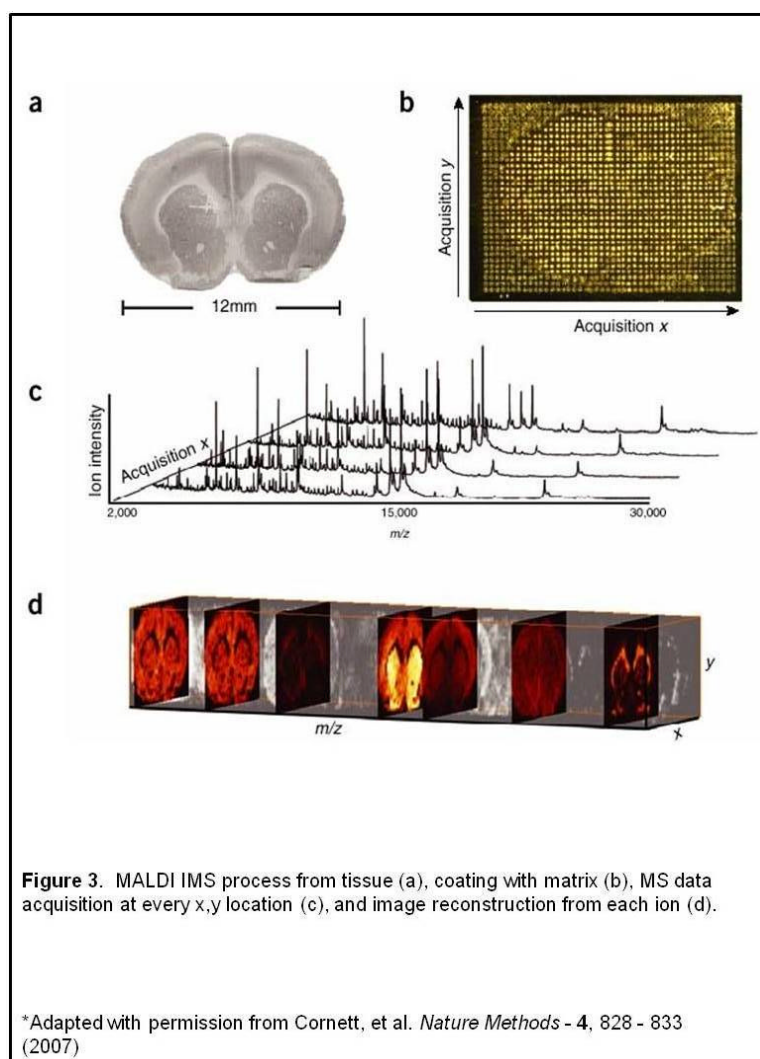
A laser irradiates the matrix and ionizes the proteins, generating 2 dimensional data containing both the proteins detected and the tissue location. The sampling positions become 'pixels' that are compiled to generate a picture or image for each molecule detected. Any given mass-to-charge (m/z) signal in the spectrum can be displayed with its relative intensity over the entire array, giving a density map of that compound in the array area. Hundreds of such pictures or images can be generated from a single acquisition experiment. MALDI IMS for proteomics has the benefit of 1) measuring intact proteins with high mass accuracy (typically better than 1 part in10,000), 2) measurement of intact proteins in their native, biologic state including PTM's, 3) *in-situ* analysis directly from tissue with location and cellular specific information and, 4) high sensitivity of intact proteins below 20 kDa (an area often overlooked in other proteomic analyses).

Figure 4. Histology directed MALDI IMS. A) An H&E breast tumor tissue is marked by a pathologist, using specific colors corresponding to particular cell/tissue types (B). (C) The marked H&E image is overlayed to a serial tissue section for MALDI analysis. (D) The marked coordinates are transferred to a robotic spotter for accurate, targeted matrix application.

*Adapted with permission from Cornett et al. *Mol Cell Proteomics*, 2006 Oct;5(10):1975-83.

MALDI IMS has been employed to generate ion density maps (images) of numerous detected analytes, including pharmecueticals[27-30], lipids[31], enzymatically cleaved proteins[32], and intact proteins[33-36]. This technology has also been used to identify biomarkers and classifiers for clinical diagnosis and potential

treatment of cancer[37], including lung cancer[38], gliomas[39], and breast cancer[40]. The technology has recently been adapted to accurately target small cellular regions within tissue biopsies, termed histology-directed IMS where a pathologist examines a histological stained tissue section to guide and confidently target the cellular regions of interest in an adjacent serial section of the biopsy, Figure 4.[41] In this way, the proteins from tumor foci or regions of adjacent "normal" tissue can be analyzed from each section, and necrotic, autolysis, connective tissue, and blood vessels can be avoided, so as not to unduly complicate the analysis.

MALDI TOF Fundamentals

Advances in interface technology have allowed MALDI and ESI sources to be coupled to virtually any mass analyzers, including quadrupole, ion trap, time-of-flight (TOF), Fourier transform ion cyclotron resonance (FT-ICR), and more recently orbitrap instruments. MALDI TOF composes the core of our MS workflow and is described here in some detail. Detailed descriptions of other MS configurations can be found here.*

Matrix-assisted laser desorption/ionization (MALDI) was developed from the work of Karas, Hillenkemp, and Tanaka during the late 1980's.[42,43] The technology uses a light absorbing molecule, or matrix, to desorb and ionize analytes, with relatively little fragmentation. An analyte is co-mixed with a solution of dissolved matrix, applied to a conductive target plate, and as the solution dries, the matrix forms a crystal lattice that incorporates the analyte. When the crystals are irradiated with a UV laser, the photons are absorbed by the crystals and the energy transformed into kinetic energy E_k. This energy conversion creates a matrix "plume" that converts the analyte into the gas phase and ionizes them, Figure 5.[44]

Suitable matrix molecules are often small, acidic aromatic compounds, such as the common 3,5-dimethyoxy-4-hydroxycinnamic acid (sinapinic acid, SA), α-cyano-4-hydroxycinnamic acid (CHCA), and 2,5-dihydroxybenzoic acid (DHB). The explosion from the MALDI process produces ions with a mix of kinetic energy, E_k. A small time delay (~200 ns) from the laser irradiation is applied, termed delayed extraction. When the extraction grid is activated and an electric field accelerates the ions, those farther from the source will receive a slightly lower push. The exact time delay is adjusted to spatially focus the ions on the detector. Ions are typically accelerated $\pm$20-25 kV into the TOF, Figure 3, which consists of a hollow field-free tube usually less than a meter in length.

The ion separation is a function of the basic principles of a charged particle in an electric field:

$$(1)\ E_p = q \cdot U$$

where E_p is the potential energy, q is the charge on the particle, and U is the strength of the electric field or voltage applied. With no hinderance on the ions, the poteintial energy is converted to kinetic, $E_p = E_k$, and is given by

$$(2)\ E_k = \frac{1}{2} \cdot m \cdot v^2$$

MALDI Plume

(a)
(b)

MALDI Ionization

Figure. 5. **Top:** Captured fluorescent images of the MALDI plume process at several time points post irradiation. **Bottom:** Description of the MALDI process. Matrix is mixed in excess of analyte. Laser irradiation creates a desorption and ionization process. During ionization, charged analyte ions are created, as well as charged matrix and matrix cluster ions. Many molecules remain neutral. The extraction grids move ions into the TOF for mass separation and detection.

*Top figure adapted with permission from *Chem. Rev.* **2003**, *103*, 395-425*

where *m* is the mass and *v* is the ion velocity, and by substitution becomes

$$(1) \quad q \cdot U = \frac{1}{2} \cdot m \cdot v^2$$

The ion velocity is the ratio of the length of the flight tube *d* and the flight time of the ion *t*, giving

$$(2) \quad v = \frac{d}{t}$$

And by substitution with equation (3),

$$(3) \quad q \cdot U = \frac{1}{2} \cdot m \cdot \left(\frac{d}{t}\right)^2$$

Solving for t, we obtain

$$(4) \quad t = d \cdot \sqrt{\frac{m}{2 \cdot q \cdot U}}$$

With d and U constant, a constant k simplifies equation (6) to

$$(5) \quad t = k \cdot \sqrt{\frac{m}{q}}$$

Thus, the flight time is inversely proportional to the mass and more specifically, to m/z (where q becomes z). Larger ions will have a longer flight time, and thus reach the detector after smaller ions. Modern MALDI instruments are incredibly fast, routinely acquiring 1000 or more spectra per second. Unlike ESI, MALDI produces almost exclusively singly charged ions, making spectral interpretation straightforward.

Imaging Mass Spectrometry Perspectives in Biology and Medicine

Understanding the molecular complexity found in both health and disease has driven research investigators to incorporate new tools and methodologies into their studies. One technology that continues to excel in this regard and enable discoveries at the molecular level is mass spectrometry (MS). In particular, one emerging field is imaging mass spectrometry (IMS), a technology that brings extraordinarily powerful capabilities to the research laboratory in that it allows images to be acquired at specific molecular weights. The early work on IMS goes back several decades with the utilization of a variety of different types of instruments to acquire images of elements and small molecules in biological specimens using secondary ion mass spectrometry (SIMS) and laser desorption ionization (LDI). One of the major advantages of SIMS is the ability to use a highly focused irradiating beam (0.1–10 microns diameter on target) to produce high resolution images in applications involving low molecular weight substances, such as drugs and metabolites, and for elemental analysis. Work with direct laser ablation techniques was also found to be useful for element and small molecule analyses using high pulse frequency lasers having target spot sizes of 1–30 microns in diameter. This technology has seen extensive use in the semi-conductor field. With the advent of MALDI, the field took a major leap forward because many molecular species were now amenable to the molecular imaging process, especially higher molecular weight species such as proteins. The first applications of MALDI MS for imaging demonstrated that signals for peptides and proteins could be obtained directly from tissues as well as other samples.

From such samples, hundreds of peptide and protein peaks can be recorded in the mass spectrum produced from a single laser ablated area on the sample of about 10–50 microns in diameter on target. Commonly, one can generate individual maps to verify the presence, molecular weight, and location of proteins that have been selected based on preliminary MS scans, 2-D gels, gene identification and sequencing, and other biochemical information. From the clinical perspective, recent advances in molecular biology and molecular technologies will have a profound impact on diagnostic pathology in the years to come. In addition to complete protein images, protein profiles (mass spectra taken from selected areas on the tissue) can be obtained from thin tissue sections. Archived tissue such as fresh frozen specimens or formalin fixed paraffin embedded (FFPE) tissue blocks may also be used to investigate the pathogenesis of human diseases. The latter involves sample preparation that includes an antigen retrieval step and proteolytic digestion with subsequent peptide identification for best results. To date, profiling and imaging MS has been applied to multiple diseased tissues, including human non-small cell lung tumors, gliomas, and breast tumors. Interrogation of the resulting complex MS data sets using modern bio-computational tools has resulted in identification of both disease-state and patient-prognosis specific protein patterns. These studies suggest that such proteomic information will become more and more important in assessing disease progression, prognosis and drug efficacy. Histology has been known for some time and its value is clear in the field of pathology. IMS brings a new dimension of molecular data, one focusing on the disease phenotype. Further, molecular information derived of this kind will be of critical importance to our understanding of molecular pathogenesis, improving therapeutic efficacy, and enhancing the quality of information that is provided to clinicians so as to markedly improve patient outcomes. One area of intense interest is the use of IMS to help define the molecular phenotypes expressed in cancer, particularly in comparing patterns in pre-lesions and tumors in human biopsies and animal models of lung, colorectal, breast, brain, skin, prostate, and ovarian cancers. Other human diseases also being studied by IMS include diabetes, Alzheimer's, Parkinsonism, schizophrenia, other neurodegenerative diseases, *Staphylococcus aureus* infections and immune system diseases, just to name a few. Protein patterns in differentiating cells are complex and shift rapidly, and new molecular tools are needed to identify not only the changes in these patterns, but also the specific proteins involved. These proteins represent potential disease-specific markers and possible drug targets. MS offers a unique high-accuracy molecular specificity that will be invaluable in understanding the molecular events in these and other investigations in both health and disease. The ability to image cells and tissues with molecular specificity will be of extraordinary benefit in such research investigations. Several papers address specific methods and protocol developments including analysis of FFPE tissues, targeted reagents for imaging, and disease biomarkers. Several papers are focused on biological applications such as bacterial peptides and proteins, proteins in neurodegenerative diseases and in healthy nervous tissue such as spinal cord, metabolomics, and bone mineralization. The ensemble of papers in this issue nicely reflects the focus of applications of MALDI MS, SIMS, and LD technologies to specific analytical tasks in biological and clinical areas. When taken together with other molecular analytical tools available today to research investigators in both biological and clinical applications, it is clear that IMS will play a strong complementary role in providing specific molecular information for the understanding of the underlying biology of health and disease.[45]

Recent MALDI IMS Developments

Several technological advances in recent years have dramatically improved the workflow, robustness, and image quality of MALDI IMS in matrix deposition, data acquisition, and image processing and analysis. Previously reported robotic deposition by a prototype acoustic spotter[46] was limited to ~200 μm lateral spot resolution. Current versions continuously move the target with constant droplet ejection, providing lateral resolution of 150 μm while reducing spotting time. Controlled mechanical spray deposition controls the humidity, measures matrix drying, and generates smaller droplets by advanced vibrational vaporization spray.[47] Further, matrix deposition by sublimation[48] coats an entire tissue with uniform sub micron crystals in less than 10 minutes, with images under 30 μm lateral resolution. Although sublimation is currently limited to endogenous lipid analysis, recrystallization of the coating is proving successful for higher mass analytes. Optimal protein analysis via MALDI has been limited to N_2 lasers and as a consequence, 20-50 Hz spectral acquisitions and 20 million shot lifetimes. Modulation of Nd:YAG lasers give comparable or superior protein spectra at laser speeds of 1 kHz and lifetimes of more than a billion laser shots.[49] Prototype instruments incorporating 5 kHz lasers are currently being investigated. In conjunction, image processing software integrates spectral processing, image processing, image visualization, and statistical analyses of image regions.[50] These advances combine to significantly improve the ease, quality, speed, and analysis of MALDI IMS. MALDI TOF IMS and the histology-directed MALDI IMS adaptation are here used as the proteomic technology to investigate the biology of skin pressure ulcers at stage IV.

References

1. Sen, C.K., et al., *Human skin wounds: a major and snowballing threat to public health and the economy.* Wound Repair Regen, **2009**. 17(6): p. 763-71.

2. Menke, N.B., et al., *Impaired wound healing.* Clin Dermatol, **2007**. 25(1): p. 19-25.

3. www.npuap.org , National Pressure Ulcer Advisory Panel.

4. Fogerty, M.D., et al., *Risk factors for pressure ulcers in acute care hospitals.* Wound Repair Regen, **2008**. 16(1): p. 11-8.

5. Fogerty, M., et al., *African Americans show increased risk for pressure ulcers: a retrospective analysis of acute care hospitals in America.* Wound Repair Regen, **2009**. 17(5): p. 678-84.

6. Mustoe, T.A., K. O'Shaughnessy, and O. Kloeters, *Chronic wound pathogenesis and current treatment strategies: a unifying hypothesis.* Plast Reconstr Surg, **2006**. 117(7 Suppl): p. 35S-41S.

7. Marko-Varga, G. and T.E. Fehniger, *Proteomics and disease--the challenges for technology and discovery.* J Proteome Res, **2004**. 3(2): p. 167-78.

8. Lescuyer, P., D. Hochstrasser, and T. Rabilloud, *How shall we use the proteomics toolbox for biomarker discovery?* J Proteome Res, **2007**. 6(9): p. 3371-6.

9. Caprioli, R.M., *Perspectives on imaging mass spectrometry in biology and medicine.* Proteomics, **2008**. 8(18): p. 3679-80.

10. Burnum, K.E.F., Sara L; Caprioli, Richard M, *Matrix-Assisted Laser Desorption/Ionization Imaging Mess Spectrometry for the Investigation of Proteins and Peptides.* Annual Review of Analytical Cahemistry, **2008**. 1: p. 689-705.

11. Hardesty, W.M. and R.M. Caprioli, *In situ molecular imaging of proteins in tissues using mass spectrometry.* Anal Bioanal Chem, **2008**. 391(3): p. 899-903.

12. Eming, S.A., et al., *Differential proteomic analysis distinguishes tissue repair biomarker signatures in wound exudates obtained from normal healing and chronic wounds.* J Proteome Res, **2010**.

13. Liebler, D. C., *Introduction to proteomics : tools for the new biology.* Humana Press: Totowa, NJ, **2002**; p ix, 198 p.

14. Friedman, D. B., et al., Isoelectric focusing and two-dimensional gel electrophoresis. *Methods Enzymol* **2009,** 463, 515-40.

15. Westermeier, R.; Schickle, H., The current state of the art in high-resolution two-dimensional electrophoresis. *Arch Physiol Biochem* **2009,** 115, (5), 279-85.

16. Unlu, M., et al., Difference gel electrophoresis: a single gel method for detecting changes in protein extracts. *Electrophoresis* **1997,** 18, (11), 2071-7.

17. Link, A. J., et al., Direct analysis of protein complexes using mass spectrometry. *Nat Biotechnol* **1999,** 17, (7), 676-82.

18. Schwartz, J. C., et al., A two-dimensional quadrupole ion trap mass spectrometer. *J Am Soc Mass Spectrom* **2002,** 13, (6), 659-69.

19. Perkins, D. N., et al., Probability-based protein identification by searching sequence databases using mass spectrometry data. *Electrophoresis* **1999,** 20, (18), 3551-67.

20. Tabb, D. L., et al., MyriMatch: highly accurate tandem mass spectral peptide identification by multivariate hypergeometric analysis. *J Proteome Res* **2007,** 6, (2), 654-61.

21. Gao, J., et al., Changes in the protein expression of yeast as a function of carbon source. *J Proteome Res* **2003,** 2, (6), 643-9.

22. Liu, H., et al., A model for random sampling and estimation of relative protein abundance in shotgun proteomics. *Anal Chem* **2004,** 76, (14), 4193-201.

23. Gygi, S. P., et al., Quantitative analysis of complex protein mixtures using isotope-coded affinity tags. *Nat Biotechnol* **1999,** 17, (10), 994-9.

24. Ross, P. L., et al., Multiplexed protein quantitation in Saccharomyces cerevisiae using amine-reactive isobaric tagging reagents. *Mol Cell Proteomics* **2004,** 3, (12), 1154-69.

25. Caprioli, R. M., et al., Molecular imaging of biological samples: localization of peptides and proteins using MALDI-TOF MS. *Anal Chem* **1997,** 69, (23), 4751-60.

26. Stoeckli, M., et al., Imaging mass spectrometry: a new technology for the analysis of protein expression in mammalian tissues. *Nat Med* **2001,** 7, (4), 493-6.

27. Khatib-Shahidi, S., et al., Direct molecular analysis of whole-body animal tissue sections by imaging MALDI mass spectrometry. *Anal Chem* **2006,** 78, (18), 6448-56.

28. Stoeckli, M., et al., Compound and metabolite distribution measured by MALDI mass spectrometric imaging in whole-body tissue sections. *International Journal of Mass Spectrometry* **2007,** 260, (2-3), 195-202.

29. Reyzer, M. L., et al., Direct analysis of drug candidates in tissue by matrix-assisted laser desorption/ionization mass spectrometry. *Journal of Mass Spectrometry* **2003,** 38, (10), 1081-1092.

30. Hsieh, Y., et al., Matrix-assisted laser desorption/ionization imaging mass spectrometry for direct measurement of clozapine in rat brain tissue. *Rapid Communications in Mass Spectrometry* **2006,** 20, (6), 965-972.

31. Puolitaival, S. M., et al., Solvent-free matrix dry-coating for MALDI imaging of phospholipids. *J Am Soc Mass Spectrom* **2008,** 19, (6), 882-6.

32. Groseclose, M. R., et al., Identification of proteins directly from tissue: in situ tryptic digestions coupled with imaging mass spectrometry. *J Mass Spectrom* **2007,** 42, (2), 254-62.

33. Burnum, K. E., et al., Imaging mass spectrometry reveals unique protein profiles during embryo implantation. *Endocrinology* **2008,** 149, (7), 3274-8.

34. Pierson, J., et al., Molecular profiling of experimental Parkinson's disease: direct analysis of peptides and proteins on brain tissue sections by MALDI mass spectrometry. *J Proteome Res* **2004,** 3, (2), 289-95.

35. Reyzer, M. L., et al., Early changes in protein expression detected by mass spectrometry predict tumor response to molecular therapeutics. *Cancer Res* **2004,** 64, (24), 9093-100.

36. Thibault, D. B., et al., MALDI tissue profiling of integral membrane proteins from ocular tissues. *J Am Soc Mass Spectrom* **2008,** 19, (6), 814-22.

37. Caprioli, R. M., Deciphering protein molecular signatures in cancer tissues to aid in diagnosis, prognosis, and therapy. *Cancer Res* **2005,** 65, (23), 10642-5.

38. Yanagisawa, K., et al., Proteomic patterns of tumour subsets in non-small-cell lung cancer. *Lancet* **2003,** 362, (9382), 433-9.

39. Schwartz, S. A., et al., Proteomic-based prognosis of brain tumor patients using direct-tissue matrix-assisted laser desorption ionization mass spectrometry. *Cancer Res* **2005,** 65, (17), 7674-81.

40. Sanders, M. E., et al., Differentiating proteomic biomarkers in breast cancer by laser capture microdissection and MALDI MS. *J Proteome Res* **2008,** 7, (4), 1500-7.

41. Cornett, D. S., et al., A novel histology-directed strategy for MALDI-MS tissue profiling that improves throughput and cellular specificity in human breast cancer. *Mol Cell Proteomics* **2006,** 5, (10), 1975-83.

42. Tanaka, K., et al., Protein and polymer analyses up to m/z 100 000 by laser ionization time-of-flight mass spectrometry. *Rapid Communications in Mass Spectrometry* **1988,** 2, (8), 151-153.

43. Karas, M.; Hillenkamp, F., Laser desorption ionization of proteins with molecular masses exceeding 10,000 daltons. *Anal Chem* **1988,** 60, (20), 2299-301.

44. Knochenmuss, R.; Zenobi, R., MALDI ionization: the role of in-plume processes. *Chem Rev* **2003,** 103, (2), 441-52.

45. Caprioli RM, Proteomics **2008**, *8,* 3679–3680.

46. Aerni, H. R., et al., Automated acoustic matrix deposition for MALDI sample preparation. *Anal Chem* **2006,** 78, (3), 827-34.

47. http://www.bdal.de/uploads/media/ImagePrep-2008-eBook.pdf

48. Hankin, J. A., et al., Sublimation as a method of matrix application for mass spectrometric imaging. *J Am Soc Mass Spectrom* **2007,** 18, (9), 1646-52.

49. Holle, A., et al., Optimizing UV laser focus profiles for improved MALDI performance. *J Mass Spectrom* **2006,** 41, (6), 705-16.

50. Stauber J et al., J *Proteome Res*, **2008**, 7 (3), 969-78.

Section 2

Chapter 2

Imaging Mass Spectrometry Applications on Human Skin Ulcers

Results and Discussion

Spatial mapping by Imaging Mass Spectrometry Offers Advancements for Rapid Definition of Human Skin Proteomic Signatures

Mass spectrometry (MS) has become an indispensable tool to detect and identify proteins in health and disease.[1-5] Proteomic approaches have proven useful for homogeneous *in vitro* studies with dermal fibroblasts or keratinocytes, but such techniques are not optimal for capturing global signatures within *in vivo* settings.[6, 7] In 2006, Huang *et al.* reported an *in vivo* mass spectrometry detection technique coupled with capillary ultrafiltration probes used to identify secreted proteins during murine wound healing.[8] Other reports applied 2D-DIGE technology to homogenized samples of scleroderma skin.[9, 10] At present, what is known of protein localization to specific cells of interest in skin is limited to indirect evidence from immunohistochemical staining within biopsies. MS technologies such as matrix-assisted laser desorption ionization (MALDI) imaging MS has high throughput potential[11, 12] and can generate many hundreds of protein-specific ion maps correlated with tissue architecture.[13-16] MALDI-IMS permits imaging of the tissue distribution for low molecular weight compounds such as metabolites.[17-20] Application of spatially retentive technologies allows for study of complex interaction between cells and their microenvironment at the molecular level, a type of systematic analysis particularly attractive for examination of the complex architecture in cutaneous samples.[15, 21-28] Additionally, MALDI MS offers the potential for detection of molecular species present in a single tissue section regardless of whether a given protein perturbation has been previously implicated or whether a specific antibody has been developed for its immunodetection. In combination with rapid advances in sample preparation[13, 15, 24, 29-31] and data processing[32, 33], IMS now offers the capability of a precise means of analyzing protein signatures within complex microenvironments that develop during pathophysiologic or pharmacologic modifications in skin diseases.[34, 35] The present study was designed to optimize MALDI techniques for the detection and definition of proteomic signatures in normal human epidermis and dermis. Two experimental approaches were employed: MALDI-MS profiling, where mass spectra were taken from discrete locations based on histology, and MALDI-IMS imaging, where complete molecular images were obtained at various MW values. In addition, proteins were identified by *in situ* tryptic digestion, sequence analysis of the fragment peptides, and protein database searching.

Results

Skin Protein Profiling/Imaging

A typical analysis of proteins directly from tissue follows two main experimental approaches: profiling and imaging. Profiling involves analysis of discrete areas of the tissue sections to enable comparisons between distinct areas on tissue sections, such as normal healthy area versus a diseased area, or between two different specimens. High-resolution imaging of a tissue section requires that the entire tissue section be analyzed from an ordered array of laser ablated spots in which spectra are acquired from those spots at

intervals that define the image resolution. Imaging software generates two-dimensional ion-maps, by plotting the intensity of signals obtained as a function of *xy* coordinates. This procedure allows for rapid assessment of protein localization and the visualization of the molecular differences between and among samples. To optimize skin-specific detection parameters, frozen sections were prepared from trunk skin removed from 3 male and 7 female adult patients who were undergoing elective surgery. Initial experiments were performed by MALDI MS in order to profile different areas of the tissue. Hematoxylin and eosin stained sections were used to determine histological coordinates for matrix application over the epidermis and dermis (Fig 1a). Visualization prior to spotting helped avoid matrix deposition over epidermal appendages such as pilosebaceous units or eccrine sweat glands that are dispersed throughout the dermis. Figures 1b & 1c show the same section before and after matrix deposition over the epidermis and dermis. We deposited 20 matrix spots per area in order to establish the protein pattern in these focal areas of interest.
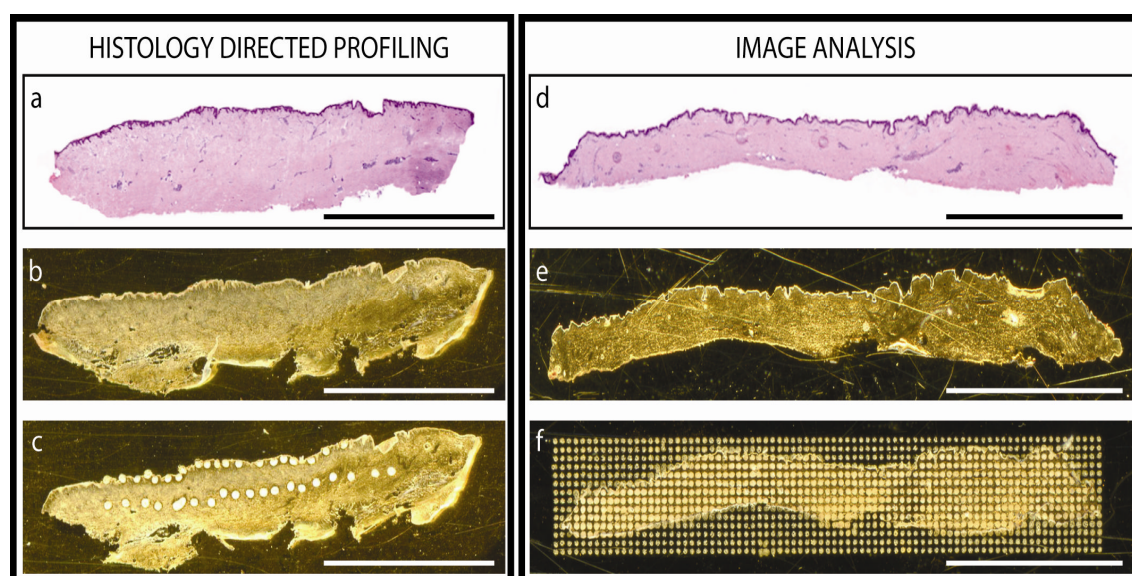
Figure 1: *a-c) illustrate a typical MALDI MS (profiling) experiment. a) shows hematoxylin and eosin staining of a normal human skin section b) shows the same tissue section mounted on a gold MALDI plate before and c) after matrix robotic deposition with 20 spots arrayed over the epidermis and 20 spots arrayed over the dermis. d-f) illustrated a typical MALDI IMS sample preparation d) shows hematoxylin and eosin staining of a different human skin section. e) shows a tissue section on a gold MALDI plate before and f) after a 200 μm spacing matrix was arrayed for IMS analysis. Scale bar = 5000 μm*

Figure 2 presents the protein profiles in the mass range from 2000 to 16,000 Da related to the epidermis (Fig 2a) and dermis (2b). In each set of data, differences were observed comparing the profiles obtained from the epidermis and dermis reflecting the expected expression differences between a stratified squamous keratinizing epithelium and the dense irregular connective tissue of the dermis. For example,

signals at m/z 10178, 11051, 11308 and 11607 were only observed in the epidermis (Fig 2a), whereas the signals at m/z 3369, 3440 and 5170 were only detected in the dermis (Fig 2b). Moreover, other peaks such as m/z 2936, 7767 and 8567 were found in both epidermis and dermis although with different expression levels. Dermal spectra showed fewer peaks than those from epidermis, especially in the high mass range (Fig 2b).
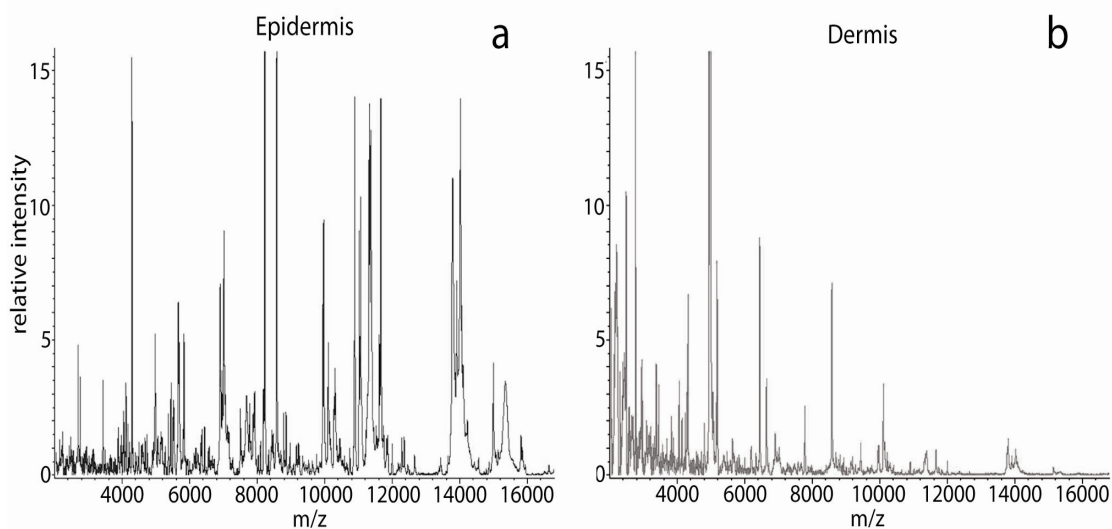
Figure 2: *averaged mass spectra from epidermis and dermis, a) profiled epidermis characteristic signals and b) profiled dermis characteristic signals. The mass spectra are averaged from 20 spots and are normalized to total ion current.*

Many dermal peaks were observed in the mass range 3-5 kDa, such as the signal at m/z 4965, the base peak of every spectrum acquired from the 20 spots deposited on the dermis of every sample. The dermis expressed many other characteristic peaks such as m/z 6432 and 6633 and also m/z 8772 and 8845. The comparison between protein profiles of the two main skin layers was carried out using averaged and normalized mass spectra in order to minimize spectrum-to-spectrum differences. Numerous protein peaks were consistently detected in both regions while others showed an apparent pattern of individuality. We attribute differences among inter-spot intensity to the sensitivity of MALDI MS that captures slightly variable tissue morphology from one dermal spot to another, i.e., one spot may be centered over an area with a high population of resident cells whereas another spot may center over a capillary endothelium and yet another spot over extracellular matrix molecules. Figures 1 e & f present optical images of a 12µm skin section mounted on a gold MALDI plate prior to and after matrix deposition for IMS analysis. We conducted preliminary matrix deposition tests and selected a 200 µm (center-to-center) pattern. Figure 3 presents a series of ion density maps or images from proteins, with different intensities, that were localized in different areas of the section.
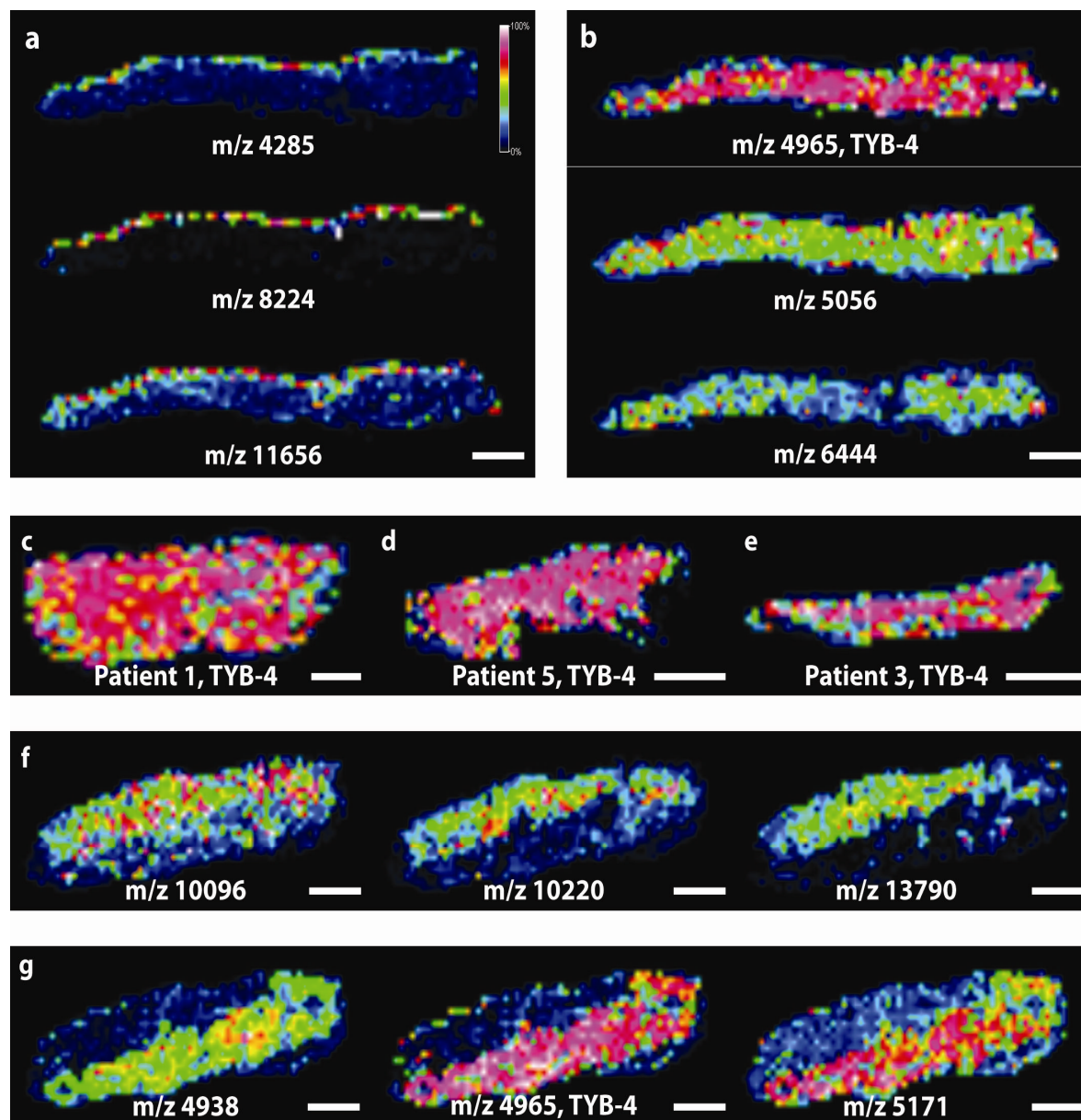
Figure 3: *illustrates a series of ion density maps from MALDI IMS. a) reveals 3 representative ions with a distribution of m/z consistent with an epidermal spatial distribution and b) reveals ions with a generalized spatial distribution throughout the dermis. c-e) show the ion density maps from 3 different patients illustrating the distribution for thymosin β-4 at m/z of 4965. f) shows ion density maps from a single patient depicting 3 m/z ions with selective spatial distribution restricted to the papillary dermis and g) ion density maps from the same patient showing site-specific distribution in the reticular dermis. Scale bar = 2000 μm*

Figure 3a shows three representative ion density maps over the epidermis related to the ions at m/z 4285, 8224 and 11,656, while Fig 3b depicts several ions with unique dermal distributions. Figure 3c-e shows

ion density maps for m/z 4965, corresponding to thymosin β-4 (TYB-4), distributed throughout the dermis in all the samples analyzed, as well as the ions at m/z 5056 and 6444. Further, IMS localized some signals, for example at m/z 10,096, 10,229 and 13,790, that were largely restricted to the upper papillary dermis (Fig 3f). Figure 3g depicts ions selectively concentrated in the reticular dermis at m/z 4938, 4965 and 5171. All 10 patients did not show this distinctive sub-localization pattern within the dermis (compare Fig 3g for m/z 4965 with Fig 3c-e). The reason of this patient-to-patient variability is not yet clear. On the basis of our IMS optimization and analysis of 10 normal patients, we found that the signal at m/z 4965 is a predominant protein in dermal regions while those at 8215, 8565 and 11,656 are uniquely expressed proteins in normal human epidermis.

Protein Identification on Tissue Sections Using *in situ* Tryptic Micro Digestion

We utilized an *in situ* tryptic micro digestion protocol to generate peptides directly on discrete areas of tissue for sequence analysis.[36, 37] Signal intensities of tryptic peptides are mediated by several factors, e.g. protein concentration differences, variation in enzymatic digestion efficiency and differences in desorption and ionization efficiencies. The protease hydrolysis step is essential to generate peptide fragments and enable identification directly from their specific location in the tissue. Peptides were sequenced using a MALDI TOF/TOF instrument and were subsequently correlated to the respective intact proteins for epidermis or dermis through a protein database search. Currently we have identified selected proteins directly from human skin using tandem MS, carried out to achieve mass accuracies of approximately 0.1 Da. Thymosine β-4 was sequenced intact off the tissue by MS/MS, whereas other proteins were identified using a *bottom-up* approach: enzymatic digestion followed by peptide sequencing. Five keratin proteins found in the epidermis are listed in the Table 1. As expected, keratin 14 is restricted to the undifferentiated epidermal stratum while keratins 1 and 10, were highly characteristic of the outer more differentiated epidermal strata. Table 1 features the peptide at m/z 2872, part of K1C10-human for which ions at m/z 1090, 1364, 1492, 1706 were also detected. Some areas of the epidermis revealed low signals for the ion at m/z 1668. This signal was detected in higher relative abundance in the dermis and corresponds to the partial protein sequence SLEYLDLSFNQIAR (Fig 4), characteristic of lumican, a prototypic leucine-rich proteoglycan with keratin sulfate side chains that binds to type I collagen fibrils and plays a role in collagen fibril assembly.[38, 39] Three more peptides were sequenced from the dermal region from signals for ions at m/z of 1753, 1225 and 1024 (Table 1). Our digestion protocol also detected collagen molecules in the dermis. These included collagen alpha-3 (VI) chain for which a total of 12 tryptic peptides from CO6A3-human were detected. Decorin, a proteoglycan from the small leucine-rich proteoglycan (SLRP) family, was also identified. Dermis also was found to have actin protein (ACTA-human) and beta-actin-like protein 2 (ACTBL-human) which, after digestion, a total of 8 and 7 peptides were detected, respectively (Table 1).

Protein	Abbreviation	Fragmented peptide	Mass
Keratin type I cytoskeletal 14*	K1C14_HUMAN	VTMQNLNDR	1089.5528
Keratin type II cytoskeletal 1b*	K2C1B_HUMAN	YQELQITAGR	1178.6127
Keratin type I cytoskeletal 10	K1C10_HUMAN	NVSTGDVNVEMNAAPGVDLTQLLNNMR	2872.4399
		VTMQNLNDR	1090.531
		VLDELTLTK	1031.5983
		SQYEQLAEQNR	1364.6627
		SQYEQLAEQNRK	1492.7627
		GSLGGGFSSGGFSGGSFSR	1706.8028
Keratin type II cytoskeletal 1	K2C1_HUMAN	SLNNQFASFIDKVR	1637.8927
		SISISVAR	831.4927
Keratin type II cytoskeletal 2 epidermal	K22E_HUMAN	GGGFGGGSSFGGGSGFSGGGFGGGGFGGGR	2398.0628
		FLEQQNQVLQTK	1474.7827
		SISISVAGGGGGFGAAGGFGGR	1837.9427
Decorin*	PGS2_HUMAN	ASYSGVSLFSNPVQYWEIQPSTFR	2763.2727
Actin	ACTA_HUMAN	AVFPSIVGRPR	1198.434
		TTGIVLDSGDGVTHNVPIYE	3196.6095
		EITALAPSTMK	1161.6184
		GYSFVTTAER	1130.5476
		AGFAGDDAPR	976.4482
		CDIDIR	734.3501
		LDLAGR	644.3726
		ILTER	631.3773
Beta-actin-like protein 2	ACTBL_HUMAN	SYELPDGQVITIGNER	1789.884
		TTGIVMDSGDGGVTHIVPIYE	3195.6506
		QEYDEAGPPIVHR	1510.7284
		AVFPSMIGRPR	1230.6775
		DLTDYLMK	998.4863
		CDVDIR	720.3345
		LDLAGR	644.3726
Collagen alpha-3 (VI) chain	CO6A3_HUMAN	AAPLQGMLPGLLAPLR	1616.943
		AGDGVPQVIVVLTDGHSK	1791.9599
		SQHPYVLTEDTLK	1530.7798
		LVDYLDVGFDTTR	1513.7533
		QINVGNALEYVSR	1462.7648
		SDDEVDDPAVELK	1431.6485
		QLGTVQQVISER	1357.7434
		VPQIAFVITGGK	1229.7252
		NNLFTSSAGYR	1229.5909
		QFGVAPFTIAR	1206.6629
		LMHLEFGR	1002.5189
		ELPNIEER	999.5105
Glypican-2	GPC2_HUMAN	GGGGSARYNQGR	1197.698
		AFVQGLETGR	1077.5687
		ETEATFR	853.405
		SCAETR	666.2875
Hemoglobin	HBB_HUMAN	LLVVYPWTQR	1273.718
		VLGAFSDGLAHLDNLK	1669.8907
		VNVDEVGGEALGR	1314.6648
Lumican	LUM_HUMAN	SLEYLDLSFNQIAR	1667.851
		ISETSLPPDMYECLR	1753.8135
		ISNIPDEYFK	1225.6069
		SVPMVPPGIK	1024.5859
Thymosin beta-4	TYB-4_HUMAN	SDKPDMAEIEKFDKSKLKKTETQEKNPLPSK ETIEQEKQAGES	4963.5830

Table 1: *proteins identified after on tissue tryptic digestion and MS/MS analysis. The proteins K1C14, K2C1B and PGS2, marked by asterisks, are preliminary identifications based on the sequence of a single peptide fragment. TYB-4 was sequenced from tissue intact by MS/MS.*

All skin samples contain a rich vascular network so the presence of three different peptides with AA sequences for hemoglobin (HBB-human) served as an internal positive control. Finally, glypican-2 (GPC2-human), a protein from the glypican family of heparan sulfate proteoglycans, was identified. This protein, known to modify cell signaling pathways and contribute to cellular proliferation and tissue growth, was spatially restricted to the dermal region as were hemoglobin, decorin, actin and actin-like proteins.
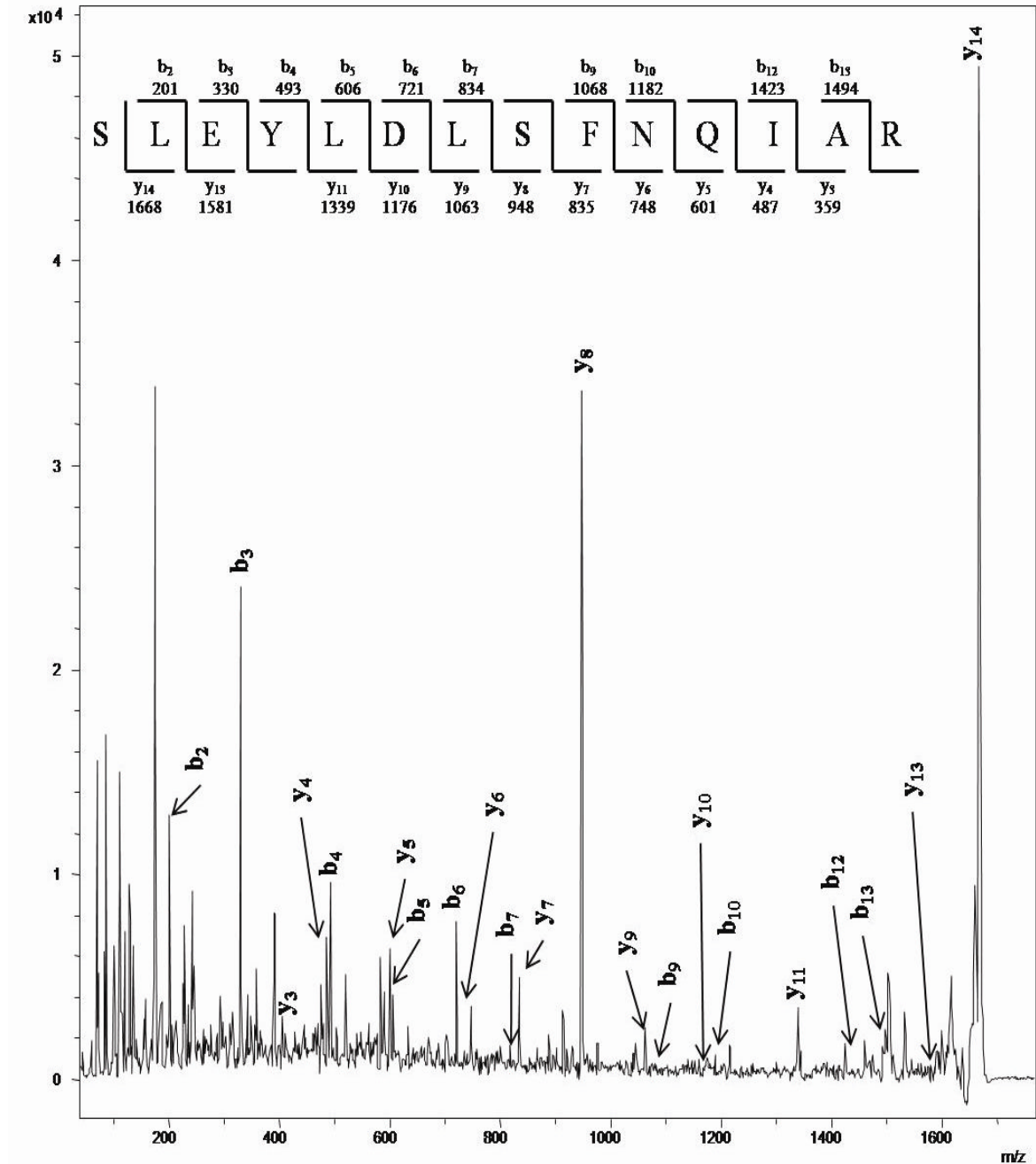
Figure 4: *MS/MS spectrum of the presumptive lumican at m/z 1668 and the peptide fragment assignment.*

Immunohistochemical Confirmation

Positive immunoreactivity for TYB-4 was present within a dermal population (presumed resident fibroblasts and immunocytes) (Figs 5a & b). These images show intense staining of capillary endothelium for TYB-4 while this secreted protein reveals a diffuse distribution over the extracellular matrix. Lumican, an extracellular matrix molecule that is incompletely characterized in the skin, was quite evident by *in situ* tryptic digestion coupled with MALDI MS.
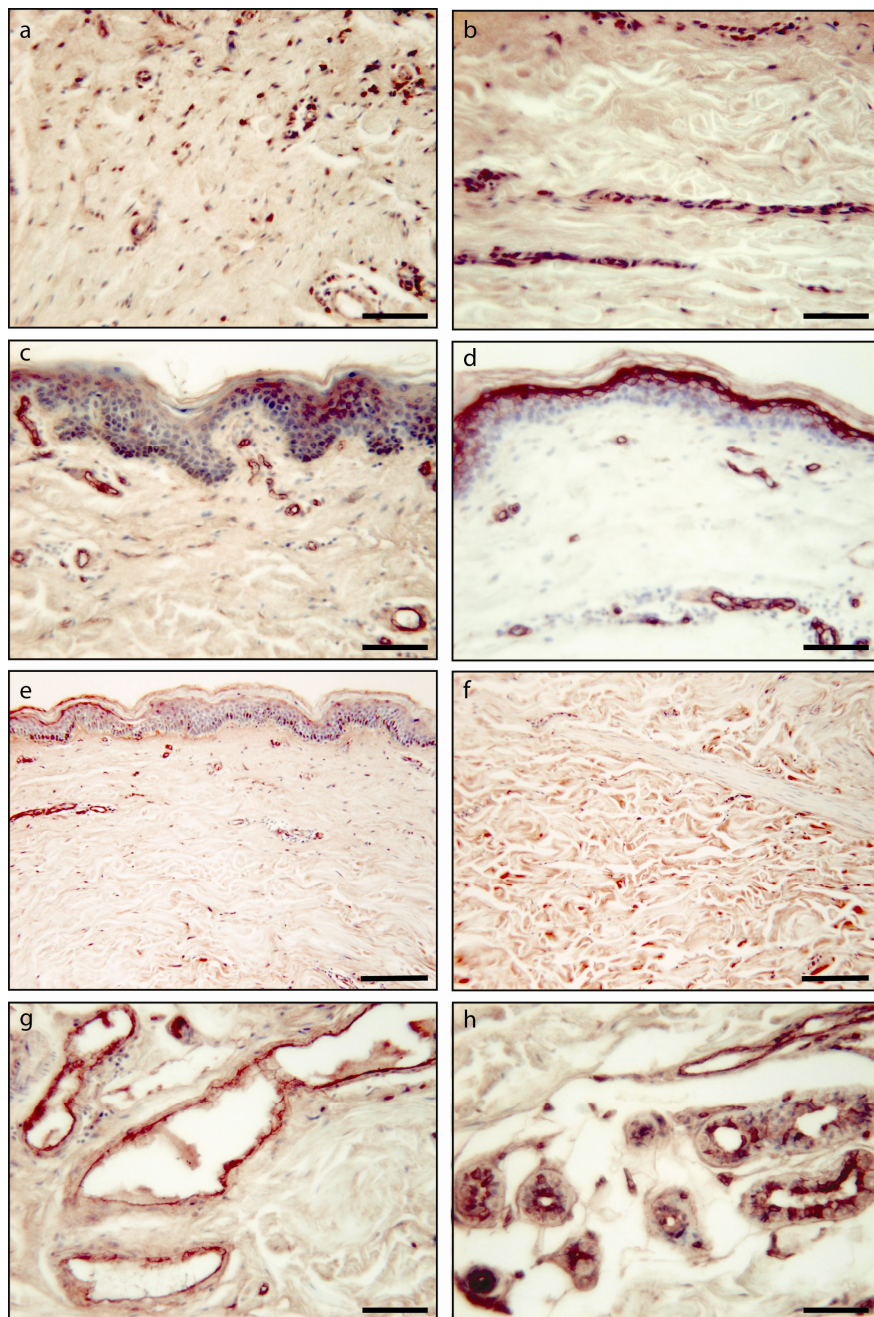
Figure 5: *immunohistochemical confirmation and distribution for thymosin β-4 and lumican a) shows thymosine β-4 in many cells within the dermis b) shows a diffuse dispersal for this secreted protein over the extracellular matrix in the reticular dermal region c-e) shows the highest distribution for lumican in*

association with capillaries. e) shows a modest staining for lumican in the uppermost papillary dermis at the dermal-epidermal junction f) shows a wide spatial dispersal pattern throughout the reticular dermis g) shows intense staining in numerous keratinocytes in the apocrine sweat gland h) shows intense staining in many keratinocytes within the secretory segment of the eccrine sweat gland. Scale bar (e & f) = 200 μm. Scale bar (all others) = 100 μm

Figure 5c-e show variable epidermal displays for lumican revealing intense immunostaining over capillaries. Lumican shows a variable distribution in the dermis with a sub-epidermal concentration that was particularly strong in one patient (Fig 5e) but displays a broad dispersal pattern throughout the reticular dermis in another patient (Fig 5f). Many keratinocytes comprising the secretory segments of the apocrine (Fig 5g) and eccrine sweat glands (Fig 5h) show intense staining for lumican.

Discussion

The protein profiles obtained in this study showed distinct differences between the focal regions of the skin (epidermis versus dermis) due to their different cellular compositions. In addition MALDI IMS was able to detect unique differences between the papillary and reticular dermis. We consistently detected constitutive markers of normal skin regions as well as unique markers indicative of individual variability. This latter finding suggests that these advanced MS techniques may find increasing applicability in the realm of individualized medicine. Since skin is a prime example of an organ with clear spatial patterns of morphologic and functional specialization[40], the potential of this type of highly sensitive and spatially precise analysis is particularly attractive for the study of cutaneous lesions. For example, it is known that skin grafts maintain unique donor site specificities. Only recently investigators have begun to uncover fibroblast gene expression mechanisms that are responsible for this phenomenon of anatomic diversity and positional variation in human skin.[40-42] With the MS techniques we have developed for analysis of skin, we can map such site-specific cutaneous nuances by virtue of their ability to provide a more comprehensive proteomic signature in register with unique tissue architecture. While protein identification in skin has been a standard approach for many decades, such discoveries have been laborious and using techniques such as Western Blotting, ELISA, and immunohistochemistry, only known proteins can be studied. Another modern proteomic approach, 2D-DIGE/MS, is limited to homogenization of whole skin biopsies and detects high-abundance proteins at a MW between 20-200 kDa, but loses spatial information at the cellular level. Technologies utilized in the present paper produced complementary data by detecting proteins in the 3-12 kDa range, a lower mass range than previously reported using other techniques. This mass range included TYB-4 that has already been implicated in events occurring during wound repair[43], mast cell exocytosis[44], activation of hair follicle stem cells[45], angiogenesis[45-46], matrix metalloproteinase expression[43] and anti-inflammatory events.[47] TYB-4 regulates dynamics of the actin cytoskeleton in cell types for which cell migration is essential.[48] We also confirmed the presence of this protein in normal human skin using immunohistochemical techniques.[49] In sum, the presence of TYB-4 in each dermal

spectrum suggests that an ample supply of this protein is held in readiness during skin homeostasis awaiting a response to stimuli. Although IMS technology detected a number of interesting proteins, in this report we restricted our focus to lumican, a protein that is less abundant and has been poorly characterized in skin.[50] Bhattacharjee *et al* depicted the presence of lumican in the subepidermal region. We confirmed a similar moderate distribution in this location. Since this proteoglycan is known to interact with collagen by limiting growth of fibril diameter[38], its distribution in this area may explain the visibly smaller caliber of the collagen fibrils in this microniche within an otherwise dense irregular connective tissue. The presence of this protein led us to examine additional locations of lumican within the skin. We have found that lumican is also present in certain differentiated keratinocytes in the outer strata of the surface epidermis as well as in the secretory keratinocytes of sweat glands. The diffuse presence within the extracellular matrix of the reticular dermis where collagen fibrils are not constrained in diameter, leads us to suspect several more unexplored roles for lumican in both the dermis as well as in keratinocytes. Our data suggest that proteomic signatures resulting from newer, more sensitive MALDI IMS techniques can be equally useful in generating novel hypotheses to explain cutaneous structure and function.

In summary, IMS offers new opportunities for the investigation of the proteome of tissues such as human skin permitting a systems biology approach for monitoring cellular modifications occurring in skin diseases. The purpose of this study was to optimize and assess the utility of mass spectrometry to analyze proteins from normal human skin using IMS to observe the distribution and localization within different areas of human skin. We highlight the potential value of high resolution images that allow for the evaluation of cutaneous proteomic details unreachable using other lower resolution investigative techniques.

The Microenvironment of Human pressure Ulcers as Defined by Imaging Mass Spectrometry

Cutaneous ulcers currently affect 6.5 million patients in the United States.[51] The problems associated with chronic wounds are large in scope imposing physical, psychosocial and economic burdens on patients, while piling up tremendous economic cost.[52] Chronic wounds are, by definition, wounds that fail to progress through normal stages of healing and thus enter a state of prolonged pathologic inflammation. Chronic wounds rarely develop in individuals who are otherwise healthy. Not surprisingly, chronic wound patients frequently suffer from co-morbidities such as obesity, diabetes and peripheral vascular disease.[51] For example in the diabetic population, roughly fifteen percent of patients develop chronic foot ulcers during their lifetime and a significant number of these will eventually require a lower extremity amputation.[53] In the US population, African-American patients or those who are trapped by a low socio-economic status have a higher incidence of pressure ulcers.[54, 55] Chronic wounds comprise a large catch-all category that includes major types such as venous stasis wounds, diabetic wounds, and pressure ulcers

as well as other minor categories. Although Mustoe *et al*. proposed a unifying hypothesis of chronic wound pathogenesis based on four main causative factors[56], these remain unproven hypotheses. The existing and sparse literature on chronic wounds has historically focused on single molecules or limited pathways.[57-61]   A recent paper based on a proteomic analysis of wound fluids comparison between an acute and venous stasis ulcer proposed several new biomarkers of chronic wound repair.[62]   Nevertheless, multifocal disturbances that maintain the chronicity of pressure ulcers remain unexplored and clinicians are in need of more sophisticated tools to provide accurate, patient-tailored assessments.   At present providers are forced to classify a wound based simply on visual impressions of the depth of involvement. The determination as to whether a wound is remaining stagnant on a given therapeutic regime or is on the road to recovery is often based on sequential photography measure. It is our supposition that improvements in patient outcomes will eventually be fostered by a molecular-based classification system that is undergirded by powerful proteomic techniques. Over the past decade, proteomics has become a vital component elucidating cellular processes in both health and disease.[63,64]   New advances in mass spectrometry (MS) provide investigators with opportunities to study molecular interactions within intact tissues.[65] In this study, MS measurements were performed to determine differences to the skin proteome when a chronic wound is present. In particular, matrix assisted laser desorption/ionization (MALDI) imaging mass spectrometry (IMS) allows for analysis of the spatial distribution of proteins directly in tissue specimens.[66] This technology generates robust molecular-weight-specific data, requires no target-specific reagents (such as antibodies), can sample intact large proteins of 100 kDa or less, and uses simple and rapid sample preparation protocols.[67]   The use of MALDI mass spectrometry makes it possible to simultaneously investigate hundreds of molecular species, especially those of higher molecular weight such as proteins, as well as lipids, drugs or metabolites by depositing matrix on tissue sections. From a generic sample, hundreds of peptide and protein peaks can be recorded in the mass spectrum produced from a single laser ablated area on the sample. In this report, MS analysis of proteins from skin tissue was performed following two main experimental approaches involving direct analysis of tissue.[66, 68, 69]   The first, termed "profiling", analyzes discrete but limited areas within a tissue section and subjects the resulting protein profiles to computational analysis. Such experiments are designed to make comparisons between representative areas on pieces of tissue or between two different specimens. Thus, replicate sampling within a focal area of interest permits the capturing of data that can achieve statistical confidence though the use of principal component analysis and hierarchical clustering analysis although fine spatial resolution is lacking. The second approach, termed "imaging", is a high spatial resolution technology that allows image acquisition at specific molecular weights directly from tissue.[70] Ion density maps are generated representing the spatial distribution of a given analyte within the tissue section as well as its relative abundance (intensity). The entire tissue section is analyzed through an ordered array of spots, or raster pattern, in which spectra are acquired at intervals that define the image resolution (e.g., every 40 μm in both the x and y directions). Two dimensional ion density maps, or images, can then be created by plotting the intensity of signal obtained as a function of its xy coordinates.[67, 71, 72]   In the current study, imaging as well as profiling mass spectrometry was applied to the examination of human pressure ulcers

to provide insights into the multi-focal disturbances that inhibit the healing of ulcerated skin and contribute to the chronicity of this poorly understood type of wound.

Results

Overview of MALDI MS Applications to Chronic Wounds

The proteomic content of frozen sections cut from pressure ulcer specimens was investigated by MALDI mass spectrometry. Prior to the distribution of matrix over frozen tissue sections, a hematoxylin and eosin stained section (H & E) was prepared for each wound. These serial sections were used to identify distinctive morphological features that defined regions of interest (Figure 6).
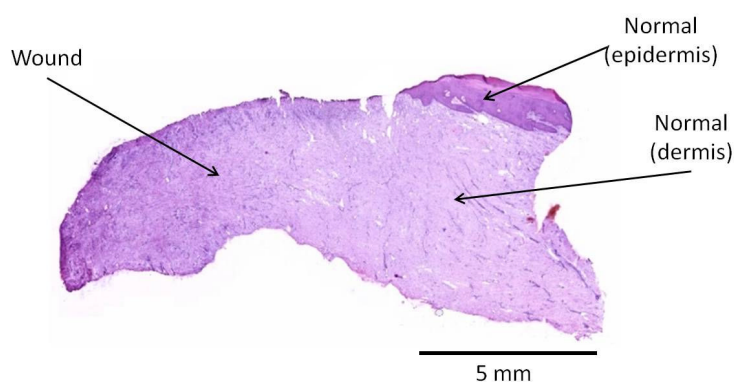
Figure 6: *histological evaluation of a representative tissue section H&E stained from an ulcer patient, highlighting 3 main areas of interest: wound, hypertrophic epidermis and the dermis adjacent to the wound bed.*

In recognition that keratinocytes play a role in modulating wound repair activities[73, 74], the hypertrophic epidermis at the edge of the wound was included in samples from patients #1-4 as was the underlying non-wounded dermis immediately adjacent to the wound bed. Two ulcer specimens instead were collected very close to the wound edge and they did not contain definitive margins with hypertrophic epidermis (patients #5 and 6). Four wound samples were collected from patients with longstanding ulcers that were showing some clinical evidence of wound improvement (Table 2). These latter samples of chronic wounds became available when these large wound beds and margins were surgically excised prior to coverage with skin flaps since it was deemed in the patient's best interest to have a swifter wound closure than could be achieved by secondary intention. In the MALDI IMS experiments, a comprehensive array of matrix spots is deposited throughout the entire tissue section without investigator bias. The obtained ion maps provided an overview of the relative intensity of the protein and peptide contents and were used as a survey or discovery tool and formed the basis for the bulk of the studies in this report.

	Patient No.	Gender	Age	Race	Body Area	Co-morbidities
Ulcer	1	female	69	caucasian	sacrum	diabetes
	2	female	37	caucasian	sacrum	diabetes, paraplegia
	3	male	18	caucasian	ischial	paraplegia
	4	male	64	caucasian	ischial	paraplegia
	5	male	26	caucasian	ischial	paraplegia
	6	male	41	caucasian	ischial	paraplegia
Normal	7	female	47	caucasian	breast	none
	8	female	47	caucasian	breast	none
	9	female	54	caucasian	breast	none

Table 2: *demographic data for the 9 patients in this study.*

Wound Molecular MS Profiling

The proteomic content of frozen sections cut from pressure ulcers specimens was investigated by MALDI mass spectrometry. Figure 7 shows the averaged and normalized mass spectral profiles in the mass range up to 20 kDa for the six pressure ulcers included in this pilot study. Three focal regions were initially targeted for MALDI MS: the wound bed, the non-eroded adjacent dermis, and the hypertrophic epidermis at the wound edge (when present). These data reveal unique spectral profiles for each region. The wound bed profile was distinctive showing comparatively more signals and with higher relative intensities within the lower mass range (from m/z 2500 up to ~4000) (Figure 7A). Profiling of the adjacent dermis showed more prevalent signals in the m/z range of 4000 and 6000 (Figure 7B). The signal at m/z 4965, for thymosin β-4 (TYB-4), was observed as the base peak of each spectrum acquired from the dermis. In the wound bed, other intense signals were the m/z 3372 and 3443, human neutrophil peptides, HNP-2 and -1 respectively (Figure 7A). Furthermore, in five of the six samples, the signal at m/z 3487 (HNP-3) was observed as one of the stronger peaks. Profiling was performed on the hypertrophic epidermis at the margin of the wound (Figure 7C). This region showed distinctive signals in the higher mass range 8-12 kDa, revealing a profile that was dissimilar to the underlying dermis or the wound bed itself. For instance, signals at m/z 9928, 11010, 11042, 11371 and 11656 were unique to this highly activated epithelium. The m/z at 10403 and 15134, were detected in a few but not all the patients. For several patients, the m/z 3373 and 3443 (HNP-2 and HNP-1) were detected in the highly activated hypertrophic epidermis at the wound's edge. This suggests that these particular peptides are not restricted to the wound bed, a finding that was later confirmed by ion density mapping (Figure 8-9) and immunohistochemistry (Figure 10). Although this report displays averaged data gathered from all six patients, this technology allows for the capture and probing of personalized wound profiles for individual wounds or patients. When this was performed, additional signals such as m/z 4279, 5653, 9958, 11308 and 15349 displayed variable representation in individual epidermal samples.
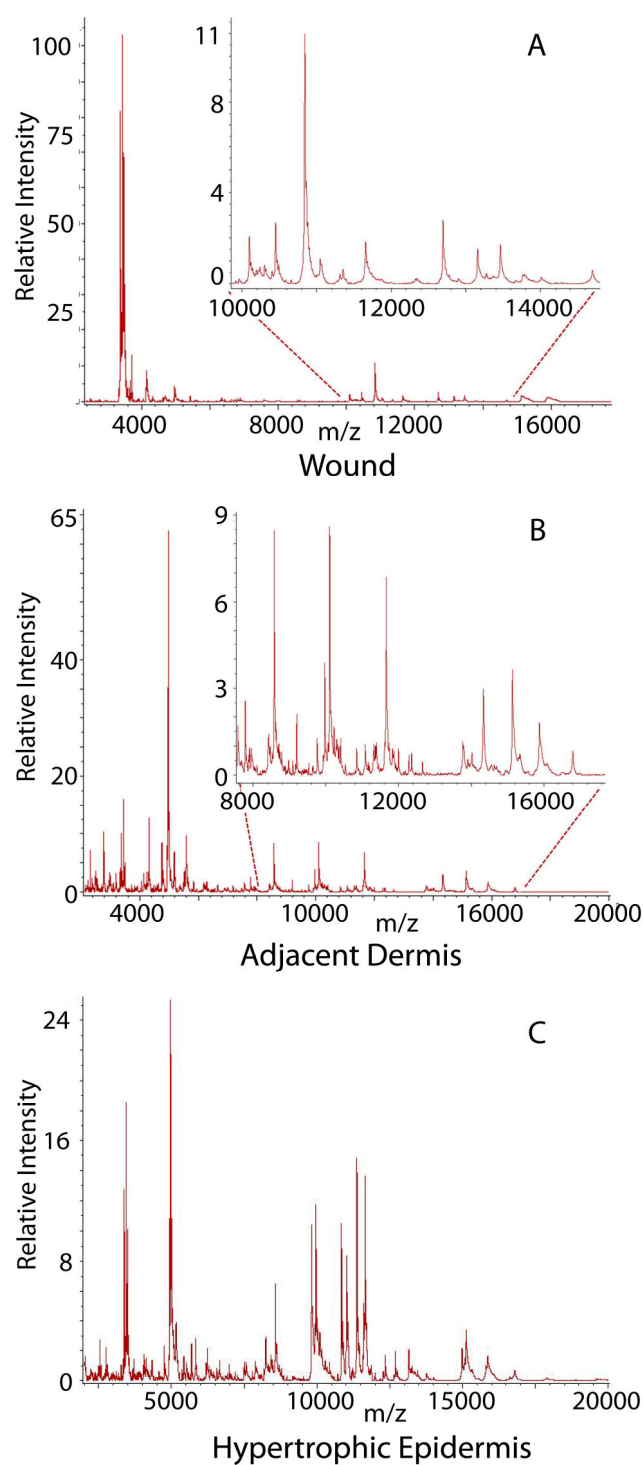
Figure 7: *spectra were acquired from 20 spots deposited in that area and then averaged and normalized to the TIC.averaged spectra from a) wound bed, b) dermis adjacent to the wound bed and c) hypertrophic epidermis.*

Molecular Imaging Produces Spatial Distribution for Molecular Features

IMS ion density maps highlight the spatial distribution of the molecules profiled within four representative pressure ulcers (Figure 9). Based on examination of scores of individual ion density maps, knowledge about the clinical status of each wound and histological scrutiny of the inflammatory features of these wounds, the left-to-right arrangement of the columns of ion density maps was selectively ordered to depict a proposed continuum from mildly inflammatory and improving wounds to highly inflammatory and non-improving wounds. Ion density maps for the same six proteins are featured for each wound to provide a visual comparison and contrast (Figure 9). Further, hematoxylin and eosin stained sections were prepared for each wound in order to identify distinctive morphological features. For purposes of comparative visualization of distinctive features within different wound areas, dual ion density maps (for HNP-3 and TYB-4) were created for each of the patients displayed in Figure 8. MALDI IMS provide complementary data to support the initial profiling data in Figure 7. For example, a prominent distribution for m/z 3372, 3443 and 3487 (HNP-2, -1 and -3) was confirmed. In four of six patients, HNP-3 was the molecule with the highest relative expression in the wound bed. Most notably, querying of individual wound beds often produced differential signals between the upper and lower wound bed (patients # 1, 3, 5 in Figure 9). In some wounds, the lower wound bed showed closer similarity to the adjacent dermis. This was true for TYB-4 in patients 1, 3 and 5 in Figure 9. TYB-4 was density mapped as the most relatively intense protein distributed in the dermis adjacent to the wound bed in all ulcer patients as well as in the dermis in normal patients. IMS data indicate in some patients a reverse correlation between the spatial distribution of TYB-4, a molecule closely correlated with intact granulation tissue with relative maturity, and HNPs, molecules closely correlated instead with those wound regions showing the highest degree of neutrophilic influx on the companion hematoxylin and eosin stained sections.
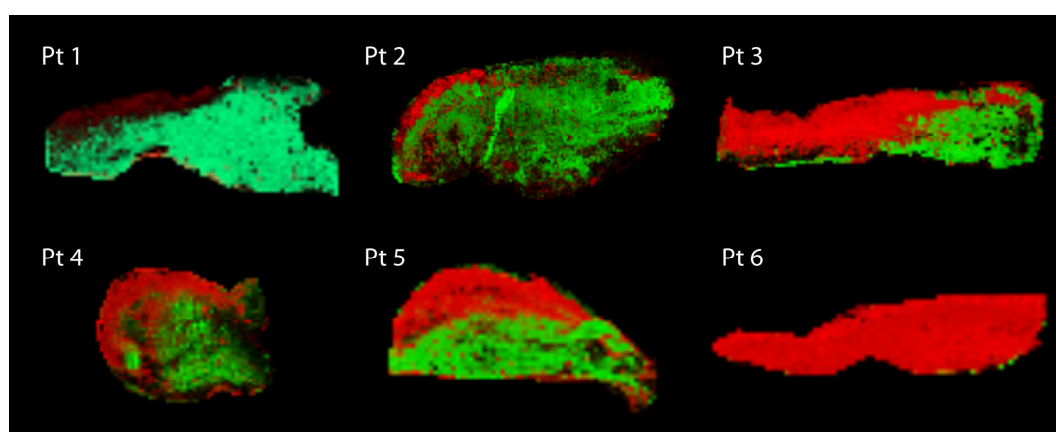
Figure 8:. *dual molecular ion density maps for selected features (HNP-3 in red and TYB-4 in green) are displayed for a simultaneous visualization of reverse distribution between wound regions.*

The exception to this complementary distribution pattern was observed in the wound from patient #6. By H & E and clinical observations, this wound was the most stagnant chronic wound in this cohort. TYB-4 was poorly expressed suggesting little evidence of a return toward normal dermis in this specimen. In the wound area from patient #1 (the wound area with the most favorable histological evidence of improvement), HNP-3 was weakly expressed. By contrast, HNP-3 was strongly expressed in the wound material from patient #2 (the wound area with the least favorable histological evidence of improvement). HNP-1 and -2 were prominent in all six chronic wounds.
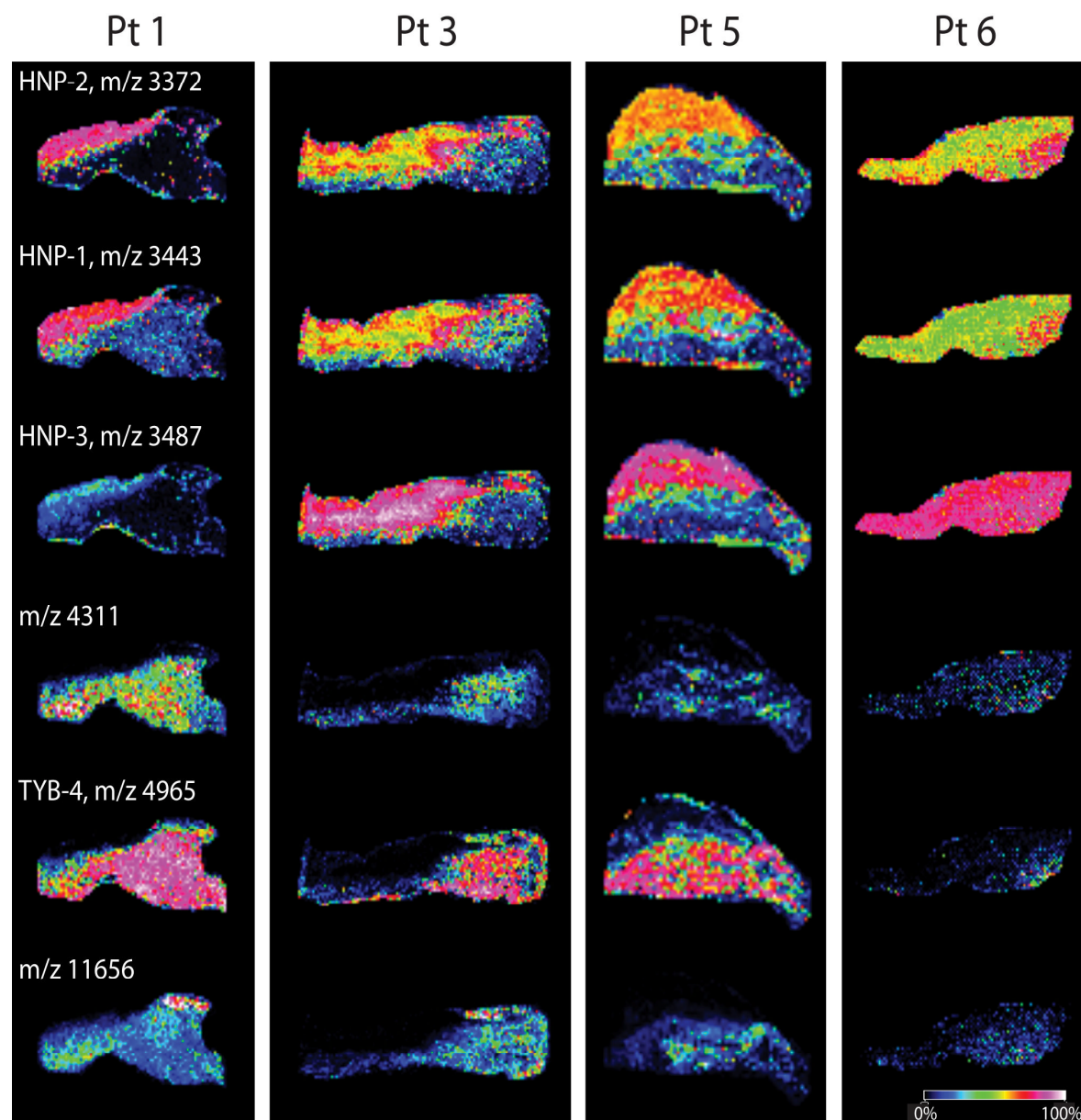
Figure 9: *IMS ion density maps for ulcer skin samples from representative patients #1, 3, 5 and 6 illustrating pattern mapping for six representative ions: m/z 3372, 3443, 3487, 4311, 4965, 11656. All wounds were taken from the edge and down to the base of stage IV pressure ulcers. The representative*

data set for each patient is arranged in a vertical column and was retrospectively grouped by a proposed molecular stratification of wound status. Wounds to the left display evidence of nascent healing (patient#1) whereas the wounds in the right column from patient #6 displayed little evidence of improvement.

Moreover some displayed relative prominent in the upper regions of the wound bed. Further, the ion with m/z 4311 was selected to feature in Figure 9 since it correlates strongly with the distribution pattern for a known protein TYB-4. Both of these are generally located in the adjacent dermis and lower portion of the wound bed where the granulation tissue is the oldest and most mature. Figure 9 also features a protein at m/z 11656. By ion density mapping, this ion was largely restricted to the hypertrophic epidermis at the wound edge but does show relatively lesser levels in the underlying adjacent dermis at the wound's edge and is present in the maturing granulation at the base of the wound bed in patient #1, the prototypic wound that shows the least inflammatory characteristics and relatively more maturity and differentiation of its lower wound bed. The latter protein was density mapped also in other samples (e.g., patients # 3 and 5), largely restricted to the hypertrophic epidermis but traces were observed in the adjacent dermis.

Immunoreactivity for α-defensins

As a complementary approach to confirm the presence of α-defensins, a non-selective HNP antisera known to recognize all three peptides forms (HNP-1, -2, and -3) was used to perform immunohistochemistry with all the normal and wound samples. As expected, HNPs are not prominent in normal human skin; nevertheless, mild immunoreactivity for HNPs was observed in the external region of the skin, the epidermis and in the circulating leukocytes within the intact capillaries of skin (Figure 10 A). Figures 10 B-D show the immunoprecipitation patterns for the HNP family in a representative wound (patient #3), that exhibited moderate inflammatory characteristics. HNPs were also present in the hypertrophic epidermis containing infiltrating neutrophils as well as within the inflamed underlying dermis at the wound edge.

Figure 10 displays: (A) normal skin with no immunoreactivity in the dermis. Modest staining is present in the basal epidermis and in leukocytes within the lumen of dermal capillaries. (B) By contrast, HNPs are prominent in the hypertrophic epidermis at the wound margin and in the underlying dermis. (C) Shows an inflammatory foci within the wound bed where cellularity is greatly increased and (D) shows a higher magnification suggesting that highest levels for the HMPs are contained within the neutrophilic granules but dispersal is equally evident from neutrophils that have released their granules.
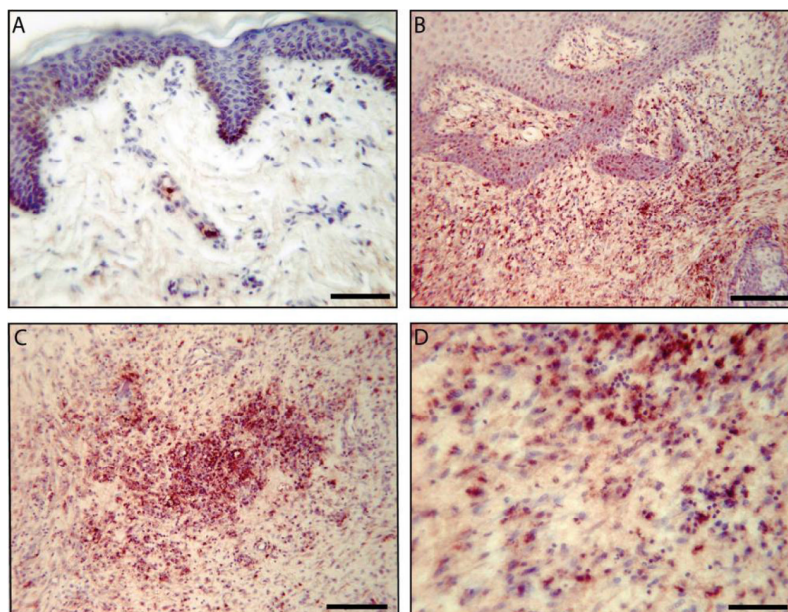
Figure 10: *immunohistochemical localization of the expression α-defensin (HNPs) in a representative paraffin-embedded companion wound section from patient #3. Scale bar (A, B) = 100 μm, scale bar (C, D) = 200 μm.*

Statistical Analysis

PCA Differentiate Pressure Ulcers Areas

PCA analyses were performed since this is a statistical method commonly used to reduce the dimensionality of a multivariate data set by displaying and ranking its variance within a data set. Here, PCA was explored and applied as a tool to define spectral clustering for the composite proteome within the upper and lower wound bed region. Figure 11 displays a two-dimensional PCA plot for the wound from the patient #1 that showed unique protein patterns between the upper and lower wound bed. By analysis of the total significant protein components in the sample, the software was able to cluster the spectra from the upper wound area to the left of the zero mark on the x-axis based on 58% of the variances in the spectra. Thus, spectra from these two regions within the wound bed were distinctively separated into two clusters.

By contrast, when the statistically recognized protein variances (PC1) in the total spectra were applied to the wound from patient #6, the mathematically derived data from the upper and lower wound regions reveal significant overlap (Figure 12). The PC1 variances were low at 30%. The lack of a definitive clustering pattern confirmed that this wound is comparatively homogenous with no distinction between an upper or lower wound area.
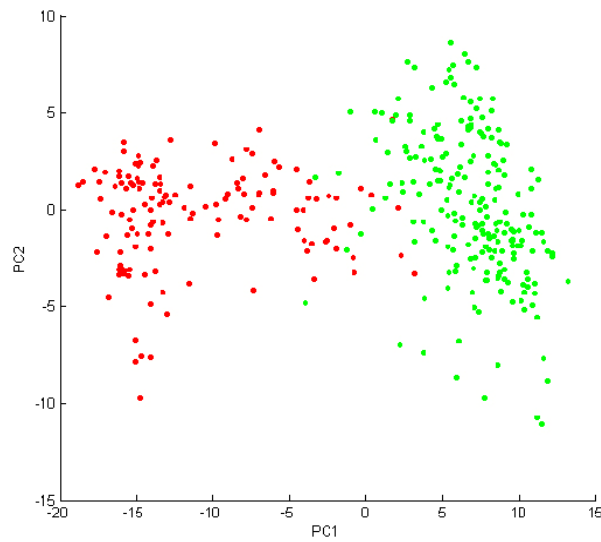
Figure 11: *a supervised principal component analysis (PCA) analysis of individual total spectra from patient #1, a representative example of healing wound. Each red dot displays a full spectrum collected from the upper wound bed and each green dot displays the significant protein features from the lower wound bed.*
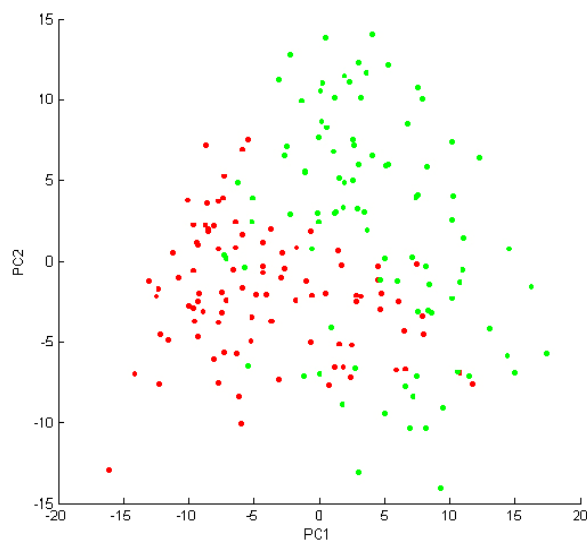
Figure 12: *a supervised principal component analysis (PCA) analysis of individual total spectra from patient #6, a representative example of non-healing wound. Each red dot displays a full spectrum collected from the upper wound bed and each green dot displays the significant protein features from the lower wound bed.*

PCA Differentiate Ulcer and Healthy Proteome

PCA analysis was also performed to compare protein signatures in normal epidermis (N=3) to those in hyperproliferative ulcer-associated epidermis (N=3) (Figure 13).
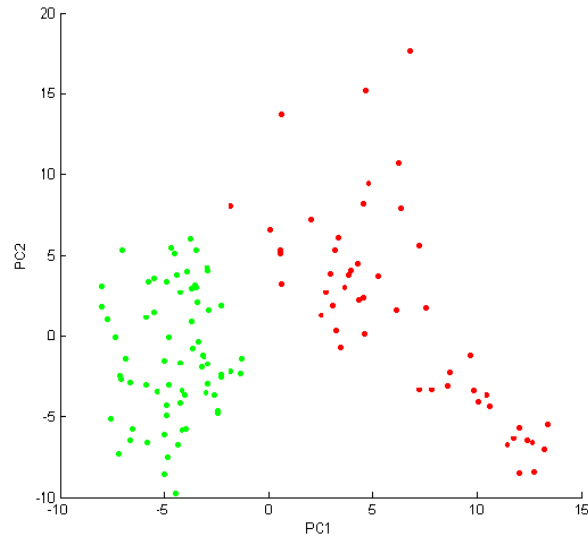
Figure 13: *displays a supervised PCA analysis comparing the averaged significant protein features between normal epidermis (normal patients, green dots) with hypertrophic epidermis at the wound margin (red dots).*
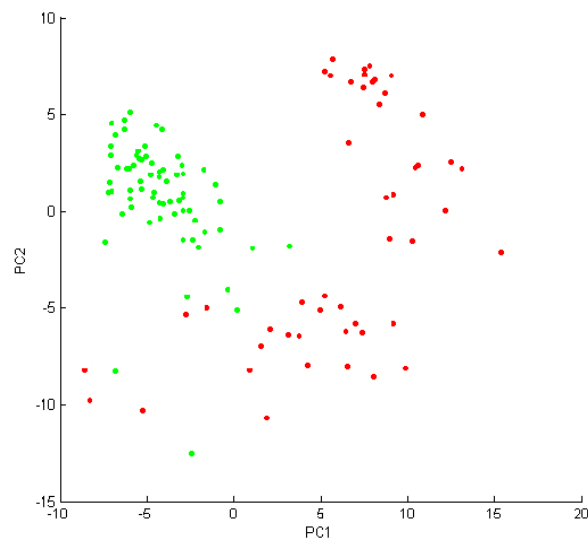
Figure 14: *displays a similar scheme comparing protein features in normal dermis (normal patients, green dots) with dermis immediately adjacent to the wound bed (red dots).*

PCA plots for these two dynamically different epidermal states revealed two clusterings in the first-dimension (PC1) based on 22% of the protein features Protein features for normal epidermis were more tightly clustered than hypertrophic epidermis. A similar PCA analysis strategy was performed to compare normal dermis to the ulcer-associated dermis at the edge of the wound bed (Figure 14). Variances in the PC1 of 28% indicated a close clustering of proteins in normal dermal tissue. The dermal data set of proteins derived from areas adjacent to ulcers showed a clear dispersed pattern that distinguished it from that of the normal dermis where proteins are in a state of equilibrium.

ROC Curves Demonstrate Ion Specificity within Wound Areas

To further validate that some pressure ulcers show signs of regionalization or stratification into distinctive upper and lower wound beds, a receiver operating characteristic curve (ROC curve) was calculated for representative m/z from the spectra collected from the wound regions of each patient. Thus, the area under the ROC curve (AUC) value (0 to 1) was used as a quantitative parameter to estimate the specificity of a given ion within the two spectral groups derived from upper and lower portion of the wound bed. Data from ROC curves document with high statistical probability that selected ions (e.g., HNPs and TYB-4) are differentially expressed in the upper and lower wound regions of patient #1. The area under the curve for these peaks closely approached 1.0, a statistically significant finding indicative of high specificity of that feature for one of the classes loaded in the model (Table 2). By contrast, upper and lower regions of the wound from patient #6 displayed very different ROC curve values for the same molecular features and failed to show statistical differences for these ions between the upper and lower wound. Such data confirmed that this wound bed has a homogenous distribution for HNPs and shows no regionalization or stratification for these particular molecules (Table 3).

Molecular features	Patient #1 wound ROC AUC values	Patient #6 wound ROC AUC values
HNP-1	0.99345	0.58461
HNP-2	0.996414	0.64354
HNP-3	0.996468	0.64880
TYB-4	0.983162	0.82157

Table 3: *area under ROC curve values (0 to 1) for selected molecular species in upper and lower wound areas of representative wounds (patient #1 and 6). Values approaching 1.0 confirm the specificity of that molecular species for one of the classes loaded in the model (upper vs. lower wound). Values much lower than 1.0 indicate the non specific distribution of the same molecular species in both classes and confirm the homogenous distribution within the tissue.*

Differentially Expressed Molecular Features

Figure 15 shows the use of another statistical tool with the power to display proteins that are either over-expressed or under-expressed in the wound bed as compared to the adjacent non-eroded dermis. Total spectra from 25 matrix spots within each focal region were collected and the relative intensity of proteins or peptides between one area versus another was plotted. A total of 96 molecular features were identified as differentially expressed within a threshold of ±5 (Δ). In our survey of wound beds versus adjacent dermis, 20 ions were over expressed in the wound and 76 ions were under expressed. Molecular features with the highest score are highlighted in Table 4.
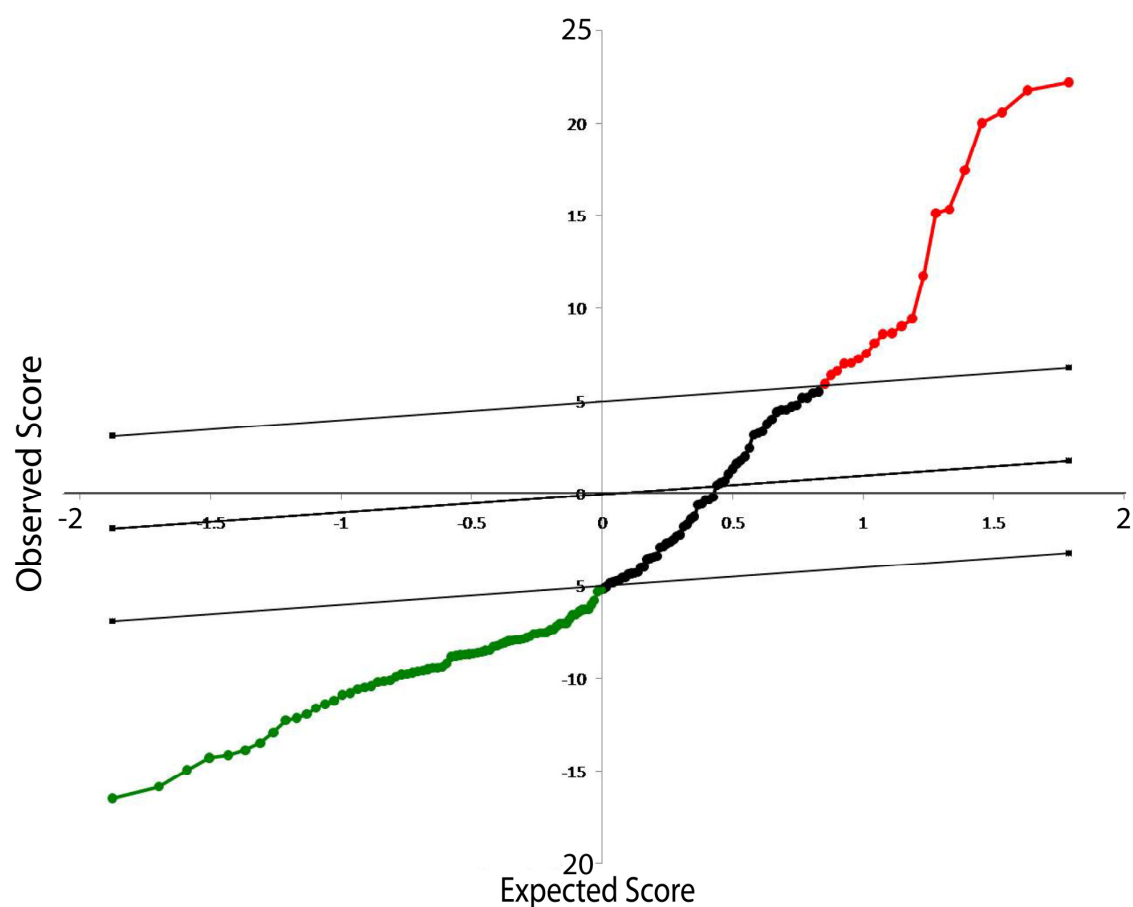
Figure 15: *significance analysis of microarrays (SAM) plot of results of wound versus adjacent dermis. Red circles indicate significant features that are over-expressed in the wound. The green circles indicate features significantly under-expressed in the tumor. Protein features (m/z) are arranged by their degree of difference in expression. Black lines represent the significance threshold (Δ) corresponding to FDR <0.01. Points distributed in either the upper right (top) or left (bottom) exhibit a higher degree of difference from threshold values.*

a)

m/z	SAM Score
3394	22
3465	21
3443	20
3412	20
3487	17
3507	15
3372	15
3526	11
3710	9
3577	9
4160	8
3549	8
3668	8
3597	7
10856	7
10838	7
10876	7
4137	6
12691	6
13459	5

b)

m/z	SAM Score
8569	16
4939	15
2777	14
4965	14
3173	14
4749	13
5172	13
2302	12
2976	12
10054	12
5047	11
5191	11
5146	11
4776	11
5475	10
7770	10
2753	10
6178	10
8608	10
4987	10
10096	10
8416	10
4310	9
5004	9
2481	9
4791	9
6224	9
2502	9
11656	9
2354	9
7887	9
5828	9
4228	9

Table 4: *top differentially expressed features as determined by SAM in wound regions versus adjacent dermis regions. Data are presented with respect to molecules within the wound bed. Feature: significant m/z values with the highest score. Class prediction ability: 94%.*

131

Discussion

This pilot report provides new proteomic insights for chronic wounds while demonstrating the potential utility of MALDI IMS for global and specific analyses. Pressure ulcers were examined since they represent the least understood of the chronic skin ulcers and ample material is available during surgical reconstruction. In current practice, pressure ulcers are rarely biopsied and sent to pathology since there is no clinical expectation that examination will supply useful prognostic clues to indicate whether or not a wound is improving. In the present study wound material normally relegated to the biohazard waste was collected for purposes of inquiry. These MALDI IMS data provided a robust molecular portrait within a spatial context. Furthermore, ion density maps revealed previously unknown differential molecular distributions for proteins in the upper (presumably more immature or stagnant or inflammatory) region of the wound bed as compared to either the lower (and presumably more mature) region of the wound bed. As expected, the data depict multiple molecular disturbances in the wound bed as compared to the adjacent intact dermal tissue. MALDI IMS approaches revealed spatial distributions for certain anti-microbial peptides, the α-defensins that have not been associated with wound beds in pressure ulcers. Although the potential for data collection in MALDI IMS studies is extensive since each pixel represents full spectra in the considered mass range, we applied a focal analysis approach with this small family of proteins as an example to demonstrate new molecular information. Recent reports have provided evidence that other antimicrobial peptides such as the β-defensins and psoriasin and RNAse 7 play a role in wound repair and are present in the surrounding epithelium.[71, 72]   These reports were based on fluids from patients with venous stasis ulcers as well as biopsies from the adjacent tissue at the edge of the wound. By contrast, the distribution of the α-defensin family has previously been poorly documented in wound repair. This family of peptides was previously implicated by immunohistochemical localization in the wound margin of a chronic venous ulcer[71] and in the wound fluids associated with superficial skin injury and venous ulcers.[72, 75]   The MALDI MS data in this report extends these findings and indicates for the first time that three members of the α-defensin family (HNP 1-3) are prominent in the wound bed of pressure ulcers. Furthermore, the variability in the intra-wound and inter-patient spatial distribution patterns suggest that this family of proteins should be further pursued as dynamic molecular indicators to ascertain whether wounds are improving, remaining stagnant or deteriorating. The ability of MALDI MS and IMS to discriminate among the closely homologus HNP molecules also shows the heightened selectivity that can be achieved by simultaneous study of molecular & spatial distributions. In this paper we contrast ion density mapping with a standard and alternative experimental approach – immunohistochemical localization. The HNP example illustrates the pros and cons between these two localization approaches. The three HNPs are currently indistinguishable by available antisera since HNP-2 is a degradation product and HNP-3 differs by a single animo acid. Nevertheless, the immunohistochemical localization was useful as a complementary technique for two reasons. It provided secondary confirmation that this family of proteins is present in pressure ulcers. Immunostaining is superior in other regards since it currently has the ability to identify cell populations associated with the HNP family. Ion density maps in our study indicate that the upper, outer portions of pressure ulcers are especially rich in HNPs. Previous studies have provided preliminary evidence that HNPs are present in wound fluids derived from acute wounds and

venous stasis ulcers.[76]   Our spatially-based finding is consistent with the expectation that this region of the wound is constantly exposed to hostile microbes in the external environment and is thus most in need of a line of defense. Dual ion density mapping for the HNP-3 and TYB-4 molecules provides a visual aid similar to dual immunefluorescence and clearly indicates the opposing spatial distribution patterns for these molecules. Collected data suggest that TYB-4 is a marker for adjacent dermis while HNP-3. HNPs and their wound bed associated distribution provide descriptive data at this point that will require further work to solidify this hypothesis. Progress using mass spectrometry to define global proteomic signatures in pressure ulcers has been made in multiple ways. Signals profiled from averaged spectra show the sensitivity to reveal scores of m/z for ions (many intact proteins) in the range of 2-20 kDa in the wound bed. Not surprisingly, PCA analyses with its patterning of significant proteomic features indicate that there may be sub-categories within the catch-all category of stage IV pressure ulcers. Some wounds show demarcation into distinctive upper and lower wound molecular environments while others are homogenous in their proteomic patterns. As more biopsies are accrued and individual spectrum are grouped and averaged according to clinical wound outcomes, it is eventually expected to be feasible to consider whether the spectrum for an individual wound matches the signature for a chronic wound that is improving or one that remains stagnant or is actually deteriorating further. The present paper provides proof-of-concept to serve as the basis for such prospective clinical tracking. Global discovery was also fruitful when significant analysis of microarrays was performed. We have accrued a listing of ions that are over- and under- expressed in the wound bed as compared to the adjacent intact dermis. Such molecules provide potential therapeutic targets for supplementation for molecules that are deficient in pressure ulcers as well as blockade for harmful proteins that are deleterious when abundant. Although the bulk of this report is designed to showcase global proteomic characterization of pressure ulcers, these same techniques appear suitable and promising as tools that can personalize medicine. MS output yields full spectra for each area of interest and provides a wound signature for that individual patient that contains individual proteins not present in the spectra of this cohort. Since patients with chronic wounds typically have concurrent illnesses, the ability and sensitivity to examine individual differences by IMS and compare them to statistically significant proteomic signatures study is expected to prove informative for individualized wound therapies in the future.

In conclusion, the data reported herein represent an initial step in the lengthy process of casting light on the etiology of skin ulcers. The findings suggest that mass spectrometry with spatial capabilities brings the requisite sensitivity that will permit an analytical, systemic examination of the similarities and differences of proteomic signatures among populations of patients with chronic skin ulcers. A novel tool such as MALDI IMS is needed to advance both the science and practice of wound care since wound providers are currently limited to classifying wounds based on crude visual parameters. In this first application of MALDI IMS to the examination of chronic pressure ulcers, distinctive and consistent molecular differences are revealed for stage IV pressure ulcers. Unique protein features among the various patients were also discovered in the pressure ulcer setting leading us to speculate that such proteomic portraits can be utilized in the growing push to provide personalized wound care that is based on an understanding of

the molecular pathophysiology in each wound. Application of MALDI IMS as either an investigation or prognostic tool has the selectivity and robustness for discovery of complex molecular events in the microenvironments of acute and chronic wounds.

Spatial Detection of Phospholipids in Human Skin Pressure Ulcers by Imaging Mass Spectrometry

Lipids perform both structural and functional roles throughout the body and are known to be important mediators of cell signaling, acting as second messengers in cellular events such as cell growth, cellular proliferation and cell death. Furthermore, lipids are the major building blocks of biomembranes, play key roles in signal transduction, and are an important reservoir of energy in biological systems. Due to these essential functions of lipids, alterations in their metabolism are pivotal occurrences resulting in many pathological conditions.[77-80] Therefore, the study of lipid distribution and relative abundance is an interesting area of research.

Traditionally, the detection of phospholipids has relied on extraction and purification prior to analysis by mass spectrometry. Perhaps for this reason and others, phospholipids have rarely been the focus of wound healing studies. Nevertheless, scant but growing evidence indicates that phospholipid signaling exerts pivotal influences on the dynamic inflammatory events within the complex environment of the wound bed.[81] Much of the work to date has focused on larger lipid species such as the class of molecules in the arachidonic acid group. Perhaps the best studied of the lipid mediators to date is sphingosine-1-phosphate. This lipid mediator is capable of stimulating favorable wound healing properties in keratinocytes as well as fibroblasts.[82, 83] Furthermore, an aberrant signaling pathway downstream of this phosopholipid is apparently responsible for pathologic angiogenesis of diabetics whereas normalization of sphingosine-1-phosphate signaling events has the potential to restore a normal type of angiogenesis.[84]

Until recently the study of lipid composition and distribution in tissue was a complex and time-consuming undertaking as intricate techniques were required to extract and separate lipid species.[85] Such preparative methods had the drawback of being laborious. The resulting data were devoid of spatial information, a problem that limited the usefulness of lipid basedinquiry in tissues with inherent site complexities such as skin and disrupted injured skin with even more dynamic architectural changes. Advances in mass spectrometry, such as matrix-assisted laser desorption/ionization (MALDI), have made it possible to directly probe protein species from tissue.[86, 87] However, the bulk of lipid species in tissue have a molecular weight below 1000 Da and this mass range rendered it difficult to identify analytes by MALDI due to the presence of matrix ions of similar weight or background interference ions resulting from the preparation of tissue sections. Only recently has direct tissue analysis of phospholipids become possible using MALDI-MS.[88-90] MALDI imaging mass spectrometry (MALDI IMS) generates ion density maps from tissue sections that allow for visualization of phospholipid localization without prior knowledge of

the specific molecules being analyzed. A discovery technique is especially necessary since the lipids that may mediate wound repair are largely unknown.

As mentioned above, MALDI-TOF mass spectrometry has become a valuable technique for the direct analysis of biomolecules from tissue.[91-94] MALDI is well suited for *in situ* analysis due to its high sensitivity, large tolerance for salts and other contaminants, and a wide mass range with little fragmentation. There are two general types of experiments conducted using MALDI for *in situ* tissue analysis: profiling and imaging. In profiling experiments, the matrix is deposited (e.g. as droplets) directly onto specific regions of interest in the tissue sections. Due to the solubility of some biomolecules in the matrix solution droplet, the spatial resolution of this method is usually limited to the size of the matrix droplet. Next, the tissue section is mass analyzed and mass spectral profiles are generated. This approach allows for the comparison of focal regions of interest within tissue. By contrast, in an imaging approach, the matrix is applied over the entire tissue section and individual mass spectra are automatically acquired across the entire tissue section. The data can be used to generate two-dimensional ion density maps (images), in which the individual peaks of each mass spectrum are represented by pixels. While the spatial resolution of this technique is limited by the diameter of the laser spot, spatial resolution below 100 μm is easily obtained.

The goal of this study was to use mass spectrometry technologies to explore the lipidomic signatures associated with the chronic wound situation in synchrony with the MALDI IMS technique thereby facilitating discovery of spatial distributions for lipid species. Pressure ulcers were selected for the present study since this sub-type is infrequently examined and its pathophysiology remains poorly understood. The pressure ulcer problem remains a growing economic threat to limited medical resources and is predicted to escalate as the geriatric population expands and as the incidence of diabetes grows. In the acute care hospital setting, the reported incidence rate for pressure ulcers in the USA ranges from 0.4% - 38%, and in long term care settings the reported incidence rate is 2.2% to 23%.[95] We speculated that the spatial distribution of phospholipid signatures may soon prove useful as a tool in the quest to objectively determine whether a chronic wound is improving or worsening. To date, there have been few reports of lipid mediators that influence wound repair in either a positive or negative manner, thus MALDI IMS was applied to an examination of pressure ulcers for the first time.

Results

Initial work was conducted to determine the optimal matrix and matrix depositing technique for analysis of lipids in two cutaneous settings: 1) ulcerated skin from stage IV pressure ulcers and 2) normal skin in physiologic equilibrium. These cutaneous samples were analyzed by MALDI mass spectrometry and MS methods were optimized for glycerophospholipid detection, in particular in the mass range 600-900 Da. For purposes of orientation, a representative H&E from the edge of a massive ulcer exhibiting slight evidence of healing is shown (Figure 16A). This figure is included to illustrate the experimental scheme for the two differing matrix deposition techniques that were utilized throughout this study. DHA matrix was deposited over the tissues by an orderly rastered pattern in order to create a defined array with spatial

resolution of 200 μm (Figure 16B). In other cases, DHB matrix was applied using a sublimation technique. The sublimation technique covered the entire tissue section with a homogeneous and relatively thin layer of matrix powder. Thus the spatial resolution was increased to a few micrometers and matrix deposition appeared nearly uniform (Figure 16C). Based on histological landmarks rendered visible after the H&E staining of each section, spectra were acquired within a region of interest. In the normal skin samples, spectra were aggregated from either epidermis or dermis from a given sample. In the ulcers, spectra were collected from the wound bed, the normal adjacent dermis and also the hypertrophic epidermis when present.
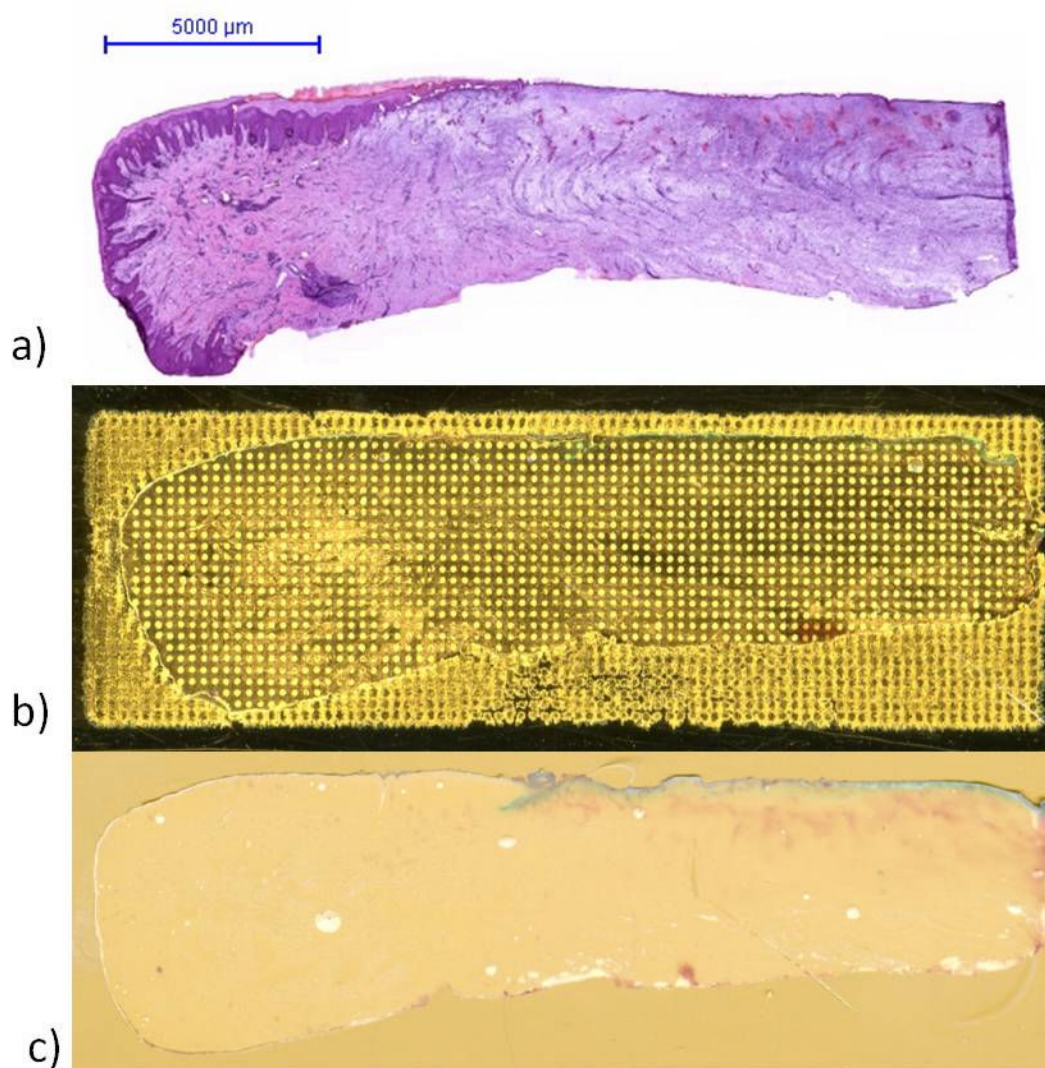
Figure 16: *scheme of the experimental setup comparing the two imaging techniques in this study. (A) photomicrograph showing hemaoxylin and eosin staining of a pressure ulcer illustrating major subregions of interest E – epidermis, AD – adjacent dermis, WB – wound bed. (B) Photomicrograph after matrix deposition with a raster pattern prior to MALDI imaging. (C) Photomicrograph showing uniform matrix coverage of the entire section using the sublimation technique prior to MALDI Scale bar = 5 mm*

MS Profiling

In direct tissue analysis, the selection of the ionization mode (negative vs. positive) determines which classes of lipids are detected. The amount of each lipid class is another critical factor that have an important influence over the *in situ* analysis by mass spectrometry.[85] Tissues were analyzed in both positive and negative ionization mode in the present study and mass spectral profiles were generated for diseased samples (pressure ulcers) and compared to normal human skin (control). Glycerophospholipids are typically divided into classes based upon their head group, and numerous classes of glycerophospholipids were identified in this study. Examination of skin (normal or ulcerated) revealed the presence of the major classes of lipids: glycerophosphocholines (PCs), glycerophosphoserines (PSs), glycerophosphoglycerols (PGs), glycerophosphoinositols (PIs) and glycerophosphates (PAs). Many glycerophospholipids were observed to have unique spatial restrictions and were noted only within the averaged spectra from a sole area of interest within the tissue section. Not surprisingly, other glycerophospholipids were broadly distributed throughout the tissue but showed distinctive relative intensity level differences among the targeted regions of interest. First, the normal control skin showed a lipid composition that markedly differed from the ulcerated skin. There were however, a few signals common to both ulcers and control human skin but these were nonetheless distinctive since expression levels were quite different (e.g. m/z at 577, 725, 734, 741, 782, 820). These ions were found stronger in the normal dermis. Others, for instance PC 32:0 (m/z 756), were noted to be more intense in the dermis adjacent to the wound and in the normal dermis, while the PA 36:3 (m/z 707) was expressed in the wound bed. Figure 17 illustrates mass spectral profiles from two different areas of a representative ulcer (the wound bed and the adjacent dermis) and the dermis from a normal skin sample generated in positive ionization mode. Wound positive profiling showed some stronger peaks in the low mass range 450-600 Da as compared to adjacent dermis (Figure 17A & B). These signals were not detected in the normal dermis (Figure 17C). Further, the base peak of all the spectra acquired in the wound area of the tissue was the ion at m/z 709, a characteristic feature of the ulcerated tissues. By contrast, the spectral profiles from adjacent dermis featured stronger signals in the mass range 650-850 Da and were devoid of signals in the low mass range but maintained the ion at m/z 709 as the base peak (Figure 17B). In positive ionization mode, mass spectra were dominated by PAs, PIs, PSs and a few PCs, with PAs and PSs species showing the greatest regional differences (Table 5). The three major PS species detected were PS 35:0, PS 37:0 and PS 41:1 and their predominant localizations were observed in the wound bed itself. Moreover in the glycerophosphate class, PA 40:3 was also heavily concentrated in the wound as was PA 26:0. The wound profiles displayed also many unique signals between m/z 880 and 1020 (Figure 17A).
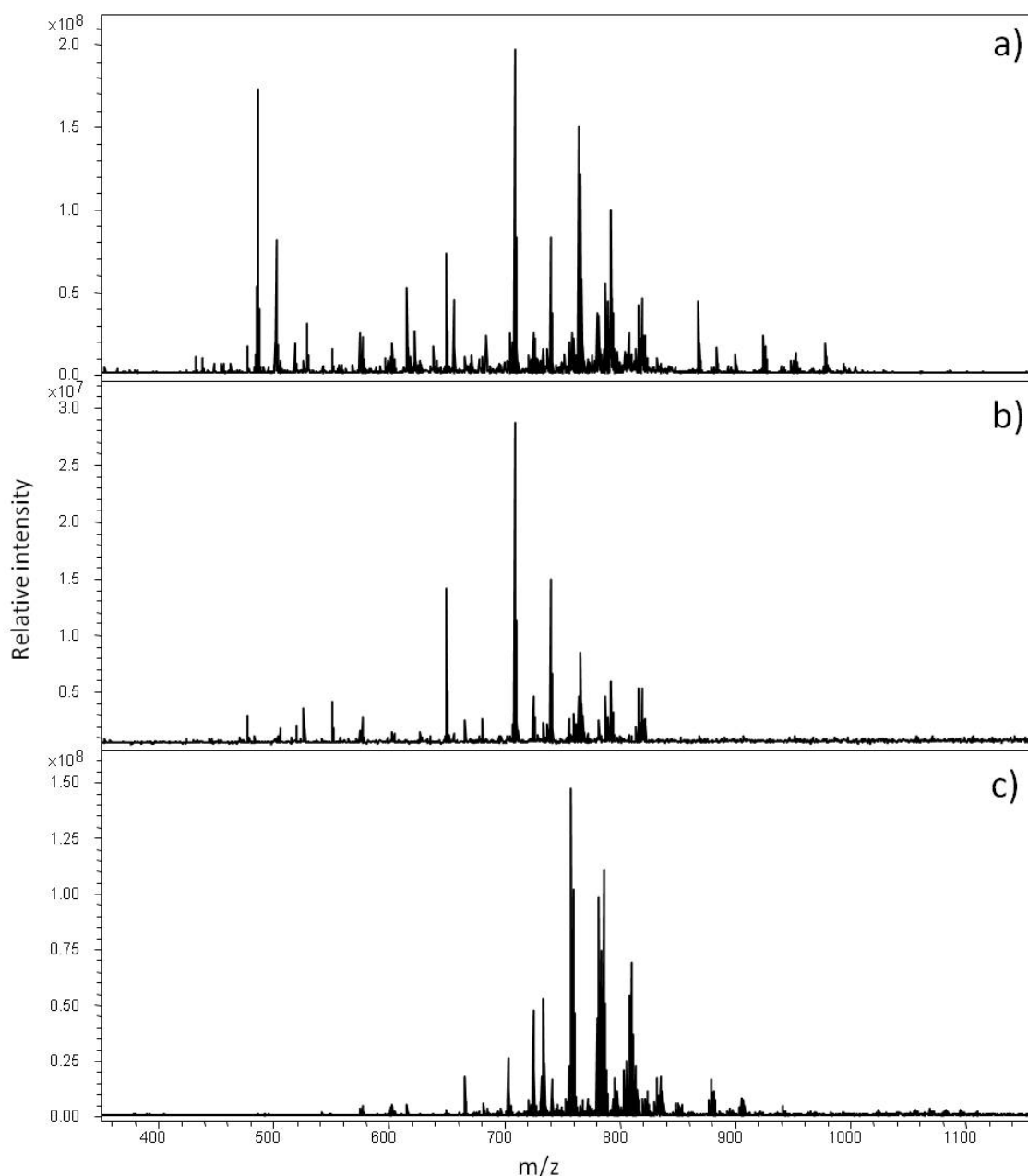
Figure 17: *shows MALDI FT-ICR spectra from a representative ulcer sample and a normal control sample collected under positive ionization mode. (A) displays ions profiled from the wound bed. (B) displays ions profiled from the adjacent dermis at the boundary of the wound as well as (C) displays the lipid pattern from the dermis of a normal patient.*

A different situation was found using negative ionization mode (Figure 18). In this case, the strongest ion detected (base peak) was at m/z 885, assigned by high mass accuracy measurement and identified as a PI 38:4 by tandem mass spectrometry (Figure 19). Furthermore, this ion didn't show a site specific localization, and was observed as the base peak in both the wound bed as well as the adjacent dermis (Figure 18A & B). The normal skins also displayed this PI as base peak (Figure 18C).
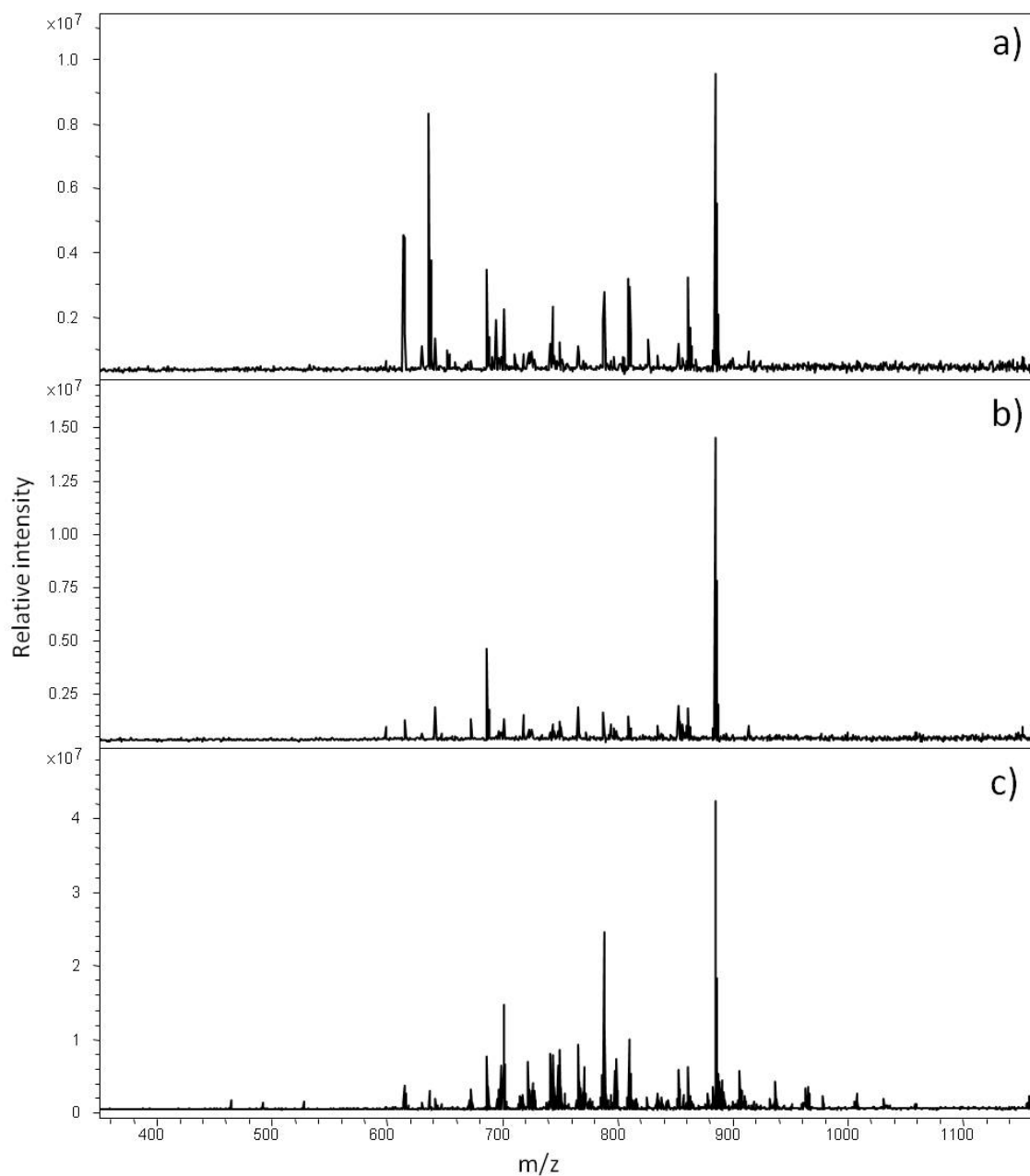
Figure 18: *shows MALDI FT-ICR spectra from a representative ulcer sample and a normal control sample collected under negative ionization mode. (A) displays ions profiled from the wound bed. (B) displays ions profiled from the adjacent dermis at the boundary of the wound as well as (C) displays the lipid pattern from the dermis of a normal patient.*

The wound bed profiled in negative ionization mode produced stronger signals in the mass range 600-700 Da than did the intact adjacent dermis. Several of these signals were unique to the wound bed (Table 6). While PEs, PIs and some PCs were recorded as characteristic of the wound bed in negative ionization mode, a glycerophosphoinositol-phosphate at m/z 1009 (PIP 16:0) was assigned in one of the sample

analyzed. Moreover, a few PAs and PGs were also observed in the low mass range, for example the ion at m/z 454, identified as PA 20:5 and the ion at m/z 465 as PA 20:0 as well as the ion at m/z 505 and the ion at m/z 509 (Table 6). In this study the mass range above 1000 Da was probed and showed very low signals. When the wound region was profiled and analyzed in this range in the positive ionization mode, some glycerophospholipid dimers were detected. Many ions in the high mass range were assigned in negative ion mode after high mass accuracy measurements (10 ppm error). Those species (Table 6) were not identified by tandem mass spectrometry because the fragmentation pattern highlighted only the fragment at m/z 290. We suggest a nominal assignment of the species as glyceroshpingolipids.
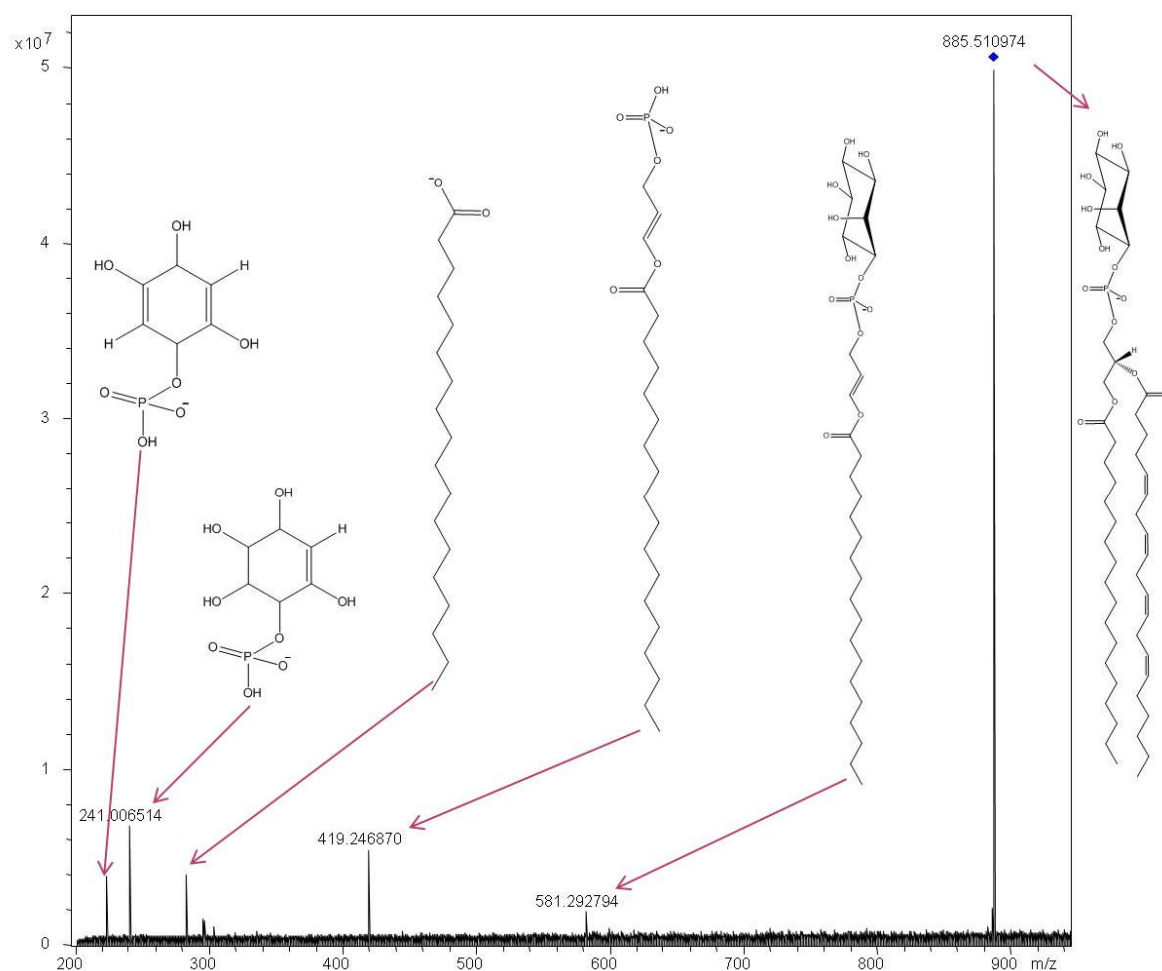
Figure 19: *represeantative MALDI FT-ICR MS/MS spectrum performed in negative ion mode to fragment the speies at m/z 885, assigned by high mass measurement as a phosphoinositol species and validated by tandem mass spectrometry as PI 38:4 (18:0- 20:4).*

MS Imaging

Although the MS profiling technique regionalized many lipid features within selected areas of interest within the wound and normal skin, IMS analyses were also performed in order to obtain ion density maps within tissue sections and to observe spot-to-spot variability across the section. Representative ion density maps for normal human skin are depicted in Figure 20. This particular patient was selected since IMS analysis additionally revealed a unique distribution for some lipid ions depending on whether the ions were located within the papillary or the reticular dermis. For example, IMS localized some glycerophospholipids in the papillary dermis, such as PA 38:4 or PC 32:0, while others were density mapped restricted to the reticular dermis, such as two PI species, the ions at m/z 851 and 853 and two TGs, the ions at m/z 879 and 881 (Table 5). This demarcation between the papillary and reticular dermis was not a feature of the majority of the normal dermal samples and illustrates that IMS of lipids has the sensitivity and capacity to detect fine nuances when they are present in patients. Ulcer samples were also analyzed by IMS (Figures 21-22). When ions were density mapped, several proved to be restricted to either the wound area or to the adjacent dermis, a finding that was expected based on the profiled spectra illustrated in Figures 17 & 18. Additionally, the IMS technique provided novel microenvironmental wound data that were not captured with profiling. For instance, while the histological examination of a stained tissue section suggested that the wound bed can be distinguished from adjacent dermis, the high resolution analysis of the whole tissue section by IMS brought to light evidence of a further partitioning of the wound bed into two distinct lipidomic signatures. Spatial displays from the ion density maps suggested (in 3 of the 6 wounds in this study) that some ions were restricted to or were considerably higher in intensity in either the upper portion or the lower portion of the wound bed or that the portion closest to the adjacent dermis which we surmise is the relatively more mature portion of the wound that more closely resembles the adjacent dermis (Figures 21 & 22). In particular, PSs species were restricted to the upper wound bed in the density maps for these 3 ulcers. The distribution of two ions was targeted to the lower wound bed: the ions at m/z 551 and 741, identified as PA 26:0 and PA 40:3 respectively. By contrast, the ion at m/z 792 was consistently associated with an upper wound distribution, the area of the wound that is most tenuous and nascent and often more colonized with a biofilm (Figure 21 & 22).

Two of the ulcers included in this survey showed little or no demarcation in ion distributions between the upper and lower wound bed (Figure 22, middle column). The uniformly high ion intensities throughout the entire wound bed in these patients were the same ions that were consistently associated in the upper/lower wounds in the other ulcers in this study. Scrutiny of the clinical descriptions for these patients and their wounds provided additional clues to explain the two diverse IMS display patterns. In retrospect, IMS display patterns in concert with gross clinical and histological evidence led us to propose a two part classification scheme.

Wounds such as the examples depicted in Figure 21 and Figure 22 (left column) were classified as "healing" based on their histological features (new collagen deposition in the wound base, robust capillary in-growth and a relative paucity of neutrophils) and gross clinical impression of wound improvement in the weeks leading up to surgical excision. Other wounds such as the example depicted in Figure 22 (middle column) were classified as "non-healing". Histologically such wounds showed little new

collagen, a paucity of capillary in-growth and an abundance of neutrophils. Clinically these patients had a higher acuity (more serious systemic condition) and longitudinal clinical assessment of these wounds indicated no evidence of improvement in the lead up period to surgery. Subsequent examination of the clinical scenarios after surgical excision followed by skin flap coverage indicated that these patients experienced significant morbidities and associated wound dehiscence.
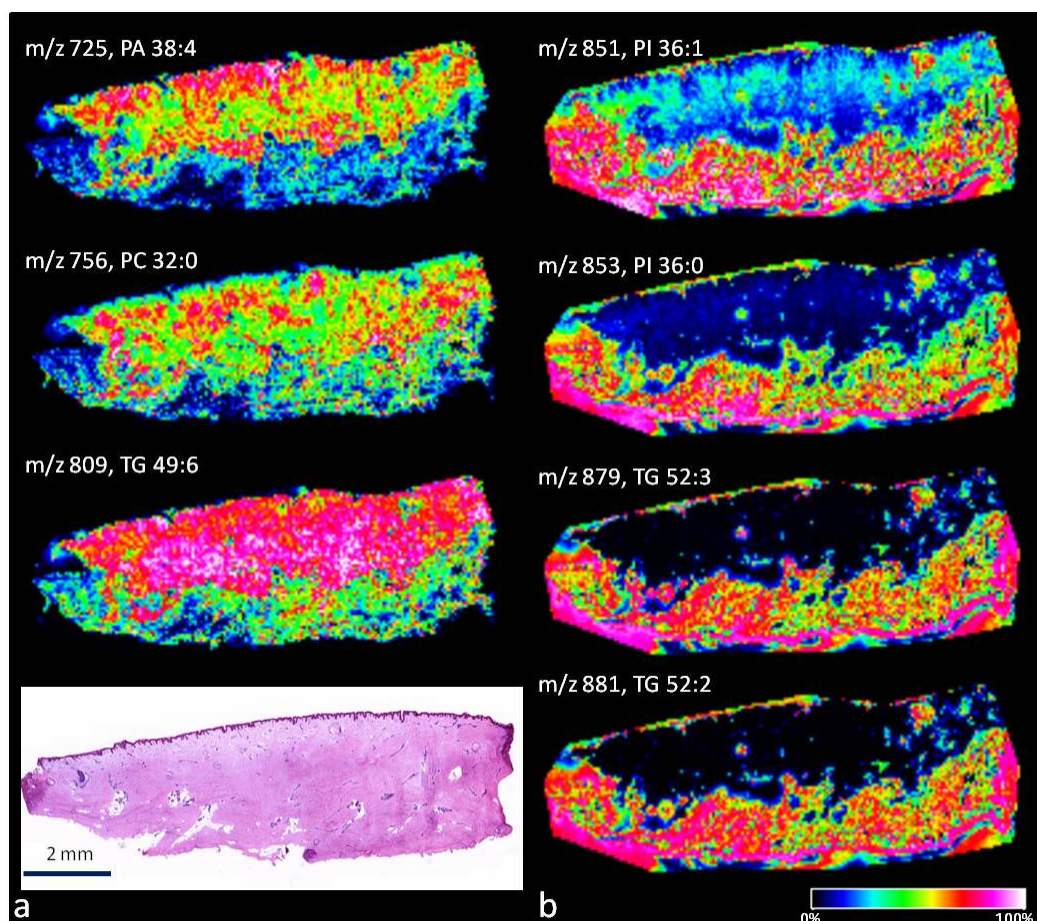
Figure 20: *shows a collection of representative ion density maps from the skin of a normal patient. Column a) shows ions with a predominant upper papillary dermal distribution. Column b) shows ions with a predominant lower reticular dermal distribution. A serial section stained with hematoxylin and eosin is included at the bottom of column a for orientation purposes. E = epidermis, PD = papillary dermis, RD = reticular dermis. Scale bar = 2 mm*

While the IMS data in this study suggest that lipid species are dynamically modified in chronic wounds, these data also suggest that the phospholipid story is a complex one. For example the m/z 868 doesn't seem to show any correlation to wound status from the images in Figure 22; however the wound in Figure 21 shows that this ion is uniquely restricted to the upper wound. The ion at m/z 979 (PI 44:0) seems

enigmatic in that it is distributed in the upper wound in Figure 21, in the upper wound and dermal area in Figure 22 (left column) and at very low levels in another wound (Figure 22 middle column). IMS validated this preliminary clinical data, since in the healing wound sample (left column in Figure 22) the ions density mapped within the wound bed of other patients as well as restricted either to the upper or lower wound beds (Figure 21), were not all restricted to the wound area in this case. Further, the relative expression levels for these lipid species characteristic of the ulcer area were found lower than the other ulcer samples involved in this study.
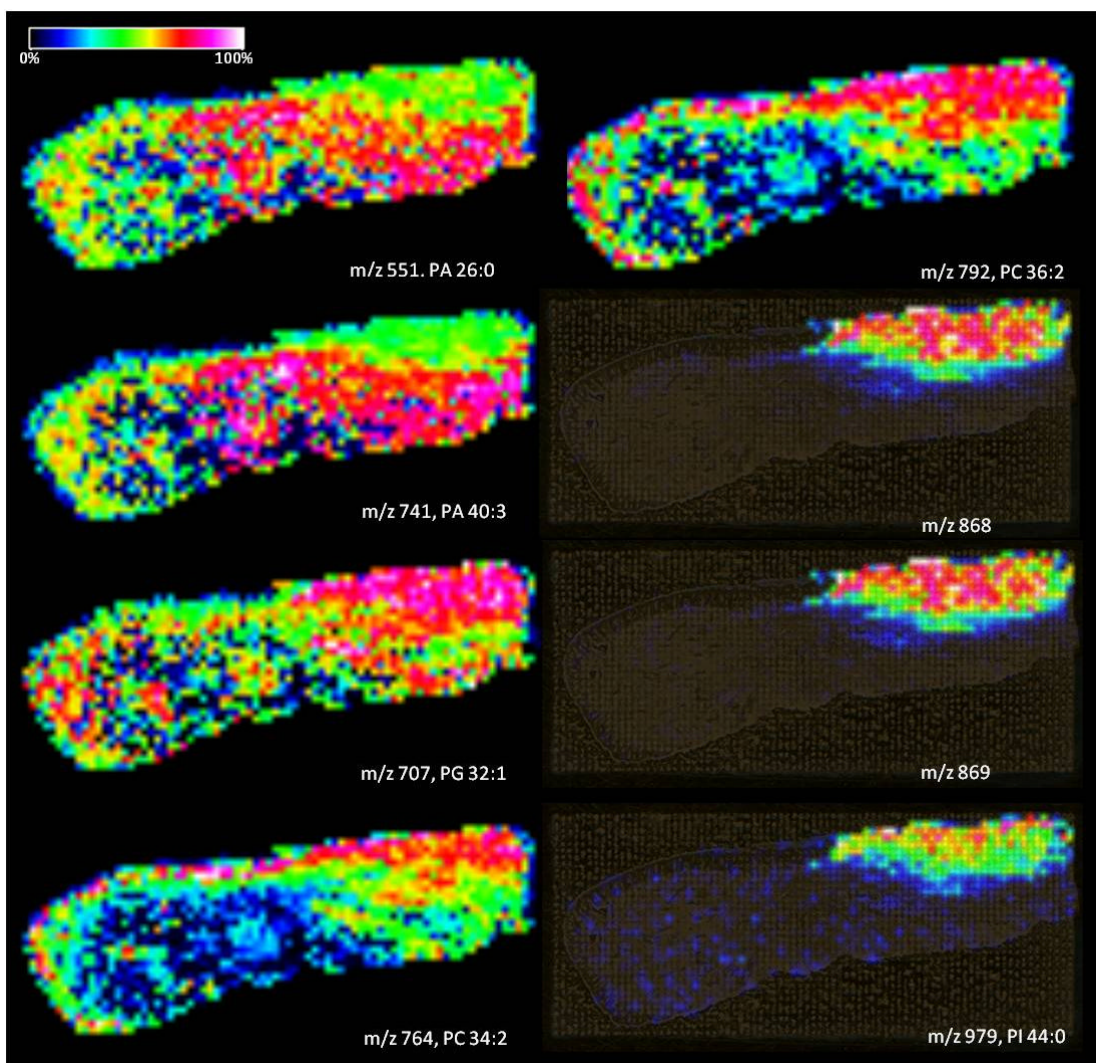
Figure 21: *shows ion density maps and spatial distribution of representative molecules in a pressure ulcer. The upper (most immature) portion of the wound is displayed in the upper right corner in the sample and shows a unique ion distribution that sets it apart from the lower more mature region (lower right corner of the sample). The ion intensity is uniquely different in the adjacent dermis that immediately borders the wound (left corner). The corresponding H & E slide for this wound is featured in Figure 16.*

An exception was found for the ions at m/z 979 and 869, largely restricted to the wound bed also in this healing wound sample. Moreover, in the non-healing sample (Figure 22, middle column), some of the wound lipid species were found higher expressed, even if not localized in any areas of the wound but just generally distributed. This finding confirmed that this sample doesn't show any evidence of improvement.
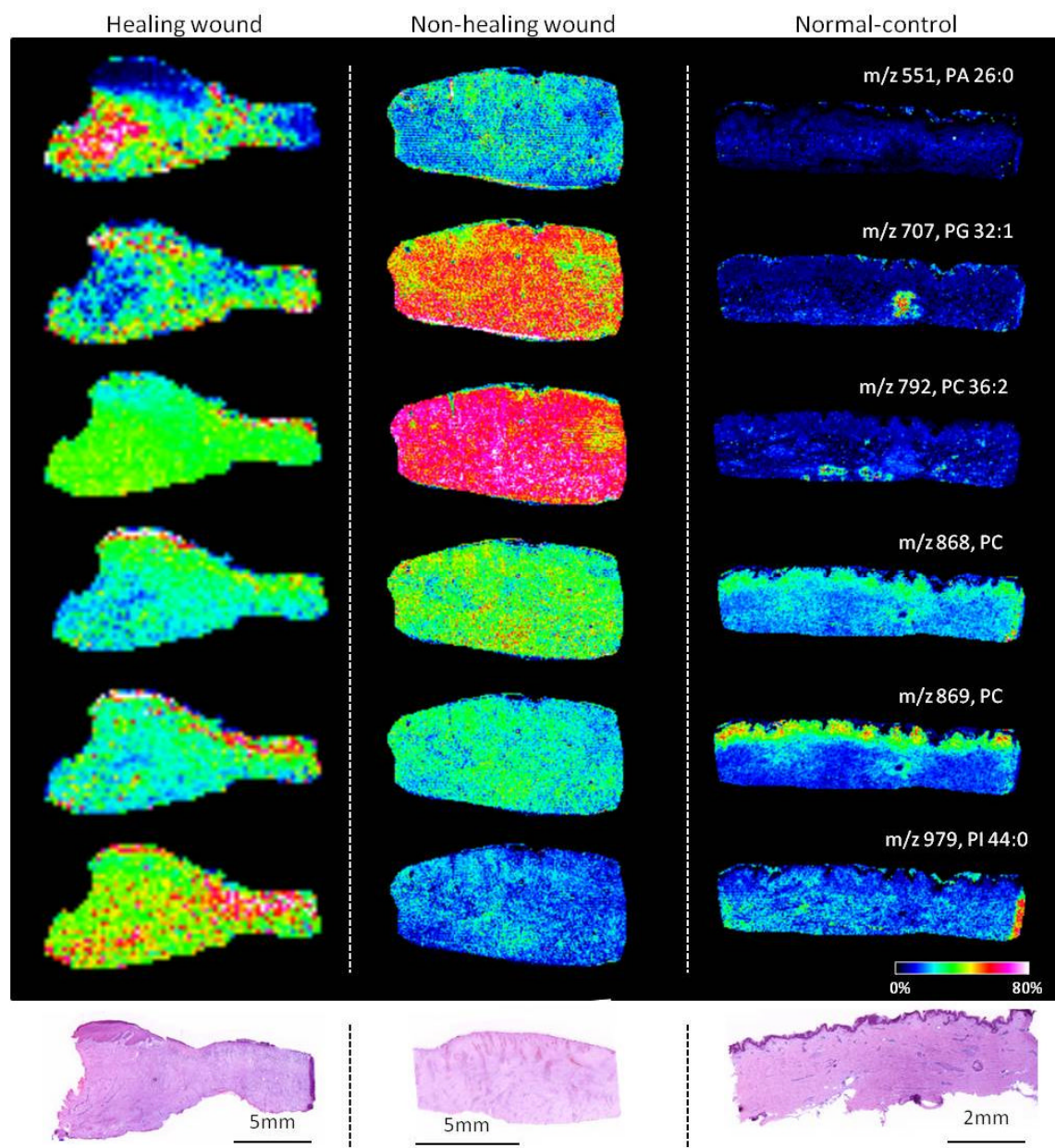
Figure 22: *shows ion density mapping for the spatial distribution of representative lipid molecules in specimens collected from an improving chronic wound (left column), a stagnant chronic wound (middle column) and normal control skin (right column). The lowest row of images shows the corresponding section stained with hematoxylin and eosin. Images in the middle column were collected using 60 μm spot-*

to-spot resolution while the right column at 40 μm. Images in the left column were collected using 200 μm resolution. E = epidermis, D = dermis, WB = wound bed Scale bar value 5 mm and 2 mm

By contrast, the 4 other patients in this study did show clinical evidence of improvement in their wounds so their wounds were classified as improving. Thus by inference the IMS lipid pattern from upper portion of these wounds was judged as a circumstance of nascent or immature healing as compared to the deeper portion of the wound bed. Further validation of the unique wound associated lipid pattern is provided by a comparative examination of the ion density maps from normal patients. In Figure 22 (right column) these IMS ion density maps document the very low presence of these ions in the dermis or epidermis of the normal skin. The ions at 868 and 869 appear to have one function in normal skin (i.e, they are found at the dermal-epidermal junction) and another one in the circumstance of a chronic wound where intensities are slightly elevated by comparison and do not shown restriction to areas of interest in the healing wound example shown in Figure 22, column left. Near the conclusion of this study an updated MALDI IMS resolution became feasible. IMS experiments were performed at 60 µm and 40 µm spatial resolution, respectively. The high resolution IMS analysis was used to reach tissue architecture details such as the epidermis and dermal structures. IMS high resolution displayed and confirmed the absence of the epidermis in the non-healing wound sample. By contrast, the high resolution IMS made it possible to visualize ions that were focally restricted in distribution to the dermal-epidermal juction in the normal sample we used as control (Figure 22, right column). IMS was sensitive enough to create ion density map also for lower signals. As mentioned in the MS profiling, the negative ionization mode highlighted the presence of some species in high mass range phospholipids within the wound bed. Using tandem mass spectrometry we were able only to assign the species of these masses as glycerosphingolipids. While the signals were very low in terms of relative intensity compared with others, the IMS technique proved sensitive enough to detect this family of molecules in the form of ion density maps.

Discussion

Since the introduction of MALDI imaging over a decade ago, this analytical tool has assumed increasing importance in biological and medical research. The novel information obtained by tissue IMS has shed new light on the multi-focal disturbances that occur in skin ulcerations. Although it has long been known that pressure ulcers represent a major inflammatory based circumstance and several lipid mediators have been associated with acute and chronic inflammation[96], the present study has been useful since it has expanded previous knowledge by examining lipids in the range between 300 and 2000 Da. Additionally, due to the spatial resolution and the possibility of analyzing a whole tissue section (imaging MS) instead few points per areas (profiling MS), sub-regions of a general wound bed were observed in an objective fashion for the first time. The latter finding opens another avenue for the classification of skin pressure ulcers. This report takes advantage of the recent developments in instrumentation and sample preparation that have expanded the options for analysis of the spatial distribution of phospholipids directly from tissue sections. While MALDI IMS has recently shown promise as an experimental tool for mapping of

phospholipids and endogenous metabolites in tissues such as brain and embryos[88, 90], this promising new approach has not been previously applied to the study of chronic wounds or normal skin in a state of physiologic equilibrium. Several salient features emerged when unknown phospholipids were probed within their spatial context. Ion density maps highlighted signals that were differentially expressed in the upper and lower regions of wound beds. This unexpected finding was a consistent feature of pressure ulcers showing signs of improvement but was not a prime feature in the most stagnant pressure ulcers included in our experimental series. This technique proved especially useful as a discovery tool since searches for targeted lipids could prove expansive, cost prohibitive and require large volumes of ulcer tissue. These data added credence to our hypothesis that a histological correlation with molecular data containing spatial identifiers offers a powerful new tool to probe the unfavorable and favorable metabolic nuances that are determinants of wound healing status and capabilities. As is frequently the case when a new technology is applied, our findings raise new challenges and leave many questions unanswered. The prime question is one of how to interpret the histological clues in light of the differential lipid intensities and spatial distributions that were detected in pressure ulcers and normal skin samples. Several ions seemed to display a "logical pattern" that showed a strong correlation with upper and lower wound bed. The histology in these cases revealed a poorly differentiated loose arrangement of granulation tissue exhibiting a high degree of inflammation and edema while the lower wound showed a diminished cellularity due to a relative abundance of collagen and decreasing density of capillaries that suggested but did not prove that this sub-region was further along in the healing/remodeling phase. Clearly the morphological characterization of the pressure ulcer wound bed is an area that has only garnered sporadic treatment in the wound healing literature[97, 99], and this further limits our ability to provide a detailed comparison and correlation of underlying histological features with our newly uncovered MALDI IMS lipid distribution. One of the stated purposes of our study was to examine the feasibility, sensitivity and potential usefulness of a new technique to the field of wound repair. Our collection of stage IV pressure ulcer wounds was random and this exploratory survey was limited in design to one static collection date. In retrospect, the MALDI IMS data in this study appeared to correlate with the clinical notes crudely describing the recent healing or non healing status of each wound. However without longitudinal tracking of these wounds it is impossible to state with certainty whether a given wound was improving, remaining stagnant or actually enlarging and getting progressively worse. Such definitive statements and correlations with lipid spatial distributions must await either a larger prospective randomized clinical trial with multiple tissue samplings or similar studies in an acute wound healing animal model where there can be tight tracking of the temporal sequence of healing. The present study demonstrated that MALDI MS for phospholipids (whether used in profiling or imaging mode) has the sensitivity to detect nuanced differences between the dermis that borders the wound and the dermis that is perfectly normal. A similar focus using MALDI MS to define the gradient in tumor associated stromal proteins as one moved away from the tumor itself showed that nearby tissue can be quite metabolically affected or exert its own influence.[100] This recent finding leads us to speculate that the imaging of lipids from the dermis at the periphery of the wound may likewise serve as a prognostic indicator of events to come. In the case of the chronic wounds, an increase or decrease in certain phospholipids may signal improvement in wound status

or the eminent threat of deterioration. Several wounds in the present study were also included in a parallel proteomic analysis. Taken together our composite data show evidence of a high degree of inflammatory markers in the adjacent dermis and hypertrophic epidermis of the same wounds. Thus MALDI IMS has allowed us to visualize that the equilibrium between a chronic wound bed and the surrounding tissue is a complex dynamic as hypothesized by others[101] and recently shown by unique transcriptional profiles of endothelial cells at the margin[102] and hypertrophic epidermis at the margin.[103, 104] We believe that this tool provides a new experimental approach to gauge the molecular perturbations associated with inflammation, bioburden, and ischemia, all hypothesized factors that determine at any given point in time whether a wound is either on the pathway toward improvement, remaining stagnant or is headed on a downward spiral toward organ failure. Another advantage of the MALDI IMS approach was its suitability as a discovery tool. The present survey exploring the feasibility of MALDI IMS to uncover relevant lipid perturbations within the pressure ulcer environment showcases the potential of one such diagnostic tool. The striking differences in the lipid profiles between upper and lower portions of the improving wounds versus the stagnant and possibly worsening wounds suggest the eventual possibility to develop prognostic tools based on lipid signatures. Broad scale interrogations that can track multiple molecular events such as the one in this report are much needed and especially appropriate for application to the field of wound healing. Pressure ulcers go through a host of processes ranging from necrosis, degradation, apoptosis, inflammation, infection, cell proliferation, matrix deposition and remodeling. Thus it is very unlikely that a single, dual or triple tracking of molecules will be successful in predicting whether a wound is healing, remaining in a stagnant state or continuing on a further downhill spiral. Whether a lipid profiling tool eventually finds utility as a clinical tool or whether it is more appropriately applied in the experimental setting as a global discovery tool will require considerably more prospective investigation. The data presented herein comprise foundational evidence that the lipidomic avenue is worthy of additional exploration and application in other chronic wound types. Furthermore, the definitive ion differences between the papillary and reticular regions of normal dermis suggest that MALDI IMS has the sensitivity to reveal subtle and heretofore undetected differences in many other disorders that fall in the realm of dermatopathology.

In summary, the application of MALDI IMS techniques to uncover the role of lipids in chronic pressure ulcers has provided solid evidence of multiple and dynamic alterations at work in this poorly understood chronic situation that is marked with architectural complexities. The ability to define a healing ulcer from a non-healing ulcer based on its lipid signature has the potential to produce a new diagnostic modality in a field where treatment regimes are currently limited to guesswork and the degree of experience of the caregiver's gross visual observations of the wound surface. Our discovery of the dynamic modulation of multiple lipid species with chronic wounds in various stages of improvement or stagnation supplies the wound healing community with a fresh new set of potential molecules that may allow for progress toward elucidation of the multitude of disturbances that perpetuate wound chronicity.

This IMS approach to the study of such pressure ulcers brings new perspectives to improve the paucity of knowledge about lipid biomolecules involved in this chronic condition. MALDI MS also offers a valid

and straightforward method for lipid species assignment and identification for a large number of the most intense signals. This work was a preliminary study carried out to explore the potential of the powerful analytical technique of mass spectrometry in the investigation of chronic disturbances occurring on human skin in case of ulceration. Technological improvement allowed us to extend the range for ion detection at the upper range to include lipid ions at 1000-1500 Da. Future research applied on a large cohort of patients can further validate these preliminary data. Our findings highlight a characteristic lipid pattern within the wound area of an ulcer tissue as well as within the normal skin layers. Such data can be used to examine causative complex molecular pathways or healing status in a new way.

m/z	*Ion*	*Species*	*ID*
487	[M+H]$^+$	PA	20:1
602	[M+H]$^+$	PC	22:0
725	[M+H]$^+$	PA	38:4
756	[M+Na]$^+$	PC	32:0
772	[M+Na]$^+$	PC	32:0
798	[M+H]$^+$	PC	34:1
800	[M+H]$^+$	PC	34:0
810	[M+Na]$^+$	PC	38:4
820	[M+H]$^+$	PC	36:4
826	[M+Na]$^+$	PC	36:1
838	[M+H]$^+$	PC	38:1
844	[M+H]$^+$	PC	38:6
852	[M+Na]$^+$	PC	42:4
853	[M+Na]$^+$	PG	42:5
872	[M+H]$^+$	PC	40:6
879	[M+H]$^+$	TG	52:3
881	[M+H]$^+$	TG	52:2
897	[M+H]$^+$	TG	55:7
907	[M+H]$^+$	TG	56:6

Table 5: *positive ion mode human skin identified species.*

m/z [M-H]⁻	*Mass defect*	*Species*	*ID*
687	0.5267	PG	30:3
699	0.5016	PA	36:2 (18:0/18:2)
701	0.4935	PA	36:1 (18:0/18:1)
770	0.5773	PE	38:2 (18:1/20:1)
788	0.7193	PS	36:1 (18:0/18:1)
797	0.6312	PG	38:4 (18:1/20:3)
835	0.5972	PI	34:1 (16:0/18:1)
836	0.5119	PS	40:5 (18:0/22:5)
838	0.5321	PS	40:4 (18:0/22:4)
857	0.4903	PI	36:4 (16:0/20:4)
859	0.5012	PI	36:3 (18:1/18:2)
861	0.5218	PI	36:2
863	0.5352	PI	36:1 (18:0/18:1)
883	0.5042	PI	38:5 (18:1/20:4)
885	0.5109	PI	38:4 (18:0/20:4)
887	0.5338	PI	38:3 (18:0/20:3)
911	0.5336	PI	40:5 (18:0/22:5)
913	0.5517	PI	40:4 (18:0/22:4)

Table 6: *negative ion mode human skin identified species.*

References

1. Aebersold R, Goodlett DR (2001) Mass spectrometry in proteomics. Chem Rev 101:269-295.

2. Chung CH, Levy S, Chaurand P, Carbone DP (2007) Genomics and proteomics: emerging technologies in clinical cancer research. *Crit Rev Oncol Hematol* 61:1-25.

3. Lahm HW, Langen H (2000) Mass spectrometry: a tool for the identification of proteins separated by gels. *Electrophoresis* 21:2105-2114.

4. Pandey A, Mann M (2000) Proteomics to study genes and genomes. *Nature* 405:837-846.

5. Roepstorff P (1997) Mass spectrometry in protein studies from genome to function. *Curr Opin Biotechnol* 8:6-13.

6. Dezitter X, Hammoudi F, Belverge N, Deloulme JC, Drobecq H, Masselot B*, et al.* (2007) Proteomics unveil corticoid-induced S100A11 shuttling in keratinocyte differentiation. *Biochem Biophys Res Commun* 360:627-632.

7. Pflieger D, Chabane S, Gaillard O, Bernard BA, Ducoroy P, Rossier J*, et al.* (2006) Comparative proteomic analysis of extracellular matrix proteins secreted by two types of skin fibroblasts. *Proteomics* 6:5868-5879.

8. Huang C-M W, C-C, Barner S, Elmets CA (2006) In vivo detection of secreted proteins from wounded skin using capillary ultrafiltration probes and mass spectrometric proteomics. *Proteomics* 6, 5805-5814.

9. Aden N, Shiwen X, Aden D, Black C, Nuttall A, Denton CP*, et al.* (2008) Proteomic analysis of scleroderma lesional skin reveals activated wound healing phenotype of epidermal cell layer. *Rheumatology (Oxford)* 47:1754-1760.

10. Pollins AC, Friedman DB, Nanney LB (2007) Proteomic investigation of human burn wounds by 2D-difference gel electrophoresis and mass spectrometry. *J Surg Res* 142:143-152.

11. Brown RS, Lennon JJ (1995) Mass resolution improvement by incorporation of pulsed ion extraction in a matrix-assisted laser desorption/ionization linear time-of-flight mass spectrometer. *Anal Chem* 67:1998-2003.

12. Vestal MJ, P; Martin, SA (1995) Delayed Extraction Matrix-Assisted Laser-Desorption Time-of-Flight Mass-Spectrometry. *Rapid Commun Mass Spectrom* 9:1044-1050.

13. Aerni HR, Cornett DS, Caprioli RM (2006) Automated acoustic matrix deposition for MALDI sample preparation. *Anal Chem* 78:827-834.

14. Chaurand P, Cornett DS, Caprioli RM (2006) Molecular imaging of thin mammalian tissue sections by mass spectrometry. *Curr Opin Biotechnol* 17:431-436.

15. Chaurand P, Norris JL, Cornett DS, Mobley JA, Caprioli RM (2006) New developments in profiling and imaging of proteins from tissue sections by MALDI mass spectrometry. *J Proteome Res* 5:2889-2900.

16. Stoeckli M, Staab D, Staufenbiel M, Wiederhold KH, Signor L (2002) Molecular imaging of amyloid beta peptides in mouse brain sections using mass spectrometry. *Anal Biochem* 311:33-39.

17. Garrett TJ, Prieto-Conaway MC, Kovtoun V, Bui H, Izgarian N, Stafford G*, et al.* (2007) Imaging of small molecules in tissue sections with a new intermediate-pressure MALDI linear ion trap mass spectrometer. *International Journal of Mass Spectrometry* 260:166-176.

18. Khatib-Shahidi S, Andersson M, Herman JL, Gillespie TA, Caprioli RM (2006) Direct molecular analysis of whole-body animal tissue sections by imaging MALDI mass spectrometry. *Anal Chem* 78:6448-6456.

19. Reyzer ML, Caprioli RM (2007) MALDI-MS-based imaging of small molecules and proteins in tissues. *Curr Opin Chem Biol* 11:29-35.

20. Reyzer ML, Hsieh Y, Ng K, Korfmacher WA, Caprioli RM (2003) Direct analysis of drug candidates in tissue by matrix-assisted laser desorption/ionization mass spectrometry. *J Mass Spectrom* 38:1081-1092.

21. Chaurand P, Sanders ME, Jensen RA, Caprioli RM (2004) Proteomics in diagnostic pathology: profiling and imaging proteins directly in tissue sections. *Am J Pathol* 165:1057-1068.

22. Chaurand P, Schwartz SA, Caprioli RM (2004) Assessing protein patterns in disease using imaging mass spectrometry. *J Proteome Res* 3:245-252.

23. Chaurand P, Schwartz SA, Caprioli RM (2004) Profiling and imaging proteins in tissue sections by MS. *Anal Chem* 76:87A-93A.

24. Cornett DS, Mobley JA, Dias EC, Andersson M, Arteaga CL, Sanders ME*, et al.* (2006) A novel histology-directed strategy for MALDI-MS tissue profiling that improves throughput and cellular specificity in human breast cancer. *Mol Cell Proteomics* 5:1975-198.

25. Cornett DS, Reyzer ML, Chaurand P, Caprioli RM (2007) MALDI imaging mass spectrometry: molecular snapshots of biochemical systems. *Nat Methods* 4:828-833.

26. Schwartz SA, Weil RJ, Thompson RC, Shyr Y, Moore JH, Toms SA*, et al.* (2005) Proteomic-based prognosis of brain tumor patients using direct-tissue matrix-assisted laser desorption ionization mass spectrometry. *Cancer Res* 65:7674-7681.

27. Stoeckli M, Chaurand P, Hallahan DE, Caprioli RM (2001) Imaging mass spectrometry: a new technology for the analysis of protein expression in mammalian tissues. *Nat Med* 7:493-496.

28. Yanagisawa K, Shyr Y, Xu BJ, Massion PP, Larsen PH, White BC*, et al.* (2003) Proteomic patterns of tumour subsets in non-small-cell lung cancer. *Lancet* 362:433-439.

29. Chaurand P, Schwartz SA, Billheimer D, Xu BJ, Crecelius A, Caprioli RM (2004b) Integrating histology and imaging mass spectrometry. *Anal Chem* 76:1145-1155.

30. Schwartz SA, Reyzer ML, Caprioli RM (2003) Direct tissue analysis using matrix-assisted laser desorption/ionization mass spectrometry: practical aspects of sample preparation. *J Mass Spectrom* 38:699-708.

31. Sugiura Y, Shimma S, Setou M (2006) Two-step matrix application technique to improve ionization efficiency for matrix-assisted laser desorption/ionization in imaging mass spectrometry. *Anal Chem* 78:8227-8235.

32. McCombie G, Staab D, Stoeckli M, Knochenmuss R (2005) Spatial and spectral correlations in MALDI mass spectrometry images by clustering and multivariate analysis. *Anal Chem* 77:6118-6124.

33. Norris JL, Cornett DS, Mobley JA, Andersson M, Seeley EH, Chaurand P*, et al.* (2007) Processing MALDI Mass Spectra to Improve Mass Spectral Direct Tissue Analysis. *Int J Mass Spectrom* 260:212-221.

34. Caldwell RL, Opalenik SR, Davidson JM, Caprioli RM, Nanney LB (2008) Tissue profiling MALDI mass spectrometry reveals prominent calcium-binding proteins in the proteome of regenerative MRL mouse wounds. *Wound Repair Regen* 16:442-449.

35. Nanney LB, Caldwell RL, Pollins AC, Cardwell NL, Opalenik SR, Davidson JM (2006) Novel approaches for understanding the mechanisms of wound repair. *J Investig Dermatol Symp Proc* 11:132-139.

36. Groseclose MR, Andersson M, Hardesty WM, Caprioli RM (2007) Identification of proteins directly from tissue: in situ tryptic digestions coupled with imaging mass spectrometry. *J Mass Spectrom* 42:254-262.

37. Groseclose MR, Massion PP, Chaurand P, Caprioli RM (2008) High-throughput proteomic analysis of formalin-fixed paraffin-embedded tissue microarrays using MALDI imaging mass spectrometry. *Proteomics,* 8 (18), 3715-24..

38. Chakravarti S, Magnuson T (1995) Localization of mouse lumican (keratan sulfate proteoglycan) to distal chromosome 10. *Mamm Genome* 6:367-368.

39. Chakravarti S, Stallings RL, SundarRaj N, Cornuet PK, Hassell JR (1995) Primary structure of human lumican (keratan sulfate proteoglycan) and localization of the gene (LUM) to chromosome 12q21.3-q22. *Genomics* 27:481-488.

40. Rinn JL, Bondre C, Gladstone HB, Brown PO, Chang HY (2006) Anatomic demarcation by positional variation in fibroblast gene expression programs. *PLoS Genet* 2:e119.

41. Rinn JL, Wang JK, Allen N, Brugmann SA, Mikels AJ, Liu H*, et al.* (2008) A dermal HOX transcriptional program regulates site-specific epidermal fate. *Genes Dev* 22:303-307.

42. Rinn JL, Wang JK, Liu H, Montgomery K, van de Rijn M, Chang HY (2008) A systems biology approach to anatomic diversity of skin. *J Invest Dermatol* 128:776-782.

43. Philp D, Scheremeta B, Sibliss K, Zhou M, Fine EL, Nguyen M*, et al.* (2006) Thymosin beta4 promotes matrix metalloproteinase expression during wound repair. *J Cell Physiol* 208:195-200.

44. Wyczolkowska J, Walczak-Drzewiecka A, Wagner W, Dastych J (2007) Thymosin beta4 and thymosin beta4-derived peptides induce mast cell exocytosis. *Peptides* 28:752-759.

45. Philp D, Nguyen M, Scheremeta B, St-Surin S, Villa AM, Orgel A*, et al.* (2004) Thymosin beta4 increases hair growth by activation of hair follicle stem cells. *FASEB J* 18:385-387.

46. Smart N, Rossdeutsch A, Riley PR (2007) Thymosin beta4 and angiogenesis: modes of action and therapeutic potential. *Angiogenesis* 10:229-241.

47. Girardi M, Sherling MA, Filler RB, Shires J, Theodoridis E, Hayday AC*, et al.* (2003) Anti-inflammatory effects in the skin of thymosin-beta4 splice-variants. *Immunology* 109:1-7.

48. Philp D, Badamchian M, Scheremeta B, Nguyen M, Goldstein AL, Kleinman HK (2003) Thymosin beta 4 and a synthetic peptide containing its actin-binding domain promote dermal wound repair in db/db diabetic mice and in aged mice. *Wound Repair Regen* 11:19-24.

49. Goldstein AL, Hannappel E, Kleinman HK (2005) Thymosin beta4: actin-sequestering protein moonlights to repair injured tissues. *Trends Mol Med* 11:421-429.

50. Bhattacharjee N, De PM, Chakravarti SK, Chakraborty MS, Neogi DK, Mukherjee KK (1995) Febrile episode among a floating population of C.R.P.F. Jawans stationed at Calcutta. *J Commun Dis* 27:70-76.

51. Sen, C.K., et al., *Human skin wounds: a major and snowballing threat to public health and the economy.* Wound Repair Regen, 2009. **17**(6): p. 763-71.

52. Menke, N.B., et al., *Impaired wound healing.* Clin Dermatol, 2007. **25**(1): p. 19-25.

53. *Consensus Development Conference on Diabetic Foot Wound Care: 7-8 April 1999, Boston, Massachusetts. American Diabetes Association.* Diabetes Care, 1999. **22**(8): p. 1354-60.

54. Fogerty, M.D., et al., *Risk factors for pressure ulcers in acute care hospitals.* Wound Repair Regen, 2008. **16**(1): p. 11-8.

55. Fogerty, M., et al., *African Americans show increased risk for pressure ulcers: a retrospective analysis of acute care hospitals in America.* Wound Repair Regen, 2009. **17**(5): p. 678-84.

56. Mustoe, T.A., K. O'Shaughnessy, and O. Kloeters, *Chronic wound pathogenesis and current treatment strategies: a unifying hypothesis.* Plast Reconstr Surg, 2006. **117**(7 Suppl): p. 35S-41S.

57. Trengove, N.J., et al., *Analysis of the acute and chronic wound environments: the role of proteases and their inhibitors.* Wound Repair Regen, 1999. **7**(6): p. 442-52.

58. Yager, D.R. and B.C. Nwomeh, *The proteolytic environment of chronic wounds.* Wound Repair Regen, 1999. **7**(6): p. 433-41.

59. Nwomeh, B.C., et al., *MMP-8 is the predominant collagenase in healing wounds and nonhealing ulcers.* J Surg Res, 1999. **81**(2): p. 189-95.

60. Diegelmann, R.F., *Excessive neutrophils characterize chronic pressure ulcers.* Wound Repair Regen, 2003. **11**(6): p. 490-5.

61. Vande Berg, J.S., et al., *Cultured pressure ulcer fibroblasts show replicative senescence with elevated production of plasmin, plasminogen activator inhibitor-1, and transforming growth factor-beta1.* Wound Repair Regen, 2005. **13**(1): p. 76-83.

62. Eming, S.A., et al., *Differential proteomic analysis distinguishes tissue repair biomarker signatures in wound exudates obtained from normal healing and chronic wounds.* J Proteome Res, 2010.

63. Marko-Varga, G. and T.E. Fehniger, *Proteomics and disease--the challenges for technology and discovery.* J Proteome Res, 2004. **3**(2): p. 167-78.

64. Lescuyer, P., D. Hochstrasser, and T. Rabilloud, *How shall we use the proteomics toolbox for biomarker discovery?* J Proteome Res, 2007. **6**(9): p. 3371-6.

65. Caprioli, R.M., *Perspectives on imaging mass spectrometry in biology and medicine.* Proteomics, 2008. **8**(18): p. 3679-80.

66. Burnum, K.E.F., Sara L; Caprioli, Richard M, *Matrix-Assisted Laser Desorption/Ionization Imaging Mess Spectrometry for the Investigation of Proteins and Peptides.* Annual Review of Analytical Cahemistry, 2008. **1**: p. 689-705.

67. Hardesty, W.M. and R.M. Caprioli, *In situ molecular imaging of proteins in tissues using mass spectrometry.* Anal Bioanal Chem, 2008. **391**(3): p. 899-903.

68. Chaurand, P., et al., *Imaging mass spectrometry of intact proteins from alcohol-preserved tissue specimens: bypassing formalin fixation.* J Proteome Res, 2008. **7**(8): p. 3543-55.

69. Caldwell, R.L. and R.M. Caprioli, *Tissue profiling by mass spectrometry: a review of methodology and applications.* Mol Cell Proteomics, 2005. **4**(4): p. 394-401.

70. Seeley, E.H. and R.M. Caprioli, *Molecular imaging of proteins in tissues by mass spectrometry.* Proc Natl Acad Sci U S A, 2008. **105**(47): p. 18126-31.

71. Cornett, D.S., et al., *MALDI imaging mass spectrometry: molecular snapshots of biochemical systems.* Nat Methods, 2007. **4**(10): p. 828-33.

72. Herring, K.D., S.R. Oppenheimer, and R.M. Caprioli, *Direct tissue analysis by matrix-assisted laser desorption ionization mass spectrometry: application to kidney biology.* Semin Nephrol, 2007. **27**(6): p. 597-608.

73. Pastar, I., O. Stojadinovic, and M. Tomic-Canic, *Role of keratinocytes in healing of chronic wounds.* Surg Technol Int, 2008. **17**: p. 105-12.

74. Stojadinovic, O., et al., *Molecular pathogenesis of chronic wounds: the role of beta-catenin and c-myc in the inhibition of epithelialization and wound healing.* Am J Pathol, 2005. 167(1): p. 59-69.

75. Andersson, M., et al., *Imaging mass spectrometry of proteins and peptides: 3D volume reconstruction.* Nat Methods, 2008. 5(1): p. 101-8.

76. Dressel, S, et al., *Differential expression of antimicrobial peptides in margins of chronic wounds.* Experimental Dermatology 2010; 19: 628–632.

77. Han, X., D.M. Holtzman, and D.W. McKeel, Jr., *Plasmalogen deficiency in early Alzheimer's disease subjects and in animal models: molecular characterization using electrospray ionization mass spectrometry.* J Neurochem, 2001. 77(4): p. 1168-80.

78. Han, X., et al., *Substantial sulfatide deficiency and ceramide elevation in very early Alzheimer's disease: potential role in disease pathogenesis.* J Neurochem, 2002. 82(4): p. 809-18.

79. Murphy, E.J., et al., *Phospholipid composition and levels are altered in Down syndrome brain.* Brain Res, 2000. 867(1-2): p. 9-18.

80. Han, X., et al., *Alterations in myocardial cardiolipin content and composition occur at the very earliest stages of diabetes: a shotgun lipidomics study.* Biochemistry, 2007. 46(21): p. 6417-28.

81. Wilgus, T., *Lipid Mediators: Important REgulators of Cutaneous Wound Inflammation.* Advances in Wound Care, 2010. 1: p. 230-235.

82. Amano, S., et al., *Increase of laminin 5 synthesis in human keratinocytes by acute wound fluid, inflammatory cytokines and growth factors, and lysophospholipids.* Br J Dermatol, 2004. 151(5): p. 961-70.

83. Watterson, K.R., et al., *Regulation of fibroblast functions by lysophospholipid mediators: potential roles in wound healing.* Wound Repair Regen, 2007. 15(5): p. 607-16.

84. Francis-Goforth, K.N., A.H. Harken, and J.D. Saba, *Normalization of diabetic wound healing.* Surgery, 2010. 147(3): p. 446-9.

85. Jackson, S.N. and A.S. Woods, *Direct profiling of tissue lipids by MALDI-TOFMS.* J Chromatogr B Analyt Technol Biomed Life Sci, 2009. 877(26): p. 2822-9.

86. Aerni, H.R., Cornett, D.S., Caprioli, R.M., *High-throughput profiling of formali-fixed paraffin-embedded tissue using parallel electrophoresis and matrix-assisted laser desoprtion ionization mass spectrometry.* Anal Chem, 2009. 81(17): p. 7490-7495.

87. Chaurand, P., et al., *Imaging mass spectrometry of intact proteins from alcohol-preserved tissue specimens: bypassing formalin fixation.* J Proteome Res, 2008. 7(8): p. 3543-55.

88. Jackson, S.N., Wang, H-Y., Woods, A.S., Ugarov, M., Egan, T., Schultz, J.A. , *Direct tissue analysis of phospholipids in rat brain using MALDI-TOFMS and MALDI-IOn Mobility-TOFMS.* J. Am Soc Mass Spectrom, 2005   16: p. 133-138.

89. Burnum, K.E.e.a., *Spatial and temporal alterations of phospholipids determined by mass spectrometry during mouse embryo implantation.* J Lipid Res, 2009. 50(11): p. 2290 - 2298.

90. Chaurand, P., Cornett, D.S., Angel, P.M., Caprioli, R.M., *Perspective: From Whole-Body Sections Down to Cellular Level, Multiscale Imaging of Phospholipids by MALDI Mass Spectrometry.* 2010. in press.

91. Schwartz, S.A., M.L. Reyzer, and R.M. Caprioli, *Direct tissue analysis using matrix-assisted laser desorption/ionization mass spectrometry: practical aspects of sample preparation.* J Mass Spectrom, 2003. 38(7): p. 699-708.

92. Chaurand, P., et al., *Imaging mass spectrometry: principles and potentials.* Toxicol Pathol, 2005. 33(1): p. 92-101.

93. McDonnell, L.A. and R.M. Heeren, *Imaging mass spectrometry.* Mass Spectrom Rev, 2007. 26(4): p. 606-43.

94. Fournier, I., M. Wisztorski, and M. Salzet, *Tissue imaging using MALDI-MS: a new frontier of histopathology proteomics.* Expert Rev Proteomics, 2008. 5(3): p. 413-24.

95. Cuddigan, J., Ayello, E.A., Sussman, C., *Pressure ulcers in America: prevalence, incidence, and implications for the future.* Advances in Skin Wound Care, 2001. 14: p. 208-215.

96. Wilgus, T.A., *Lipid Mediators: Important Regulators of Cutaneous Wound Inflammation.* Advances in Wound Care, 2010. 1: p. 230-236.

97. Edsberg, L.E., *Pressure ulcer tissue histology: an appraisal of current knowledge. .* Ostomy Wound Manage, 2007. 53: p. 40-49.

98. Vande Berg, J.S., Rudolph, R., *Pressure (decubitus) ulcer: variation in histopathology--a light and electron microscope study.* . Hum Pathol, 1995. 26: p. 195-200.

99. Diegelmann, R.F., *Excessive neutrophils characterize chronic pressure ulcers. Wound Repair Regen*, 2003. 11: p. 490-495.

100. Oppenheimer, S.R., et al., *Molecular analysis of tumor margins by MALDI mass spectrometry in renal carcinoma. J Proteome Res*, 2010. 9(5): p. 2182-90.

101. Mustoe, T.A., O'Shaughnessy, K., Kloeters, O., *Chronic wound pathogenesis and current treatment strategies: a unifying hypothesis.* . Plastic Recontr Surg, 2006. 117: p. 35S - 41S.

102. Roy, S., Patel, D., Khanna, S., Gordillo, G. M., Biswas, S., Friedman, A., Sen, C. K, *Transcriptome-wide analysis of blood vessels laser captured from human skin and chronic wound-edge tissue.* . Proc Natl Acad Sci USA, 2007. 104: p. 14472 - 14477.

103. Tomic-Canic, M., and Brem, H. , *Gene array technology and pathogenesis of chronic wounds.* Am J Surg, 2004. 188: p. 67-72.

104. Stojadinovic, O., et al., *Molecular pathogenesis of chronic wounds: the role of beta-catenin and c-myc in the inhibition of epithelialization and wound healing.* Am J Pathol, 2005. 167(1): p. 59-69.

Section 2

Chapter 3

Imaging Mass Spectrometry Applications on Human Skin Ulcers

Materials and Methods

Spatial mapping by Imaging Mass Spectrometry offers advancements for rapid definition of human skin proteomic signatures

Tissue Specimen Collection and Processing

Following institutional review board approval, skin samples were obtained from the trunk region of normal health patients undergoing elective surgical procedures (N=10). Samples were snap frozen in liquid nitrogen and stored in -80°C freezer until ready to processing. Companion pieces were also fixed in 10% neutral buffered formalin embedded in paraffin, sectioned and stained for immunohistochemical confirmation of proteins discovered during MS analysis.

Frozen Tissue Preparation

Human skin samples were sectioned at 12 μm using a cryostat (CM 3050 S, Leica Microsystems GmbH, Wetzlar, Germany) at a setting of -20° C. Serial sections were collected on MALDI gold plates (Applied Biosystem Inc, Foster City, CA, USA) for MS analysis. After thaw mounting, gold plates were placed in a desiccator for 10 min to allow tissue adherence and to equilibrate to room temperature. Serial sections collected on microscope slides were cut and stained with Hematoxylin and Eosin in order to plan for matrix placement for MALDI MS studies.

Tissue Fixation and Contaminant Removal

Before matrix deposition, each plate was rinsed at room temperature with solvent.[1] Solvents tested included 70% isopropanol followed 95% isopropanol, 70% methanol followed by 95% methanol, 70% ethanol followed by 95% ethanol, dual rinses in 100% hexane, and dual rinses in 100% toluene. Each rinsing procedure lasted for 30 sec. Protein spectra were evaluated for TIC (total ion current), background noise and the number of peaks recorded. The TIC proved highest for isopropanol and lowest for toluene. Ethanol produced comparable data, but for IMS, more ions were localized in epidermis layer after isopropanol washing. In the cases of hexane and toluene, only a few signals in the low mass range were detected. Overall, isopropanol was determined to show the highest relative signaling intensities and the highest number of peaks observed. Our final procedure of choice consisted of 70% isopropanol followed by 95 % isopropanol for 30 sec each and 30 min of vacuum desiccation. The aim of the described procedure was to remove interfering species, such as salts and lipids, that can promote adduct formation, ion suppression and poor matrix crystallization.[2]

Tissue Preparation for Profiling

A robotic acoustic droplet ejection system was used for matrix deposition (Portrait 630 reagent multi-spotter, Labcyte, Sunnyvale, CA).[3] Two different areas of interest, epidermis and dermis, were targeted

for deposition of multiple spots of MALDI matrix. Sinapinic acid (20 mg/mL) in 1:1 ACN/0.1% TFA (aq.) was deposited over a series of 6 iterations at 10 droplets per iteration. After completion of matrix deposition, gold plates were immediately returned to vacuum dessication at room temperature until MS analysis the same day.

Tissue Preparation for Imaging

MALDI matrix was spotted by the robotic spotter (Labcyte Portrait 930). Sinapinic acid (20 mg/mL) in 1:1 ACN/0.1% TFA (aq.) was spotted *on tissue* into an array incorporating 200 µm (center-to-center) spacing between individual spots, each with a diameter of 150 µm. The robotic spotter deposited over a series of 20 iterations at 1 drop per iteration. Profiling and imaging analysis were carried out by Autoflex MALDI-TOF mass spectrometer (Bruker Daltonics, Billerica, MA, USA) operating in positive polarity and linear mode.

Tissue Preparation for Tryptic Digestion

Trypsin solution was prepared in 50 mM acetic acid[4, 5] and activated by adding 500 µL of 100 mM ammonium bicarbonate, reaching pH ~8.0 with a final concentration of 0.038 µg/µL. Enzyme solution was automatically spotted onto frozen sections using the robotic spotter in a 200 µm array, over a series of 30 iterations at three droplets per iteration and 120 sec time intervals per iteration to allow for drying. Trypsin digestion proceeded at room temperature (~22° C) for ~3 h. Following digestion, a matrix solution containing 10 mg/ml of α–cyano-4-hydroxy-cinnamic acid (CHCA) in 1:1 ACN/0.5% TFA (aq.) was spotted. Peptide spectra were acquired using Ultraflextreme MALDI-TOF/TOF mass spectrometer (Bruker Daltonics, Billerica, MA, USA). The mass spectrometer was operated with positive polarity *reflectron* mode and spectra acquired in the range of m/z 400-4700.

MS/MS Sequence Analysis of Tryptic Peptides and Protein Identification

Digested peptides were isolated as *precursor ions* (*parent ions*) and fragmented to generate MS/MS spectra. Latter were converted into a single MASCOT generic format data file and run against the Swiss Prot database to match tryptic peptide sequences to their respective intact proteins. MS/MS spectrum searches were performed with a mass tolerance of 0.3 Da and fragment ion tolerance of ± 0.1 Da. Search criteria also included up to three missed cleavages and variable modifications, such as methionine (M), histidine (H) and tryptophan (W) oxidation and also N-terminal (N-term) acetylation.

Immunoistochemistry: an overview

Immunohistochemistry or IHC refers to the process of localizing antigens (e.g. proteins) in cells of a tissue section exploiting the principle of antibodies binding specifically to antigens in biological tissues.[6] It

takes its name from the roots "immuno," in reference to antibodies used in the procedure, and "histo," meaning tissue (compare to immunocytochemistry). Immunohistochemical staining is widely used in the diagnosis of abnormal cells such as those found in cancerous tumors. Specific molecular markers are characteristic of particular cellular events such as proliferation or cell death (apoptosis). IHC is also widely used in basic research to understand the distribution and localization of biomarkers and differentially expressed proteins in different parts of a biological tissue. Visualising an antibody-antigen interaction can be accomplished in a number of ways. In the most common instance, an antibody is conjugated to an enzyme, such as peroxidase, that can catalyse a colour-producing reaction. Alternatively, the antibody can also be tagged to a fluorophore, such as fluorescein or rhodamine. There are two strategies used for the immunohistochemical detection of antigens in tissue, the direct method and the indirect method. In both cases, many antigens also need an additional step for unmasking, which often makes the difference between staining and no staining. Unlike immunocytochemistry, the tissue does not need to be permeabilized because this has already been accomplished by the microtome blade during sample preparation. Detergents like Triton X-100 are generally used in immunohistochemistry to reduce surface tension, allowing less reagent to be used to achieve better and more even coverage of the sample.

The *direct method* is a one-step staining method, and involves a labeled antibody (e.g. FITC conjugated antiserum) reacting directly with the antigen in tissue sections. This technique utilizes only one antibody and the procedure is therefore simple and rapid. However, it can suffer problems with sensitivity due to little signal amplification and is in less common use than indirect methods. The indirect method involves an unlabeled primary antibody (first layer) which reacts with tissue antigen, and a labeled secondary antibody (second layer) which reacts with the primary antibody. (The secondary antibody must be raised against the IgG of the animal species in which the primary antibody has been raised.) This method is more sensitive due to signal amplification through several secondary antibody reactions with different antigenic sites on the primary antibody. The second layer antibody can be labeled with a fluorescent dye or an enzyme. In a common procedure, a biotinylated secondary antibody is coupled with streptavidin-horseradish peroxidase. This is reacted with 3,3'-Diaminobenzidine (DAB) to produce a brown staining wherever primary and secondary antibodies are attached in a process known as DAB staining. The reaction can be enhanced using nickel, producing a deep purple/gray staining. Diluted filtered Hematoxylin can also be used in the staining of cells and produces a blue color.

The *indirect method*, aside from its greater sensitivity, also has the advantage that only a relatively small number of standard conjugated (labeled) secondary antibodies needs to be generated. For example, a labeled secondary antibody raised against rabbit IgG, which can be purchased "off the shelf," is useful with any primary antibody raised in rabbit. With the direct method, it would be necessary to make custom labeled antibodies against every antigen of interest. IHC is an excellent detection technique and has the tremendous advantage of being able to show exactly where a given protein is located within the tissue examined. It is also an effective way to examine the tissues .This has made it a widely-used technique in the neurosciences, enabling researchers to examine protein expression within specific brain structures. Its

major disadvantage is that, unlike immunoblotting techniques where staining is checked against a molecular weight ladder, it is impossible to show in IHC that the staining corresponds with the protein of interest. For this reason, primary antibodies must be well-validated in a Western Blot or similar procedure. The technique is even more widely used in diagnostic surgical pathology for typing tumors (e.g. immunostaining for e-cadherin to differentiate between DCIS -ductal carcinoma in situ: stains positive- and LCIS (lobular carcinoma in situ: does not stain positive).[7]

Immunohistochemical Staining on Normal Skin Tissue Sections

Immunohistochemical staining was performed using commercial antibodies specifically directed against thymosin β-4 (Abcam, Cambridge, MA) and lumican (R&D Systems, Minneapolis, MN). Formalin-fixed paraffin embedded normal skins were sectioned at 5 μm, placed on slides and warmed overnight at 60°C. The slides were deparaffinized and rehydrated with graded alcohols ending in tris buffered saline (TBS-T Wash Buffer, LabVision, Freemont, CA). For thymosin β-4 staining, pepsin (ready-to-use or RTU, Invitrogen, Camarillo, CA) was applied for 20mins at 37°C. Endogenous peroxidases and non-specific background were blocked by subsequent incubations in peroxidase block (RTU, DAKO, Carpenteria, CA) and serum-free protein block (RTU, DAKO). Primary antibody to thymosin β-4 was used at 1:1000 for 1 hour, followed by incubation in EnVision+ HRP labelled polymer (RTU, DAKO). For lumican staining, proteinase K (RTU, DAKO) was applied for 5 mins. Endogenous peroxidases were blocked as before. Non-specific background, secondary, and tertiary labelling of target was accomplished by use of Vector's ABC Elite Goat IgG kit (Vector Laboratories, Burlingame, CA). Primary antibody to lumican was used at 1:300 for 1 hour. Slides were rinsed with TBS-T between each reagent treatments and all steps were carried out at room temperature unless otherwise noted. Visualization of both antibodies was achieved with Nova Red chromogen (Vector Laboratories). Slides were counterstained with Mayer's hematoxylin, dehydrated through a series of alcohols and xylenes, and then coverslipped with Acrytol Mounting Media (Surgipath, Richmond, IL). Microscopic examination and imaging was performed with an Olympus BH-2 microscope with a Polaroid digital microscope camera 2 (Melville, NY).

The Microenvironment of Human Pressure Ulcers as Defined by Imaging Mass Spectrometry

Profiling and Imaging Mass Spectrometry

In this pilot examination of pressure ulcers, MS analysis of proteins was performed following two main experimental approaches involving direct analysis of tissue.[8-10] The first, termed "profiling", analyzed discrete but limited areas within the tissue section producing protein profiles that were subjected to computational analysis. Experiments were designed to make

comparisons between representative areas within ulcer regions or between two different specimens (ulcers versus normal intact skin). Replicate sampling within focal area of interest permitted data capture that achieved statistical confidence though principal component analysis. The second approach, termed "imaging", is a high spatial resolution technology that produced image acquisition at specific molecular weights.[11]   The entire tissue section was analyzed through an ordered array of spots, or raster pattern, in which spectra were acquired at intervals that defined the image resolution. Two dimensional ion density maps were generated representing the spatial distribution of a given analyte within the tissue section as well as its relative abundance (intensity).[12-14]

Tissue Specimen Collection and Processing

Samples were obtained from patients on the Plastic Surgery Service who were undergoing surgical excision of large Stage IV pressure ulcers prior to coverage with a local skin flap. In this pilot study, a wide variety of wound healing conditions were sampled. Some wounds were showing clinical evidence of improvement but were excised and flapped to speed recovery. Other wounds were showing no evidence of improvement or responsiveness to therapy. To maintain a degree of standardization among these large complex ulcers, sample collection was restricted to the edge of the wound. Intact normal skin samples from patients undergoing elective cosmetic surgical procedures were also obtained and used as controls. Consent was obtained to use these specimens for research purposes in accordance with Vanderbilt's Institutional Review Board. Samples were wrapped in aluminum foil, snap frozen in liquid nitrogen and were stored at -80°C until they were ready for preparation for mass spectrometry analysis. Companion pieces from the same sample were also fixed in 10% neutral buffered formalin (NBF) for later use in immunohistochemical (IHC) analysis for confirmation of proteins discovered during the MS analysis. Table 1 displays demographic data and wound locations (N = 6) as well as the normal controls (N = 3). This study was designed as an exploratory examination to determine the potential utility of mass spectrometry for the analysis of pressure ulcers. Thus patients and wound areas with diverse clinical features were surveyed.

Tissue Preparation, Fixation and Contaminant Removal

Human skin samples collected for proteomic analysis were sectioned at 12µm using a cryostat (CM 3050 S, Leica Microsystems GmbH, Wetzlar, Germany) set at -20° C. Serial sections were collected and thaw mounted on either a MALDI gold coated plate (Applied Biosystem Inc, Foster City, CA, USA) for MS analysis or on a microscope slide (Fisher Scientific, Pittsburg, PA, USA) for subsequent hematoxylin and eosin (H & E) staining for histological orientation. Plates affixed with skin specimens were then placed in a desiccator for at least 10 min. After drying under vacuum and prior to matrix deposition, each plate was rinsed with isopropanol.[1]   Skin samples

were submerged in 70% isopropanol followed by 95 % isopropanol for 30 sec each with gently swirling. Tissue sections were again dried within a vacuum desiccator for at least 30 min before matrix deposition. The aim of the rinsing procedure was to remove interfering species, such as salts and lipids, that can promote adduct formation, ion suppression and poor matrix crystallization.[2]

Immunohistochemical Staining

Immunohistochemical staining was performed on companion ulcer samples and normal human skin samples using a commercial antisera directed against HNP-1+2+3 (#Ab64763, Abcam, Inc, Cambridge, MA) and thymosin β-4 (#Ab14335, Abcam). Formalin-fixed paraffin embedded skin specimens were sectioned at 5 μm, were deparaffinized and rehydrated with graded alcohols ending in Tris buffered saline (TBS-T Wash Buffer, LabVision, Freemont, CA). For HNP 1+2+3 localization, proteinase K (RTU, DAKO) was applied for 5 min as an antigen retrieval agent. For thymosin β-4 staining, pepsin (ready-to-use or RTU, Invitrogen, Camarillo, CA) was applied for 20mins at 37°C. Endogenous peroxidases and non-specific background in both were blocked by incubations in peroxidase block (RTU, DAKO, Carpenteria, CA) and serum-free protein block (RTU, DAKO). Primary antibody to HNP-1+2+3 was used at 1:2,500 and primary antibody to thymosin β-4 was used at 1:1,000, both for 1 h followed by incubation in EnVision+ HRP Labelled Polymer (RTU, DAKO). Slides were rinsed with TBS-T between each reagent treatment and all steps were carried out at room temperature. Visualization of immunoreactivity was achieved with Nova Red chromogen (Vector Laboratories). Slides were counterstained with Mayer's hematoxylin, dehydrated through a series of alcohols and xylenes, and then coverslipped with Acrytol Mounting Media (Surgipath, Richmond, IL). Microscopic examination and image capture were performed with an Olympus BH-2 microscope with a Polaroid digital microscope camera 2 (Melville, NY).

Matrix Deposition for MS Analysis

MALDI matrix, sinapinic acid (SA) 20 mg/ml in 50% ACN/0.1% TFA (aq.), was applied by a robotic acoustic droplet ejection system (Portrait 630, Labcyte, Sunnyvale, CA) to create a series of spots within the tissue section.[3] Matrix was spotted over a series of 10 iterations while depositing 10 droplets (~170 μl per drop) during each iteration. Three different regions of interest (hypertrophic epidermis, dermis immediately adjacent to the wound and the wound bed), were targeted for analysis based on the specific tissue architecture of the matching serial section stained with hematoxylin and eosin. After completion of matrix deposition (15 spots per region of interest), the sample plate was immediately returned to vacuum dessicator at room temperature until MS analysis.

For high spatial resolution images, the same matrix solution was robotically spotted directly over the entire tissue into an array of spots with 200 μm (center-to-center) spacing and each spot having diameter of approximate 150 μm. In this case, SA was automatically spotted into the array over a series of 20 iterations at one drop per iteration to achieve a total spot volume of 3.4 nL Further, α-cyano-4-hydroxycinnamic acid (CHCA), 10 mg/ml in 50% ACN/0.5% TFA (aq.), was automatically deposited on the wound bed as well as on the adjacent dermis for MS/MS experiments. Finally, since HNPs show an an animo acid sequence with 6 cysteines linked by 3 disulfide bond bridges, 1,5-diaminonaphtalene (DAN) matrix was used for reducting condition prior to the performance of MS/MS experiments.[15]

MALDI MS-MS/MS Analysis

Data were acquired with an Autoflex II MALDI-TOF mass spectrometer (Bruker Daltonics, Billerica, MA, USA) equipped with a smart beam laser and a linear TOF. The instrument was operated under automated mode with a method optimized for acquisition at a mass range of 2000 to 20,000 Da. Mass spectra were acquired from each array spot in positive ionization mode. Acquired spectra for profiling were processed using Flex Analysis 3.3 software (Bruker Daltonics, Billerica, MA, USA). Prior to statistical analysis, mass spectra were baseline-corrected, smoothed, recalibrated and subjected to signal-to-noise thresholding using ClinProTools 2.2 software (Bruker Daltonics, Billerica, MA, USA). Multiple spectra from each individual patient were averaged for each of the regions of interest within the complex biopsy. Peaks lists were created from the average spectra; the peak intensities and area under curve (AUC) were calculated. Images generation was carried out using Flex Imaging 2.1 (Bruker Daltonics, Billerica, MA, USA). Mass spectra (within each matrix spot) obtained after each image sequence acquisition were normalized to the total ion current (TIC) prior to processing for the ion density mapping procedures. Thus, MS/MS experiments for protein and peptide identification were carried out using a Ultraflextreme MALDI TOF-TOF (Bruker Daltonics, Billerica, MA, USA) equipped with a reflectron TOF and operating in positive ion mode. Proteins were identified by a MASCOT search engine, using the Swiss-Prot database. The MS/MS spectrum search was performed with search criteria including up to three missed cleavages and variable modifications, a parent ion tolerance of 0.1 Da and a fragment ion tolerance of ± 0.3 Da. The α-defensins peptides (HNP-1 and -2) were identified by *de novo* sequence loading the AA sequence from Swiss Prot database and matching the peptide fragments with a MS/MS tolerance of ± 0.5 Da.

Statistical Analysis : an overview

Principal Component Analysis (PCA) is a broadly used mathematical technique designed to extract, display and rank the variance within a data set.[16] The overall goal of PCA is to reduce

the dimensionality of a data set while simultaneously retaining the information present in the data. In data sets with many groups of variables, variables often show similar behavior and contain redundant information. In the case of mass spectra, the variables are represented by the intensity at defined masses. According to the resolution, the number of these variables can be very high. The PCA reduces the number of dependent variables contained within the spectra set via replacing groups of variables by a single new variable. By this, a set of new variables, so-called principal components will be generated. Each principal component (PC) is a linear combination of the original variables. All principal components are orthogonal to each other, so there is no redundant information. In many cases (depending on the complexity of the data set), only few PCs (compared to the large number of original variables) contain most of the variance. The full set of PCs is as large as the original set of variables, nevertheless only the first PCs are of interest mostly; higher PCs contain very detailed spectra information and the highest PCs contain spectra noise. Actually, each sample (spectrum) can be plotted in an m-dimensional space of variables. The PCA ranks the variables according to their influence on the data set. Upon PCA calculation, the original coordinates of the diagram are transformed to new coordinates ranked by the variance each coordinate explains. The new axes are called PCs. PC1 describes the largest variance within the data set; PC2 describes the second largest variance, and is orthogonal to PC1, etc. The variance explained by a PC is calculated as sum of the individual variance. The PCA is managed by an external MATLAB® software tool, which is integrated in ClinProTools.

Receiver Operating Characteristic Curve (ROC). ClinProTools calculates a Receiver Operating Characteristic (ROC) curve for each peak within peak calculation. The ROC curve gives a graphical overview about specificity and sensitivity of a test or, within ClinProTools, an evaluation of the discrimination quality of a peak.[17]   The sensitivity represents the true positive fraction (TPF) and the specificity the true negative fraction (TNF). The fraction of false negatives (FNF) together with the TPF give a sum of 1 (100%); and the fraction of the false positives (FPF) together with the TNF also give a sum of 1 (100%). In ClinProTools, the ROC curve is generated similar as explained above whereby a peak is considered as the random variable, which can be interpreted as a test separating two populations. The peak area or the intensity of the peak represents the threshold that is used to reach the separation into the two groups. On the x-axis the '1-specificity' in terms of the false positives is given and on the y-axis, the sensitivity in terms of the true positives is recorded; for this it is assumed that the first loaded class is the diseased one and the second loaded class is the non-diseased one. Both axes are given in values between 0 and 1. At the bottom of the plot, the peak number, peak position and AUC value are given. If the data is separable by a univariate approach considering only one peak as a test criterion the ROC Curve View may already indicate this peak by a high AUC value close to 1.0. ROC curves and their AUC values are only estimations and become more confident with an increasing number of samples.

Significance Analysis of Microarray (SAM). SAM is a statistical technique for finding significant genes in a set of microarray experiments. It was proposed by Tusher, Tibshirani and Chu.[18]   The software was written by Balasubramanian Narasimhan and Robert Tibshirani. The input to SAM is gene expression measurements from a set of microarray experiments, as well as a response variable from each experiment. The response variable may be a grouping like *untreated, treated* [either unpaired or paired], a multiclass grouping (like breast cancer, lymphoma, colon cancer, etc), a quantitative variable (like blood pressure) or a possibly censored survival time. SAM computes a statistic d_i for each gene i, measuring the strength of the relationship between gene expression and the response variable. It uses repeated permutations of the data to determine if the expression of any genes are significantly related to the response. The *cutoff* for significante is determined by a tuning parameter delta (Δ), chosen by the user based on the false positive rate. One can also choose a fold change parameter, to ensure that called genes change at least a pre-specified amount.

Statistical Analysis on Human Skin Mass Spec Data

Multiple spectra per region of interest (the general wound, the upper and lower wound bed, adjacent dermis, hypertrophic epidermal margin) were selected from the obtained MALDI-IMS data. Comparisons of the different cutaneous regions of interest were conducted using principal component analysis (PCA) and receiver operating characteristic curves (ROC curves). PCA was used to generate classification models based on protein profile patterns whereas the ROC curves were used to further confirm the existence of two disparate sub-regions within the wound bed regions. Furthermore, in order to understand how the molecular micro-environment within the wound bed itself can influence adjacent areas, PCA was performed comparing the wound bed to the adjacent dermis and this adjacent "wound associated" dermis with the normal dermis from normal patients. The same statistical analysis was carried out for the hypertrophic epidermis at the wound margin versus the normal epidermis from normal healthy patients. Differentially expressed features within the wound area and the adjacent dermis were elucidated using the significance analysis of microarrays (SAM) for paired data.[19]   Features with a false discovery rate (FDR) less than 0.01% were considered as potentially significant. For the differentially expressed features identified between the wound area and the adjacent dermis, a support vector machine (SVM) classifier was used to assess the class prediction ability of each individual feature. The prediction accuracy was estimated using a leave-one-out-cross-validation algorithm.

Spatial Detection of Phospholipids in Human Pressure Ulcers by Imaging Mass Spectrometry

Chemicals

Matrix 2,5-dihydroxy-benzoic acid (DHB) as well as 2,5-dihydroxy-acetophenone (DHA) were purchased from Acros Organics (Morris Plains, NJ, USA). Aniline was purchased from Sigma-Aldrich (St Louis, MO, USA).

Tissue Sectioning

Informed consent to collect and study discarded tissues was obtained in accordance with guidelines at Vanderbilt's Institutional Review Board. Skin samples were obtained from the trunk region of normal healthy patients undergoing elective surgical procedures (N = 8). Tissues from stage IV pressure ulcers over the bony prominences (the sacrum, ischial tuberosity or greater trochanter) were collected when rotational flaps were used to provide skin coverage. Samples were snap frozen in liquid nitrogen and were stored in the -80°C freezer until ready for processing. Skin samples were serially sectioned at 12μm using a cryostat (CM 3050 S, Leica Microsystems GmbH, Wetzlar, Germany) set at -20° C. Serial sections were collected on a MALDI gold plate (Applied Biosystem Inc, Foster City, CA, USA) for MS analysis. After thaw mounting, gold plates were placed in a desiccator for 10 min to allow for tissue adherence to the plate and for equilibration to room temperature. Serial sections were collected on microscope slides for immediate staining with hematoxylin and eosin to visualize areas of interest (wound, adjacent margin, hypertrophic epidermis at the margin) and provide coordinates for the MALDI MS studies.

Sample Preparation

Two different sample preparation protocols were used to prepare the tissue sections for imaging analysis, direct profiling or MS/MS experiments.[4, 20] For profiling and subsequent MS/MS experiments, MALDI matrix was spotted by a robotic acoustic droplet ejection system (Portrait 630 reagent multi-spotter, Labcyte, Sunnyvale, CA, USA) to create a series of spots within focal regions on the tissue sections. Two regions of interest, the epidermis and dermis, were targeted for analysis of the normal skin while three regions of interest were considered for the ulcer samples (hypertrophic epidermis at the wound's edge when present, adjacent dermis abutting the wound bed and the wound bed itself). After completion of matrix deposition, the gold plate was immediately returned to vacuum desiccation at room temperature until MS analysis that same day. A solution consisting of 2,5- DHB, 20 mg/ml in 50% ACN (aq.), was spotted for positive ionization mode MS analysis while 2,5- DHA, 10 mg/ml in 50% ACN (aq.) was used for negative ionization mode. The latter matrix solution contained aniline (6%) to facilitate the ionization of some lipid species. Either DHB or DHA was spotted over a series of 10 iterations while depositing 10 droplets (~170 pL per drop) during each iteration to achieve a total spot volume of ~1.7 nL. The same

robot spotter was used to prepare samples for imaging analysis in negative ionization mode, creating an array incorporating 200 μm (center-to-center) spacing between individual matrix spots with an approximate diameter of 150 μm. In this case, DHA was automatically spotted into the array over a series of 20 iterations at one drop per iteration (total volume per spot ~3.4 nL). Conversely, for positive imaging analysis, DHB matrix was sublimed. Approximately 300 mg of DHB were added to the bottom section of a sublimation apparatus (Chemglass Life Science, Vineland, NJ, USA) and the sublimation was carried out at 88 mTorr , at 120°C. After 8 minutes, the gold plate with the tissue on the upper surface became uniformly coated with this thin matrix layer. The aim of this procedure was to allow the mass spectrometer to acquire spectra with a spatial resolution higher than is possible by the array of evenly spaced spots. Imaging sequences were acquired at 60 and 40 μm raster pattern using this sample preparation protocol.

Mass Spectrometers

For lipid investigation of human skin, several mass spectrometers were needed. Lower spatial resolution imaging MS in positive ionization mode (200 um) was performed on an UltraFlextreme MALDI TOF-TOF instrument (Bruker Daltonic, Billerica, MA, USA) in reflectron mode, accumulating 150 laser shots per position at 1000 Hz laser frequency over m/z range of 400-1200. Higher spatial resolution imaging MS (60 and 40 um) of sublimed skin sections was also performed by the same instrument. The laser intensity was adjusted before each imaging experiment to yield optimal results. Negative ionization mode images as well as high mass accuracy measurements were performed using a 9.4 T Ape-Qe MALDI FT-ICR instrument (Bruker Daltonic, Billerica, MA, USA). The LIPID metabolites and pathways strategy (LIPID MAPS) online resource was used to search for possible lipid structures that could match our experimental mass (±0.005 Da,). Although only one theoretical mass matched in each case, multiple fatty acid isobars with the same exact mass are possible. Thus, MALDI MS/MS fragmentation of phospholipids was implemented to determine the fatty acid chains with greater confidence. All MALDI MS/MS experiments were performed on a MALDI linear ion trap quadrupole mass spectrometer (MALDI-LTQ, Thermo Electron, San Jose, CA, USA) equipped with a 337 N_2 laser. For fragmentation of phospholipids, matrix solutions (DHB and DHA) were hand spotted. Glyceroshpingolipids MS/MS were conducted using the LIFT cell of the UltraFlextreme MALDI TOF-TOF instrument.

For each experiment, external calibration was performed using 300 nL of a mixture of standard peptides, deposited onto the sample plate after matrix deposition. In both polarities, this mixture provides 9 calibration points in the mass range between 428 and 1460 and allows mass accuracy for phospholipids to be typically better than 10 ppm across a skin ulcer image.

Data Processing

Spectra acquired for profiling experiments were processed using FlexAnalysis software (Bruker Daltonic, Billlerica, MA, USA). Thresholding to minimize the signal-to-noise ratio was conducted by baseline subtraction and smoothing. Two-dimensional density maps (images) were created using FlexImaging 2.1

software (Bruker Daltonic, Billlerica, MA, USA). Prior to generation of ion density maps, acquired spectra were normalized to the total ion current (TIC) in order to minimize spectrum-to-spectrum differences in peak intensity. Spectra from tandem MS studies (MS^2 and MS^3) were created after acquisition by Xcalibur Qual Browser software (Thermo Electron, San Jose, CA, USA). The resulting fragmentation patterns were matched into the LipidMap web database using the exact mass from the high mass accuracy measurements as the basis for assignment of the lipid species.

References

1. Seeley EH, Oppenheimer SR, Mi D, Chaurand P, Caprioli RM (2008) Enhancement of protein sensitivity for MALDI imaging mass spectrometry after chemical treatment of tissue sections. *J Am Soc Mass Spectrom* 19:1069-1077.

2. Schwartz SA, Reyzer ML, Caprioli RM (2003) Direct tissue analysis using matrix-assisted laser desorption/ionization mass spectrometry: practical aspects of sample preparation. *J Mass Spectrom* 38:699-708.

3. Aerni, H.R., D.S. Cornett, and R.M. Caprioli, *Automated acoustic matrix deposition for MALDI sample preparation.* Anal Chem, 2006. 78(3): p. 827-34.

4. Groseclose MR, Andersson M, Hardesty WM, Caprioli RM (2007) Identification of proteins directly from tissue: in situ tryptic digestions coupled with imaging mass spectrometry. *J Mass Spectrom* 42:254-262.

5. Groseclose MR, Massion PP, Chaurand P, Caprioli RM (2008) High-throughput proteomic analysis of formalin-fixed paraffin-embedded tissue microarrays using MALDI imaging mass spectrometry. *Proteomics* 8:18, 3715-3724.

6. Ramos-VAra JA, (2005) Technical Aspects of Immunoistochemistry. *Vet. Pathol.* 42 (4) 405-426.

7. O'Malley F, Pinder S (2006) Breast Pathology 1st Ed. Elsevier ISBN 978-0-443-06-680-1.

8. Burnum, K.E.F., Sara L; Caprioli, Richard M, *Matrix-Assisted Laser Desorption/Ionization Imaging Mess Spectrometry for the Investigation of Proteins and Peptides.* Annual Review of Analytical Cahemistry, 2008. 1: p. 689-705.

9. Chaurand, P., et al., *Imaging mass spectrometry of intact proteins from alcohol-preserved tissue specimens: bypassing formalin fixation.* J Proteome Res, 2008. 7(8): p. 3543-55.

10. Caldwell, R.L. and R.M. Caprioli, *Tissue profiling by mass spectrometry: a review of methodology and applications.* Mol Cell Proteomics, 2005. 4(4): p. 394-401.

11. Seeley, E.H. and R.M. Caprioli, *Molecular imaging of proteins in tissues by mass spectrometry.* Proc Natl Acad Sci U S A, 2008. 105(47): p. 18126-31.

12. Hardesty, W.M. and R.M. Caprioli, *In situ molecular imaging of proteins in tissues using mass spectrometry.* Anal Bioanal Chem, 2008. 391(3): p. 899-903.

13. Cornett, D.S., et al., *MALDI imaging mass spectrometry: molecular snapshots of biochemical systems.* Nat Methods, 2007. 4(10): p. 828-33.

14. Herring, K.D., S.R. Oppenheimer, and R.M. Caprioli, *Direct tissue analysis by matrix-assisted laser desorption ionization mass spectrometry: application to kidney biology.* Semin Nephrol, 2007. 27(6): p. 597-608.

15. Fukuyama, Y., S. Iwamoto, and K. Tanaka, *Rapid sequencing and disulfide mapping of peptides containing disulfide bonds by using 1,5-diaminonaphthalene as a reductive matrix.* J Mass Spectrom, 2006. 41(2): p. 191-201.

16. Jolliffe IT (2002) Principal Component Analysis 2nd edition Springer.

17. Http://www.bdal.de Basics on data preparation, model generation and spectra classification, Receiver Operating Characteristic, Bruker Daltonics, ClinProTools help software.

18. Tusher V et al. *Significance Analysis of Microarrays Applied to Transcriptional Responses to Ionizing Radiation* Proc. Natl. Acad. Sci. USA, 2001, 98, 5116-5121.

19. Oppenheimer SR, Mi D, Sanders ME, Caprioli RM (2010) *Molecular Analysis of Tumor margins by MALDI Mass Spectrometry in Renal Carcinoma* J. Proteome Res., 9, 2182-2190.

20. Hankin, J.A., R.M. Barkley, and R.C. Murphy, *Sublimation as a method of matrix application for mass spectrometric imaging.* J Am Soc Mass Spectrom, 2007. 18(9): p. 1646-52.

T his thesis work confirmed the usefulness of mass spectrometry as investigative tool in many fields. For instance, it's clear the role of mass spectrometry as analytical technique in the characterization of compounds of pharmacological interest. It appears also clear the role of the hyphenated techniques in the separation and purification of a complex mixture such as a food. Food is considered as a source of nutrients and often as a source of compounds involved in many biological activities in humans. The MS approach allows to observe molecules at specific molecular weights and thanks to the high resolution measurements it allows to gain important information about the molecular formula as well as about the double bonds present in the structures. The accuracy of an MS measurement is needed when a compound present in a complex matrix needs to be characterized. Mass spectrometry was used in this thesis work also for the study of real human samples from patients with a disease. In the last decade, advancement in instrumentation and sample preparation, make it possible the tissues investigation at a cellular level. The current clinical prognostic and diagnostic tools are limited to the paucity of information at a molecular level. Most of the time, clinicians are forced to a crude overview or a photographic measurement for the evaluation of a skin wound state. Now, using newer instrumentations and advanced technologies, it is possible to study a biopsy not only in terms of histological evaluation but also in terms of molecular contents without any alteration of the tissue architecture. Imaging mass spectrometry poses new clues in this way. In the past, tissue analysis were carried out only on homogenized fractions. At date, by imaging mass spectrometry it's possible to analyze discrete areas or the whole biopsy and obtain molecular information. Further, the generated ion density maps allows to have an overview of the distribution and the localization of a species at a specific molecular weight. This is useful for the definition of specific areas of a tissue, for the screening of drugs metabolites as well as for the definition of a wound state according to the distribution of a wound marker and its localization within the wound bed edge. MS technology continues to excel in this regard and enable discoveries at the molecular level. In particular, the emerging field of imaging mass spectrometry brings extraordinarily powerful capabilities to the research laboratory in that it allows images to be acquired at specific molecular weights. When taken together with other molecular analytical tools available today to research investigators in both biological and clinical applications, it is clear that IMS will play a strong complementary role in providing specific molecular information for the understanding of the underlying biology of health and disease. Understanding the molecular complexity found in both health and disease has driven research investigators to incorporate new tools and methodologies into their studies.

Publications on International Scientific Journals:

1. Di Donna L, Mazzotti F, Naccarato A, Salerno R, Tagarelli A, Taverna D, Sindona G, Secondary Metabolites of Olea Europaea Leaves as Markers for the Discrimination of Cultivars and Cultivation Zones by Multivariate Analysis, *Food Chemistry* **2010**, 121, 2, 462-469. Impact factor: 3.146 Times cited: 0

2. Di Donna L, De Luca G, Mazzotti F, Napoli A, Salerno R, Taverna D, Sindona G, Statin-like Principles fo Bergamot Fruit (Citrus Bergamia): Isolation of 3-hydroxymethylglutaryl Flvonoid Glycosides, *J. Nat, Prod.* **2009**, 72, 7, 1352-4. Impact factor: 3.159 Times cited: 3

3. Di Donna L, Mazzotti F, Salerno R, Tagarelli A, Taverna D, Sindona G, Characterization of New Phenolic Compounds from Leaves of Olea Europaea L. by High-resolution Tandem Mass Spectrometry, *Rapid Commun. Mass Spectrom.* **2007**; 21: 3653–3657. Impact factor: 2.971 Times cited: 1
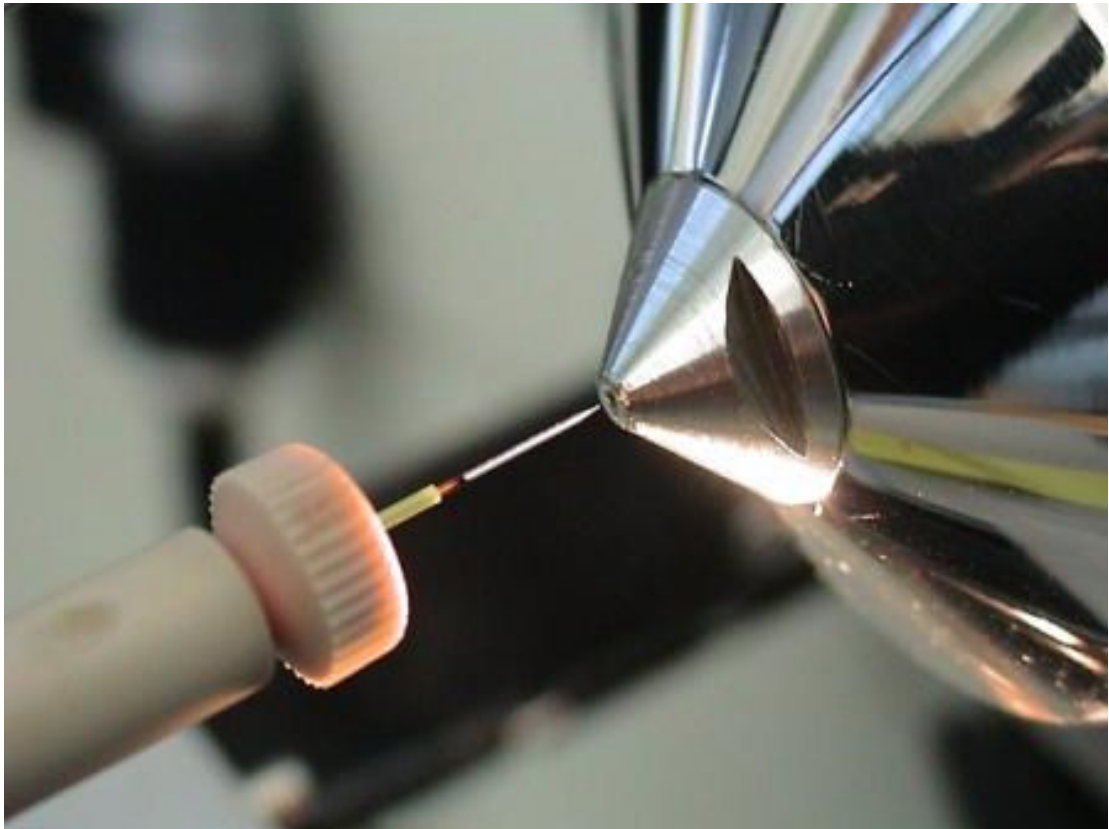
Conference Oral Presentations:

1. Taverna D, Nanney LB, Pollins AC, Sindona G, Caprioli RM, Investigation of Human Skin Proteome by Imaging Mass Spectrometry, 6° MS Pharmaday, Milano (Italy), October 6-8 **2010**. Abstract book pag. Or 03.

2. Taverna D, Salerno R, Di Donna L, Mazzotti F, Sindona G, Characterization of New Flavonoids in Pummelo Juice by High Resolution Mass Spectrometry and High Resolution Nuclear Magnetic Resonance, 1° French-Italian Conference on Mass Spectrometry - Massa **2008**, Fundamentals and applications of mass spectrometry, Siena (Italy), June 30 – July 4 **2008**. Abstract book pag.55.

Conference Poster Presentations:

1. Taverna D, Mazzotti F, Caprioli RM, Sindona G, Detection of Isomeric Dioleyl Glycerides by Ion Mobility Mass Spectrometry. A Modern Approach to the Evaluation of Olive Oil Aging, 15 th IUFoST World Congress of Food Science and Technology, Cape Town, Sputh Africa, August 22-26 **2010.** Abstract book pag 5, cod P0701.

2. Taverna D, Nanney LB, Pollins AC, Sindona G, Caprioli RM, Investigation of the Cutaneous Proteome in Humans: Imaging MS of Biopsies from Skin Ulcers, 58th ASMS Conference on Mass Spectrometry and allied topics, Salt Lake City, Utah USA, May 23-27 **2010**. Abstract book pag. 130.

3. Di Donna L, De Luca G, Napoli A, Mazzotti F, Taverna D, Sindona G, Structural Characteristic of New Statin-like Flavonoids Glycosides in Citrus Bergamia by High Resolution Mass Spectrometry, 57th ASMS Conference on Mass Spectrometry and allied topics, Philadelphia, Pennsylvania, USA, May 31 – June 4 **2009**. Abstract book pag. 119.

4. Taverna D, Salerno R, Di Donna L, Mazzotti F, Sindona G, Characterization of new flavonoids in Pummelo juice by high resolution tandem mass spectrometry, IV Convegno Congiunto delle Sezioni Sicilia e Calabria della SCI, Rende (Cs), December 1-3, **2008**. Abstract book pag. P75.

5. Taverna D, Salerno R, Di Donna L, Mazzotti F, Sindona G, Characterization of New Flavonoids in Pummelo Juice by High Resolution Tandem Mass Spectrometry, Convegno Nazionale della Divisione di Chimica Analitica della Società Chimica Italiana, il ruolo della Chimica Analitica nella tutela della salute, Arcavacata di Rende (Cs), September 21-25 **2008**. Abstract book pag. 126.

6. Aiello D, Di Donna L, Indelicato S, Moschidis P, Napoli A, Taverna D, Sindona G, Allergeni delle noci, One Day Meeting on Mass Spectrometry methods in clinical diagnosis, Aci Sant'Antonio, Lavinaio (Ct), Italy, June 20, **2008**.

7. Taverna D, Salerno R, Di Donna L, Mazzotti F, Sindona G, Nuovi Composti Flavonoidici Presenti in Allium Porrum: Determinazione Mediante Spettrometria di Massa Tandem ad Alta Risoluzione, Convegno Congiunto delle Sezioni Calabria e Sicilia della Società Chimica Italiana, Messina, Italy, December 3-4 **2007**. Abstract book pag.89.

8. Salerno R, Di Donna L, Mazzotti F, Taverna D, Sindona G, Determination of New Flavonoidic Compounds by High Resolution ESI-MS/MS in Allium Porrum, Italian Annual Meeting on Mass Spectrometry, September 2-5, **2007**, Lucca, Italy.

An ion source